#42

IN THE UNITED STATES PATENT AND TRADEMARK OFFICE

Applicant:	McDonald *et al.*.	Group Art Unit:	1647
Serial No.:	09/360,242	Examiner:	Landsman, R.
Filed:	July 22, 1999		

For: *METHODS AND COMPOSITIONS FOR TREATING SECONDARY TISSUE DAMAGE AND OTHER INFLAMMATORY CONDITIONS AND DISORDERS*

DECLARATION PURSUANT TO 37 C.F.R. §1.132

Commissioner for Patents
U.S. Patent and Trademark Office
P.O. Box 1450
Alexandria, VA 22313-1450

Sir:

I, JOHN R. McDONALD, declare as follows:

1. I am an inventor of and am familiar with the subject matter of the above-captioned application.

2. I received B.Sc. and Ph.D. degrees at Napier College, Edinburgh, completed successful postdoctoral appointments in Canada and The United States before leaving academia for the biotechnology industry (Boulder CO, and San Diego CA). I have been involved in all aspects of the Research and Development process from project planning through IND filing. My research has focused upon growth factor signal transduction, multiple sclerosis, and the purification and characterization of neurotrophic factors and growth factor-mitotoxin fusion proteins. I have received several peer-reviewed awards and grants, including a US National Institutes of Health Small Business Innovation Research Grant. I am co-author of over fifty publications, and a named inventor on nine patent applications.

3. I am a founder of Osprey Pharmaceuticals Limited, Canada, and I was Vice-President Research & Development and a Director at the company.

4. I have read the Office Action, mailed February 19, 2003, that issued in connection with the above-captioned application. It is my understanding that the claims are rejected by the Examiner over Roby *et al.* (Oncology Reports 3:175-179, 1996) as being anticipated or obvious. I understand that anticipation requires that a reference disclose all elements as claimed and obviousness requires a suggestion in a reference to do that which applicant has done.

5. As described below, Roby *et al.* does not disclose chemokine targeting agent-toxin conjugates that bind to chemokine receptors. The data and results presented in Roby *et al.* are inconsistent with a conclusion that its conjugates bind to chemokine receptors on cells and that its conjugates are internalized upon binding to chemokine receptors on cells. Furthermore, as described below, the C-terminus of chemokines, such as MSGA/GROα, is not responsible for receptor binding.

Roby *et al.* describes a study that evaluated the feasibility of targeted delivery of daunorubicin to melanoma cancers cells. A **C-terminal peptide** from the CXC chemokine MSGA/GROa was conjugated to daunorubicin. As demonstrated below and in the attached references, the C-terminal portion of this chemokine does not mediate binding to chemokine receptors; the data in Roby *et al.* are consistent with this conclusion. In addition, the data in Roby *et al.* do not support a conclusion that the resulting conjugate is internalized by binding to receptors on melanoma cells.

6. **Analysis**

A. Expression of Chemokine Receptors on Target Cells

IL-8, which has significant homology to MSGA/GROα, binds to the same receptors (see, Moser *et al.* (1991) *J. Biol. Chem. 266*:10666-10671 Clark-Lewis *et al.* (1994) *J. Biol. Chem. 269*:16075-16081; Kim *et al.* (1994) *J.*

Biol. Chem. 269:132909-132915). as MSGA/GROα. Also, it is known that the chemokine MSGA/GROa binds to IL-8RB/CXCR2 and IL-8RA/CXCR1 with high and low affinity, respectively (see, *e.g.*, Kim *et al.* (1994) *J. Biol. Chem. 269*:132909-132915). It also is known that many chemokine receptors including CXCR1 and CXCR2 are expressed on a wide variety of cancers including ovarian cancers. In fact, both receptors have been shown to be highly expressed on human SKOV-3 ovarian cancer cells (Venkatakrishnan *et al.* (2000) *J. Biol. Chem. 275*: 6868-6875). Hence, if the conjugate of Roby *et al.* binds to chemokine receptors for MSGA/GROα, then it should bind to SKOV-3 cells.

Roby *et al.*, however, shows that SKOV-3 ovarian cancer cells **are not** susceptible to the C-terminal peptide targeted drug (Tables I and II). Thus, the C-terminal peptide of MGSA/GROα does not bind to chemokine receptors.

This result indicates that the C-terminal peptide that is used to target the drug in Roby *et al.* is not binding to an MSGA/GROα receptor, since it would also bind to SKOV-3 cells, which express MSGA/Groα receptors. Further, as discussed below, it is unlikely that the conjugate engages another protein/growth factor receptor and undergoes internalization in view of the cytotoxic kinetic data presented by Roby *et al.*

B. Chemokine receptor binding and activation sites reside on the N-terminus and NOT the C-terminus of the molecule.

As described in the application and known to those of ordinary skill in the art the chemokine superfamily is divided into four subgroups (CXC, CC, C and CX3C) based on the position of up to four conserved cysteine residues. Most chemokines belong to the CXC and CC subgroups. The different chemokines have between 15 and 50% identity in their primary structures, but they share conserved three-dimensional structures. It is their highly conserved and shared three dimensional structures that are responsible for receptor binding and function. Early structural studies were carried out with the CXC ligand, IL-8, which as noted above, has significant homology to MSGA/GROa and binds to

the same receptors (see, Moser *et al.* (1991) *J. Biol. Chem. 266*:10666-10671 Clark-Lewis *et al.* (1994) *J. Biol. Chem. 269*:16075-16081; Kim *et al.* (1994) *J. Biol. Chem. 269*:132909-132915).

Subsequent studies on several chemokines confirmed the conserved nature of the three dimensional structure among chemokines and that subtle differences in the protein conformation accounts for their functional differences. Structurally, chemokines including MSGA/GROa, are made up a flexible N-terminus (up to 11 amino acids preceding the first cysteine) followed by a conformational rigid N-terminal loop region, then 3 anti-parallel beta strands and finally, a C-terminal alpha helix. Structural studies have established that the **N-terminal region of all chemokines is essential for chemokine receptor binding, activation and internalization.** The rigid loop region following the second N-terminal cysteine of CXC and CC chemokines is responsible for initial ligand interaction or "docking" with the extracellular domain of the receptor which facilitates the access of the flexible N-terminal region (prior to the first cysteine) for receptor activation. The 30s loop (a few amino acids numbered around 30-36 from the N-terminus) is not directly involved in receptor binding, but along with the disulfides provide a scaffold that determine the conformation of the sites that are critical for receptor binding and activation. (see, *e.g.*, Clark-Lewis *et al.* (1995) *J. Leukoc. Biol. 53*:703-711; Baysal *et al.* (2001) *Proteins 43*:150-160).

The C-terminal alpha helix does NOT bind to chemokine receptors, but has a stabilizing effect on the three dimensional structure. (see, *e.g.*, Clark-Lewis *et al.* (1994) *J. Biol. Chem. 269*:16075-16081; Clark-Lewis *et al.* (1991) *J. Biol. Chem. 266*:23128-34; Zhang *et al.* (1991) *J. Biol.Chem. 269*:15918-15924). For example, functional studies on peptides of IL-8 (an analog of MSGA/GROa; as noted IL-8 and MSGA/GROa selectively bind to the

same receptors (IL8A/CXCR1 and IL-8B/CXCR2) show that a 1-51 amino acid peptide with the entire C-terminal *α* helix missing competes with the full length IL-8 for binding to the receptor and exhibits activity (see, Clark-Lewis *et al.* (1991) *J. Biol. Chem. 266*:23128-23134, 23131). Further, a 22 amino acid C-terminal peptide containing the whole C-terminal a helix **does not** to bind to the receptor or show any activity (page 23132 of the same reference). The Roby *et al.* peptide (MGSA/GRO*α* 47-71) has striking primary and secondary structure homology to the Clark-Lewis peptide.

Despite extensive structural studies on numerous chemokines over the last 15 years there have been no reports preceding or subsequent to that of the cited Roby *et al.* describing C-terminals of chemokines (or peptides thereof) that bind to any signal transducing receptor (chemokine or not). Therefore, the peptide used in the conjugate of Roby *et al.* does not bind to a chemokine receptor. Thus, the conjugate does not target chemokine receptors and is not composed of a chemokine-receptor targeting agent.

C. Kinetics of Chemokine receptor Internalization

High affinity binding of many chemokines including MSGA/GROa, results in rapid (within minutes) receptor desensitization and internalization by receptor mediated endocytosis (see, Chuntharapai *et al.* (1995) *J. Immunol. 155*:2587-2594; Mueller *et al.* (1997) *J. Biol. Chem. 272*:8207-8214; Yang *et al.* (1999) *J. Biol. Chem. 274*:11328-11333; Solari *et al.* (1997) *J. Biol. Chem. 272*:9617-9620). Internalization leads to a dramatic drop in the availability of cell surface receptors leaving the cells unresponsive to further ligand effects until the cells have time to recycle or express new receptors. In the case of CXCR2, the MSGA/GROa specific receptor, recovery was shown to take several hours without receptor expression levels reaching 100% of the initial expression levels (see, Chuntharapai *et al.* (1995) *J. Immunol. 155*:2587-2594). In the same study, MSGA/GROa was shown to be internalized and to down regulate receptors by 50% in 10 min at a concentration of 0.2 nM.

If the conjugate of Roby *et al.* was utilizing a chemokine receptor (and one of ordinary skill in the art would expect CXCR2) or any classic protein/growth factor receptor that requires internalization, the drug would have been taken up rapidly. Given the multi-mechanisms of action of daunorubicin (which is taken into cells by diffusion as outlined below) and the short term experiments described by Roby *et al.* (page 178, Table II), evidence of cell death of most of the susceptible (most metabolically active) cancer cells at lower doses would have been expected. The ID_{50} of the free and conjugated drug is in the micro-molar range and by definition so would the C-peptide (as it is conjugated 1:1 to the drug). This, however, is not what was observed in Roby *et al.* The >1000 ng/ml of ID 50 value for conjugate early incubation time points for the "target cells" in Table II (page 179) is calculated to give a concentration of at least 2000 times greater than the nM value reported by Chuntharapi *et al.* It would be charitable to expect an "active" peptide to lose this much activity when compared to the parent molecule. Roby *et al.* sum up the results of the shorter term drug incubation experiments summarized in Table II by stating "We can see from these tests that the observed tendency for long exposure (of daunorubicin and conjugate) is maintained" (page 178). This would suggest that both unconjugated and conjugated drug are taken up by the cells by a mechanism other than by a classic protein receptor route. It is most likely that the conjugated drug is taken up by diffusion as is the free drug. The Roby *et al.* data supports this conclusion.

D. Cellular uptake and Mechanism of Action of Daunorubicin

Daunorubicin (Cerubidin®, DaunoXome) is one of the lipophilic anthracycline antibiotics long used in cancer therapy (see, *e.g.*, Weiss (1992) *Semin Oncol 19*:670-686). The mechanisms of action(s) of these antibiotics include the inhibition of function and breakage of DNA, inhibition of transcription by inhibition of topoisomerase II, metal ion chelation, and generation of free

radicals (see, *e.g.*, Bakker *et al.* (1995) *Current Pharmaceutical Design 1*:1133-1144). The anthracyclines are used in cancer therapy and are toxic to a wide range of cancer cells; there are only a few unresponsive cancers (see, Weiss *et al.* (1992) *Semin Oncol 19*:670-86). Due to their lipophilic nature, these compounds are readily taken up by cells by simple diffusion (see, Bakker *et al.* (1995) *Current Pharmaceutical Design 1*:1133-1144). In fact, to exploit this property, derivatives of daunorubicin, which are on the market, have been designed to increase their lipophilic nature (see, *e.g.*, Michieli *et al.* (1996) *Haematologica 81*:295-301). The process of diffusion is time-, temperature-, concentration-dependent and energy independent (see, *e.g.*, Nagasawa *et al.* (1996) *Biol. Pharm. Bull. 19*:100-105). Efflux of the drugs is facilitated by energy-dependent membrane pumps. The intracellular concentration is determined by a balance of these two processes and is a major determinant for the cytotoxic effects or the drugs. Tumor cells show differences in their intrinsic or acquired resistance to the drug.

The data presented by Roby *et al.* show properties and functions characteristic of daunorubicin. Figures 3 through 6 and Tables I and II show that the free drug and conjugate at high concentrations are capable of killing ovarian carcinoma cells and fibrosarcoma cells as well as melanomas as would be expected of the broad spectrum cancer therapeutic. The high concentrations of drug needed in the short term experiments and the need for long term exposure is far more consistent with cellular uptake of the drug by diffusion rather than by internalization. The differences in ID_{50} values among the cell lines used could be a reflection of differences in the activity, in the accumulated intracellular drug concentration or the active state of the cells (e.g., different rates of proliferation). The result also can be a reflection of differences in the tumor

cells' intrinsic level of resistance to the drug. It must be pointed out that even resistant strains succumb to the drug albeit at higher doses (see, *e.g.*, Michieli *et al.* (1996) *Haematologica 81*:295-301; Michieli *et al.* (1999) *Haematologica 84*:1151-1158).

Roby *et al.* states that "the conjugate greatly increases the activity of daunorubicin on melanoma cells" and concludes "that the reason for such a dramatic increase is unknown" (bottom of page 178). The inference that Roby *et al.* is trying to make is that the conjugate targets the drug to these cells. These conclusions, however, clearly contradict the data in the paper. As noted, SKOV-3 cancer cells are known to robustly express the MSGA/GROa receptors, but the activity of the conjugates on these cells is decreased.

Thus, the paper is describing phenomenology. The only explanation for the data is that the conjugate is sequestered in some way. Chemokines bind to glycosaminoglycans (GAGS) including heparin and heparan sulfate, chondroitin sulfate and dermatan sulfate (see, *e.g.*, Proudfoot *et al.* (2001) *J. Biol. Chem. 276*:10620-10626). They bind with much lower affinities than to chemokine receptors. These GAGS are expressed to a varying degree on the surface of cells and are not internalized. These GAGS are thought to help localize the chemokines to the area of inflammation and disease, increase their local concentration in vivo and facilitate chemokine receptor binding. It has been shown that the binding site for these proteoglycans has been located in the C-terminal alpha helix of some chemokines where a number of basic amino acid residues (lysine and arginine, also present in the peptide discussed here). The Roby *et al.* C-terminal peptide contains these amino acid residues. In a tissue culture dish without the stabilizing and high affinity binding effect of an N-terminal portion of a chemokine, this charged molecule will bind to a number of charged surfaces including the tissue culture dishes, various proteins and GAGS in the serum and cell medium as well as to the surface of most cells. Soluble GAGS have been shown to inhibit binding to GAGS on cells.

Therefore, while it is impossible to unequivocally interpret the data of Roby *et al.* (Tables I and II), a possible explanation for the increased, decreased and no change in sensitivity among the cell lines (Table I) is differences in GAG type, expression levels, affinities and number of binding sites on the different cells and this would be after binding to miscellaneous other surfaces. Finally, given that most cells express GAGS, Roby *et al.* does not demonstrate targeted delivery.

7. **Summary**

a) Roby *et al.* does not show that a chemokine targets a toxin to melanoma cancer cells specifically nor that such conjugate of a C-terminal peptide and a drug is internalized. Given the information available at the time of publication of Roby *et al.*, one of ordinary skill in the art would not design a conjugate for targeting to chemokine receptors that lacks the N-terminal regions known to be required for cell-specific targeting (i.e., receptor binding, activation and internalization). Despite extensive work on peptides from all parts numerous chemokine proteins, there are no reports of any chemokine C-terminal peptide that is internalized or biologically active before or after that of Roby *et al.*

b) Further, Roby *et al.* does not report studies of receptor internalization, cross-linking studies or receptor identification on target cells and alleged non-target cells. The kinetics of cellular uptake and activity on different cancer cell targets exhibited by the conjugate are entirely consistent with the known properties of the free drug. Thus Roby *et al.* does not disclose, teach or suggest conjugates that target toxins leukocytes, nor that different chemokine-targeting ligands confer different cellular specificities nor use of such conjugates for treatment of disorders that share a common underlying pathology.

* * *

I further declare that all statements made herein of my own knowledge are true and that all statements made on information and belief are believed to be true; and further, that these statements were made with knowledge that willful false statements and the like so made are punishable by fine or imprisonment, or both, under Section 1001 of Title 18 of the United States Code, and that such willful false statements may jeopardize the validity of the application or any patent resulting therefrom.

_____
JOHN R. McDONALD

Date: _____
25020-601B

Vol. 206, No. 2, 1995
January 17, 1995

BIOCHEMICAL AND BIOPHYSICAL RESEARCH COMMUNICATIONS
Pages 792-798

CELL-BINDING AND GROWTH-STIMULATING ACTIVITIES OF THE C-TERMINAL PART OF HUMAN MGSA/GROα

Philippe Roby and Michel Page[1]

Department of Biochemistry, Faculty of Medicine, Université Laval, Québec G1K 7P4, Canada

Received December 9, 1994

The FITC-labeled C-terminal alpha-helix portion of human MGSA/groα (MGSA 47-71) was shown, using flow cytometry, to bind to human melanoma cells Hs294t but not to non-melanoma cells. MGSA (47-71) is capable to induce specifically DNA synthesis of melanoma cells. These results indicate that the C-terminal portion of human MGSA is sufficient for its biological activity, thus raising questions about the importance of dimerization and of the N-terminal ELR box of the molecule which has been proposed.

Cell growth factors and/or cytokines bind to specific receptors which transmit their effect by means of various intermediates and protein kinases (1).

One of the major interest of these various proteins is their importance in cancer growth, in which many proteins are involved, either as an endocrine, paracrine and autocrine control. Study of those growth factors contributes to the understanding of the mechanisms of cancer progression.

Melanoma is a very aggressive type of skin cancer characterized by proliferation of pre-melanocyte. The incidence of this kind of cancer is progressing exponentially among the caucasian population (2). Growth factors involved in the growth of melanoma cells include basic fibroblast growth factor, epidermal growth factor and melanocyte stimulating hormone (3). In 1988, a new melanoma growth factor was discovered. This factor was characterized and cloned as the oncogene GROα (or Melanoma Growth Stimulating Activity (MGSA)). From the cDNA sequence, it was possible to determine that MGSA was an analogue of interleukin-8 (4). The latter and its analogues (including

[1] To whom correspondence should be addressed.

Abbreviations: MGSA: Melanoma Growth Stimulating Activity. ELR box: Glutamate, leucine Arginine Box. DMSO: Dimethyl sulfoxide. Fmoc:Fluorene methoxy carbonyl. TFA: Trifluoroacetic acid. FITC: Fluorescein isothiocyanate. FCS: Fetal calf serum.

0006-291X/95 $5.00

MGSA, NAP-2 and about 6 others) are members of a family of small proteins called chemokines (5). These proteins are chemotactic and stimulatory factors for neutrophils (for the CXC sub-family) or macrophages (for the CC sub-family) (6). MGSA is a member of the CXC sub-family named for two characteristic cysteine residues on the N-terminal side (7).

The 3-dimensional structure of interleukin-8 shows that it is a dimer made of two sub-units each composed of a compact array of 3 beta sheets with a C-terminal protruding alpha helix (8). Recently, studies with mutated interleukin-8 molecules have shown that 3 amino acids at the N-terminal portion of the molecule (glutamate, leucine and arginine, the ELR box) were essential for activity. These amino acids are conserved in all members of the CXC sub-family, including MGSA (9). However, the 3-dimensional structure raises the possibility that the C-terminal α-helix could be the receptor binding moiety of MGSA. Studies on the structure-activity relashionship of MGSA are essential for designing specific agonists or antagonists.

This is the first report of the biological activity of the C-terminal portion of MGSA as a first step in the elucidation of the structure-activity relationship of this growth factor.

MATERIALS AND METHODS

Hs294t and CCl-121 cells were obtained from the American Type Culture Collection (Rockville MA). RPMI 1640 is from ICN Biomedicals Canada ltd (Mississauga Ont.). Fetal bovine serum is from Cansera (Rexdale Ont.) Fmoc amino acids, synthesis resin and synthesis reagents were obtained from Novabiochem (LaJolla CA). TFA and acetonitrile were obtained from Omega Chemical Company inc. (Quebec Que.). Anisole, ethyl methyl sulfide, Trypan Blue and DMSO come from Aldrich Chemical Company (St-Louis MO). Ethanethiol, trichloroacetic acid and Scintiverse II come from J.T. Baker Canada (Toronto Ont.). Fluorescein isothiocyanate and bovine serum albumin were purchased from Sigma Chemical Company (St-Louis MO). Alamar Blue, from Alamar (Sacramento CA). 3H-Thymidine was obtained from ICN pharmaceuticals (Mississauga Ont.).

SYNTHESIS OF MGSA (47-71)

MGSA (47-71) was synthesized using solid-phase peptide synthesis as previously described (10). Briefly, Fmoc-amino acid -oPfp were added one by one in sequence to a Biolynx 4175 semi-automatic peptide synthesizer (LKB) loaded with a resin bearing Fmoc-Lysine. Synthesis proceeded from the C-terminal to the N-terminal part of the following peptide : NGRKACLNPASPIVKKIIEKMLNSDK, which correspond to amino acids 47-71 of human MGSA (4). After completion, the peptide was cleaved from the resin and deprotected with 93% TFA, 3% anisole, 3% ethanethiol and 1% ethyl methyl sulfide. The crude peptide was washed once with ether and purified by HPLC on a delta-pak C18 column (Waters (Mississauga Ont.)) with a 30-50% acetonitrile : water + 0,05% TFA gradient using a LC 925 system connected to a 996 photodiode array (Waters).

Purity of the peptide was measured by Capillary Zone Electrophoresis on a Bio-Focus 3000 system (Bio-Rad Laboratories (Mississauga Ont.) using a 24μx25mm cartridge. 20μg of sample were dissolved in 100μl of 0,01M PO4 buffer pH 2,5 and run under a 10kV current for 15 minutes in 0,1M phosphate buffer pH 2,5.

LABELING OF MGSA (47-71)

The pure peptide was labeled with FITC as follows: 500μg of MGSA (47-71) were dissolved in 500μl of 0,1M carbonate buffer pH 9,0. Then, 67μl of a 2mg/ml solution of FITC in dimethyl sulfoxyde were added in 5μl steps with agitation. The solution was allowed to react for 16 hours at 4°C in the dark. We then added 60μl of a 1M solution of ammonium chloride and 30μl of glycerol.

After 2 hours at 4°C, the labeled peptide was purified on a PD-10 column (Pharmacia Biotech (Baie D'Urfe Que.)) equilibrated with phosphate buffered saline. The coupling ratio of FITC was measured by absorption at 495nm.

CELL-BINDING ASSAYS

Hs294t and CCl-121 cells were harvested by scraping and counted using Trypan Blue. One hundred thousand cells were added to a test tube and suspended in 1ml of PBS + 0,1% BSA. Various amounts of FITC-labeled peptide (0, 40ng, 50ng, 60ng, 80ng, 100ng, 200ng, 500ng and 1000ng) were added and the cells were incubated for 1 hour at 4°C. They were then washed twice with 5ml of PBS + 0,1% BSA and resuspended in 1ml of FACS-Flow (Becton Dickinson). Flow Cytometry on a FACS-Sort (Becton Dickinson (Mississauga Ont.)) was used to measure the fluorescence of 5000 cells. Binding was measured by the ratio of the medians of fluorescence peaks of labeled cells divided by the median of the fluorescence peak of unlabeled cells.
Controls were also run with 100ng of labeled peptide incubated 1 hour at 37°C with 10μg of an anti-MGSA monoclonal antibody (developed in our laboratory) before being added to the cells.

^{3}H-THYMIDINE ASSAY

A 24-well plate was seeded with 50000 Hs294t or CCl-121 cells per well suspended in 1ml of RPMI 1640 + 10% fetal calf serum. The plate was incubated for 24 hours at 37°C in a humid atmosphere of 5% CO2. The cells were then washed once with 1ml of RPMI 1640 and then each well filled with 1ml of RPMI 1640 without serum. After 24 hours, the cells were washed as above and various quantities of MGSA (47-71) were added (0, 100ng, 10ng, 1ng, 100pg and 10pg) in 1ml of RPMI 1640 in duplicate. 2 wells were filled with 1ml of RPMI 1640 + 10% FCS. The cells were incubated for 16 hours at 37°C 5% CO2 and then 2μCi of 3H Thymidine in RPMI 1640 were added, and the cells incubated for 6 more hours.
The cells were washed twice with cold PBS and incubated 20 minutes in cold methanol, then 20 minutes in cold 5% trichloroacetic acid. They were then washed twice in water, dissolved in 200μl NaOH 1M and 150μl of the solution was added to scintillation vials filled with 5ml of Scintiverse II. Radioactivity was them measured on a Rackbeta II (LKB) counter.

ALAMAR BLUE ASSAY(11)

Two 96-wells plates were seeded with 5000 Hs294t or CCL-121 cells per well suspended in 100μl of RPMI 1640 + 10% FCS. The plates were incubated for 24 hours at 37°C in a humid, 5% CO2 atmosphere. Each plate was then washed and 100μl of RPMI 1640 without serum added. After 24 hours, the cells were washed again and concentrations of MGSA identical to those used in the 3H-thymidine assay were added
Tests were made after 0, 2, 3 and 4 days. Wells were washed with RPMI 1640. Then,10 μl of Alamar Blue were added and the plate incubated for 2 hours. Fluorescence was then measured on a Cytofluor 2300 (Millipore) at excitation 530nm and emission 590nm.

RESULTS AND DISCUSSION

CELL-BINDING OF MGSA (47-71)

Cell-binding assays using a FITC-labeled MGSA (47-71) peptide show that this molecule is able to bind to Hs294t cells, as shown by the increased fluorescence of the cells incubated with the peptide [fig.1] A way to measure that effect was to look at the ratio of the median of the fluorescence peak of labeled cells divided by the median of the unlabeled cells [fig. 2]. These results show that a near linear ratio was obtained with concentrations of FITC-labeled MGSA, varying from 0 to 100ng/ml. At higher concentrations, a plateau was reached. When fibrosarcoma CCL-121 cells were used, concentrations up to 1000ng/ml of MGSA (47-71)-FITC showed no significant labeling [fig.3], suggesting that these cells have no receptors for MGSA. The specific binding on melanoma cells was confirmed by assays with the peptide incubated with an anti-MGSA monoclonal antibody obtained in our laboratory which blocked MGSA binding (data not shown).

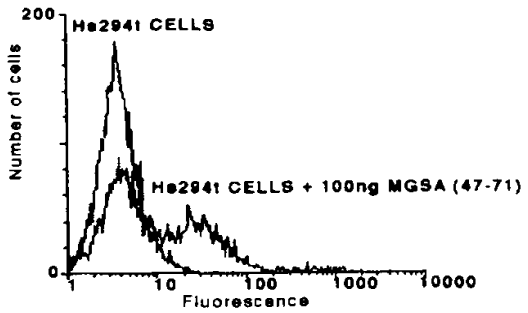

Fig.1. Binding assay of 100ng MGSA (47-71)-FITC to 100 000 Hs294t cells (1-hour incubation).

3H-THYMIDINE ASSAYS

3H-Thymidine incorporation was 160% of control in human melanoma Hs294t cells stimulated with MGSA (47-71) with an optimal concentration at 10ng/ml [fig. 4]. This concentration is higher than the concentration already reported for complete MGSA, which is around 0,6 to 6ng/ml (12). However, it clearly stands above the background, while a similar assay with CCL-121 shows no significant 3H-thymidine incorporation at any peptide concentration (data not shown). This indicates that the increase in radioactivity is caused by the peptide binding to the receptor and not simply by a change in culture conditions.

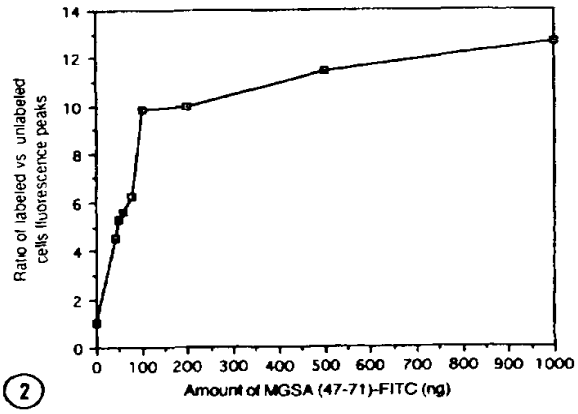

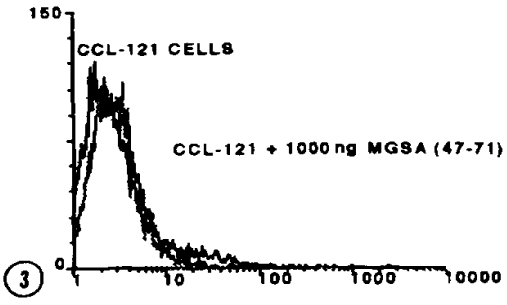

Fig. 2. Ratios of the fluorescence peaks of MGSA (47-71)-FITC-labeled Hs294t cells versus unlabeled cells measured by flow cytometry.

FIG 3. Binding assay of 1000ng MGSA (47-71)-FITC to 100 000 CCL-121 cells (1-hour incubation).

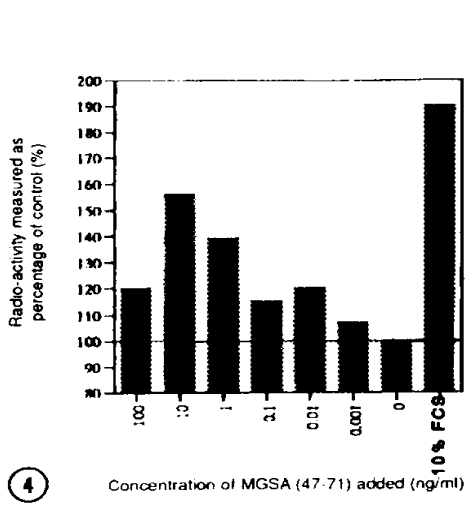

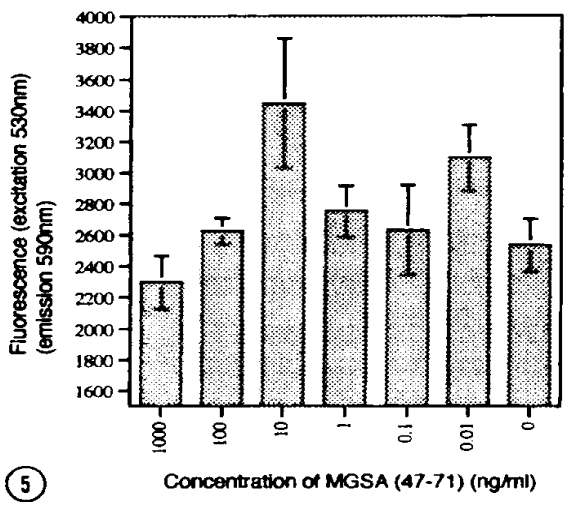

Fig. 4. 3H-Thymidine incorporation assay on Hs294t cells incubated with various concentrations of MGSA (47-71).

Fig. 5. Cell growth measurement assay of Hs294t cells with MGSA (47-71) added to culture medium by the Alamar Blue fluorometric method.

ALAMAR BLUE ASSAYS

The measurement of cell growth by the Alamar Blue assay confirms the results obtained by 3H-Thymidine incorporation, with a maximum cell growth at a concentration of 10ng/ml of MGSA (47-71) [fig. 5]. The largest difference between cells incubated with peptide and control was seen after 3 days of incubation. After this period, we could observe some cell death and fluorescence began to decrease. Similar tests performed on CCL-121 cells show no significant increase in cell number compared with control for any peptide concentration used.

DISCUSSION

Results show for the first time that the C-terminal portion (47-71) of MGSA binds specifically to human melanoma cell receptors. Incubation of the peptide with an anti-MGSA antibody before the addition to melanoma cells confirms these results and shows that the C-terminal α-helix of MGSA is sufficient for receptor recognition and binding.

Results obtained by 3H-thymidine incorporation and Alamar Blue indicate that MGSA (47-71) is capable of promoting cell-growth of melanoma cells *in vitro* at 10ng/ml but has no activity on cells without specific receptors. These results

show that the binding of the C-terminal α-helix of MGSA non-only is sufficient for binding but it is also a mitogen for melanoma cells.

However, These findings however, raise some interesting questions. The first is that in solution, the closest analog of MGSA, interleukin-8, is a dimeric molecule and recent studies (13) have shown that this cytokine seems to act as a monomer on the receptor. Our results seem to confirm this hypothesis since it is very unlikely that MGSA (47-71) is capable of dimerization (it has a +5 charge in solution) but nevertheless this peptide is active.

Other workers have shown that the N-terminal ELR (glutamate, leucine, arginine) box is essential for the neutrophil stimulating activity of interleukin-8 (9). However, while this ELR box is conserved at the same position in MGSA, it does not seem to be essential for receptor binding nor for growth-stimulating activity on melanoma cells. This may be due to the fact that either the ELR box is an essential component for proper folding of the CXC chemokines, or the receptor on melanoma cells and the one on neutrophils are different. Indeed, two receptors have been identified by cross-linking with MGSA in placenta, one of 58kDa and one of 78kDa. The 78kDa appears to be the primary receptor on Hs294t cells (14), while the molecular weight of the interleukin-8 receptors on neutrophils varies from 55 to 65kDa. (15). MGSA (47-71) will be tested on neutrophils to elucidate at least the second possibility.

Nevertheless these studies show that specific growth stimulation of human melanoma cells may be obtained with the short C-terminal MGSA (47-71) peptide thus opening the possibility of designing small antagonists against this growth factor.

REFERENCES

1- Aggarwal, B., and Gutterman, J. (1992) Human Cytokines, 411pp. Blackwell Scientific Publications, Boston.
2- Balch, C.M., Houghton, A. and Peters, L. (1989) in Cancer Principles and Practice of Oncology (DeVita, V.T., Hellman, S. and Rosenberg, S.A. Ed.). pp 1499-1542. J.B. Lippincott Company, Philadelphia.
3- Rodeck, U., Melber, K., Kath, R., Menssen H.D., Varello, M., Atkinson, B. and Herlyn, M. (1991) J. Invest. Dermatol. 97(1), 20-26.
4- Richmond, A., Balentien, E., Thomas H.G., Flaggs, G., Barton, D.E., Spiess, J., Bordoni, R., Francke, U. and Derynck, R. (1988) EMBO J. 7, 2025-2033.
5- Durum, S. (1992) ImmunologyToday 13(12), 514-515.
6- Schall, T.J. (1991) Cytokine 3, 165-183.
7- Oppenheim, J., Zachariae, C.O.C., Mukaida, N. and Matsushima, K. (1991) Annu. Rev. Immunol. 99, 617-648.
8- Clore, G.M., Appella, E., Yamada, M., Matsushima, A. and Gronenborg, A.M. (1990) Biochemistry 29, 1689.
9- Clark-Lewis, I., Schumacher, C., Baggilioni, M. and Moser, B. (1991) J. Biol. Chem. 266, 23128.
10- Levesque, A., Page, M., Huard, G., Noel, C. and Bejaoui, N. (1991) Anticancer Research 11, 2215-2222.

11- Page, B., Page, M. and Noel, C. (1993) Int. J. of Oncology 3, 473-476.
12- Richmond, A. and Thomas, H. G. (1988) J. of Cell. Biochemistry 36, 185-198.
13- Rajarathnam, K., Sykes, B.D., Kay, C.M., Dewald, B., Geiser, T., Baggiolini, M. and Clark-Lewis, I. (1994) Science 264, 90-92.
14- Cheng, Q.C., Han, J.H., Thomas, H.G., Balentian, E and Richmond, A. (1992) Journal of Immunology 148 (2), 451-456.
15- Horuk, R. (1994) Immunology Today 15 (4), 169-174.

THE JOURNAL OF BIOLOGICAL CHEMISTRY
Vol. 276, No. 14, Issue of April 6, pp. 10620–10626, 2001
Printed in U.S.A.

The BBXB Motif of RANTES Is the Principal Site for Heparin Binding and Controls Receptor Selectivity*

Received for publication, December 1, 2000
Published, JBC Papers in Press, December 14, 2000, DOI 10.1074/jbc.M010867200

Amanda E. I. Proudfoot‡§, Sarah Fritchley¶, Frédéric Borlat‡, Jeffrey P. Shaw‡, Francis Vilbois‡, Catherine Zwahlen‖, Alexandra Trkola, David Marchant‡‡, Paul R. Clapham‡‡, and Timothy N. C. Wells‡**

*From the ‡Serono Pharmaceutical Research Institute, 14 Chemin des Aulx, 1228 Plan-les-Ouates, Geneva, Switzerland, ¶Department of Surgery, The Medical School, University of Newcastle upon Tyne, Newcastle upon Tyne NE2 4HH, United Kingdom, ‖Institut de Chimie Organique, Université de Lausanne, BCH, 1015 Lausanne, Switzerland, **Department of Medicine, Division of Infectious Diseases and Hospital Epidemiology, University Hospital Zurich, Ramistrasse 100, 8091 Zurich, Switzerland, and the ‡‡Wohl Virion Centre, Department of Molecular Pathology, The Windeyer Institute for Medical Sciences, University College Medical School, London W1T 4JF, United Kingdom*

The chemokine RANTES (regulated on activation normal T cell expressed and secreted; CCL5) binds selectively to glycosaminoglycans (GAGs) such as heparin, chondroitin sulfate, and dermatan sulfate. The primary sequence of RANTES contains two clusters of basic residues, ^{44}RKNR^{47} and ^{55}KKWVR^{59}. The first is a BBXB motif common in heparin-binding proteins, and the second is located in the loop directly preceding the C-terminal helix. We have mutated these residues to alanine, both as point mutations as well as triple mutations of the 40s and 50s clusters. Using a binding assay to heparin beads with radiolabeled proteins, the ^{44}AANA^{47} mutant demonstrated an 80% reduction in its capacity to bind heparin, whereas the ^{55}AAWVA^{59} mutant retained full binding capacity. Mutation of the ^{44}RKNR^{47} site reduced the selectivity of RANTES binding to different GAGs. The mutants were tested for their integrity by receptor binding assays on CCR1 and CCR5 as well as their ability to induce chemotaxis *in vitro*. In all assays the single point mutations and the triple 50s cluster mutation caused no significant difference in activity compared with the wild type sequence. However, the triple 40s mutant showed a 80-fold reduction in affinity for CCR1, despite normal binding to CCR5. It was only able to induce monocyte chemotaxis at micromolar concentrations. The triple 40s mutant was also able to inhibit HIV-1 infectivity, but consistent with its abrogated GAG binding capacity, it no longer induced enhanced infectivity at high concentrations.

Chemokines selectively recruit and activate leukocyte populations, both during routine immunosurveillance and also during inflammation. The migration of cells is believed to require immobilization of the chemokines on proteoglycans in the extracellular matrix and on the endothelial cell (2, 3). The glycosaminoglycan (GAG)[1] moiety of the proteoglycan shows a wide range of structures, with heparin, heparan sulfate, chondroitin sulfate, and dermatan sulfate being important members of the family. Changes in the type of intensity of proteoglycan expression are known to happen in a wide variety of inflammatory diseases. It has been suggested that these changes in glycosaminoglycan expression play a role in the localization of the inflammatory response, by localizing inflammatory cytokines and chemokines (4–7).

Chemokines are a large family of small proteins with a remarkably highly conserved three-dimensional monomeric structure (Ref. 8 and Fig. 1). This conserved structure is mediated by the formation of two disulfide bridges imposed by the conserved 4-cysteine motif rather than identity at the level of primary sequence, which can be as low as 20%. The majority of chemokines (MIP-1α and -1β being the exceptions)[2] are highly basic proteins with an isoelectric point around pH 9.0. All chemokines are able to bind heparin, although with varying affinities. We have previously shown that selectivity exists for the chemokine/GAG interaction for four chemokines investigated: IL-8, RANTES, MIP-1α, and MCP-1 (9). RANTES was shown to have the greatest range of selectivity with an affinity 3 orders of magnitude higher for heparin than for chondroitin sulfate. Despite its acidic isoelectric point, MIP-1α is still able to bind to GAGs, showing that the interaction is not simply a global electrostatic attraction of basic chemokines with acidic glycosaminoglycans. The complexation of chemokines with glycosaminoglycans prevents the binding of the chemokines to their receptors in most cases (9). However, the GAG/chemokine interaction has also been reported to potentiate the activity of chemokines in some cases (10, 11).

The *XBBXBX* and *XBBBXXBX* motifs, where B represents a basic residue, have been shown to be a common heparin-binding motif for several proteins (12, 13). Inspection of the RANTES sequence showed that it had two clusters of basic residues: a BBXB cluster on the 40s loop (^{44}RKNR^{47}) and another cluster of basic residues toward the C-terminal on the 50s loop (^{55}KKWVR^{59}). The C-terminal region has been shown to be implicated in GAG binding for chemokines such as PF4 (14), IL-8 (15), and MCP-1 (16) but not necessarily through BBXB motifs. We have mutated the charged amino acids in these sequences, as point mutations as well as triple mutations, to

* The costs of publication of this article were defrayed in part by the payment of page charges. This article must therefore be hereby marked "*advertisement*" in accordance with 18 U.S.C. Section 1734 solely to indicate this fact.

§ To whom correspondence should be addressed: Serono Pharmaceutical Research Institute, 14, Chemin des Aulx, 1228 Plan les Ouates, Geneva, Switzerland. Tel.: 41-22-706-98-00; Fax: 41-22-794-69-65; E-mail: amanda.proudfoot@serono.com.

[1] The abbreviations used are: GAG, glycosaminoglycan; IL, interleukin; RANTES, regulated on activation normal T cell expressed and secreted; CHO, Chinese hamster ovary; HPLC, high pressure liquid chromatography; HSQC, heteronuclear single quantum coherence; HIV-1, human immunodeficiency virus, type 1; WT, wild type.

[2] The following chemokines with the new standardized nomenclature (1) are cited: IL-8, CXCL8; SDF-1, CXCL12; MIP-1α, CCL3; MIP-1β, CCL4; RANTES, CCL5; and MCP-1, CCL2.

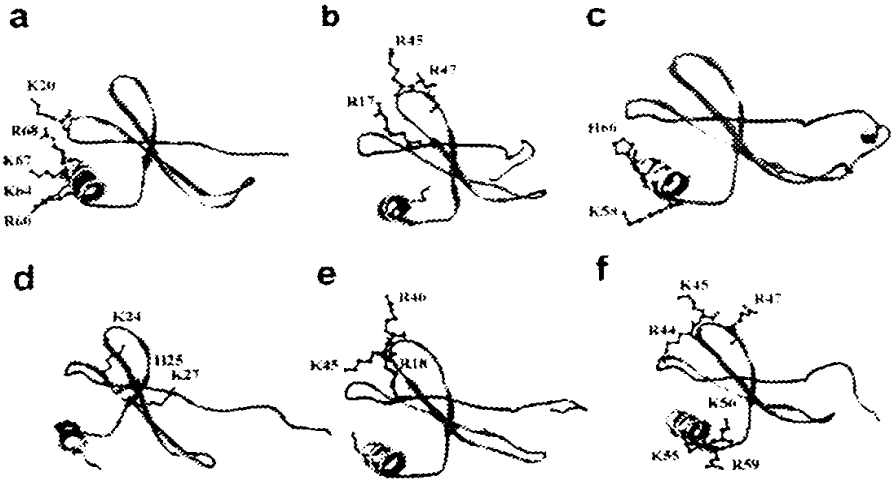

FIG. 1. **Chemokine monomers indicating the basic GAG binding residues.** *A*, interleukin-8 (15). *b*, MIP-1α (36, 40). *c*, MCP-1 (16). *d*, SDF-1α (38). *e*, MIP-1β (37). *f*, the residues of RANTES mutated in this study. The images of chemokine monomers were produced using the program SwissPDBViewer (31) and the ray-tracing program POV-RAY. The Research Collaboratory for Structural Bioinformatics entries of the structures were: IL-8, 1il8; MIP-1α, 1b53; MCP-1, 1dok; SDF-1α, 1a15; Mip-1β, 1hum; and RANTES, 1eqt.

alanine residues. These studies did not identify a major role for any single amino acid, but our findings demonstrate that the triple mutation of the 40s cluster abrogates 80% of the heparin binding capacity, whereas mutation of the 50s cluster has no effect. Furthermore, additional experiments indicated that these basic residues in the 40s loop are also important for CCR1 but not for CCR5 binding, indicating an overlapping epitope on RANTES for CCR1 and GAG binding.

EXPERIMENTAL PROCEDURES

Reagents—Unless otherwise stated, all chemicals were purchased from Sigma. The heparin used in the binding assays was the low molecular weight species (5–30 kDa) supplied by Sigma (H3393). Enzymes were from New England Biolabs, and chromatographic material was from Amersham Pharmacia Biotech. CHO/CCR1 transfectants were generated as described (42), CHO/CCR5 transfectants were a kind gift of Dr. Matthias Mack (43), RBL/CCR5 transfectants were provided by Dr. Martin Oppermann (28), and HeLa-CD4 cells were provided by Dr. David Kabat. Env pseudotyped, luciferase-expressing reporter viruses were produced using the calcium phosphate technique (17).

Generation of Nonheparin-binding Mutants—The point mutations were introduced by inversed polymerase chain reaction. The DNA was alkali-denatured and diluted to a concentration of ~10 pg/reaction to avoid the incorporation of unmutated DNA into the transformation reaction. The mutagenesis primers used are shown below with the mutated bases shown in bold: R44A (sense), 5′-TTT GTC ACC **GCA** AAG AAC CGC CAA G-3′, and R44A (antisense), 5′-GAC GAC TGC TGG GTT GGA GCA CTT G-3′; R45A (sense)5′-TTT GTC ACC CGA **GCG** AAC CGC CAA G-3′, and R45A (antisense), 5′-GAC GAC TGC TGG GTT GGA GCA CTT G-3′; R47A (sense), 5′-CGA AAG AAC **GCC** CAA GTG TGT GCC A-3′, and R47A (antisense), 5′-GGT GAC AAA GAC GAC TGC TGG GTT G-3′; R44A/K45A/R47A (^{44}AANA^{47}) (sense), 5′-TTT GTC ACC **GCA GCG** AAC **GCC** CAA GTG TGT GCC AAC-3′, and R44A/K45A/R47A (^{44}AANA^{47}) (antisense), 5′-GAC GAC TGC TGG GTT GGA GCA CTT GCC-3′; K55A (sense), 5′-GCC AAC CCA GAG **GCG** AAA TGG GTT CGG-3′, and K55A (antisense), 5′-ACA CAC TTG GCG GTT CTT TCG GGT GAC-3′; K56A (sense), 5′-AAC CCA GAG AAG **GCA** TGG GTT CGG GAG-3′, and K56A (antisense), 5′-GGC ACA CAC TTG GCG GTT CTT TCG GGT-3′; K59A (sense), 5′-AAG AAA TGG GTT **GCG** GAG TAC ATC AAC-3′, and K59A (antisense), 5′-CTC TGG GTT GGC ACA CAC TTG GCG-3′; and K55A/K56A/R59A (^{55}AAWVA^{59}) (sense), 5′-GCC AAC CCA GAG **GCG GCA** TGG GTT **GCG** GAG TAC ATC-3′, and K55A/K56A/R59A (^{55}AAWVA^{59}) (antisense), 5′-ACA CAC TTG GCG GTT CTT TCG GGT GAC AAA GAC-3′. Amplification was performed in a DNA thermal cycler (Perkin-Elmer 480) for 35 cycles using *Pfu* Turbo DNA polymerase. Polymerase chain reaction products were purified, and DNA was ligated and transformed into Top 10 F′ competent cells (Invitrogen). The sequence of the mutants was verified by DNA sequence analysis using an ABI370 DNA sequencer.

Protein Purification and Characterization—The mutant proteins were purified as described for simultaneous multiple purifications of recombinant RANTES proteins (18). ^{15}N RANTES was produced as previously described (19). The purity and authenticity of ^{15}N RANTES and the mutants were verified by reverse-phase HPLC and mass spectroscopy.

NMR Spectroscopy of the Interaction of RANTES and Heparin Disaccharides—NMR experiments were recorded at 30 °C on a Bruker DRX600 spectrometer equipped with triple axis gradients using a 5-mm triple inverse resonance probe head. Heparin disaccharides I-A, II-A, and II-S were added to a solution containing 300 μM ^{15}N-labeled RANTES at pH 3.2 in a 0.6:1 ratio. Two-dimensional ^{1}H-^{15}N HSQC experiments were recorded using the sensitivity enhancement technique (20). Data matrices consisting of 128 × 512 complex points were acquired, and the spectral widths were 8390 Hz in the ^{1}H dimension and 1460 Hz in the ^{15}N dimension. The differences in chemical shift Δδ between free and bound protein were evaluated using the following equation (21).

$$\Delta\delta = \sqrt{(\Delta\delta\ ^{1}\mathrm{H})^2 + 0.17(\Delta\delta\ ^{15}\mathrm{N})^2} \qquad \text{(Eq. 1)}$$

Heparin-Sepharose Chromatography—50 μg of RANTES and mutants were loaded onto heparin-Sepharose CL-6B, packed in a HR5/5 column, equilibrated in 25 mM Tris/HCl, pH 8.0, and 50 mM NaCl, and eluted with a linear gradient of 0–2 M NaCl in 25 mM Tris/HCl, pH 8.0, using a Smart system (Amersham Pharmacia Biotech).

Mono S (Cation Exchange) Chromatography—50 μg of RANTES and the mutants were loaded onto a Mono S HR5/5 prepacked cation exchange column equilibrated in 50 mM sodium acetate, pH 4.5, using a Smart system (Amersham Pharmacia Biotech). Protein was eluted with a 0–2 M NaCl gradient.

Heparin Binding Assay—RANTES and the mutants were measured for their ability to bind to immobilized heparin according to Ref. 22. Wild type RANTES and the triple 40s and 50s RANTES mutants were radiolabeled with ^{125}I by Amersham Pharmacia Biotech to a specific activity of 2200 mCi/mol. 96-well filter plates were soaked with binding buffer (50 mM HEPES, pH 7.2, containing 1 mM $CaCl_2$, 5 mM $MgCl_2$, 0.15 M NaCl, and 0.5% bovine serum albumin). Serial dilutions of heparin in the binding buffer were carried out to cover the range of 20 mg/ml-1 μg/ml. The assay was performed in a total volume of 100 μl by adding 25 μl of the heparin dilutions, 25 μl 0.4 nM [^{125}I]chemokine, 25 μl of heparin beads (0.2 μg/ml in water), and 25 μl of binding buffer to each well. The assays were carried out in triplicate. The plates were incubated at room temperature with agitation for 4 h. The filter plates were washed three times with 200 μl of washing buffer using a vacuum pump to remove unbound iodinated chemokine. 50 μl of scintillant was added to each well, and radioactivity was counted in a β-scintillation counter (Wallac) for 1 min/well. Data were analyzed using GraFit Software.

Equilibrium Competition Receptor Binding Assays—The assays were carried out on membranes from CHO transfectants expressing CCR1 and CCR5 using a scintillation proximity assay. Competitors were prepared by serial dilutions of the unlabeled chemokines in binding buffer to cover the range 10^{-6}–10^{-12} M. The binding buffer used was 50 mM HEPES, pH 7.2, containing 1 mM $CaCl_2$, 5 mM $MgCl_2$, 0.15 M NaCl, and 0.5% bovine serum albumin. Wheatgerm scintillation proximity

TABLE I
Mass spectrometric analysis of the RANTES mutants

Mutation	Expected mass	Experimental mass
Wild type	7847.03	7846.69 ± 0.09
R44A	7761.92	7761.20 ± 0.1
K45A	7789.94	7790.49 ± 0.16
R47A	7761.92	7762.32 ± 0.11
R44A/K45A/R47A	7619.72	7619.91 ± 0.11
K55A	7789.94	7791.00 ± 0.02
K56A	7789.94	7791.01 ± 0.02
R59A	7761.92	7760.67 ± 0.06
K55A/K56A/R59A	7647.73	7645.23 ± 0.06

assay beads (Amersham Pharmacia Biotech) were solubilized in phosphate-buffered saline to 50 mg/ml and diluted in the binding buffer to 10 mg/ml, and the final concentration in the assay was 0.25 mg/well. Membranes expressing CCR1 or CCR5 were stored at −80 °C and diluted in the binding buffer to 80 μg/ml. Equal volumes of membrane and bead stocks were mixed before performing the assay to reduce background. The final membrane concentration was 2 μg/ml and that of ^{125}I-RANTES was 0.1 nM. The plates were incubated at room temperature with agitation for 4 h. Radioactivity was measured, and data were analyzed as described above for the heparin binding assay.

Chemotaxis Assays—The proteins were analyzed for their ability to induce the directional migration of freshly isolated monocytes purified from buffy coats and RBL/CCR5 transfectants (23) using the modified micro-Boyden chamber as previously described (24). For monocyte chemotaxis, 3-μm pore size filters were used, and the chambers were incubated for 30 min at 37 °C, whereas for the RBL/CCR5 assays, filters with 12-μm pores were used, and the incubation time was 45 min.

HIV-1 Infection Enhancement Assay—The extent of virus entry was determined using a single-cycle infection assay as described previously (17, 25). One day before infection, HeLa-CD4 cells were seeded at a density of 1 × 10^4/well of a 96-well tissue culture plate. Cells were with chemokines during the infection period (simultaneous addition of virus and chemokine) or left untreated. Cells were infected with murine leukemia virus Env pseudotyped HIV-1 (*e.g.* HIV-1$_{MuLV}$) for 2 h at 37 °C in the presence or absence of chemokines, in a total infection volume of 100 μl. Unbound virus was removed after 2 h by washing, and fresh medium lacking chemokines was added back to the cells. 72 h post-infection, the cells were washed once with phosphate-buffered saline and lysed in 50 μl of reporter lysis buffer (Promega, Inc.). The luciferase activity in a mixture of 100 μl of luciferase substrate (Promega) and 30 μl of cell lysate was measured in relative light units using a DYNEX MLX microplate luminometer.

Inhibition of HIV Infectivity—HIV inhibition assays were performed as described (26). Briefly, 1 × 10^5 phytohaemaglutinin/IL-2-stimulated peripheral blood mononuclear cells were exposed to 50 μl of chemokine for 30 min at 37 °C. 1000 TCID50 of the CCR5-using HIV-1 strain, SI-2 (27), was then added in a volume of 50 μl. Following 3 h of incubation at 37 °C, the cells were washed three times and resuspended in RPMI 1640 (Life Technologies, Inc.), 20% fetal calf serum, and 10% IL-2 (Roche Molecular Biochemicals) containing the relevant chemokine. After 7 days culture at 37 °C, the samples were assayed for supernatant p24.

RESULTS

Purification and Characterization of the RANTES Mutants—The enzymic digestion using Endoproteinase Arg C of the MKKKWPR-RANTES mutant constructs yielded proteins that had the expected sequence as ascertained by mass spectroscopy (Table I). The proteins were all >90% pure as estimated by reverse-phase HPLC with the exception of the R47A mutant, which was 80% pure.

Heparin Disaccharide/RANTES Interaction as Measured by NMR—Preliminary studies (data not shown) have shown that RANTES interacts with various heparin disaccharides, namely I-S, I-A, II-S, and II-A. The binding of RANTES to the heparin disaccharides was investigated further by two-dimensional NMR. ^{15}N HSQC spectra of ^{15}N-labeled RANTES were recorded in the absence and in the presence of heparin disaccharides. Upon binding to RANTES, the disaccharide causes changes of the resonance positions in the ^{15}N HSQC of the protein. These changes were then mapped to the binding surface of the protein. Residues in the 40s as well as in the 20s exhibit significant changes in chemical shifts in the presence of the disaccharide I-A (Fig. 2).

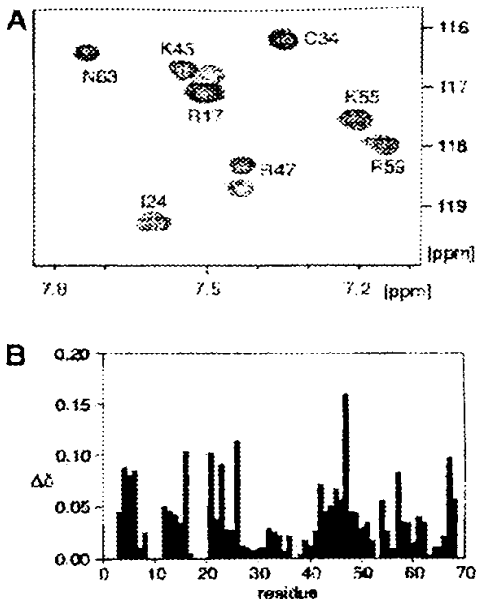

FIG. 2. **^{1}H-^{15}N HSQC NMR spectrum of ^{15}N-RANTES in the presence of heparin disaccharide I-A.** *A*, region of the ^{1}H-^{15}N HSQC spectrum of ^{15}N-labeled RANTES. *Solid line*, RANTES in the absence of disaccharide; *dotted line*, RANTES and heparin disaccharide I-A in a ratio of 0.6:1 (mol/mol). *B*, chemical shift differences of the ^{15}N HSQC of the protein between the free (no disaccharide) and bound (I-A) state.

Heparin Affinity and Mono S Chromatographies—RANTES elutes at 0.8 M NaCl on heparin affinity chromatography. Because the mutations carried out remove a basic residue presumed to play a role in heparin binding, a decrease of the concentration of NaCl required to elute all the mutants was observed for the mutations with the exception of K56A (Table II). Similarly, as can be predicted on the removal of basic residues, a decrease in NaCl concentration was required to elute the proteins from the Mono S column, again with two exceptions, K45A and K56A. The difference in NaCl concentration required for elution from the Mono S column and that required for the elution from the heparin column was determined for all mutants. Only the mutants in the 40s region showed a positive value, indicating that these residues may play a role in the specific interaction with heparin. (15)

Equilibrium Competition Assays—The integrity of the recombinant proteins was verified using receptor binding assays on two RANTES receptors, CCR1 and CCR5, using ^{125}I-MIP1α as the radiolabeled ligand in both cases. RANTES had an IC_{50} of 4.9 ± 2.5 nM (n = 4) for CCR1 and an IC_{50} of 2.15 ± 2.11 nM for CCR5 in these heterologous binding competition assays. All of the single mutations resulted in RANTES proteins that showed similar affinities to both receptors, with the largest deviation being 3-fold compared with the WT protein for K45A and R47A on CCR1 (results not shown). Both triple mutants showed very similar affinities compared with the WT protein for CCR5 (Fig. 3*B*). The ^{55}AAWVA^{59} RANTES mutant had an IC_{50} of 4.74 ± 2.98 nM (n = 3) for CCR5, and ^{44}AANA^{47} RANTES had an IC_{50} of 6.8 ± 2.8 nM (n = 4). However, the triple mutations had a more significant effect on the affinity for CCR1. The triple 50s mutant still retained high affinity for CCR1 with an IC_{50} of 17.6 ± 6.6 nM (n = 3), 3-fold less than that of RANTES (Fig. 3*A*). The greatest effect was demonstrated by

TABLE II
Molarity of NaCl required for elution from heparin and Mono S (cation exchange) columns

Mutant	Heparin	Mono S	Δ NaCl$^{Hep\,S}$	Δ NaCl$^{Mono\,S}$	$\Delta\Delta$ NaCl
Wild type	0.80	0.91			
R44A	0.61	0.82	0.19	0.09	0.10
K45A	0.65	0.97	0.15	0.04	0.11
R47A	0.65	0.84	0.15	0.07	0.08
R44A/K45A/R47A	0.47	0.70	0.33	0.21	0.11
K55A	0.70	0.86	0.10	0.05	−0.05
K56A	0.90	0.94	−0.10	0.07	−0.17
R59A	0.79	0.85	0.01	0.06	−0.05
K55A/K56A/R59A	0.70	0.75	0.10	0.16	−0.06

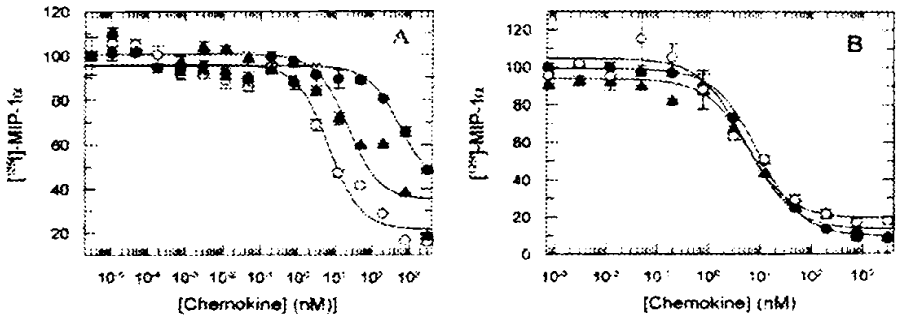

FIG. 3. **CCR1 and CCR5 equilibrium competition assays.** Competition binding assays were performed on membranes from CHO-K1 cell lines expressing CCR1 and CCR5 using 0.1 nM ^{125}I-MIP-1α as tracer and varying dilutions of WT RANTES (○), ^{44}AANA^{47} RANTES (●), and ^{56}AAWVA^{59} RANTES (◆). Results were analyzed by the Grafit software, using a single-site model. All points were run in triplicate. Data are representative of four independent experiments.

the triple 40s mutant. In all of the experiments performed, ^{44}AANA^{47} RANTES showed a 50–100-fold loss of affinity for CCR1, with a mean IC_{50} of 380 ± 147 nM (n = 5) (Fig. 3*A*).

In Vitro Chemotaxis Assays—The ability of the mutants to activate RANTES receptors was assessed by their ability to induce monocyte chemotaxis mediated through CCR1 and chemotaxis of RBL/CCR5 transfectants. Again, as observed in the receptor binding studies, the single mutations did not significantly alter the ability of the protein to induce monocyte chemotaxis (results not shown), and the triple 50s mutant had an EC_{50} value comparable with the WT protein, although a reduction in efficacy was observed (Fig. 4*A*). In accordance with its decreased affinity for CCR1, the triple 40s mutant had a significantly reduced ability to recruit monocytes, only showing full efficacy at 1 μM (Fig. 4*A*). The triple mutations were further analyzed, and both were able to recruit T cells (results not shown) as well as RBL/CCR5 transfectants with EC_{50} values comparable with the WT protein (Fig. 4*B*). The efficacy of the triple 40s mutant was reduced in both cases.

Heparin Binding Assay—Because the point mutations all exhibited activity comparable with the WT protein, only the triple mutations were further analyzed. Iodinated WT and the ^{55}AAWVA^{59} RANTES mutant bound to the heparin beads with maximum counts of 22,000 cpm in the absence of, or with low concentrations of competitor (Fig. 5). However, the maximum number of counts for iodinated ^{44}AANA^{47} RANTES was only 4,000. The three proteins were iodinated simultaneously by Amersham Pharmacia Biotech, and verification of their specific radioactivities confirmed that they were identical. The IC_{50} values obtained for the competition with heparin were 0.018 and 0.016 μg/ml, respectively, for WT RANTES and ^{55}AAWVA^{59} RANTES. The IC_{50} observed for the triple 40s RANTES mutant 0.022 μg/ml (Fig. 5, *inset*) was also very similar to the WT, indicating that the residual binding capacity of the triple 40s RANTES retained the same affinity for heparin.

We next compared the ability of four GAG families to compete for ^{125}I-RANTES and the triple 40s mutant. RANTES shows 3 orders of magnitude difference in its affinity for heparin (IC_{50}, 0.01 mg/ml), heparan sulfate (IC_{50}, 0.086 mg/ml), dermatan sulfate (IC_{50}, 0.75 mg/ml), and chondroitin sulfate (IC_{50} 2.7 mg/ml) (Fig. 6*A* and Ref. 22). This selectivity for the four GAG families is largely lost on mutation of the BBXB motif in the 40s loop (Fig. 6*B*). As discussed above, the affinity for heparin is not changed, but there is now only a 24-fold difference between the affinity for heparin (IC_{50}, 0.02 mg/ml) and chondroitin sulfate (IC_{50}, 0.48 mg/ml). The affinities for heparan sulfate (IC_{50}, 0.03 mg/ml) and dermatan sulfate (IC_{50}, 0.21 mg/ml) for the triple mutant are also slightly higher compared with WT RANTES. In summary, the triple 40s mutant loses the ability to discriminate between the four GAG families.

Inhibition of HIV-1 Infectivity—The triple 40s and 50s mutations were tested in their ability to inhibit the infection of peripheral blood mononuclear cells by the R5 strain, SL-2 in comparison with RANTES. As is shown in Fig. 7, the 50s cluster mutation retains full inhibitory properties, whereas the 40s cluster is still an efficient inhibitor in accordance with its receptor pharmacology but shows a reduction in potency compared with the parent RANTES protein.

Enhancement of HIV-1 Infectivity—The ability of the triple 40s mutant was compared with the WT protein and the non-aggregating mutant, E66S-RANTES, in its ability to enhance HIV-1 infection *in vitro* at micromolar concentrations. As shown in Fig. 8, abrogation of GAG binding in the triple 40s mutant has a similar effect to the removal of aggregation properties in the E66S-RANTES mutant (25, 28), and enhancement of HIV-1 infection, which is observed for both RANTES and N-terminal analogues such as AOP-RANTES (29), is no longer induced at concentrations superior to 1 μg/ml.

DISCUSSION

Chemokines are involved in the selective activation and recruitment of cells in inflammation and routine immunosurveillance. To direct the migration of cells, it has been suggested (2)

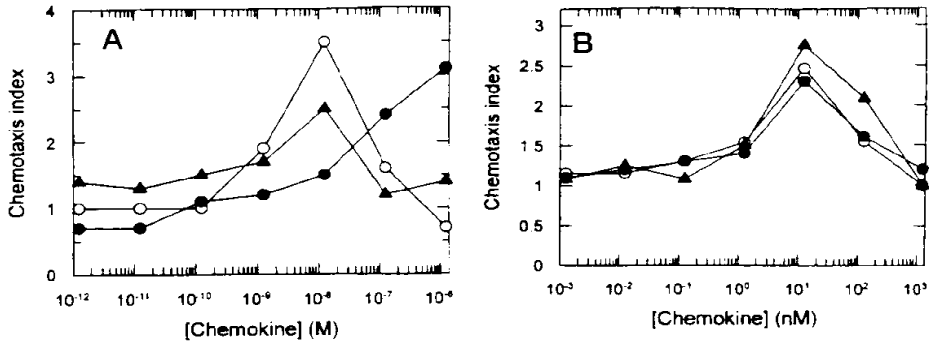

FIG. 4. **Chemotaxis induced by RANTES and the triple mutations in the 40s and 50s loops.** Chemotaxis assays were carried out using modified Boyden chambers as described in the text. *A*, monocytes; *B*, RBL/CCR5 transfectants. WT RANTES (○), ^{44}AANA^{47} RANTES (●), and ^{55}AAWVA^{59} RANTES (◆).

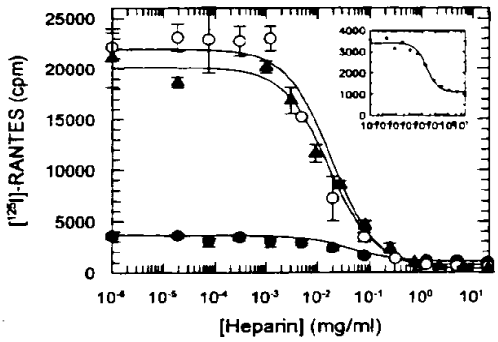

FIG. 5. **Competition binding assay of ^{125}I-RANTES and mutants to immobilized heparin.** The binding of 0.1 nM iodinated WT RANTES (○), ^{44}AANA^{47} RANTES (●), and ^{55}AAWVA^{59} RANTES (▲) to heparin-Sepharose beads in the presence of increasing concentrations of heparin was carried out as described in the text. Analysis was performed using a single-site model with Grafit software. Data points are in triplicate, and the data are representative of three separate experiments.

that cells migrate along gradients of attractant that are formed by the interaction of the chemokine with matrix components and proteoglycans. Because the expression of glycosaminoglycans is clearly regulated at the site of inflammation, this may be one of the ways that cellular recruitment is targeted. Although all chemokines interact with glycosaminoglycans and heparin, there is clearly selectivity in this interaction (9, 30). It appears that RANTES shows the greatest selectivity for the different GAG families, because its affinities for heparin and chondroitin sulfate differ by 3 orders of magnitude (9). This interaction could thus introduce a level of selectivity that is lacking from the receptor/ligand profiling observed by *in vitro* binding and activation assays that have resulted in the chemokine system being described as rather redundant.

It was thought for some time that the receptor-binding region of chemokines was located in the flexible N-terminal segment and in the 20s loop (32–34), whereas GAG binding was located in the C-terminal region of these proteins (15, 35). However, as the GAG-binding motifs for more chemokines are mapped, it appears that this is not a rigid rule. As shown in Fig. 1, GAG binding sites are found in the 20s loop in two CXC chemokines, IL-8 and SDF-1, although the sites are spatially situated on different sites of the monomer (Fig. 1, *a* and *d*). The 40s loop is found to be the site of GAG interaction for the CC chemokines MIP-1α and MIP-1β (Fig. 1, *b* and *e*), whereas the C-terminal helix is involved in IL-8 and MCP-1 GAG binding (Fig. 1, *a* and *c*). Thus, we decided to investigate two clusters of basic residues on RANTES because there was structural support in favor of both sites (Fig. 1*f*).

The affinities of chemokines binding to heparin have been measured by a variety of techniques. Binding to heparin-Sepharose columns is often used. The MIP-1α R18A, R46A, and R48A mutants no longer bound to this column (36), and the MIP-1β R46A mutant could no longer bind when the chromatography was carried out in the presence of NaCl at physiological concentration (37). However, IL-8 (15), SDF-1 (38), and the mutants of RANTES that we have generated were all able to bind to a heparin-Sepharose column but were eluted at a lower concentration of NaCl than the WT proteins. However, a comparison with cation exchange chromatographies indicated that only the mutants in the 40s region appeared to have specificity for heparin. The role of the 40s region was further supported by the shift of Lys^{45} and Arg^{47} observed on the binding of a disaccharide to ^{15}N-labeled RANTES, although the binding of the disaccharide appeared to cause more perturbation than that observed for IL-8 (15). The assay with iodinated ligands to immobilized heparin unambiguously identified that the 40s region has a major contribution to the capacity of RANTES to bind to this glycosaminoglycan moiety, whereas the cluster of basic residues in the 50s loop preceding the C-terminal helix plays no role in heparin binding.

It should be noted that the GAG binding sites are not restricted to the BBXB motif. The binding sites of three of the chemokines studied do in fact have this motif: SDF-1, with ^{24}KHLK^{27}, MIP-1α ^{45}KRSR^{48} and MIP-1β ^{45}KRSK^{48}. On the other hand, the principal residues in IL-8, Lys^{20}, Lys^{64}, and Arg^{68} (15), as well in MCP-1, Lys^{59} and Arg^{66} (16), are spatially separate.

It has been reported that cell surface GAG expression is not essential for the activity of chemokines *in vitro*, although they do serve a role in chemokine sequestration (39). Abrogation of the GAG binding sites either has no effect on receptor binding and activation in the case of IL-8, SDF-1, and MIP-1β or has a profound effect as has been reported for MIP-1α binding to CCR1 (40). We have seen both scenarios for RANTES; the mutation of the ^{44}RKNR^{47} has no significant effect on its binding to and activation of CCR5 but profoundly affects its interaction with CCR1. This observation is supported by the lack of effect of CCR5 activation by the mutation of R46A in MIP-1β (37), whereas mutations in the same region of MIP-1α profoundly affect CCR1 binding but have not been reported for CCR5. Inspection of the amino acid composition of the putative extracellular loops of these two receptors yields an indication why these differential effects are observed. CCR1 has 18 acidic Asp and Glu residues, only 10 which contribute basic charge (7 Lys and Arg and 6 His, which contributes 0.5 positive charge),

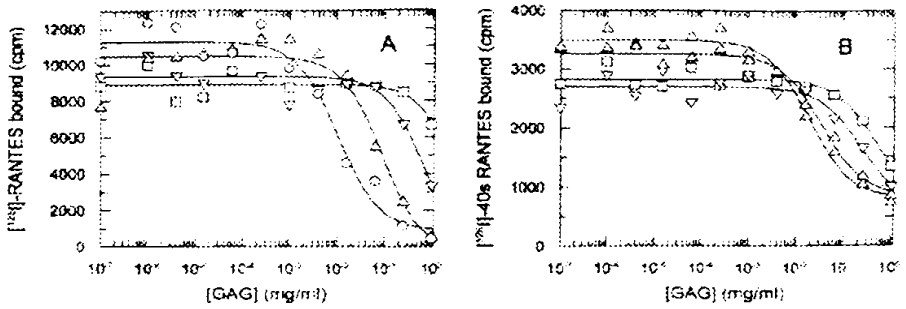

FIG. 6. **Competition of RANTES and the triple 40s mutant by different GAGs from immobilized heparin.** Iodinated WT RANTES (*A*) and iodinated ^{44}AANA^{47} RANTES (*B*) were incubated with heparin-Sepharose beads and increasing concentrations of heparin (○), heparan sulfate (△), dermatan sulfate (▽) and chondroitin sulfate (□) as described in the text. Analysis was performed as in Fig. 5, and the data are representative of two separate experiments.

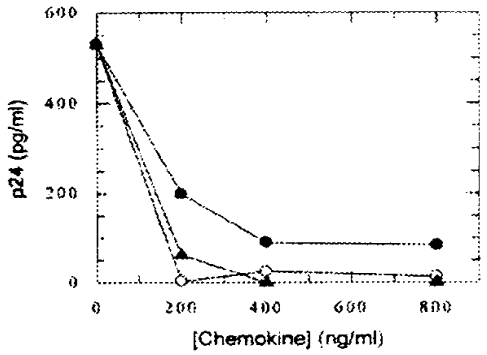

FIG. 7. **Inhibition of HIV-1 infection by RANTES and the mutants.** The HIV infection assay of peripheral blood mononuclear cells with the R5 HIV-1 strain, SL-2, was carried out as described in the text, and inhibition by WT RANTES (○), ^{44}AANA^{47} RANTES (●), and ^{56}AAWVA^{59} RANTES (◆) was measured. Supernatant p24 was measured after 7 days.

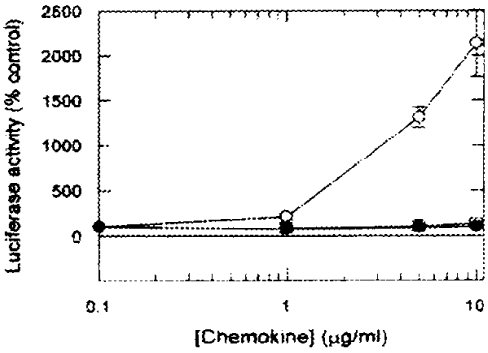

FIG. 8. **RANTES-induced enhanced HIV-1 infection is abrogated by mutation of the heparin binding site.** WT RANTES (○), ^{44}AANA^{47} RANTES (●), and E66S-RANTES (□) were incubated with HeLa-CD4 cells at the concentrations indicated for the 2-h infection period with HIV-1_{MuLV} as described in the text. The extent of viral infection was measured by determination of luciferase activity 3 days after infection.

whereas CCR5 has 7 acidic and 8 basic (7 Lys and Arg and 2 His) residues. Thus, it appears that the net electrostatic surface of CCR1 is likely to be negative, whereas in CCR5 it will be neutral. This indicates that perturbation of the electrostatic charge of CCR1 ligands may play a major role in the receptor interaction, but interaction of CCR5 and its ligands may involve interactions that are less electrostatic in nature. This argument is supported by mutagenesis studies where the important residue in the N-loop of RANTES was the charged residue Arg^{17} for CCR1 binding, whereas for CCR5 binding the hydrophobic residues in RANTES are Phe^{13} and Ile^{15} (34) and Phe^{13} in MIP-1β were critical (41). However, in these studies the role of the residues in the 40s loop in contributing to receptor binding was not investigated. The biological significance of the loss in affinity for CCR1 by the ^{44}AANA^{47} RANTES mutant is shown by its lack in ability to induce chemotaxis of freshly isolated monocytes, which express CCR1 as the predominant RANTES receptor (24).

It was surprising to note that the ^{125}I-labeled triple 40s mutant that bound to the heparin beads retained the same affinity for heparin as observed for the WT protein. This observation indicates that although this region is probably the preponderant GAG binding site, there must be other residues that also contribute. One hypothesis can be drawn from inspection of the three-dimensional structure, where His^{23} is shown to be spatially close and could therefore play a role in this binding pocket. We are currently investigating this possibility. We have previously shown that RANTES exhibits a significant degree of selectivity for different GAG families (9). Thus, the selectivity previously described for the four GAG families by RANTES appears to be mediated to a major extent by the BBXB motif on the 40s loop.

The importance of the RANTES/GAG interaction in HIV-1 infectivity has been highlighted by the observations that at high concentrations RANTES enhances viral infection (25, 29). These effects have been attributed to the property of RANTES to oligomerize on heparin (9, 25), which implies that the interaction with GAGs plays an important role. Effectively, RANTES mutants that are not able to oligomerize do not exhibit this enhancing effect (25). Here we show that the 80% reduction of the ability of the RANTES protein to bind to heparin similarly prevents the protein from inducing enhanced viral infectivity. However, the ability of RANTES to inhibit HIV-1 infectivity depends on its ability to bind to CCR5, thereby preventing the virus from interacting with its coreceptor. The triple 40s mutant retains fully functional CCR5 binding activity and is still able to inhibit HIV-1 infectivity of R5 HIV-1 strains.

This study has identified the principal heparin binding domain of RANTES but has revealed several questions that need to be addressed. First, determining which are the residues or regions that are responsible for the residual heparin binding activity; second, dissecting the individual residues in this pocket that play a predominant role in GAG binding and/or in CCR1 binding; and third, addressing the question of whether increased viral infection is principally due to the fact that it facilitates interaction with the coreceptor through oligomerization, or whether the interaction of RANTES with GAGs induces

cellular activation through a novel signal transduction mechanism. Lastly, we believe that such mutants will allow us to address the important question of the relevance of GAG binding to cellular recruitment *in vivo*, which has been hypothesized for many years without having been validated experimentally and further investigate the role of GAG binding in controlling inflammation.

Acknowlegment—We thank Christine Power for critical reading of the manuscript.

REFERENCES

1. Zlotnik, A., and Yoshie, O. (2000) *Immunity* **12,** 121–127
2. Rot, A. (1992) *Immunol. Today* **13,** 291–294
3. Springer, T. A. (1994) *Cell* **76,** 301–314
4. Roberts, C. R., Wight, T. N., and Hascall, V. C. (2000) *The Lung* (Crystal, R. G., West, J. B., Weibel, E., and Barnes, P. J., ed) Lippincott-Raven, Philadelphia
5. Jackson, D. G. (1997) *Biochem. Soc. Trans.* **25,** 229–234
6. Wasty, F., Alavi, M. Z., and Moore, S. (1993) *Diabetologia* **36,** 316–322
7. Marquezini, M. V., Strunz, C. M., Dallan, L. A., and Toledo, O. M. (1995) *Cardiology* **86,** 143–146
8. Wells, T. C., and Proudfoot, A. E. (1999) *Inflamm. Res.* **48,** 353–362
9. Kuschert, G. S., Coulin, F., Power, C. A., Proudfoot, A. E., Hubbard, R. E., Hoogewerf, A. J., and Wells, T. N. (1999) *Biochemistry* **38,** 12959–12968
10. Webb, L. M., Ehrengruber, M. U., Clark-Lewis, I., Baggiolini, M., and Rot, A. (1993) *Proc. Natl. Acad. Sci. U. S. A.* **90,** 7158–7162
11. Wagner, L., Yang, O. O., Garcia-Zepeda, E. A., Ge, Y., Kalams, S. A., Walker, B. D., Pasternack, M. S., and Luster, A. D. (1998) *Nature* **391,** 908–911
12. Cardin, A. D., and Weintraub, H. J. (1989) *Arteriosclerosis* **9,** 21–32
13. Hileman, R. E., Fromm, J. R., Weiler, J. M., and Linhardt, R. J. (1998) *Bioessays* **20,** 156–167
14. Mayo, K. H., Ilyina, E., Roongta, V., Dundas, M., Joseph, J., Lai, C. K., Maione, T., and Daly, T. J. (1995) *Biochem. J.* **312,** 357–365
15. Kuschert, G. S., Hoogewerf, A. J., Proudfoot, A. E. I., Chung, C. W., Cooke, R. M., Hubbard, R. E., Wells, T. N. C., and Sanderson, P. N. (1998) *Biochemistry* **37,** 11193–11201
16. Chakravarty, L., Rogers, L., Quach, T., Breckenridge, S., and Kolattukudy, P. E. (1998) *J. Biol. Chem.* **273,** 29641–29647
17. Conner, R. I., Sheridan, K. E., Ceradini, D., Choe, S., and Landau, N. R. (1997) *J. Exp. Med.* **185,** 621–628
18. Proudfoot, A. E. I., and Borlat, F. (2000) *Chemokine Protocols* (Proudfoot, A. E. I., Wells, T. N. C., and Power, C. A., eds) pp. 75–87, Humana Press, Totowa, NJ
19. Chung, C. W., Cooke, R. M., Proudfoot, A. E. I., and Wells, T. N. C. (1995) *Biochemistry* **34,** 9307–9314
20. Kay, L. E., Keifer, P., and Saarinen, T. (1992) *J. Am. Chem. Soc.* **114,** 10663–10665
21. Farmer, B. T., Constantine, K. L., Goldfarb, V., Friedrichs, M. S., Wittekind, M., Yanchunas, J., Jr., Robertson, J. G., and Mueller, L. (1996) *Nat. Struct. Biol.* **3,** 995–997
22. Kuschert, G. S., Hubbard, R. E., Power, C. A., Wells, T. N. C., and Hoogewerf, A. J. (1997) *Methods Enzymol.* **287,** 369–378
23. Oppermann, M., Mack, M., Proudfoot, A. E., and Olbrich, H. (1999) *J. Biol. Chem.* **274,** 8875–8885
24. Proudfoot, A. E., Buser, R., Borlat, F., Alouani, S., Soler, D., Offord, R. E., Schroder, J. M., Power, C. A., and Wells, T. N. (1999) *J. Biol. Chem.* **274,** 32478–32485
25. Trkola, A., Gordon, C., Matthews, J., Maxwell, E., Ketas, T., Czaplewski, L., Proudfoot, A. E., and Moore, J. P. (1999) *J. Virol.* **73,** 6370–6379
26. Reeves, J. D., and Simmons, G. (2000) in *Chemokine Protocols* (Proudfoot, A. E. I., Wells, T. N. C., and Power, C. A., eds) pp. 209–222, Humana Press, Totowa, NJ
27. Simmons, G., Wilkinson, D., Reeves, J. D., Dittmar, M. T., Beddows, S., Weber, J., Carnegie, G., Desselberger, U., Gray, P. W., Weiss, R. A., and Clapham, P. R. (1996) *J. Virol.* **70,** 8355–8360
28. Czaplewski, L. G., McKeating, J., Craven, C. J., Higgins, L. D., Appay, V., Brown, A., Dudgeon, T., Howard, L. A., Meyers, T., Owen, J., Palan, S. R., Tan, P., Wilson, G., Woods, N. R., Heyworth, C. M., Lord, B. I., Brotherton, D., Christison, R., Craig, S., Cribbes, S., Edwards, R. M., Evans, S. J., Gilbert, R., Morgan, P., and Hunter, M. G. (1999) *J. Biol. Chem.* **274,** 16077–16084
29. Gordon, C. J., Muesing, M. A., Proudfoot, A. E. I., Power, C. A., Moore, J. P., and Trkola, A. (1999) *J. Virol.* **73,** 684–694
30. Witt, D. P., and Lander, A. D. (1994) *Curr. Biol.* **4,** 394–400
31. Guex, N., and Peitsch, M. C. (1997) *Electrophoresis* **18,** 2714–2723
32. Hebert, C. A., Vitangcol, R. V., and Baker, J. B. (1991) *J. Biol. Chem.* **266,** 18989–18994
33. Clark-Lewis, I., Schumacher, C., Baggiolini, M., and Moser, B. (1991) *J. Biol. Chem.* **266,** 23128–23134
34. Paavianathan, D. R., Kuta, E. G., Artis, D. R., Skelton, N. J., and Hebert, C. A. (1997) *Biochemistry* **36,** 9642–9648
35. Stuckey, J. A., St. Charles, R., and Edwards, B. F. (1992) *Proteins* **14,** 277–287
36. Koopmann, W., and Krangel, M. S. (1997) *J. Biol. Chem.* **272,** 10103–10109
37. Koopmann, W., Ediriwickrema, C., and Krangel, M. S. (1999) *J. Immunol.* **163,** 2120–2127
38. Amara, A., Lorthioir, O., Valenzuela, A., Magerus, A., Thelen, M., Montes, M., Virelizier, J. L., Delepierre, M., Baleux, F., Lortat-Jacob, H., and Arenzana-Seisdedos, F. (1999) *J. Biol. Chem.* **274,** 23916–23925
39. Ali, S., Palmer, A. C. V., Banerjee, B., Fritchley, S. J., and Kirby, J. A. (2000) *J. Biol. Chem.* **275,** 11721–11727
40. Graham, G. J., Wilkinson, P. C., Nibbs, R. J., Lowe, S., Kolset, S. O., Parker, A., Freshney, M. G., Tsang, M. L., and Pragnell, I. B. (1996) *EMBO J.* **15,** 6506–6515
41. Laurence, J. S., Blanpain, C., Burgner, J. W., Parmentier, M., and Liwang, P. J. (2000) *Biochemistry* **39,** 3401–3409
42. Coulin, F., Power, C. A., Alouani, S., Peitsch, M. C., Schroeder, J. M., Moshizuki, M., Clark, I. I., and Wells, T. N. C. (1997) *Eur. J. Biochem.* **248,** 507–515
43. Mack, M., Luckow, B., Nelson, P. J., Cihak, J., Simmons, G., Clapham, P. R., Signoret, N., Marsh, M., Stangassinger, M., Borlat, F., Wells, T. N. C., Schlondorff, D., and Proudfoot, A. E. I. (1998) *J. Exp. Med.* **187,** 1215–1224

THE JOURNAL OF BIOLOGICAL CHEMISTRY
Vol. 269, No. 22, Issue of June 3, pp. 15918–15924, 1994
Printed in U.S.A.

Structure/Activity Analysis of Human Monocyte Chemoattractant Protein-1 (MCP-1) by Mutagenesis

IDENTIFICATION OF A MUTATED PROTEIN THAT INHIBITS MCP-1-MEDIATED MONOCYTE CHEMOTAXIS*

(Received for publication, October 27, 1993, and in revised form, March 1, 1994)

Yu Jun Zhang, Barbara J. Rutledge, and Barrett J. Rollins‡

From the Department of Medicine, Dana-Farber Cancer Institute, Harvard Medical School, Boston, Massachusetts 02115

Monocyte chemoattractant protein-1 (MCP-1) is a monocyte-specific chemoattractant and activator and is a member of the chemokine-β family of cytokines. To identify regions of MCP-1 which are required for its biological activity, we constructed human MCP-1 mutants that were expressed in eukaryotic cells and tested for their ability to attract monocytes *in vitro*. Deletion of amino acids 2–8 destroyed activity, suggesting that the amino-terminal region is necessary for activity. Within the deleted region, mutation of aspartate 3 to alanine produced a protein with 9% of wild-type activity, whereas mutation of asparagine 6 to alanine produced a protein with 52.9% of wild-type activity. Mutation of amino acids within the first intercysteine loop yielded variable results. Changing tyrosine 28 to aspartate or arginine 30 to leucine each produced proteins with essentially no monocyte chemoattractant activity. The side chains of these amino acids are predicted to point into a putative receptor binding cleft, and these loss-of-function mutations are consistent with this model. Also consistent is the retention of 60% of wild-type activity after mutation of serine 27 to glutamine, since the side chain of serine 27 is predicted to point away from the binding cleft. However, mutation of arginine 24, which lies outside of this area, to phenylalanine produced a protein with only 5% of wild-type activity, suggesting more complex interactions. Truncations of the carboxyl terminus, as well as mutation of aspartate 68 to leucine, generated proteins with 10–20% of wild-type activity. (Another carboxyl-terminal insertional mutation demonstrated that *O*-linked carbohydrate in MCP-1α may be added to a threonine in the carboxyl-terminal region.) These findings are consistent with a structural model of dimeric MCP-1 which is similar to interleukin-8, in which amino acids that point into a cleft between the two carboxyl-terminal α-helices of the subunits are important for receptor binding. In addition, however, amino acids at the amino terminus and others outside of the interhelical cleft are also essential for activity. The carboxyl-terminal α-helix is not required for signaling *per se* but is required for maximal specific activity. Finally, four mutant proteins partially inhibited the ability of wild-type MCP-1 to attract monocytes *in vitro*. In particular, mutant 7ND (deletion of amino acids 2–8) inhibited MCP-1 activity by 50% at a molar ratio of 75:1, displaced MCP-1 from its receptor on monocytes at a similar ratio, and bound to a single class of receptors on human monocytes with a K_d of 2.6 nM. However, 7ND bound only to 10% of the number of receptors to which MCP-1 bound, suggesting that part of its inhibitory activity may be due to binding to MCP-1 itself.

Chemokines are proinflammatory cytokines that attract and activate specific types of leukocytes (for review see Refs. 1 and 2). Members of this protein family share common structural motifs, in particular the positions of 4 cysteines, as well as other highly conserved regions of primary structure. Despite their structural similarities, most chemokines have nonoverlapping target cell specificities. Chemokines can be grouped into two subfamilies based on structural and genetic criteria. In the chemokine-α proteins, a single amino acid is interposed between the 2 cysteines nearest the amino terminus (for this reason they are also known as C-*X*-C proteins), and their genes cluster on the long arm of chromosome 4. In the chemokine-β proteins, the 2 cysteines nearest the amino terminus are adjacent to each other (thus C-C proteins), and their genes cluster on the long arm of chromosome 17. In terms of secondary or tertiary structure, it is unlikely that the intervening amino acid in the chemokine-α proteins has much significance (3).

For the most part, chemokine-α family members attract and activate neutrophils, although other target cells have been identified. A great deal of structural data has been generated for two chemokine-α proteins, namely platelet factor 4 and IL-8,[1] the latter of which is a neutrophil-specific chemoattractant. Crystal and solution structures for IL-8 have been solved, and both suggest that IL-8 is a homodimer in which the carboxyl-terminal α-helices of each subunit overlie two three-stranded anti-parallel β-sheets (4–6). This provides a cleft between the two α-helices which is predicted, by analogy to other structures, to be an IL-8 receptor binding region. However, mutational analysis has demonstrated an absolute requirement for the amino terminus of IL-8, in particular amino acids 4–6 (glutamate-leucine-arginine (ELR)), for neutrophil chemotaxis and activation (7, 8).

In contrast to the chemokine-α proteins, chemokine-β proteins tend to attract and activate monocytes. In particular, monocyte chemoattractant protein-1 (MCP-1) attracts monocytes *in vitro* at subnanomolar concentrations (9, 10). MCP-1 expression has been detected in a variety of pathologic conditions that involve monocyte accumulation and activation, including atherosclerosis. Much less is known about the structure of MCP-1 than the structures of IL-8 or platelet factor 4. For example, there is no direct evidence that MCP-1 is active as a dimer. By analogy to IL-8, however, proper disulfide bridging

* This work was supported in part by United States Public Health Service Grant CA53091 and by a grant from the Sandoz/DFCI Drug Development Program. The costs of publication of this article were defrayed in part by the payment of page charges. This article must therefore be hereby marked "*advertisement*" in accordance with 18 U.S.C. Section 1734 solely to indicate this fact.

‡ Recipient of a Junior Faculty Research Award from the American Cancer Society. To whom correspondence should be addressed: D930, Dana-Farber Cancer Institute, 44 Binney St., Boston, MA 02115.

[1] The abbreviations used are: IL-8, interleukin 8; MCP-1, monocyte chemoattractant protein-1.

is probably necessary for activity (11). Because of their similar primary structures, MCP-1 is predicted to have a higher order structure like that of IL-8 (3). In fact, it has been shown that mutation of 2 amino acids in the putative receptor binding domain between the two α-helices of the presumed MCP-1 dimer destroys its ability to attract monocytes (12).

Because regions outside the interhelical cleft of IL-8 are clearly necessary for activity, we hypothesized that a similar situation would apply to MCP-1. We have constructed a series of mutants involving the amino terminus, the first intercysteine loop, and the carboxyl-terminal α-helix of MCP-1 and tested them for their ability to attract monocytes *in vitro*. We have also examined these mutants for their ability to block the activity of wild-type MCP-1. Our results point to the amino terminus and specific areas of the first intercysteine loop as being necessary for monocyte chemoattraction and to the carboxyl-terminal α-helix as a region required for maximal potency.

MATERIALS AND METHODS

Construction of Epitope-tagged MCP-1 and MCP-1 Mutations—Starting with pGEM-hJE34 (human MCP-1 cDNA in pGEM-7 (Promega, Madison, WI)) (13) as template, recombinant polymerase chain reaction was used to insert 30 nucleotides immediately 5′ to the termination codon (position 366) encoding the amino acid sequence GGDYKDDDDK. The last 8 amino acids of this insert represent the so-called FLAG epitope (14), and the first 2 glycines were included to provide a "spacer" between MCP-1 sequences and the epitope. Sequence analysis of the resulting cDNA revealed no other base alterations, and the entire cDNA was cloned into the expression vector pmt21 (a derivative of p91023(B) (15)) to yield a plasmid designated pFX2. Similar techniques were used to insert the FLAG epitope and spacer immediately 3′ to the codon for aspartate 3 in processed MCP-1 (nucleotide position 146); this expression plasmid was designated pFX3. (The amino terminus of proteolytically processed MCP-1 is glutamine and is designated as position 1 in this study.) With pFX2 as template, recombinant polymerase chain reaction was used to insert termination codons or single amino acid changes as listed in Fig. 4. All mutations were confirmed by sequence analysis of both DNA strands. (Sequences for oligonucleotides used in generating FLAG epitope-tagged MCP-1 or its mutations are available on request.) Wild-type MCP-1 was purchased from Genzyme Corp. (Cambridge, MA).

Expression of MCP-1 and Its Derivatives—COS cells were suspended in serum-free Dulbecco's modified Eagle's medium at 5×10^6 cells/ml. Four $\times 10^6$ cells (0.8 ml) were placed in a cooled electroporation cuvette with a 0.4-cm gap, 10 μg of plasmid DNA was added, and the cells were electroporated at 0.36 kV, 960 microfarads (yielding a time constant of 16–17 ms). Cells were allowed to recover in the cuvette at room temperature for 10 min and were then plated in a 100-mm dish in Dulbecco's modified Eagle's medium with 10% bovine calf serum. After 24 h, the medium was changed to serum-free Dulbecco's modified Eagle's medium. After an additional 48 h, conditioned medium was collected, cells and debris were removed by centrifugation, and the medium was stored at −20 °C.

Immunoblotting—Conditioned medium from transfected COS cells was concentrated ~ 50-fold using a Centricon-10 device (Amicon, Danvers, MA), boiled in sample buffer, and subjected to electrophoresis through a 12% polyacrylamide gel in SDS. Proteins were electrophoretically transferred to nitrocellulose and probed either with an anti-FLAG M2 monoclonal antibody (International Biotechnologies, Inc., New Haven, CT) or with rabbit anti-MCP-1 antiserum (13). Blots were developed using the appropriate horseradish peroxidase-conjugated secondary antibody and substrate solution (Vector Laboratories, Burlingame, CA).

Quantitation of MCP-1 and Its Derivatives—MCP-1 was expressed as a FLAG fusion protein in *Escherichia coli* using the FLAG biosystem and purified using anti-FLAG M2 affinity gel (International Biotechnologies, Inc.). Known amounts of pure FLAG-MCP-1 fusion protein were included in every immunoblot for MCP-1 produced by COS cells. Immunoblots were then analyzed by laser densitometry (Pharmacia Biotech Inc.), and the mass of each COS cell-produced protein was determined by reference to the FLAG-MCP-1 fusion standard. The amount of COS cell supernatant loaded in each well generated an immunoblot signal within the linear response range of the laser densitometer. When possible, samples were quantitated using both anti-FLAG and anti-MCP-1 antibodies. There were no disparities between the amounts of protein determined with the two antibodies except when one of the epitopes was absent (see "Results").

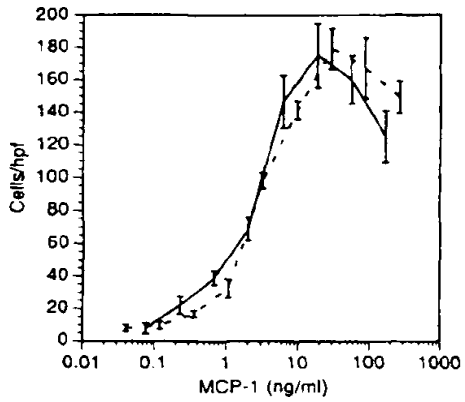

FIG. 1. Wild-type MCP-1 and carboxyl-terminal epitope tagged MCP-1 (FX2) were produced by transient transfection of COS cells and quantitated by Western blotting as described under "Materials and Methods." Varying amounts of both proteins were used in monocyte chemotaxis assays, and the number of monocytes per high powered field (*hpf*) which migrated in response to each protein was counted. *Solid line*, wild-type MCP-1; *dotted line*, FX2.

Monocyte Chemotaxis—Human peripheral blood mononuclear cells were prepared from volunteers as described (16). Chemotaxis assays were performed using a multiwell chamber fitted with a polycarbonate filter having 5-μm pores, as described. Each COS cell supernatant was tested over a wide range of dilutions, and the concentration of monocyte chemoattractant activity in each supernatant was defined as the inverse of the dilution producing half-maximal chemotactic response (17).

Purification of 7ND—Mutant 7ND was expressed in stably transfected Chinese hamster ovary cells as described (18, 19). Conditioned medium was loaded onto an anti-FLAG M2 affinity gel (International Biotechnologies, Inc.), the column was washed with phosphate-buffered saline, and protein was eluted using 0.1 M glycine hydrochloride (pH 3.0) followed by neutralization using Tris base. Protein was quantified by Bradford assay (30) and its purity assessed by SDS-polyacrylamide gel electrophoresis followed by staining with Coomassie Blue.

Radioiodination of 7ND—Pure 7ND was radioiodinated using Bolton-Hunter reagent (DuPont NEN) and separated from unincorporated reagent by gel filtration chromatography. Analysis by SDS-polyacrylamide gel electrophoresis showed a single radioactive species of appropriate M_r. Specific activity was in the range of 120–204 μCi/μg.

Receptor Binding—Human monocytes were purified from Leukopaks obtained from the Blood Component Laboratory at the Dana-Farber Cancer Institute. Peripheral blood mononuclear cells were isolated by Ficoll-Hypaque density centrifugation, and monocytes were purified by centrifugal counterflow elutriation as described (20). Binding experiments using radioiodinated 7ND or MCP-1 (DuPont NEN) were performed as described (20).

RESULTS

Epitope-tagged MCP-1—Using polymerase chain reaction, we modified wild-type MCP-1 cDNA so that it encoded a protein with a FLAG epitope tag. In the tagged protein, the amino acid sequence GGDYKDDDDK appears after the carboxyl-terminal threonine of processed MCP-1. This protein, designated FX2, was expressed by transient transfection in COS cells and quantitated by densitometric analysis of an immunoblot using an anti-FLAG antibody and a standard amount of FX2 purified from a bacterial expression system. Serial dilutions of conditioned medium from COS cells transfected with FX2 were used in a monocyte chemotaxis assay as shown in Fig. 1. At the same time, wild-type MCP-1 was also produced by COS cell transfection (16) and quantitated by densitometric analysis of a Western blot using an anti-MCP-1 antiserum and a standard amount of FX2. This material was also tested in a monocyte

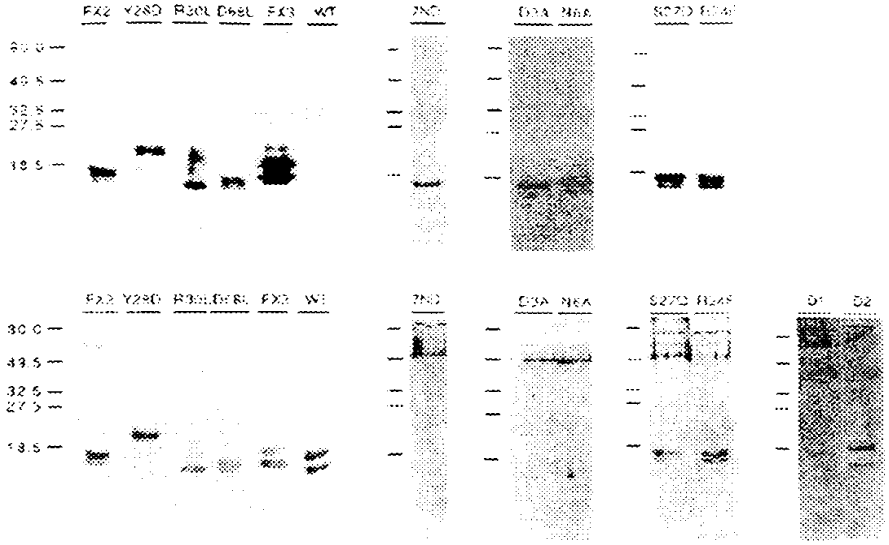

FIG. 2. Wild-type (WT) and mutant MCP-1 proteins were produced by transient transfection of COS cells. Conditioned medium from transfections was boiled in reducing SDS-containing sample buffer and fractionated by electrophoresis through SDS-containing 15% polyacrylamide gels. Proteins were blotted onto nitrocellulose, and immunoblots were developed using either an anti-FLAG monoclonal antibody (*upper panel*) or a rabbit anti-MCP-1 antiserum (*lower panel*). Protein designations correspond to those listed in Fig. 1. Molecular size markers are indicated for each separately processed gel.

chemotaxis assay. Fig. 1 shows that both proteins had similar dose-response characteristics. Using the quantitation results from immunoblotting, analysis of the dose-response curves showed that the specific activity of FX2 is 408,000 units/ml, and that of wild-type MCP-1 is 442,000 units/ml. Both values compare favorably with the specific activity determined for purified, eukaryotically produced, recombinant MCP-1, suggesting that the epitope tag in this position does not interfere with MCP-1's ability to attract monocytes *in vitro* (16, 21).

Construction and Expression of MCP-1 Mutants—FX2 was used as a template for the introduction of a variety of mutations. To quantify each mutant protein, conditioned medium from transfected COS cells was analyzed by immunoblotting. Representative examples are shown in Fig. 2. Although most mutants were produced in high quantity, the carboxyl-terminal deletion mutations, D1 (consisting of amino acids 1–62 of processed MCP-1) and D2 (amino acids 1–68), were either unstable or inefficiently produced. Sufficient D1 and D2 could be produced for analysis, but detection by immunoblot using anti-MCP-1 required concentrating the conditioned medium. Since their carboxyl termini were deleted, the anti-FLAG antibody could not be used.

It is possible that the apparently low levels of D1 and D2, as determined by immunoblotting, might be due to loss of antigenic determinants in the carboxyl-terminal domain which are normally detected by the anti-MCP-1 antiserum. To rule this out, we engineered a FLAG epitope tag near the amino terminus of both deletion mutants as well as wild-type MCP-1 (the amino-terminal FLAG-tagged full-length protein is denoted FX3). Immunoblotting detected large amounts of FX3, suggesting that insertion of the FLAG epitope in this position did not effect secretion or stability. However, even with the anti-FLAG antibody, only low levels of carboxyl-terminal deletion proteins carrying the amino-terminal tag could be detected. Thus both D1 and D2 are either unstable or inefficiently secreted. By performing several transfections and pooling media, enough D1 and D2 were produced for further analysis.

Electrophoretic Analysis of MCP-1 Mutants—The electrophoretic mobility of MCP-1 mutations in SDS-containing polyacrylamide gels was not predictable. The largest alterations in mobility were associated with the least conservative amino acid substitutions, *e.g.* Y28D. A number of mutations showed more than one band, which is most likely due to post-translational modification by COS cells. For example, wild-type MCP-1 is often secreted by eukaryotic cells in α and β forms which differ because of the presence of O-linked carbohydrate in the α form (22). Glycosylation is not necessary for its *in vitro* chemoattractant activity (16). In the course of other experiments, we inserted a 5-amino acid substrate for cAMP-dependent protein kinase between lysine 75 and threonine 76, the 2 amino acids at the carboxyl terminus of wild-type MCP-1. Expression of this mutation in COS cells (Fig. 3) shows that the carbohydrate-containing α form is not detected. This suggests that the inserted sequences have altered the substrate recognition site for a glycosyl transferase and that the O-linked carbohydrate may be added to a threonine in this region, *i.e.* threonine 76, or perhaps threonine 75. However, then one would then expect that the carboxyl-terminal deletion mutants, D1 and D2, should show only a single band, and although this is true for preparations of D1, preparations of D2 show a second, lower molecular weight band. D2 still has a serine (serine 63) near its carboxyl terminus, whereas D1 does not. Whether D2's second species is due to utilization of this potential glycosylation site or to proteolytic degradation is currently unknown.

It is possible that lower molecular weight bands of some of the other, non-carboxyl-terminal truncation transfectants shown in Fig. 2 might be due to proteolytic degradation. This is unlikely for two reasons. First, the anti-FLAG antibody detected its epitope in all proteins in which it was expressed. Since the epitope was placed at the carboxyl terminus, carboxypeptidase activity would have been revealed as loss of the FLAG epitope in one of the bands still recognized by anti-MCP-1. This was not observed. Second, the rabbit anti-MCP-1 serum detected all forms of MCP-1 except for the amino-terminal deletion and amino-terminal point mutations (Fig. 2). Thus the predominant epitopes detected by this serum are at the amino terminus of MCP-1, and aminopeptidase activity would have been revealed as loss of anti-MCP-1 reactivity in one of the bands still recognized by anti-FLAG. This was only observed for the amino-terminal deletion and point mutants.

Activity of MCP-1 Mutations—Based on modeling considerations as well as structure/activity data from other chemokines (in particular IL-8), we constructed MCP-1 mutations in three regions: the amino terminus, the first intercysteine loop, and the carboxyl-terminal predicted α-helix (Figs. 4 and 7). At the amino terminus, insertion of the FLAG epitope after aspartate

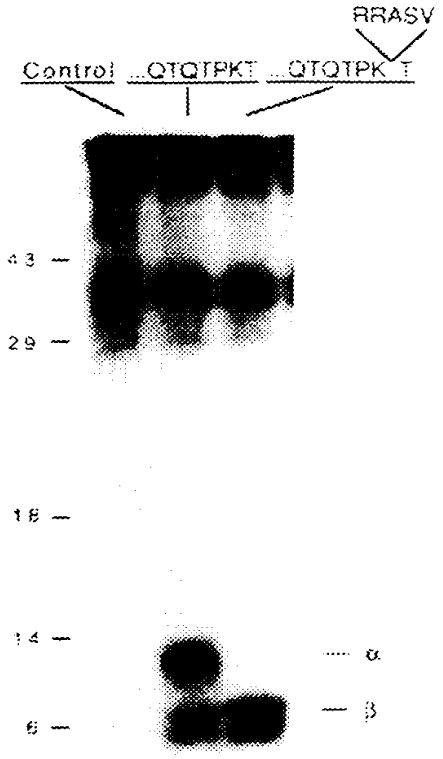

FIG. 5. Using recombinant polymerase chain reaction, nucleotide sequences encoding the amino acid sequence RRASV were introduced near the end of the MCP-1 cDNA coding region as indicated. After transient transfection of indicated expression vectors into COS cells, cells were radiolabeled with [^{35}S]methionine, and conditioned medium was subjected to immune precipitation using anti-MCP-1 antiserum. Immune precipitates were electrophoresed through a 15% polyacrylamide gel. *From left to right: first lane*, vector alone; *second lane*, wild-type MCP-1; *third lane*, MCP-1 with RRASV insert.

3 in wild-type MCP-1 destroyed the protein's monocyte chemoattractant activity (FX3). Consistent with that finding was the fact that deletion of amino acids 2–8 also yielded an inactive protein. In an attempt to accomplish finer mapping, we changed the 2 charged amino acids in this region (aspartate 3 and asparagine 6) to alanine. Changing aspartate 3 significantly reduced the activity of the protein, whereas changing asparagine 6 yielded a protein that retained 52.9% of wild-type MCP-1's activity.

Next, we constructed four point mutations in the first intercysteine loop. Mutations of arginine 24 to phenylalanine (R24F), tyrosine 28 to aspartate (Y28D), and arginine 30 to leucine (R30L) all produced proteins with activities that were only a fraction of wild-type. However, mutation of another polar amino acid in the same region, namely serine 27 to glutamine (S27Q), produced a protein with 60% of wild-type activity.

Finally, manipulations of the carboxyl-terminal α-helix produced proteins that were still able to signal but had reduced potency compared with wild-type. Deletions of half (D2) or all (D1) of the α-helix yielded proteins with 17 and 11.3% of wild-type activity, respectively. In the predicted model structure of dimeric MCP-1, aspartate 68 projects into the cleft between the two α-helices (3). Mutation of this amino acid to leucine (D68L) had the same effect as deletion of the entire helix.

Competition for Biological Effects—We next tested mutations for their ability to inhibit monocyte chemotaxis *in vitro* in response to nonmutated MCP-1. To a fixed concentration of FX2, we added increasing amounts of medium conditioned by COS cells expressing mutant proteins. We found that Y28D, R24F, 7ND, and D3A demonstrated an ability to inhibit wild-type MCP-1 to varying degrees (data not shown). 7ND appeared to be most potent and was examined in greater detail. Fig. 5 shows that pure 7ND inhibited MCP-1's ability to attract monocytes with an ID_{50} at a molar ratio of 75:1 or a concentration of 35 nM in the presence of 5 ng/ml MCP-1. This inhibition is specific for MCP-1, since 7ND did not inhibit monocyte chemotaxis in response to 10^{-7} M formyl-methionyl-leucyl-phenylalanine (data not shown).

To test 7ND's ability to bind to monocytes, we performed receptor binding assays on human monocytes using ^{125}I-7ND. In self-displacement assays (Fig. 6*A*), 7ND recognized a single class of receptor on human monocytes with a K_d of 2.6 ± 0.23 nM, which is approximately 3-fold lower than the affinity of wild-type MCP-1 for its receptor in similar experiments (Fig. 6*B*), *i.e.* 0.94 ± 0.36 nM. That this receptor is probably the MCP-1 receptor was demonstrated by displacement experiments in which excess unlabeled 7ND was able to displace ^{125}I-MCP-1 from monocytes (Fig. 6*B*). Similarly, excess unlabeled MCP-1 efficiently displaced ^{125}I-7ND (Fig. 6*A*). The derived K_d for ^{125}I-7ND was the same whether cold 7ND or MCP-1 was used for displacement. However, the K_d for ^{125}I-MCP-1 approached that of ^{125}I-7ND when cold 7ND was used for displacement. Interestingly, experiments using ^{125}I-MCP-1 identified 8,145 ± 1430 binding sites/cell (average of five experiments), whereas those using ^{125}I-7ND identified only 840 ± 563 sites/cell (average of six experiments).

Based on the observation of 7ND's ability to inhibit FX2 activity, we tested a peptide comprising the first 10 amino acids of processed MCP-1. This peptide neither had intrinsic monocyte chemoattractant activity, nor did it inhibit the activity of wild-type MCP-1.

DISCUSSION

In the absence of structural data for MCP-1, there is no complete context in which to interpret our results. The arguments that follow rely heavily on the structural modeling work of Gronenborn and Clore (3) and on biochemical and gel filtration results that predict the existence of MCP-1 dimers[2] (23). If the modeling is correct, MCP-1 should have the structure schematized in Fig. 7, in which we have indicated amino acids that were mutated in this study. Of course, this structure requires confirmation by crystal analysis or NMR-derived solution structure.

Our mutations focused on three regions of MCP-1. First, amino acids in the amino-terminal region appear to be absolutely required for MCP-1's monocyte chemoattractant activity. Both 7ND (amino-terminal deletion mutant) and FX3 (amino-terminal insertion mutant) had almost no activity compared with wild-type MCP-1. Furthermore, at least 1 charged amino acid in this region, aspartate 3, is necessary for activity, whereas the only other charged amino acid in this region, asparagine 6, is not. These results are reminiscent of work implicating the amino-terminal region of IL-8, in particular amino acids 4–6 (ELR), in neutrophil activation and receptor binding (7, 8). Although the importance of ELR might have been inferred by its conservation among the neutrophil-active chemokine-α proteins, there is no similar conservation of aspartate 3 or its neighboring amino acids among the monocyte-active chemokine-β proteins. Thus it remains to be determined whether this portion of MCP-1 contains a monocyte chemoattractant motif that would impart similar activity to another protein, as

[2] Y. J. Zhang and B. J. Rollins, manuscript in preparation.

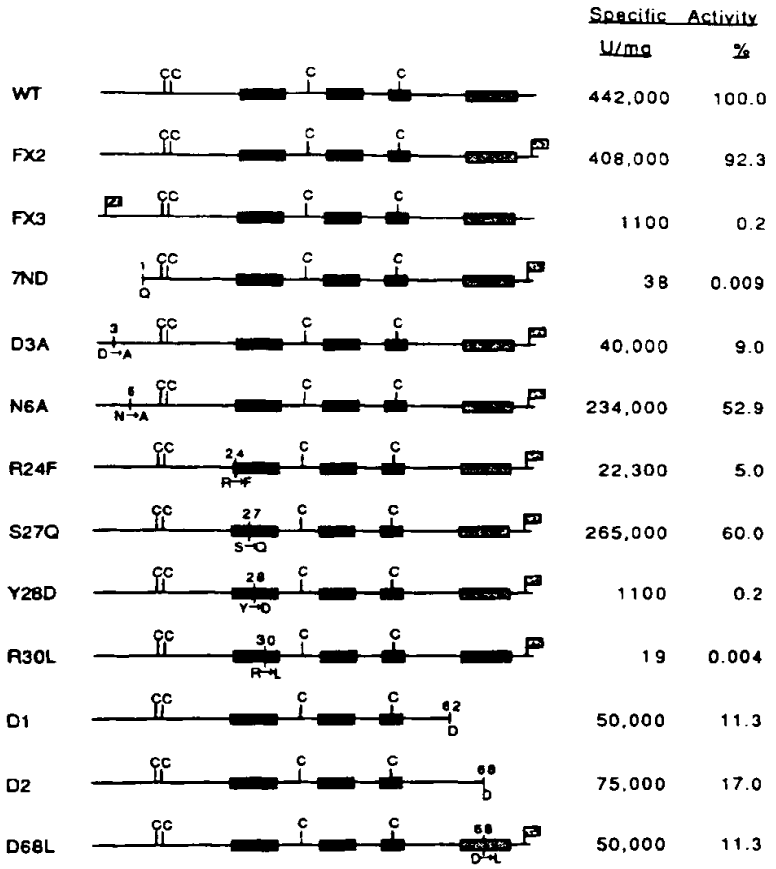

FIG. 4. **Schematic representation of MCP-1 mutations.** *WT* is wild-type, and other designations are described under "Results." Each mutation was expressed by transient transfection of COS cells. The concentration of monocyte chemoattractant activity in the conditioned medium of transfected COS cells was determined by *in vitro* monocyte chemotaxis assay as described under "Materials and Methods." The concentration of MCP-1 or mutated MCP-1 protein in conditioned medium was determined by densitometric analysis of immunoblots. Conditioned medium of COS cells transfected with a control vector contained 15 units/ml (of monocyte chemoattractant activity), whereas conditioned medium of COS cells transfected with vectors encoding FX2 or wild-type MCP-1 contained 400–600 units/ml.

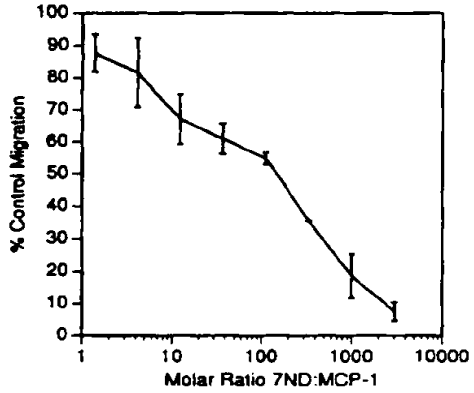

FIG. 5. 7ND was purified as described under "Materials and Methods," and increasing amounts were mixed with 5 ng/ml wild-type MCP-1. Mixtures were then tested in monocyte chemotaxis assays. *Error bars* represent the standard error for two separate wells in a single experiment, and this experiment is representative of two others.

the addition of ELR imparts neutrophil chemoattractant properties to platelet factor 4 (24).

Second, alteration of 2 amino acids in the first intercysteine loop, tyrosine 28 and arginine 30, almost completely destroyed monocyte chemoattractant activity. These results are similar, but not identical, to those of Beall *et al.* who demonstrated that a double tyrosine 28/arginine 30 mutation lost monocyte chemoattractant activity (12). In contrast to their results, our single Arg-30 → Leu (R30L) mutation had no activity, whereas their single Arg-30 → Val mutation retained activity. The disparity may be due to the different substitutions. Regardless of this difference, according to the predicted structural model of MCP-1, the side chains of tyrosine 28 and arginine 30 should point into the interhelical cleft, and loss of monocyte chemoattractant activity in Y28D and R30L is consistent with this region's putative role in receptor binding. Also consistent is the persistently high activity of S27Q, since the side chain of serine 27 is predicted to point away from the cleft (3). Valente *et al.* (25) also indicated the importance of this region in receptor binding by demonstrating that a peptide composed of amino acids 13–35 had chemoattractant activity and competed with MCP-1 for receptor binding. However, these activities required nearly millimolar concentrations of peptide.

Receptor interactions in this region are probably more complicated than this model suggests since mutation of arginine 24, which lies completely outside the interhelical cleft, to phenylalanine drastically reduced monocyte chemoattractant activity. IL-8's corresponding amino acid in this position is also

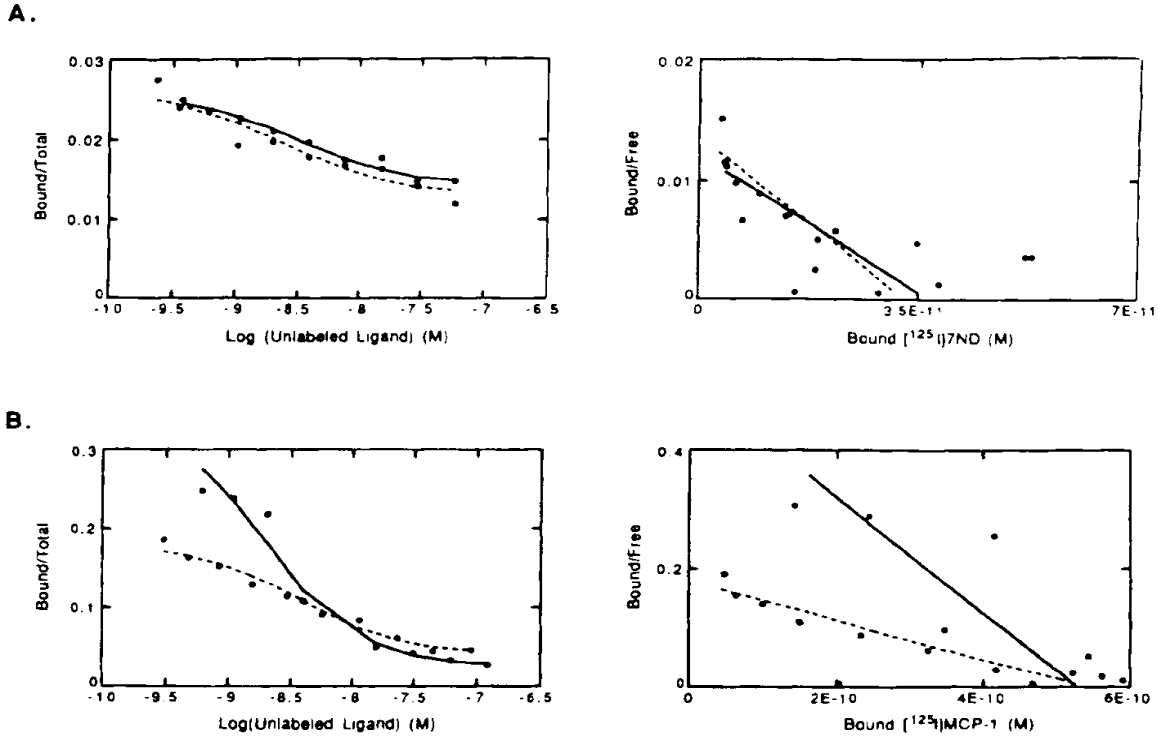

FIG. 6. *Panel A*, ^{125}I-7ND (0.12 nM) was added to 10^7 elutriated monocytes in the presence of increasing amounts of unlabeled MCP-1 (*closed circles, solid lines*) or 7ND (*open circles, dotted lines*). Binding was determined as described (20), and data were analyzed using the Ligand program (29). *Left*, displacement curves; *right*, Scatchard transformation. *Panel B*, ^{125}I-MCP-1 (0.12 nM) was added to 10^7 elutriated monocytes in the presence of increasing amounts of unlabeled FX2 (*closed circles, solid lines*) or 7ND (*open circles, dotted lines*), and binding and data analysis were determined as in *panel A*. *Left*, displacement curves; *right*, Scatchard transformation.

phenylalanine, but phenylalanine is not conserved among other neutrophil-active chemokine-α proteins. In fact, a number of chemokine-β proteins also have phenylalanine in this position. In IL-8, this amino acid is involved in hydrogen bond interactions that stabilize the loop between the second and third β-sheets (6). Although this region is not predicted to be involved in similar interactions in MCP-1, nonetheless alteration of arginine 24 may have disrupted other intrachain stabilization interactions. It is certainly possible that some mutants, such as R24F, may have lost activity because the introduced mutations severely disturbed the three-dimensional structure of the proteins. However, our extensive study of 7ND showed that it bound with high affinity to specific receptors on monocytes (most likely the MCP-1 receptor itself, based on displacement data), suggesting that this mutant, at least, had sufficient conservation of its three-dimensional structure to permit receptor binding.

Third, mutation and deletion in the carboxyl-terminal region of MCP-1 yielded proteins that were still capable of eliciting a monocyte chemotactic response, but with much lower potency. This is similar to carboxyl-terminal truncation variants of IL-8 which also displayed 10–20-fold lower activities (8). In IL-8, some of this reduction may be because the α-helix binds heparin, which enhances the activity of IL-8 (26). Preliminary data suggest that heparin also enhances the activity of MCP-1,[3] and it will be of interest to determine if MCP-1's α-helix is responsible for this enhancement.

Taken together, these results imply that like IL-8 (27) and C5a (28), MCP-1 contacts its receptor at multiple sites. The structurally compact region of C5a is believed to contact the extracellular amino terminus of its receptor, and the more disordered carboxyl terminus is believed to contact regions within the receptor's 7-transmembrane core at a point below the plane of the cell surface (28). It is tempting to ascribe analogous binding functions to domains of MCP-1 identified in the present work, *e.g.* MCP-1's interhelical cleft might bind to extracellular portions of the MCP-1 receptor, whereas the amino terminus might penetrate the receptor's 7-transmembrane core. The properties of mutant 7ND are consistent with this model: 7ND binds to specific receptors on monocytes and displaces wild-type MCP-1 from its receptor, suggesting that 7ND binds to the MCP-1 receptor without activating the signaling cascade. The absence of signaling by 7ND might be due to the absence of contacts with the receptor's 7-transmembrane core which are ordinarily supplied by the amino-terminal region of MCP-1. However, there is currently no direct evidence for such interactions.

Interestingly, some mutations, such as 7ND, R24F, Y28D, and D3A, were able to inhibit wild-type MCP-1's chemoattractant properties. As noted above, 7ND appears to be a competitive inhibitor of MCP-1, perhaps by blocking wild-type MCP-1's amino terminus from interacting with the receptor. However, the number of binding sites/monocyte for ^{125}I-7ND was only 10% of the number of binding sites for ^{125}I-MCP-1, and the K_d for ^{125}I-MCP-1 in the presence of excess cold 7ND was 3-fold lower than its K_d in the presence of excess cold MCP-1 (see Fig. 6). These confusing results might be explained by invoking a model that relies on two assumptions: (i) that MCP-1 forms dimers and that 7ND can bind and inactivate wild-type monomeric subunits, and (ii) that MCP-1 has a similar affinity for

[3] Y. J. Zhang and B. J. Rollins, unpublished observations.

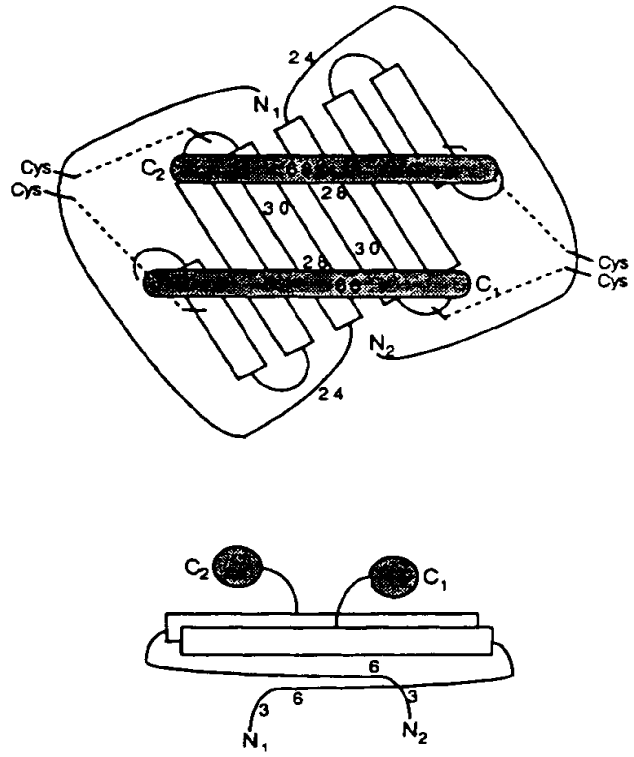

FIG. 7. **Hypothetical structure of MCP-1 dimer, by analogy to IL-8's structure, based on work of Gronenborn and Clore (3).** *Rectangles* indicate β-pleated sheets, *stippled cylinders* indicate α-helices, and *dotted lines* indicate disulfide bonds. Amino termini are depicted as extending below the plane defined by the β-sheets, but their positioning is arbitrary because these regions are disordered in IL-8 structures. Single amino acids substituted in the present study are indicated by their numbered positions.

two distinct receptors, whereas 7ND recognizes only one of these which represents 10% of the total receptor number for MCP-1. Our preliminary data suggest that MCP-1 does form dimers under physiologic conditions and that 7ND can bind to wild-type MCP-1.[2] According to this model, 7ND would efficiently displace ^{125}I-MCP-1 by a combination of mechanisms, namely competition at one set of receptors (10%) and dominant suppression at the other (90%). This model is highly speculative, and experiments are now under way to determine directly if 7ND acts as a dominant suppressor and if there are two classes of MCP-1 receptor. Regardless of their mechanisms of action, these mutants are interesting structures on which to base further work on MCP-1 inhibitors.

Acknowledgments—We acknowledge the technical assistance of Catherine Ernst and Christian Edwards and the secretarial assistance of Bethany Osborne.

REFERENCES

1. Oppenheim, J. J., Zachariae, C. O. C., Mukaida, N., and Matsushima, K. (1991) *Annu. Rev. Immunol.* **9**, 617–648
2. Schall, T. J. (1991) *Cytokine* **3**, 165–183
3. Gronenborn, A. M., and Clore, G. M. (1991) *Protein Eng.* **4**, 263–269
4. Baldwin, E. T., Weber, I. T., St. Charles, R., Xuan, J. C., Appella, E., Yamada, M., Matsushima, K., Edwards, B. F., Clore, G. M., and Gronenborn, A. M. (1991) *Proc. Natl. Acad. Sci. U. S. A.* **88**, 502–506
5. Clore, G. M., Appella, E., Yamada, M., Matsushima, K., and Gronenborn, A. M. (1990) *Biochemistry* **29**, 1689–1696
6. Clore, G. M., and Gronenborn, A. M. (1992) *Cytokines* **4**, 18–40
7. Hebert, C. A., Vitangcol, R. V., and Baker, J. B. (1991) *J. Biol. Chem.* **266**, 18989–18994
8. Clark-Lewis, I., Schumacher, S., Baggiolini, M., and Moser, B. (1991) *J. Biol. Chem.* **266**, 23128–23134
9. Leonard, E. J., and Yoshimura, T. (1990) *Immunol. Today* **11**, 97–101
10. Rollins, B. J. (1991) *Cancer Cells* **3**, 517–524
11. Tanaka, S., Robinson, E. A., Yoshimura, T., Matsushima, K., Leonard, E. J., and Appella, E. (1988) *FEBS Lett.* **236**, 467–470
12. Beall, C. J., Mahajan, S., and Kolattukudy, P. E. (1992) *J. Biol. Chem.* **267**, 3455–3459
13. Rollins, B. J., Stier, P., Ernst, T. E., and Wong, G. G. (1989) *Mol. Cell. Biol.* **9**, 4687–4695
14. Prickett, K. S., Amberg, D. C., and Hopp, T. P. (1989) *Biotechniques* **7**, 580–589
15. Wong, G. G., Witek, J. S., Temple, P. A., Wilkens, K. M., Leary, A. C., Luxenberg, D. P., Jones, S. S., Brown, E. L., Kay, R. M., Orr, E. C., Shoemaker, C., Golde, D. W., Kaufman, R. J., Hewick, R. M., Wang, E. A., and Clark, S. C. (1985) *Science* **228**, 810–815
16. Rollins, B. J., Walz, A., and Baggiolini, M. (1991) *Blood* **78**, 1112–1116
17. Falk, W., Goodwin, R. H., Jr., and Leonard, E. J. (1980) *J. Immunol. Methods* **33**, 239–247
18. Kaufman, R. J., Murtha, P., and Davies, M. (1987) *EMBO J.* **6**, 187–193
19. Rollins, B. J., and Sunday, M. E. (1991) *Mol. Cell. Biol.* **11**, 3125–3131
20. Ernst, C. A., Zhang, Y. J., Hancock, P. R., Rutledge, B. J., Corless, C. L., and Rollins, B. J. (1994) *J. Immunol.* **152**, 3541–3549
21. Yoshimura, T., Robinson, E. A., Tanaka, S., Appella, E., and Leonard, E. J. (1989) *J. Immunol.* **142**, 1956–1962
22. Jiang, Y., Valente, A. J., Williamson, M. J., Zhang, L., and Graves, D. T. (1990) *J. Biol. Chem.* **265**, 18318–18321
23. Rollins, B. J., Yoshimura, T., Leonard, E. J., and Pober, J. S. (1990) *Am. J. Pathol.* **136**, 1229–1233
24. Clark-Lewis, I., Dewald, B., Geiser, T., Moser, B., and Baggiolini, M. (1993) *Proc. Natl. Acad. Sci. U. S. A.* **90**, 3574–3577
25. Valente, A. J., Rozek, M. M., Schwartz, C. J., and Graves, D. T. (1991) *Biochem. Biophys. Res. Commun.* **176**, 309–314
26. Webb, L. M. C., Ehrengruber, M. U., Clark-Lewis, I., Baggiolini, M., and Rot, A. (1993) *Proc. Natl. Acad. Sci. U. S. A.* **90**, 7158–7162
27. Schraufstatter, I. U., Barritt, D. S., Ma, M., Oades, Z. G., and Cochrane, C. G. (1993) *J. Immunol.* **151**, 6418–6428
28. Siciliano, S. J., Rollins, T. E., DeMartino, J., Konteatis, Z., Malkowitz, L., van Riper, G., Bondy, S., Rosen, H., and Springer, M. S. (1994) *Proc. Natl. Acad. Sci. U. S. A.* **91**, 1214–1218
29. Munson, P. J. (1992) *MacLigand*, version 4.93. Analytical Biostatistical Section, Division of Computer Research and Technology, National Institutes of Health, Bethesda, MD
30. Bradford, M. M. (1976) *Anal. Biochem.* **72**, 248–254

PROTEINS: Structure, Function, and Genetics 43:150–160 (2001)

Elucidating the Structural Mechanisms for Biological Activity of the Chemokine Family

Canan Baysal[1]* and Ali Rana Atilgan[2]
[1]*Faculty of Engineering and Natural Sciences, Sabanci University, Tuzla, Istanbul, Turkey*
[2]*Polymer Research Center and School of Engineering, Bogazici University, Bebek, Istanbul, Turkey*

ABSTRACT **Chemokines are a family of proteins involved in inflammatory and immune response. They share a common fold, made up of a three-stranded β-sheet, and an overlaying α-helix. Chemokines are mainly categorized into two subfamilies distinguished by the presence or absence of a residue between two conserved cysteines in the N-terminus. Although dimers and higher-order quaternary structures are common in chemokines, they are known to function as monomers. Yet, there is quite a bit of controversy on how the actual function takes place. The mechanisms of binding and activation in the chemokine family are investigated using the gaussian network model of proteins, a low-resolution model that monitors the collective motions in proteins. It is particularly suitable for elucidating the global dynamic characteristics of large proteins or the common properties of a group of related proteins such as the chemokine family presently investigated. A sample of 16 proteins that belong to the CC, CXC, or CX_3C subfamilies are inspected. Local packing density and packing order of residues are used to determine the type and range of motions on a global scale, such as those occurring between various loop regions. The 30s-loop, although not directly involved in the binding interface like the N-terminus and the N-loop, is identified as having a prominent role in both binding/activation and dimerization. Two mechanisms are distinguished based on the communication among the three flexible regions. In these two-step mechanisms, the 30s-loop assists either the N-loop or the N-terminus during binding and activation. The findings are verified by molecular mechanics and molecular dynamics simulations carried out on the detailed structure of representative proteins from each mechanism type. A basis for the construction of hybrids of chemokines to bind and/or activate various chemokine receptors is presented. Proteins 2001;43:150–160.** © 2001 Wiley-Liss, Inc.

Key words: cytokines; transmembrane receptors; leukocytes; collectivity in binding; low-resolution models

INTRODUCTION

Chemokines are a large family of proteins that act as chemoattractants and activators of leukocytes in the inflammatory response of the immune system (see Baggiolini[1] and references cited therein). They are attractive targets for the blockade of inflammatory disease progression. The activities of chemokines are mediated through their binding to specific seven-helix transmembrane receptors. Chemokine receptors may be specific for one ligand or they may bind several chemokines. A subset of chemokine receptors function as co-receptors for infectious agents, human immunodeficiency virus type 1 (HIV-1), among others.[2] Understanding the structural basis for receptor selectivity has become an important goal because the binding of chemokines to co-receptors blocks HIV-1 infection at the entry level. Elucidating the intrinsic conformational features, on both global and local scales, may be essential for an assessment of the effect of mutations and for devising mutants with more efficient receptor selectivity.

Much work on chemokines has dealt with elaborating on function of the chemokines from structure, which is founded on a common scaffold whereby the well-defined regions contain a series of three antiparallel β-strands and a C-terminal α-helix. The region preceding the β1-strand is divided into two sections containing the disordered N-terminus and a somewhat more ordered N-loop. These two sections are joined by a short peptide segment (2–5 residues) terminated on each side by two of the four conserved cysteines in the family. The section connecting the β1- and β2-strands is called the 30s-loop, as it contains residues indexed in the 30s, and has been implicated in playing some role in receptor binding and/or activity.[3,4] Similarly, the loop joining the β2- and β3-strands is called the 40s-loop. The C-terminus α-helix is followed by several residues that do not have a defined structure. Two disulfide bridges are formed between the four structurally conserved cysteines: The first cysteine in the N-terminus is linked to a cysteine located in the 30s-loop, whereas the second is linked to that in the β3-strand.

The finding that the monomeric forms are functional, despite the fact that many chemokines are commonly found in dimeric or higher-order quaternary structures,[5–10] has led to the earlier models for the interaction of the protein with the receptor.[5] Considerable effort has been

*Correspondence to: Canan Baysal, Faculty of Engineering and Natural Sciences, Sabanci University, Tuzla 81474, Istanbul, Turkey. E-mail: canan@sabanciuniv.edu

Received 4 August 2000; Accepted 1 December 2000
Published online 20 February 2001

devoted to understanding the effect of point mutations,[9–14] truncation mutants,[9,13,15,16] and hybrids[3,11,13] on chemokine function, by studying their chemotaxis, release, and binding. Thus, regions in the N-terminus and the N-loop have been identified as the primary binding/activation interfaces, and a two-site model of interaction between chemokines and their receptors has been proposed.[12,13] Studies that directly probe the dynamics of chemokines are scarce and relatively more recent.[4,17,18] In all these studies, backbone dynamics have been probed by ^{15}N relaxation measurements. Such studies provide insight on the residues involved in binding/activation mechanisms, especially through slow conformational exchange. Crump et al.[4] point out that structure alone does not provide details on the dynamics of the protein; in particular, information on functionally sensitive regions are not accessible through a static picture of the molecule. Thus, although considerable structural and dynamical data on various chemokines have accumulated, there is no direct evidence on the common mechanisms at play within the family. By contrast, computational approaches for examining the role of a whole family of proteins is prevented due to time limitations brought about, for example, by molecular dynamics (MD) simulations. Consequently, information regarding large-scale motions, binding and activation mechanisms, and their applications towards the discovery of chemokines with improved binding features has not been available.

To elucidate the structural mechanisms for functional activity, we mainly use a recently proposed dynamics model. It is a simple and analytical approach,[19] which has proved to characterize the equilibrium motions of folded proteins efficiently,[20] for instance, flexibility–enzymatic activity relationships of HIV-1 reverse transcriptase,[21] folding nucleus stability relationships of bacterial signal transduction protein CheY,[22] or the common dynamic features of proteins with similar architectures.[23] A similar coarse-grained approach has been used to study domain motions in large proteins.[24,25] The method presently used, called the gaussian network model (GNM), is based on an analysis of the two structure-based parameters that play an eminent role in equilibrium dynamics of folded proteins[19,20]: (1) the packing density, which is the total number of bonded and nonbonded "contacting" α-carbons located within a sphere of 7 Å radius about a central α-carbon, and (2) the packing order that numerates these contacting α-carbon pairs. Within the time scale of equilibrium fluctuations, which may be associated with a frequency spectrum, different frequencies contribute to different types of motion.[26] Lower frequencies associated with longer wavelengths correspond to the fluctuation of groups of residues with relatively larger amplitudes,[24,27] whereas higher frequencies with shorter wavelengths are mainly responsible for the most dominant pairwise interactions.[22] Therefore, the former range is attributed to the motions that are relevant to function, while the latter is ascribed to the regions that are more stable than others.[20–22,28] As such, a modal decomposition of these vibrational motions allows to elucidate both the global and local motions, by considering the slowest and fastest modes, respectively.

In the present study, we confine our attention to the most cooperative motions revealed by the lowest frequency, or the largest wavelength. The peaks and sinks observed in these concerted fluctuations indicate regions that may be important for binding and catalytic activity.[20,21,28] To capture the common features coupled to the intrinsic flexibility of the structure, we therefore investigate the fluctuations and correlations of fluctuations corresponding to the longest wavelength for 16 members of the chemokine family. In turn, we identify the underlying mechanisms that manipulate the binding to receptors. Our findings are corroborated by MD and molecular mechanics (MM) calculations carried out on the detailed molecular structures of selected chemokines.

MATERIALS AND METHODS

Gaussian Network Model of Proteins

Details on the basic postulates of the GNM approach may be found in Bahar et al.[19] and Haliloglu et al.[29] In the present study, we give only a brief description of the calculations involved. For a protein of N residues, the inter-residue potential of the coarse-grained model is given by

$$\mathcal{H} = \frac{1}{2}\gamma\, tr(\Delta\mathbf{R}^T\Gamma\Delta\mathbf{R})$$

where γ is a single-parameter stiffness constant for representing all pairwise interactions in the folded state, $\Delta\mathbf{R}$ is the N-dimensional hypervector of the fluctuation vectors $\Delta\mathbf{R}_1, \Delta\mathbf{R}_2, \ldots, \Delta\mathbf{R}_N$ of the α-carbons, tr designates the trace of the matrix enclosed in parentheses, and the superscript T denotes the transpose. Γ is the $N \times N$ symmetric Kirchhoff matrix, whose entries are defined as

$$\Gamma_{ij} = \begin{cases} -H(r_c - r_{ij}) & i \neq j \\ -\sum_{i \neq j}^{N} \Gamma_{ij} & i = j \end{cases} \qquad (1)$$

where the diagonal entries ($i = j$) represent the packing density of the α-carbons and the off-diagonal elements depict the packing geometry. Here, r_{ij} is the distance between the ith and jth α-carbons, $H(x)$ is the Heavyside step function given by $H(x) = 1$ for $x > 0$ and $H(x) = 0$ for $x \leq 0$, and r_c is the upper limit for the separation between two residues in contact. The value $r_c = 7.0$ Å was originally adopted, which includes all neighbors within the first coordination shell around a central residue.[19]

Experimental results refer to either the square of the root-mean-square deviations (RMSD), $\langle \Delta\mathbf{R}_i \cdot \Delta\mathbf{R}_j \rangle$ reported in NMR derived structures, or the X-ray crystallographic temperature factors,

$$B_i = 8\pi^{2/3} < \Delta\mathbf{R}_i \cdot \Delta\mathbf{R}_i >$$

of the high-resolution structure of chemokines. It was shown that[19]

$$\langle \Delta\mathbf{R}_i \cdot \Delta\mathbf{R}_j \rangle = (3k_BT/\gamma)[\Gamma^{-1}]_{ij} \qquad (2)$$

where a proper choice of γ is obtained by normalizing the theoretical results with those given by the experiments.

The dynamic characteristics of a folded protein are described in terms of its natural frequencies ω_p, $2 \le p \le N$, of Γ, and the shapes of the corresponding modes of motion $\mathbf{u}_p$, $2 \le p \le N$, of Γ ($p = 1$ corresponds to rigid body motion). The auto ($i = j$) or cross-correlation of fluctuations associated with the pth frequency of the motion, $\langle \Delta\mathbf{R}_i \cdot \Delta\mathbf{R}_j \rangle_p$, are found from[19,29]

$$\langle \Delta\mathbf{R}_i \cdot \Delta\mathbf{R}_j \rangle_p = (3k_BT/\gamma)[\omega_p^{-1}\mathbf{u}_p\mathbf{u}_p^T]_{ij} = (3k_BT/\gamma)\omega_p^{-1}[\mathbf{u}_p]_i[\mathbf{u}_p]_j \tag{3}$$

where ω_p are the eigenvalues of the Kirchhoff matrix Γ and the subscripts designate the elements of the matrices (or vectors) enclosed in brackets.

Molecular Mechanics Calculations

The consistent valence force field (CVFF) implemented within the Molecular Simulations InsightII 98.0 (Molecular Simulations, San Diego, CA) software package was used in the MM calculations.[30] Initially, the structure of the protein obtained from the Protein Data Bank (PDB)[31,32] is solvated in a 5-Å layer of water surrounding it, resulting in ~1,250 water molecules for the proteins studied here. Group-based cutoffs are employed with a 9.5-Å cutoff distance. A switching function is used with the spline and buffer widths set to 1.0 and 0.5 Å, respectively. The system is energy minimized to 0.01 kcal/mol/Å of the derivative, using conjugate gradients method. In this study, we are interested in the relative displacements of the atoms, and the criterion for terminating the minimization must be selected accordingly. Extensive testing on various proteins have shown us that the usage of a more stringent criterion (e.g., 10^{-4} kcal/mol/Å) affects the absolute value of the energy attained, whereas the final atomic locations are within ~0.01 Å of their absolute minima at a derivative of 0.1 kcal/mol/Å. The RMSD between the original PDB and the energy minimized C_α coordinates is ~0.8 Å for the proteins studied in this work. These coordinates of the molecule are treated as the main coordinates of the equilibrium structure.

The procedure for perturbing the C_α atom is as follows: (1) the coordinates of the C_α of the selected residue is perturbed by adding equal displacements d in each of the x-, y-, and z-directions, which leads to a distorted local structure; (2) the new coordinates of the displaced C_α atom is fixed in space, whereas the rest of the protein atoms are free to move; (3) the energy of the protein is minimized to 0.1 kcal/mol/Å of the derivative; (4) the rearranged atomic coordinates in response to the perturbation are recorded for further analysis; (5) the coordinates are reset to those of the equilibrium structure and the process (1–4) is repeated over all the C_α atoms.

The N sets of protein coordinates obtained at the end of the MM calculations are organized into the perturbation–response matrix of order $3N \times 3N$, where the displacement experienced by residue i in response to a perturbation placed at residue k is denoted by $\Delta\mathbf{R}_{ik}$

$$\Delta\mathbf{R} = \begin{bmatrix} \Delta\mathbf{R}_{11} & \Delta\mathbf{R}_{12} & \cdots & \Delta\mathbf{R}_{1N} \\ \Delta\mathbf{R}_{21} & \Delta\mathbf{R}_{22} & \cdots & \Delta\mathbf{R}_{2N} \\ \vdots & \vdots & & \vdots \\ \Delta\mathbf{R}_{N1} & \Delta\mathbf{R}_{N2} & \cdots & \Delta\mathbf{R}_{NN} \end{bmatrix} \tag{4}$$

In all the MM calculations presented below, displacements $d = 0.5$ Å is used. Note that various d within the range 0.1–1.0 Å yield identical and almost symmetrical perturbation–response behavior, indicating that this size of displacement is within the range of linear response.

$\Delta\mathbf{R}$ multiplied by its transpose yields the $3N \times 3N$ second moment matrix $\mathbf{A} = \Delta\mathbf{R}\,\Delta\mathbf{R}^T$, which carries the average effect of all the perturbations. Alternatively, $\mathbf{A}$ may be viewed as an $N \times N$ matrix, whose ijth element is the 3×3 second moment matrix of correlations between the x-, y-, and z-components of the fluctuations $\Delta\mathbf{R}_i$ and $\Delta\mathbf{R}_j$ of residues i and j; i.e.,

$$\mathbf{A}_{ij} = \begin{bmatrix} \langle \Delta X_i \Delta X_j \rangle & \langle \Delta X_i \Delta Y_j \rangle & \langle \Delta X_i \Delta Z_j \rangle \\ \langle \Delta Y_i \Delta X_j \rangle & \langle \Delta Y_i \Delta Y_j \rangle & \langle \Delta Y_i \Delta Z_j \rangle \\ \langle \Delta Z_i \Delta X_j \rangle & \langle \Delta Z_i \Delta Y_j \rangle & \langle \Delta Z_i \Delta Z_j \rangle \end{bmatrix} \tag{5}$$

Finally, the cross-correlations between residues i and j in response to the inserted perturbations is given by

$$\langle \Delta\mathbf{R}_i \cdot \Delta\mathbf{R}_j \rangle = \frac{1}{N} \quad tr\,\mathbf{A}_{ij}) \tag{6}$$

Molecular Dynamics Simulations

CVFF implemented within the InsightII 98.0 software package was used in the MD simulations.[30] As in the MM calculations, a cage of water molecules of 5 Å thickness is formed around the protein structure obtained from the PDB,[31,32] resulting in ~1,250 water molecules for the proteins studied here. All atoms are treated explicitly. The system is energy minimized to 0.01 kcal/mol/Å of the derivative using the conjugate gradients method. The initial structure is thus that treated as the equilibrium structure in the MM calculations. A time step of 1 fs is used, and the temperature is kept fixed at 300 K by coupling to an external heat bath[33] with a relaxation time constant of 0.01 ps. Initial velocities are generated from a Boltzmann distribution with an average temperature of 300 K. Integration is carried out by the velocity Verlet algorithm. Group-based cutoffs are used with a 9.5 Å cutoff distance; a switching function is used with the spline and buffer widths set to 1.0 and 0.5 Å, respectively. The neighbor list is updated whenever any atom moves more than one-half the buffer width. The system is equilibrated for 200 ps, and data are collected for the next 1 ns. The cage of water is found to remain around the protein at the end of all simulations. Atomic positions are saved every 500 steps, yielding $M = 2{,}000$ coordinate sets.

The snapshots recorded during the MD simulations are organized in the fluctuation trajectory matrix of order $3N \times M$,

TABLE I. Proteins Investigated in the Present Study

Chemokine	PDB code	No. of residues	Subfamily	Quaternary structure	Reference	Mechanism type
MCP-1	1dol	71	CC	Monomer	42	II
MCP-3	1bo0	76	CC	Monomer	43	II
vMIP-II	1vmp	71	CC	Monomer	36	II
Eotaxin	1eot	74	CC	Monomer	38	I
HCC-2	2hcc	66	CC	Monomer	44	I
RANTES	1rto	136	CC	Dimer	45	II
MIP-1α	1b53	138	CC	Dimer	46	II
MIP-1β	1hum	138	CC	Dimer	46	I
SDF-1	1sdf	67	CXC	Monomer	13	I
IL-8	1ik1	71	CXC	Monomer	6	I
MIP-2	1mi2	146	CXC	Dimer	47	I
MGSA/GROα	1msg	144	CXC	Dimer	48	I
GROβ	1qnk	138	CXC	Dimer	35	I
NAP-2	1nap	264	CXC	Tetramer	49	I
PF4	1plf	260	CXC	Tetramer	50	I
Fractalkine	1b2t	77	CX_3C	Monomer	18	I

PDB, Protein Data Bank.

$$\Delta\mathbf{R} = \begin{bmatrix} \Delta\mathbf{R}_1(t_1) & \Delta\mathbf{R}_1(t_2) & \cdot & \Delta\mathbf{R}_1(t_M) \\ \Delta\mathbf{R}_2(t_1) & \Delta\mathbf{R}_2(t_2) & \cdot & \Delta\mathbf{R}_2(t_M) \\ \Delta\mathbf{R}_3(t_1) & \Delta\mathbf{R}_3(t_2) & \cdot & \Delta\mathbf{R}_3(t_M) \\ \cdot & \cdot & \cdot & \cdot \\ \cdot & \cdot & \cdot & \cdot \\ \Delta\mathbf{R}_n(t_1) & \Delta\mathbf{R}_n(t_2) & \cdot & \Delta\mathbf{R}_n(t_M) \end{bmatrix} \quad (7)$$

The fluctuation trajectory matrix of eq. 7 is the counterpart of the perturbation response matrix of eq. 4. The $3N \times 3N$ second moment matrix $\mathbf{A}$ is calculated by $\mathbf{A} = \Delta\mathbf{R}\,\Delta\mathbf{R}^T$. Finally, the cross-correlations are obtained from[34]

$$\langle \Delta\mathbf{R}_i \cdot \Delta\mathbf{R}_j \rangle = \frac{1}{M} \; tr(\mathbf{A}_{ij}) \quad (8)$$

RESULTS AND DISCUSSION

The chemokines studied in the present work, their PDB code, subfamilies, and quaternary structures are listed in Table I. We have tried to include all the chemokines whose structures have been solved by X-ray diffraction (XRD) or nuclear magnetic resonance (NMR); the monomeric form has been used when possible; otherwise, higher-order quaternary structures are used. There are two main subfamilies of chemokines. In the CXC subfamily, the N-terminal cysteine residues are separated by a single residue, whereas in the CC subfamily, these cysteines are adjacent. The chemokines inspected here mainly belong to CC and CXC subfamilies, except for fractalkine that is of type CX_3C. Note that GNM analysis is applied to all the chemokines listed in Table I, whereas the time-consuming MD and MM calculations are carried out on vMIP-II and SDF-1 only.

30s-Loop Emerges As a Major Contributor to Chemokine Function

We first point out the major difference between the CC and CXC subfamilies. Figure 1 exhibits the experimental positional fluctuations of α-carbons as well as those computed by the GNM theory and MD simulations. Note that although MD is applied to the all-atom protein solvated in explicit water, in contrast to GNM, which treats the protein as a set of interacting beads of α-carbons, the correspondence between the results is remarkable, as also demonstrated in the crystallographic B-factors of α-amylase inhibitor.[34] All three approaches identify the N- and C-termini as well as the N-, 30s-, and 40s-loops as the most mobile regions both in the CC and CXC subfamilies. However, a different picture emerges upon consideration of the contribution of only the lowest frequency counterpart of these fluctuations. Average atomic displacements as a function of residue index considering only the lowest frequency ($i = j$, $p = 2$ in eq. 3) are displayed in Figure 2a and b for representative CC and CXC chemokines, respectively. Peaks are obtained in the *N*- and 40s-loops in both cases, whereas the 30s-loop is "dead" in the CC subfamily, and "alive" in the CXC subfamily. The existence of a single residue inserted between the two cysteines results in a structural disturbance that supplies a vast amount of flexibility to the 30s-loop during collective motions.

This observation might indicate the 30s-loop as having a critical role in the diverse chemokine function. In fact, although the main residues of focus in experimental studies for binding/activation are located in the N-terminus and N-loop of chemokines, the 30s-loop has been identified as an important region through structure comparison,[18,35] backbone dynamics,[4,18] and mutation[3,13] studies. In particular, dynamics experiments provide the most concrete evidence on the role of the 30s-loop. For instance, extensive NMR dynamics experiments have been carried out on fractalkine, a CX_3C chemokine that binds the CX_3CR1 receptor.[18] Slow conformational exchange on the millisecond (ms) to microsecond (μs) time scale at residues 13, 31, 35, and 49 has been observed. Moreover, as a result of titration of fractalkine with a peptide from the N-terminus of CX_3CR1, the most highly shifted cross-peaks

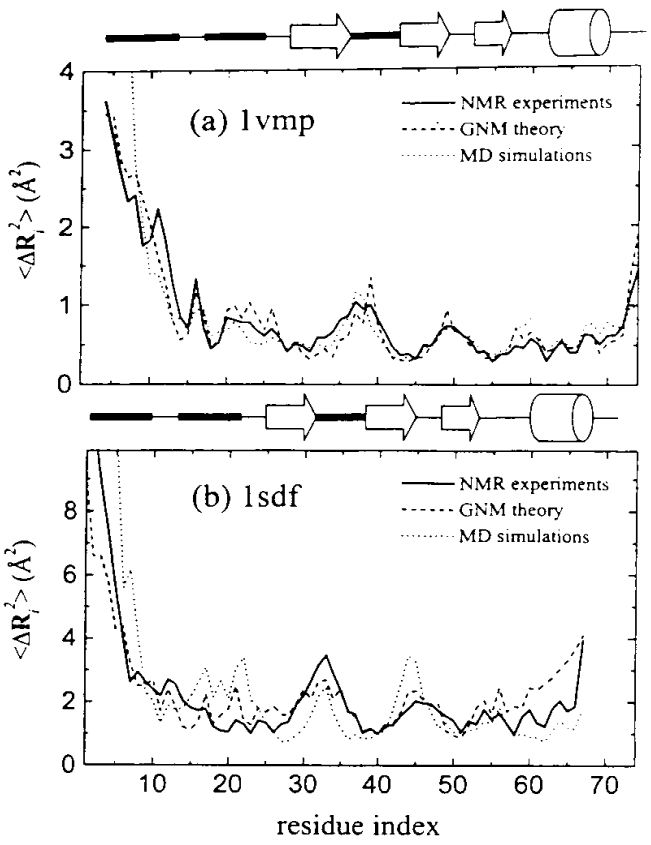

Fig. 1. Mean square fluctuations of α-carbons, $\langle \Delta \mathbf{R}_i \cdot \Delta \mathbf{R}_j \rangle$, for (a) 1vmp (CC) and (b) 1sdf (CXC); results from NMR experiments are compared with those from gaussian network model (GNM) theory ($i = j$ in eq. 2) and MD simulations ($i = j$ in eq. 8). Positions of the secondary structural units are shown along the residue indices.

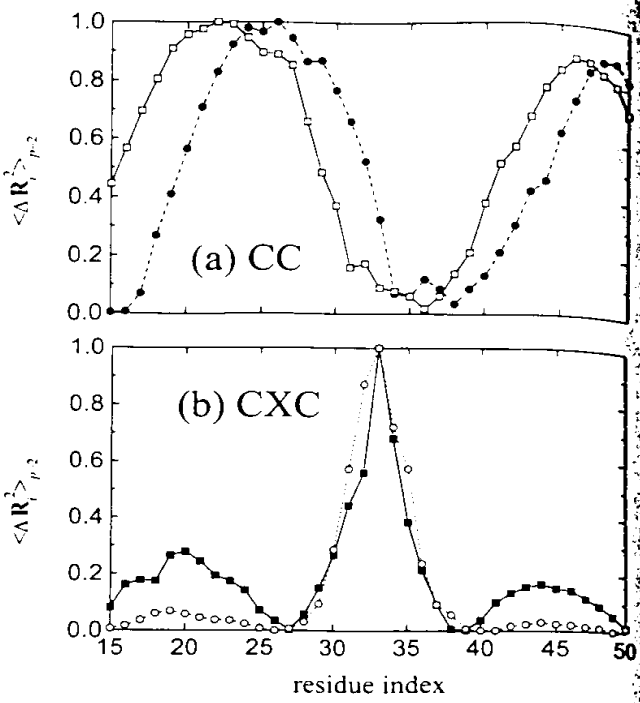

Fig. 2. Mean square fluctuations of α-carbons of selected chemokines during global motions ($i = j$, $p = 2$ in eq. 3). **a:** CC family members 1dol (□) and 1vmp (●). **b:** CXC family members 1ikl (○) and 1sdf (■). The values for the residues between 15 and 50 are presented and are normalized so that the maximum value in this interval is 1. The 30s-loop is located at residues 32–39 in 1dol, 35–41 in 1vmp, 26–40 in 1ikl, and 30–36 in 1sdf. Compared with the overall fluctuations presented in Figure 1, the 30s-loop does not exhibit collective fluctuations in the CC family, whereas it remains highly correlated in the CXC family.

in 2D ^{1}H-^{15}N HSQC spectra are displayed at residues 6–17 as well as the 30s-loop. Similarly, dynamics experiments on vMIP-II,[36] eotaxin,[4] and IL-8[37] identified slow conformational exchange through residues residing within the 30s-loop as well as the N-terminus and the N-loop. All these findings lend support to the view that the 30s-loop is actively involved in binding/activation mechanisms along with the N-terminus and the N-loop.

CC and CXC Proteins Differ in the Way They Construct Dimers

Many chemokines have been shown to form symmetric dimers and even higher-order multimers. The structural form of the CC dimer is different from that of the CXC. The dimer interface of the former is at the N-terminal of the protein, centered around the conserved cysteines and involves many of the residues implicated in receptor binding. The latter, on the other hand, involves antiparallel positioning of the β1-strands, leaving the N-terminus free. Experimental evidence implies that in solution, at concentrations at which receptor binding and biological activity are observed, the predominant form is monomeric.[6,9,11] This is conceivable, since thermodynamics will strongly favor dimerization at the high concentrations at which protein structures are determined; in contrast, the functional concentrations of chemokines are at least 10,000-fold lower. Nevertheless, the distinct forms of the dimers formed by the two chemokine families may provide clues as to how binding and activity take place. The analysis used in the previous section identifies a major difference between the way the CC and CXC chemokines operate, and this may also suffice to explain their corresponding dimerization mechanisms.

The dimerization of CC chemokines at the N-termini may be an expected scenario, as proteins tend to associate at their most flexible regions unless there is a disturbance. Such a disturbance is provided by the "alive" 30s-loop that displays cooperative fluctuations in the CXC chemokines, and is in direct contact with the N-terminus. Thus, here the proteins cannot associate at their initial option at the N-termini; they dimerize by forming a six-stranded β-sheet by the approach of the β1- and β1'-strands of the two subchains as the alternative. This scenario outlines the propensity of dimerization in the CC and CXC chemokines. Whether the dimer will actually form depends on the specific interactions that take place at the dimer interface, once the fold places the associating regions at

the correct positioning. For example, the MIP-1b dimer is locked into position due to the proper interactions between the Phe13 of one subunit with Thr9′ and Leu34′ of the other subunit. A structural alignment of vMIP-II, on the other hand, reveals that Leu16, Asp12′, and Leu37′, which are located in the corresponding positions, form a series of unfavorable interactions. Hence, vMIP-II cannot dimerize.[36]

Intrinsic Flexibility Is Manifested in Convoluted Interactions

There are a large variety of chemokines receptors; some chemokines bind to multiple receptors, some may just bind without activation, and others also activate the receptor. To illuminate the common grounds, we revert to the cross-correlations (eq. 3) that provide a complete picture of the "convoluted" interactions between various regions of the molecule. The term "convolution" represents the transitivity of interactions. For instance, the ith atom may be in contact with the jth that is in turn contacting the kth, but the ith atom is not necessarily in contact with the kth. By contrast, the fluctuations of the ith atom may be correlated with the kth. The former picture is revealed by the contact matrix, whereas the latter may be visualized by the correlation maps (eq. 2 for all frequencies and eq. 3 for a specific set of frequencies). Constructing the cross-correlation maps associated with the most cooperative motions indicate, in a coarse grained manner, the communication between different parts of the native structure that play a significant role in biological activity. In physical terms, two fluctuations occurring in the same sense of direction essentially yield a positive correlation; the opposite is true for a negative correlation.

The experimental evidence compiled for various chemokines supports the view that the core of the protein, where the α-helix packs to the β-strand, sustains the N-loop and the N-terminus, that have been known to contribute to the receptor binding and activation,[3,9,11,13,14,17,36,38] and presents them to the receptor in an optimal fashion.[38] Also, as outlined in the previous section, the 30s-loop emerges as a major contributor to function whose role remains to be determined. We therefore focus on the interrelations of these three regions in the interpretation of the correlation maps. Hence, these will be denoted by three symbol + or − codes, for the N-loop–N-terminus, N-loop–30s-loop, and N-terminus–30s-loop interactions, respectively. If the correlations between the N-loop and the N-terminus are used as a starting point, and assumed to be positively correlated, their interactions with the 30s-loop may be explained in two possible ways: either the 30s-loop is positively correlated with both N-loop and the 30s-loop (+,+,+), or it is negatively correlated with both of them (+,−,−). The remaining combinations, i.e., (+,−,+) and (+,+,−), are self-contradictory and cannot be achieved. Similarly, for a negatively correlated N-loop and N-terminus, only (−,+,−) and (−,−,+) are accessible.

Figure 3 presents the cross-correlation maps of 1sdf for all frequencies obtained by GNM theory, MM simulations, and MD calculations. In all three approaches, regions that are strongly and weakly coupled to each other are reproduced well. This finding is striking in view of the coarse graining inherent in GNM as opposed to the detailed molecular structure employed in MM and MD calculations. As pointed out earlier, long wavelength modes are expected to accentuate the collective motions occurring in proteins; therefore, residue correlations for $p = 2$ are investigated in depth below. In subsequent calculations, GNM which requires computation times on the order of minutes as opposed to MD or MM with a time cost of days is applied to all the chemokines listed in Table I, whereas the latter two methods are used to analyze selected proteins only.

Contour plots for cross-correlations pertaining to the longest wavelengths ($p = 2$) are produced for all the chemokines listed in Table I. Two types of communications emerge from the four possible combinations listed earlier, denoted type I (−,−,+) and type II (−,+,−) and are presented in Figure 4. Note that exactly the same picture emerges for all chemokines sharing the same type of mechanism, and only the representative cases of SDF-1 and vMIP-II are shown. The mechanism types realized by the whole set of proteins studied here are listed in the last column of Table I. Also note that type I involves both CC and CXC chemokines, implying that a certain category is not unique to a given subfamily.

The above findings are supported by MD and MM calculations carried out on SDF-1 and vMIP-II, selected proteins from each mechanism type. The cross-correlation maps obtained by these methods are identical to those in Figure 4 and are not displayed in this investigation. In MM calculations, external perturbation of residues in the 30s-loop, especially Asn33 and Cys34 provoke the largest amount of displacement at the N-terminus residues Tyr7 and Arg8 in SDF-1. In contrast, a disturbance of residues in the 30s-loop of vMIP-II, especially Lys40 and Pro41, provokes the largest amount of displacement at Tyr18 and Gln19 of the N-loop. Moreover, these responses are reciprocal; i.e. perturbations in the indicated residues of the N-terminus or the N-loop trigger the largest displacements at the corresponding 30s-loop residues, although the MM approach introduced in this work intrinsically need not be symmetric. Thus, both the MD simulations and the perturbation–response analysis performed on the detailed molecular structure of the proteins conforms with the positively correlated regions pointed out by the low resolution model. Note that these changes in location do not occur due to the close proximity of the above mentioned residues. For instance, in vMIP-II the equilibrium distance between residue pairs (18,40), (18,41), (19,40), and (19,41) are 10.55, 14.16, 11.72, and 14.83 Å, respectively. These values are significantly larger than that of the 7 Å radius of the first coordination shell. Thus, a more complicated communication between residues is at play, which involves the convoluted interactions discussed in the previous section.

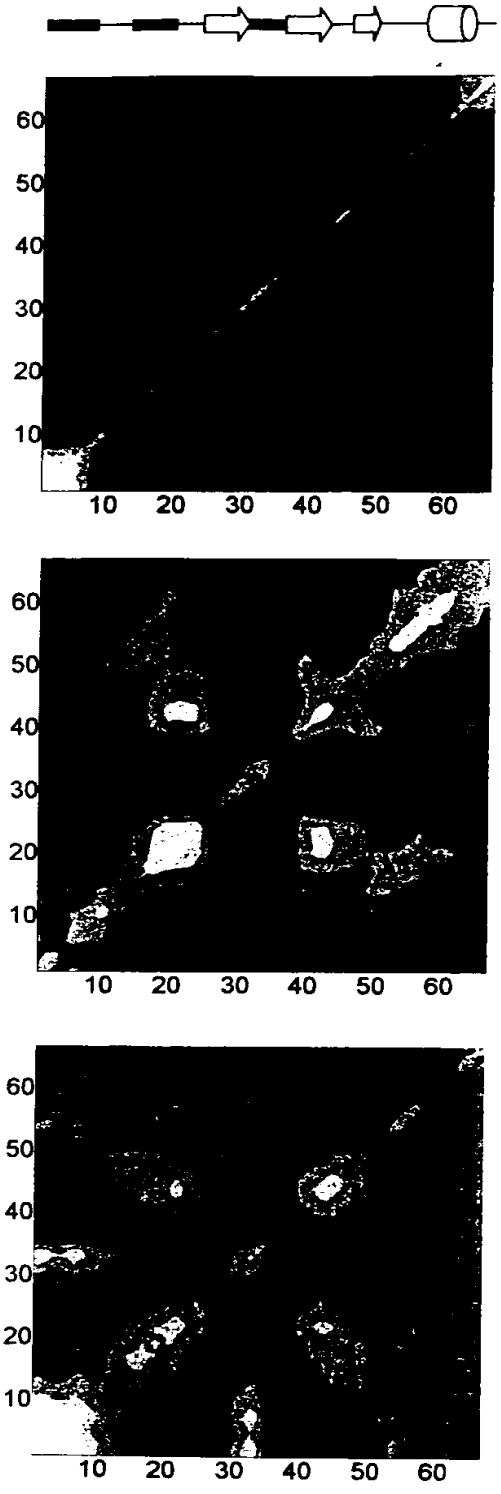

Fig. 3. Correlation maps of 1sdf residue fluctuations (contour plot of $(\Delta R_i \cdot \Delta R_j)$; all modes). **a:** Gaussian network model (GNM) theory (eq. 2). **b:** MM calculations (eq. 6). **c:** MD simulations (eq. 8). Positions of the secondary structural units are shown along the top. The most negatively correlated regions are shown in black and the most positively correlated regions in white. The GNM calculations that involve an appreciable amount of coarse graining. MM calculations that involve a perturbation-response analysis, and MD simulations that reflect the time average of the fluctuations around the equilibrium structure all reproduce the same picture, where the correlated and anticorrelated motions occur between the same residue pairs.

Structural Mechanisms Control Binding and Activity

The above relations may be used in identifying mechanisms for binding and activation. Model proteins representing type I and II interactions are displayed in Figure 5. It should be stressed that the structural organization of the core is unique to the proteins classified within the same type (e.g., eotaxin, a CC protein, is classified as having a type I mechanism), although all chemokines have commonly been characterized by the same overall fold.

Crump et al.[13] proposed a two-step model for the interaction of SDF-1 with CXCR4, wherein the N-loop forms the first contact between the ligand and receptor serving as an initial docking step. Subsequently, the N-terminal residues bind to a groove among the transmembrane helices and further induce a change in the receptor conformation that leads to its activation. More specifically, as displayed in Figure 4a, the N-loop fluctuating in the opposite direction to both the 30s-loop and the N-terminus does the initial binding. Next, the 30s-loop, which moves in the same direction as the N-terminus, pushes the latter into the binding site to make it perform its function. Thus, the model of Crump et al.[13] is consistent with the type I interactions of Figure 5a.

With type II interactions, a positive correlation exists between the 30s- and N-loops, as exhibited in Figures 4b and 5b. Thus, we propose that this time the 30s-loop leads the N-loop to do its initial binding. Once the contact is formed, the flexible N-terminal undergoes a series of conformations and binds with the help of specific interactions with the receptor. Therefore, for type II proteins, specificity may not be crucial for the initial contact to the receptor site.

There is a wealth of experimental findings to support the two mechanisms proposed above. For example, interleukin-8 (IL-8) is identified as having a type I mechanism. According to our hypothesis, the N-loop does the initial binding with the help of high specificity, and the 30s-loop aids the N-terminus. Experimentally, residues 10–22 (N-loop) and 30–35 (30s-loop) were found to be critical, as well as the ELR (Glu–Leu–Arg) motif in the N-terminus.[39] The ELR region is anchored to the 30–35 turn, which possibly provides the correct geometry for the control of the ELR motif conformation.[3] Individual substitutions to residues 10–15 have no functional consequences, but hybrid experiments indicate they are essential.[3] This is consistent with type I mechanism, the N-loop does not receive the aid of 30s-loop to access the conformations necessary for binding,

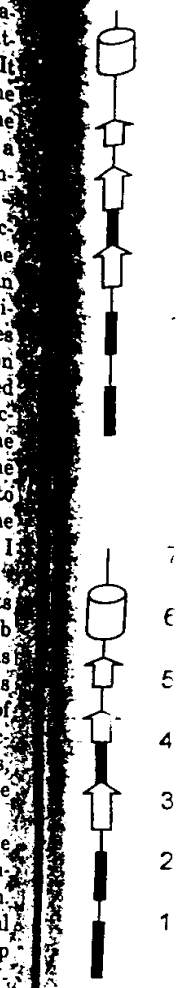

Fig. 4. C
motions of se
(type II). Posi
residue indice
black and the
both interacti
N-terminus; h
regions are re

and c collec
to realize th
Similarly
models bas
chemokine
chemokine.
having type
type I. Thu
N-loop doe
30s-loop. It
SDF-1, sinc
the 30s-loo

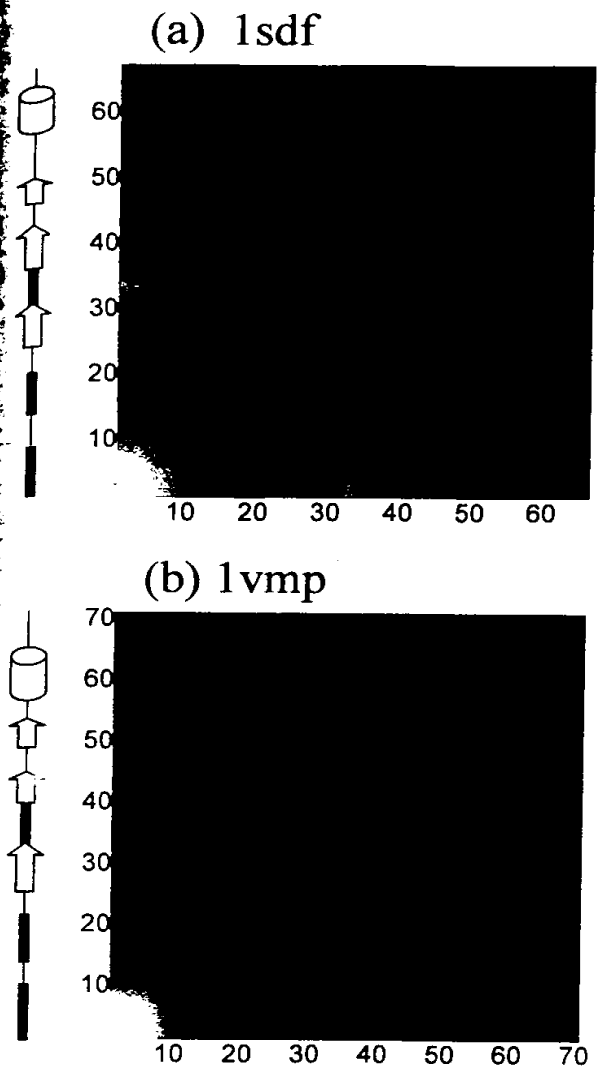

Fig. 4. Correlation map for residue fluctuations during collective motions of selected chemokines (p = 2 in eq. 3). **a:** 1sdf (type I). **b:** 1vmp (type II). Positions of the secondary structural units are shown along the residue indices. The most negatively correlated regions are shown in black and the most positively correlated regions are shown in white. In both interaction types, the N-loop is negatively correlated with the N-terminus; however, the correlations of the 30s-loop with these two regions are reversed.

and a collective effort of residues in this region is necessary to realize the function.

Similarly, data on vMIP-II and SDF-1 support the models based on Figures 4 and 5. Both proteins bind the chemokine receptor CXCR4, although the former is a CC chemokine. In the above analysis, vMIP-II is identified as having type II mechanism as opposed to SDF-1, which is of type I. Thus, according to our hypothesis, in VMP-II the N-loop does the initial binding with the help of the 30s-loop. It therefore needs less specificity compared with SDF-1, since the latter lacks the cooperativity offered by the 30s-loop during binding. In fact, vMIP-II lacks the

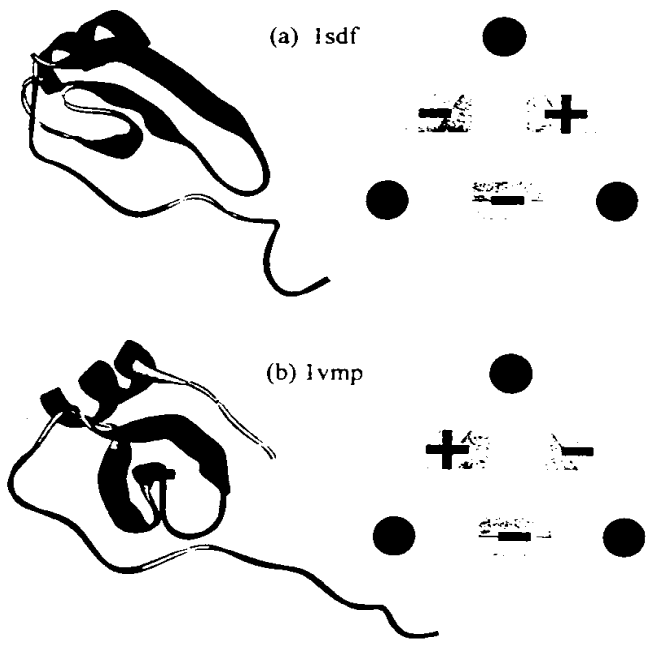

Fig. 5. Communications among the flexible units that modulate binding to receptors in two different types of interactions. The N-terminus is in green, the N-loop in red, and the 30s-loop in blue. Note the different structural organization of the core in (**a**) 1sdf (type I) and (**b**) 1vmp (type II).

RFFESH motif in the N-terminus, which has been identified as critically important in SDF-1 binding.[13] Moreover, the ability of vMIP-II to bind several other receptors also corroborates the proposition that specificity is less important at the N-loop of this protein due to type I mechanism being at play.

Apparent concerted motion between the 30s-loop and N-terminus has been reported in eotaxin,[38] a CC protein that displays type I mechanism. Eotaxin is known to bind CCR3 specifically, as compared with, e.g., RANTES or MCP-3, which are known to bind other receptors as well. Both findings are consistent with the type I mechanism, which dictates that (1) the N-loop requires specificity in binding, and (2) the motions of the N-terminus and the 30s-loop are correlated.

That a high amount of specificity is required for type I binding mechanism is also corroborated by hybrid studies on IL-8 and growth-related protein (GRO), which show that substitution of several residues following the cysteines is necessary to attain binding specificity, whereas single substitutions within the loop have small effects.[3,11] In contrast, many type II chemokines can bind several receptors, indicating the diminished role of specificity at the N-loop. For instance, vMIP-II is known to bind CCR1, CCR2, CCR3, CCR5, and CXCR4 (a function that is realized by the N-loop), whereas it activates only CCR3.

Furthermore, by constructing N-terminal peptides of SDF-1 only [SDF-1(1–8) and SDF-1(1–9)], it has been demonstrated that the peptides do not assume the conformations necessary for binding to the receptor.[13] This implies that the protein scaffold, and more specifically,

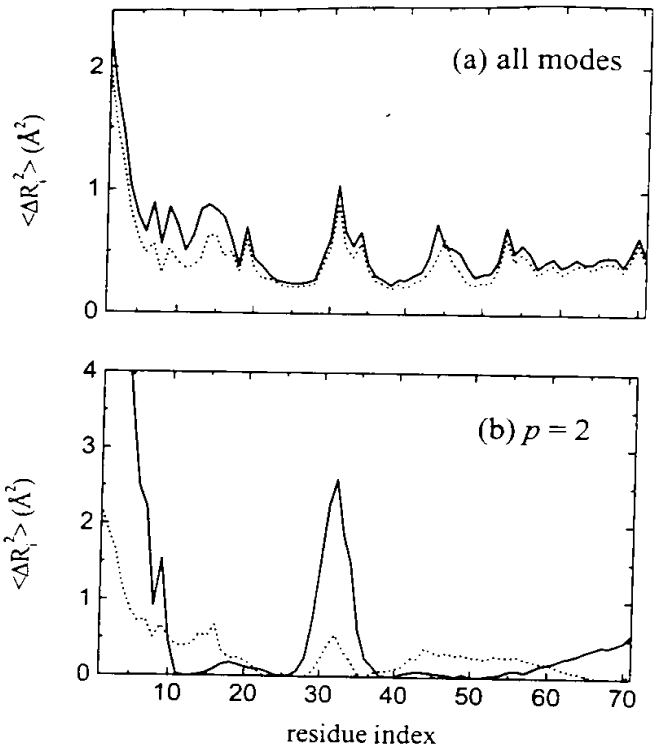

Fig. 6. Comparison of mean square fluctuations of α-carbons, $\langle \Delta \mathbf{R}^2 \rangle$, for IL-8 dimer in unbound form and in complex with a fragment of CXCR1 receptor (PDB codes 1il8 and 1ilq, respectively). **a:** The contribution of all modes present; a restriction in only the motion of the N-loop directly located at the binding interface is observed. **b:** The collective motions (p = 2 in eq. 3) are considered; a dampening in the N-terminus and 30s-loop autocorrelations occur, indicating that these regions, although located far from the binding interface, contribute to the binding mechanism.

interactions with the 30s-loop may be important for determining the optimal conformation of the N-terminal region for binding to the receptor. Another piece of evidence supporting this view comes from analysis of the only known structure of a chemokine in complex with a receptor fragment. This belongs to the N-terminal peptide of CXCR1 in complex with IL-8 (PDB code: 1ilq),[40] where the receptor fragment binds to the groove between the N-loop and the β3-strand, and the N-terminus and 30s-loop are distant. Our calculations have shown that the N-terminus and the 30s-loop have not lost their overall flexibility in the bound form (Fig. 6a), as would be expected, as these regions are remotely located to the binding groove. This is in contrast to the behavior of the N-loop located at the binding interface, which somewhat looses its flexibility upon binding. The β3-strand that is restricted by a network of hydrogen bonds has limited mobility in bound and unbound forms. Conversely, atomic fluctuations due to low wavelength motions (p = 2 in eq. 3) are characterized by a dampening in all the above-mentioned regions (Fig. 6b), implying that a large amount of cooperativity is lost upon binding. This observation is directly related to the transitivity of interactions discussed in the previous subsection and exemplified by the ^{15}N NMR relaxation experiments conducted by Olejniczak et al.[41] They have demonstrated on phosphotyrosine binding domain of the insulin receptor substrate complexed to a tyrosine-phosphorylated peptide that some residues that are remotely located at the binding interface may still lose their mobility upon binding.

These observations call for monitoring the binding and activity of different types of chemokine proteins, whose most flexible parts are specifically designed by hybrida... The following conjecture must be the motivation behind the pioneering experimental studies:[3,9,11,13,14,36,38] Since the chemokine family seemingly has the same scaffold with carefully selected mutations/chimeras, one should in principle be able to make chemokine proteins bind/activate each other's receptor. In the present study, we propose further that to be interconvertible, the proteins must initially reveal the same mechanism, that is, they must exhibit the same convoluted interactions. SDF-1, GRO, and IL-8 all have type I framework and, for this reason, the chimeras of GRO may be substituted for SDF-1 functionality,[13] IP-10 for IL-8,[3] and GRO for IL-8 or IL-8 for GRO.[11] Note that these studies are pertinent to type I mechanism and they show that the communicating structural parts and specificity are the two indispensable ingredients of protein function. These results with additional experiments on proteins that belong to type II interactions, as well as those that belong to the CC family but that exhibit a type I mechanism, may suggest that satisfying the underlying structural mechanism is a prerequisite.

We also note that although the remaining mechanism types defining the interactions between the N-terminus, N-loop, and 30s-loop, i.e., (+,+,+) and (+,−,−) combinations, are not observed among the chemokines investigated in this work, they cannot be ruled out. However, both demand a positive correlation between the N-loop and the N-terminus. This implies that they must concertedly interact with various parts of the receptor. Thus, both scenarios are highly unlikely, since the former presumes a perfect coordination between these highly flexible parts, and the latter ignores the modulating role of the 30s-loop altogether, relying heavily on specificity.

CONCLUSIONS

A low-resolution model that monitors the collective motions in proteins[19] is used to elucidate the structural mechanisms for biological activity of the proteins in the chemokine family based on the analysis of 16 chemokines. Since the model used in this report relies on deriving dynamics information from structural data, the findings are supported by MM and MD calculations performed on the detailed structures of selected proteins solvated in water. Mainly, we observe a collaborative effort among three flexible regions—the N-terminus, N-loop, and 30s-loop—during binding and activity. There has been some debate in literature on the role of the 30s-loop in chemokine dynamics. In the present study, we demonstrate the

importance of this highly flexible region and identify how it is used. It is not directly involved in the protein function and has similar overall mobility in all the chemokines. Only when the contributions to the collective (low wavelength) motions are considered does its role in both dimerization and binding/activity become apparent.

Two mechanisms are proposed for chemokine binding and activity to transmembrane receptors. In type I, the N-loop does the initial binding due to specificity, and the 30s-loop later assists N-terminus affiliation with the receptor. In type II, the 30s-loop aids the binding of the N-loop, and activation is achieved by the flexible N-terminus due to specific interactions with the receptor. Note that in each case the 30s-loop is a source of external force that diminishes the importance of specificity between residues at the binding interface. It should be pointed out that the methods used in this work provide a means of measuring the amount of correlations between regions within the proteins, but falls short of pointing out the sequence of events. Nevertheless, from the wealth of experimental data, it seems likely that in either mechanism the N-loop makes an initial contact with the receptor, followed by that of the N-terminus.

The combination of structural and mutagenesis data should contribute to the development of effective therapies against chronic microphage-mediated inflammatory diseases. The design of chimeras is a widely used method to probe structure–activity relationships in various chemokines. The present approach provides a systematic analysis of the regions involved in collaborative motions. We underline the fact that a successful hybrid should involve residues in the N-terminus, N-loop, and the 30s-loop, as long as the two proteins belong to the same mechanism type. The structural differences in the core regions are reflected in the distinct mechanisms displayed by each type. Thus, it is possible to achieve the more ambitious goal of constructing successful hybrids between types, only when further specific mutations in the core region, that interconvert the scaffold without sacrificing the stability, are made. However, the coarse-grained approach used in the present study prevent us from commenting on specificity; namely, the precise residues required. Moreover, point mutations at key residues that completely destroy the binding/activation mechanisms[10,12] cannot be elucidated by the current approach.

It is obvious that neither the large N-loop nor the highly extended N-terminus is free to explore the vast amount of conformational space accessible to peptides of this length, since the first ~20 residues of chemokines directly involved in protein function are not sufficient for performance. Possibly, this fragment is fluctuating between a few conformations including that of the bound form, such that when the chemokine approaches the receptor, the correct conformation is quickly attained.[4] This dynamic equilibrium is maintained by the scaffold formed by the protein core and the correlated fluctuations in the 30s-loop. As also corroborated by Mizoue et al.,[18] some conformational flexibility should be required for residues involved in ligand–receptor interactions to accommodate a complementary binding surface. Dynamics information that come from either experimental or theoretical sources is useful mainly for identifying regions of proteins involved in binding. The fact that residues that do not make direct contacts with the ligand may still become motionally restricted upon binding[41] point to the transitivity of interactions, explored in this study. The role of flexibility in proteins may be discerned, once a relationship between such dynamic data and binding is established.

REFERENCES

1. Baggiolini M. Chemokines and leukocyte traffic. Nature 1998;392: 565–568.
2. Mellado M, Rodriguez-Frade JM, Vila-Coro AJ, de Ana AM, Martinez AC. Chemokine control of HIV-1 infection. Nature 1999;400:723–724.
3. Clark-Lewis I, Dewald B, Loetscher M, Moser B, Baggiolini M. Structural requirements for interleukin-8 function identified by design of analogs and CXC chemokine hybrids. J Biol Chem 1994;269:16075–16081.
4. Crump MP, Spyracopoulos L, Lavigne P, Kim K-S, Clark-Lewis I, Sykes BD. Backbone dynamics of the human CC chemokine eotaxin: fast motions, slow motions, and implications for receptor binding. Protein Sci 1999;8:2041–2054.
5. Rajarathnam K, Sykes BD, Kay CM, et al. Neutrophil activation by monomeric interleukin-8. Science 1994;264:90–92.
6. Rajarathnam K, Clark-Lewis I, Sykes BD. ^{1}H NMR solution structure of an active monomeric interleukin-8. Biochemistry 1995;34:12983–12990.
7. Handel TM, Domaille PJ. Heteronuclear NMR assignments and solution structure of the monocyte chemoattractant protein-1 (MCP-1) dimer. Biochemistry 1996;35:6569–6584.
8. Rajarathnam K, Kay CM, Dewald B, et al. Neutrophil-activating peptide-2 and melanoma growth-stimulatory activity are functional as monomers for neutrophil activation. J Biol Chem 1997; 272:1725–1729.
9. Paavola CD. Monomeric monocyte chemoattractant protein-1 (MCP-1) binds and activates the MCP-1 receptor CCR2B. J Biol Chem 1998;273:33157–33165.
10. Laurence JS, Blanpain C, Burgner JW, Parmentier M, LiWang PJ. CC chemokine MIP-1β can function as a monomer and depends on Phe13 for receptor binding. Biochemistry 2000;39: 3401–3409.
11. Lowman HB, Slagle PH, DeForge LE, et al. Exchanging interleukin-8 and melanoma growth-stimulating activity receptor binding specificities. J Biol Chem 1996;271:14344–14352.
12. Pakianathan DR, Kuta EG, Artis DR, Skelton NJ, Hebert CA. Distinct but overlapping epitopes for the interaction of a CC-chemokine with CCR1, CCR3, and CCR5. Biochemistry 1997;36: 9642–9648.
13. Crump MP, Gong J-H, Loetscher P, et al. Solution structure and basis for functional activity of stromal cell-derived factor-1: dissociation of CXCR4 activation from binding and inhibition of HIV-1. EMBO J 1997;16:6996–7007.
14. Lowman HB, Fairbrother WJ, Slagle PH, et al. Monomeric variants of IL-8: effects of side chain substitutions and solution conditions upon dimer formation. Protein Sci 1997;6:598–608.
15. Gong J-H, RANTES and MCP-3 antagonists bind multiple chemokine receptors. J Biol Chem 1996;271:10521–10527.
16. Laurence JS, LiWang AC, LiWang PJ. Effect of N-terminal truncation and solution conditions on chemokine dimer stability: nuclear magnetic resonance structural analysis of microphage inflammatory protein 1β mutants. Biochemistry 1998;37:9346–9354.
17. Liwang AC, Cao JJ, Zheng H, Lu Z, Peiper SC, LiWang PJ. Dynamics study of the anti-human immunodeficiency virus chemokine viral microphage-inflammatory protein-II (VMIP-II) reveals a fully monomeric protein. Biochemistry 1999;38:442–453.
18. Mizoue LS, Bazan JF, Johnson EC, Handel TM. Solution structure of the CX_3C Chemokine domain of fractalkine and its interaction with an N-terminal fragment of CX_3CR1. Biochemistry 1999;38:1402–1414.
19. Bahar I, Atilgan AR, Erman B. Direct evaluation of thermal

fluctuations in proteins using a single parameter harmonic potential. Fold Design 1997;2:173–181.
20. Bahar I, Atilgan AR, Demirel MC, Erman B. Vibrational dynamics of folded proteins: significance of slow and fast modes in relation to function and stability. Phys Rev Lett 1998;80:2733–2736.
21. Bahar I, Erman B, Jernigan RL, Atilgan AR, Covell DG. Collective dynamics of HIV-1 reverse transcriptase: examination of flexibility and enzyme function. J Mol Biol 1999;285:1023–1037.
22. Demirel MC, Atilgan AR, Jernigan RL, Erman B, Bahar I. Identification of kinetically hot residues in proteins. Protein Sci 1998;7:2522–2532.
23. Keskin O, Jernigan RL, Bahar I. Proteins with similar architecture exhibit similar large-scale dynamic behavior. Biophys J 2000;78:2093–2106.
24. Hinsen K. Analysis of domain motions by approximate normal mode calculations. Proteins 1998;33:417–429.
25. Hinsen K, Thomas A, Field MJ. Analysis of domain motions in large proteins. Proteins 1999;34:369–382.
26. Kitao A, Go N. Investigating protein dynamics in collective coordinate space. Curr Opin Struct Biol 1999;9:164–169.
27. Go N, Noguti T, Nishikawa T. Dynamics of a small protein in terms of low-frequency vibrational modes. Proc Natl Acad Sci USA 1983;80:3696–3700.
28. Frauenfelder H, McMahon B. Dynamics and function of proteins: the search for general concepts. Proc Natl Acad Sci USA 1998;95:4795–4797.
29. Halilioglu T, Bahar I, Erman B. Gaussian dynamics of folded proteins. Phys Rev Lett 1997;79:3090–3093.
30. Dauber-Osguthorpe P, Roberts VA, Osguthorpe DJ, Wolff J, Genest M, Hagler AT. Structure and energetics of ligand binding to proteins: *Escherichia coli* dihydrofolate reductase-trimethoprim, a drug-receptor system. Proteins 1988;4:31–47.
31. Abola EE, Bernstein FC, Bryant SH, et al., eds. Bonn: Data Commission of the International Union of Crystallography; 1987. p 107.
32. Bernstein FC, Koetzle TF, Williams GJB, et al. The protein data bank: a computer based archival file for macromolecular structures. J Mol Biol 1977;112:535–542.
33. Berendsen HJC, Postma JPM, van Gunsteren WF, DiNola A, Haak JR. Molecular dynamics with coupling to an external bath. J Chem Phys 1984;81:3684–3690.
34. Doruker P, Atilgan AR, Bahar I. Dynamics of proteins predicted by molecular dynamics simulations and analytical approaches: application to α-amylase inhibitor. Proteins 2000;40:512–524.
35. Qian YQ, Johanson KO, McDevitt P. Nuclear magnetic resonance solution structure of truncated human GROβ [5–73] and its structural comparison with CXC chemokine family members GROα and IL-8. J Mol Biol 1999;294:1065–1072.
36. Liwang AC, Wang Z-X, Sun Y, Peiper SC, Liwang PJ. The solution structure of the anti-HIV chemokine vMIP-II. Protein Sci 1999;8:2270–2280.
37. Grasberger BL, Gronenborn AM, Clore GM. Analysis of the backbone dynamics of interleukin-8 by ^{15}N relaxation measurements. J Mol Biol 1993;230:364–372.
38. Crump MP, Rajarathnam K, Kim K-S, Clark-Lewis I, Sykes BD. Solution structure of eotaxin, a chemokine that selectively recruits eosinophils in allergic inflammation. J Biol Chem 1998;273:22471–22479.
39. Leong SR, Lowman HB, Liu J, et al. IL-8 single chain homodimers and heterodimers: interactions with the chemokine receptors CXCR1, CXCR2, and DARC. Protein Sci 1997;6:609–617.
40. Skelton NJ, Quan C, Reilly D, Lowman H. Structure of a CXC chemokine-receptor fragment in complex with interleukin-8. Structure 1999;7:157–168.
41. Olejniczak EJ, Zhou M-M, Fesik SW. Changes in the NMR derived motional parameters of the insulin receptor substrate 1 phosphotyrosine binding domain upon binding to an interleukin 4 receptor phosphopeptide. Biochemistry 1997;36:4118–4124.
42. Lubkowski J, Bujacz G, Boque L, Domaille PJ, Handel M, Wlodawer A. The structure of MCP-1 in two crystal forms provides a rare example of variable quaternary interactions. Nat Struct Biol 1997;4:64–69.
43. Kim KS, Rajarathnam K, Clark-Lewis I, Sykes BD. Structural characterization of a monomeric chemokine: monocyte chemoattractant protein-3. FEBS Lett 1996;395:277–282.
44. Sticht H, Escher SE, Schweimer K, Forsmann WG, Rosch P, Adermann K. Solution structure of the human CC chemokine 2: a monomeric representative of the CC chemokine subtype. Biochemistry 1999;38:5995–6002.
45. Skelton NJ, Aspiras F, Ogez J, Schall TJ. Proton NMR assignments and solution conformation of Rantes, a chemokine of the CC type. Biochemistry 1995;34:5329–5342.
46. Lodi PJ, Garrett DS, Kuscewski J, et al. Solution structure of the chemokine HMIP-1β/ACT-2 by multidimensional NMR: a novel chemokine dimer. Science 1994;263:1762–1767.
47. Shao W, L. F. Jerva, West J, Lolis E, Schweitzer BI. Solution structure of murine macrophage inflammatory protein-2. Biochemistry 1998;38:8303–8313.
48. Kim KS, Clark-Lewis I, Sykes BD. Solution structure of Gro melanoma growth stimulary activity determined by NMR spectroscopy. J Biol Chem 1994;269:32909–32915.
49. Malkowski MG, Wu JY, Lazar JB, Johnson PH, Edwards BFP. The crystal structure of recombinant human neutrophil-activating peptide-2 (M6L) at 1.9 Å resolution. Biochemistry 1995;270:7077–7087.
50. St Charles R, Walz DA, Edwards BFP. The three dimensional structure of bovine platelet factor 4 at 3.0 Å resolution. J Biol Chem 1989;264:2092–2099.

Structure-activity relationships of chemokines

Ian Clark-Lewis,* Key-Sun Kim,† Krishnakumar Rajarathnam,† Jiang-Hong Gong,* Beatrice Dewald,‡ Bernhard Moser,‡ Marco Baggiolini,‡ and Brian D. Sykes†

*The Biomedical Research Centre and Department of Biochemistry and Molecular Biology, The University of British Columbia, Vancouver, British Columbia, Canada; †The Protein Engineering Network of Centres of Excellence and Department of Biochemistry, The University of Alberta, Edmonton, Canada; ‡The Theodor-Kocher Institute, University of Bern, Bern, Switzerland

Abstract: Structural analysis of chemokines has revealed that the α/β structural-fold is highly conserved among both the CXC and CC chemokine classes. Although dimerization and aggregation is often observed, the chemokines function as monomers. The critical receptor binding regions are in the NH_2-terminal 20 residues of the protein and are the least ordered in solution. The flexible NH_2-terminal region is the most critical receptor binding site and a second site also exists in the loop that follows the two disulfides. The well-ordered regions are not directly involved in receptor binding but, along with the disulfides, they provide a scaffold that determines the conformation of the sites that are critical for receptor binding. These general requirements for function are common to all the chemokines. For the CC chemokines, receptor activation and receptor binding regions are separate within the 10 residue NH_2-terminal region. This has allowed identification of high affinity analogs that do not activate the receptor and are potent antagonists. *J. Leukoc. Biol.* **57: 703–711; 1995.**

Key Words: protein engineering • inflammation · interleukin-8 • monocyte chemoattractant protein • peptide synthesis

BACKGROUND

The chemoattractant cytokines (chemokines) are a super family of proinflammatory mediators that promote the recruitment of multiple lineages of leukocytes and lymphocytes [1]. They can be released by many different types of tissue cells, and, in some cases platelets, after activation. Continuous local release of chemokines at sites of inflammation could mediate the ongoing migration of effector cells in chronic inflammation. Chemokines have been strongly implicated in a wide range of human acute and chronic inflammatory diseases, including arthritis, respiratory diseases, and arteriosclerosis [2]. Experiments using blocking antibodies suggest that chemokines can be responsible for cellular infiltration and pathology of model diseases [3, 4].

The human chemokine polypeptides are 70–80 residues in length that share substantial sequence similarity (24% or higher identity) (**Fig. 1**). Alignment of the sequences indicates that they can be classified into two families, one with the first two cysteines separated by one residue (C-X-C chemokines) and the other with the first two cysteines adjacent (C-C chemokines). The remaining two cysteines are conserved. Furthermore, sequence comparisons suggest that they will share some similarity in tertiary structure. The similarity in chemokine genes suggests that they arose by duplication of an ancestral gene. The C-X-C chemokine genes are clustered on chromosome 4 and the C-C chemokine genes are found on chromosome 17, with the translocation possibly indicating the point of divergence of the two gene families [1]. The two chemokine families can also be distinguished functionally. The C-X-C chemokines stimulate predominately neutrophils, except for platelet factor 4(PF4) and γ-interferon inducible protein (IP10). The function of PF-4 and IP10 is uncertain and their membership of the C-X-C chemokine family is based on sequence similarity (Fig. 1). The C-C chemokines are functionally distinct from the C-X-C chemokines in that they do not affect neutrophils and generally stimulate multiple cell types: their targets include monocytes, lymphocytes, basophils, and eosinophils.

The molecular targets for chemokines are their cell surface receptors. The neutrophil receptors for the C-X-C chemokines have been identified by using interleukin-8 (IL-8) as the ligand. IL-8 receptor 1 (IL-8R1) has high affinity only for IL-8, whereas IL-8 receptor 2 (IL-8R2) has high affinity for IL-8 and all the other neutrophil-stimulating C-X-C chemokines tested [5–7]. Both receptors were functional when expressed in a T lymphoma cell line (Jurkat) [8], however, their individual contribution to the response of neutrophils to C-X-C chemokines has not been assessed. For the C-C chemokines, two distinct receptors have been characterized, one that binds macrophage inflammatory protein (MIP)-1α and RANTES [9, 10] and two variants of a receptor that binds monocyte chemotactic protein-1 (MCP)-1 [11]. Functional and receptor binding studies imply the existence of additional receptors with distinct specificity [12]. Given the complexity of chemokine functions and the diversity of the broader chemokine-related receptor family, the existence of other receptors seems certain [13].

STRUCTURE

Summary of current knowledge

Until very recently, IL-8 was the only high-resolution human chemokine structure known. The IL-8 structure, as

Abbreviations: IL-8, interleukin-8; IL-8R, IL-8 receptor; MIP, macrophage inflammatory protein; MGSA, melonoma growth stimulatory activity; MCP, monocyte chemoattractant protein; PF4, platelet factor 4; IP10, γ-interferon inducible protein.

Reprint requests: Ian Clark-Lewis, The Biomedical Research Centre, UBC, Vancouver, BC, V6T 1Z3, Canada.

Received January 10, 1995; accepted January 20, 1995.

```
CXC FAMILY
IL-8       AVLPRSAKELRCQCIKTYSKPFHPKFIKELRVIESGPHCANTEIIVKLSD-GRELCLDPKENWVQRVVEKFLKRAENS
NAP-2            AELRCMCIKTTS-GIHPKNIQSLEVIGKGTHCNQVEVIATLKD-GRKICLDPDAPRIKKIVQKKLAGDESAD
MGSA/GROα    ASVATELRCQCLQTLQ-GIHPKNIQSVNVKSPGPHCAQTEVIATLKN-GRKACLNPASPIVKKIIEKMLNSDKSN
      GROβ    APLATELRCQCLQTLQ-GIHLKNIQSVKVKSPGPHCAQTEVIATLKN-GQKACLNPASPMVKKIIEKMLKNGKSN
      GROγ    ASVVTELRCQCLQTLQ-GIHLKNIQSVNVRSPGPHCAQTEVIATLKN-GKKACLNPASPMVQKIIEKILNKGSTN
ENA78    AGPAAAVLRELRCVCLQTTQ-GVHPKMISNLQVFAIGPQCSKVEVVASLKN-GKEICLDPEAPFLKKVIQKILDGGNKEN
PF-4       EAEEDGD-LQCLCVKTTS-QVRPRHITSLEVIKAGPHCPTAQLIATLKN-GRKICLDLQAPLYKKIIKKLLES
γIP-10           SRTVRCTCISISNQPVNPRSLEKLEIIPASQFCPRVEIIATMKKKGEKRCLNPESKAIKNLLKAVSKEMSKRSP

CC FAMILY
MCP-1      QPDAINAPVTC-CYNFTNRKISVQRLASYRRIT-SSKCPKEAVIFKTIV-AKEICADPKQKWVQDSMDHLDKQTQTPKT
MCP-2      QPDSVSIPITC-CFNVINRKIPIQRLESYTRIT-NIQCPKEAVIFKTKR-GKEVCADPKERWVRDSMKHLDQIFQNLKP
MCP-3      QPVGINTSTTC-CYRFINKKIPKQRLESYRRTT-SSHCPREAVIFKTKL-DKEICADPTQKWVQDFMKHLDKKTQTPKL
RANTES      SPYSSDTTPC-CFAYIARPLPRAHIKEY-FYT-SGKCSNPAVVFVTRK-NRQVCANPEKKWVREYINSLEMS
MIP-1α     ASLAADTPTAC-CFSYTSRQIPQNFIADY-FET-SSQCSKPGVIFLTKR-SRQVCADPSEEWVQKYVSDLELSA
MIP-1β     APMGSDPPTAC-CFSYTARKLPRNFVVDY-YET-SSLCSQPAVVFQTKR-SKQVCADPSESWVQEYVYDLELN
I309          MQVPFSRC-CFSFAEQEIPLRAILCY-RNT-SSICSNEGLIFKLKR-GKEACALDTVGWVQRHRKMLRNCPSKRK
```

Fig. 1. Alignment of human chemokine sequences.

determined by both NMR spectroscopy [14] and X-ray diffraction techniques [15], was a noncovalent homodimer. Each monomer has a disordered NH_2-terminal, a loop region, three antiparallel β-strands, and a COOH-terminal α-helix. In the dimer the β-strands form a six-stranded β-sheet with the helices transversing the dimer interface (**Fig. 2**). The recent crystal structure of human PF-4 indicates that it is a tetramer and the fold of the monomeric subunit is similar to that of IL-8 [16]. For the C-C chemokines, MIP-1β is the only structure that has been completely solved [17]. The backbone trace of the MIP-1β monomer is very similar to that of IL-8, despite the difference in dimerization, the low pH used, and the altered positions of the first two cysteines in the sequence.

A crucial finding from all the structural studies thus far is that the C-X-C and C-C chemokines have strikingly similar monomeric folds. Thus, when the polypeptides are compared, they all have a flexible NH_2-terminal region followed by a loop, three antiparallel β-strands, and a single COOH-terminal α-helix (Fig. 2).

GROa/melonoma growth stimulatory activity structure (MGSA)

GROα/MGSA is a chemoattractant for neutrophils, however, unlike IL-8, it binds with high affinity only to IL-8R2 and not IL-8R1 [6, 7]. To help understand the structural basis for the receptor selectivity and other reported activities of GROα/MGSA, we determined the three-dimensional structure of chemically synthesized GROα/MGSA by ^1H NMR spectroscopy [18]. GROα/MGSA has a dimeric fold similar to IL-8, although there are some regions with conformational differences, including the ELR motif and NH_2-terminal loop region (Fig. 2). The secondary structural regions of the GROα/MGSA monomer backbone superimposed on IL-8 with a 1.2-Å root mean square deviation. In the dimer the relationship between the monomers is slightly different, such that the helices are closer together. In this respect, the structure was more similar to the IL-8 crystal structure than to the IL-8 NMR structure. The interdimer interactions are weaker than for IL-8, implying a higher dimer dissociation constant. Another group also determined the structure of recombinant GROα/MGSA by NMR [19] and it is almost identical to that of synthetic GROα/MGSA [18]. For GROα/MGSA and IL-8, the structures of both synthetic and recombinant proteins are virtually identical [14, 18–20], suggesting that both approaches to obtaining protein for structural and functional studies are valid.

Dimerization

Monomers versus dimers

The compact, symmetrical nature of the familiar IL-8 dimer structure led to the widespread presumption that the dimer form must be important for function. This notion is extended further by the finding that MIP-1β has an entirely different mode of dimerization. Thus, it has been suggested that all the C-X-C chemokines have the six-stranded β-sheet dimer, whereas all the C-C chemokines have an end-on-end dimer structure and, moreover, that this structural difference may account for the functional differences between the two families.

Here we present the case for the opposite view: that the functional form is the monomer and dimerization is not relevant for interaction with the functional receptor. The

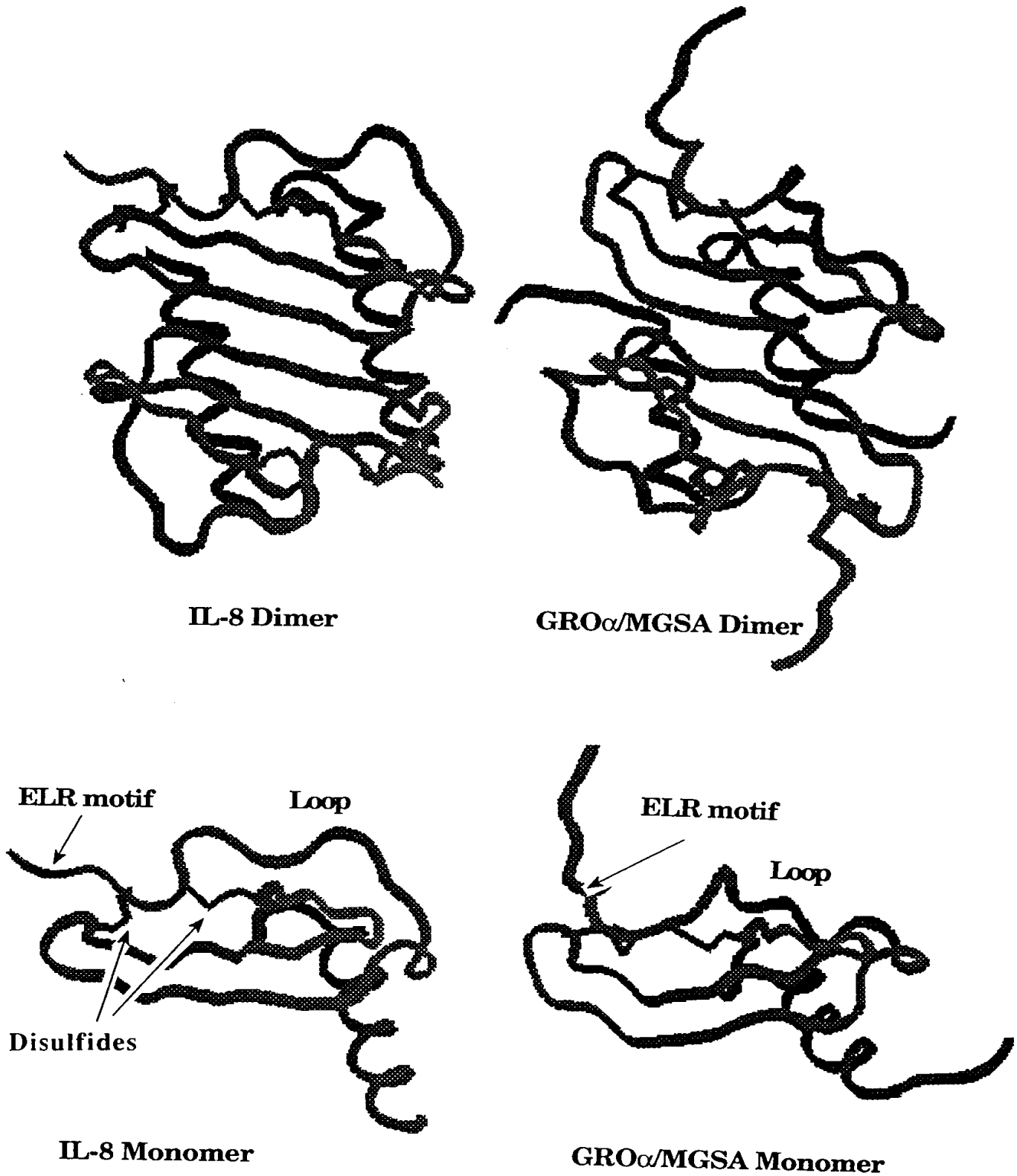

Fig. 2. The IL-8 dimer and a single subunit of the dimer, GROα/MGSA dimer, and single subunit of the dimer.

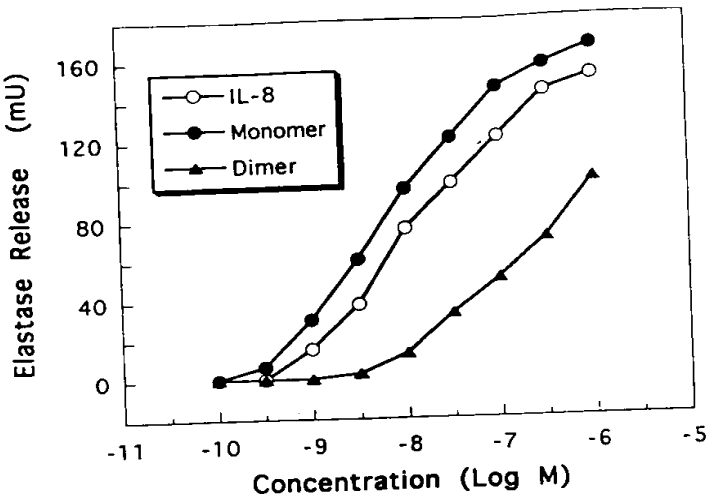

Fig. 3. The neutrophil elastase release activity of native IL-8 4-72 (○) disulfide-linked dimer (R26L)(▲) and the IL-8 monomer (L25NMe)(●). Release was assayed as described elsewhere [36].

rationale for the monomer hypothesis is twofold: (1) ligands for the G protein-coupled seven transmembrane receptors are mostly small peptides or nonpeptide hormones and mediators, therefore the binding site of the structurally similar chemokine receptors is unlikely to accommodate chemokine dimers and (2) by necessity, protein structures are determined at high concentration (>1 mM), and thus the thermodynamics will strongly favor dimerization. In contrast, the functional concentrations of chemokines are 0.1–100 nM, i.e., at least 10,000-fold lower.

A functional IL-8 monomer

To test the hypothesis that IL-8 functions as a monomer, we designed and synthesized a monomeric analogue [21]. A single polypeptide backbone modification, an *N*-methyl leucine instead of leucine at position 25, was made to prevent association of the monomers. Sedimentation equilibrium and NMR studies verified that the analogue remained a monomer even at millimolar concentrations. The monomer was fully active in receptor binding and in vitro functional assays. Thus, the synthesized analogue was both monomeric and in vitro a fully functional ligand.

Covalent dimers of IL-8

To further understand the role of the dimer we designed a stable disulfide-bridged dimer, in addition to the stable monomer described above. Because of the antiparallel arrangement of the subunits, the only residue in the polypeptide that could be substituted to give a single disulfide-bridged dimer was *Arg26*. Fortunately, our substitution analogues indicated that *Arg26* was not required for function [22]. The (R26C) IL-8 was functional, although 15-fold less potent than IL-8 (**Fig. 3**). The lower potency of the dimer could be due to additional structural constraints caused by the introduced disulfide. On the other hand, if the normal ligand is a monomer, dimerization could reduce binding and/or receptor activation. Native IL-8 has been cross-linked as a dimer on the receptor [23], although this does not address the possibility that the initial binding and receptor-activating form is the monomer, which can subsequently form dimers that are then cross-linked.

Implications of the monomer analogue for receptor interactions of native IL-8

Our stable monomer analogue results unequivocally demonstrate that IL-8 can function as a monomer. The experiment with the analogue does not rule out the possibility that native IL-8 may be able to function both as a monomer and as a dimer. However, our sedimentation studies suggest that native IL-8 does dissociate (K_d 10 μM) and monomers predominate at physiological concentrations. Other physical studies [24] using sedimentation, fluorescence, and calorimetry also revealed similar dissociation kinetics (K_d 21 and 18 μM, respectively). It might be argued that the local IL-8 concentrations at the functional cell surface receptor are enhanced by secondary interactions with nonfunctional binding molecules, resulting in "presentation" of the dimer form. However, as yet there is no experimental evidence that the dimerization is necessary for interaction with ancillary binding molecules. The simplest explanation of our findings and those of others is that the active form is the monomer.

Nevertheless, it is useful to discuss various ligand-receptor interaction models given that native IL-8 and most other chemokines have a tendency to dimerize. One possibility is that the receptor activation needs the dimer but that the two monomers bind separately. However, our results with the monomeric analogue argue against reformation of the IL-8 dimer on the receptor because the same mechanisms that prevent dimerization in solution would also prevent association on the receptor. A study of the binding interactions between a peptide corresponding to the NH_2-terminal region of IL-8R1 and the IL-8 dimer [26] suggest that one receptor peptide can bind each monomer (see later discussion). Therefore, as there is only one sequence related to the peptide in the whole receptor, it is likely that only one IL-8 subunit can bind at one time. The possibility remains that the receptor binds two separate monomers independently at different sites. However, if this were the case, then IL-8 would be still binding as a monomer and this model would be consistent with our conclusions that IL-8 functions as a monomer. This latter model raises the separate question of the stoichiometry of binding, which has not been fully addressed.

Dimerization of other chemokines

Within the C-X-C chemokine family, GROα/MGSA is a dimer by NMR [18, 19]. Hydrogen exchange studies suggested that the interactions that stabilize the dimer are weaker than those for IL-8. We found that GROα/MGSA had a K_d of 73 μM at pH 5.0 but the K_d was 7.7 μM at pH 7.0, thus illustrating the pH dependence of the subunit interactions. However, GROα/MGSA clearly dissociates into monomers at physiological pH and concentration range. In general, it is likely that the monomer-dimer equilibrium is highly dependent on the experimental conditions. PF-4 [27] and low-affinity PF-4 [28] have been detected as monomers, dimers, and tetramers in solution by NMR, however, the equilibrium favors the monomer forms at lower concentrations. The dissociation constants for the chemokines are summarized in **Table 1.**

The C-C chemokine, MIP-1β, has been detected as an end-on-end dimer by NMR under acidic conditions (pH

TABLE 1. Summary of Dimerization of Chemokines

C-X-C chemokines	
IL-8	K_d 21 μM[a], K_d 18 μM, PBS pH 7.4[b], 10 mM, 100 mM Na phosphate pH 7.0
GROα/MGSA	K_d 73 μM, 100 mM Na acetate, pH 5.0[c]; 7.7 μM, 100 mM Na phosphate, pH 7.0[c]
NAP-2	K_d 100 μM, 100 mM NaCl, 50 mM Na phosphate, pH 7.0[c]
LAPF-4[d]	Monomer favored at concentrations <0 mM, pH 5.5[e]
PF-4	Monomer favored at concentrations 100 mM, pH <5.0[f]
C-C chemokines	
MCP-1	K_d 33 μM[a], 570 μM, 100 mM Na phosphate, pH 6.6[c]
MCP-2	K_d 58 μM, 100 mM Na phosphate, pH 6.6[c]
MCP-3	Monomer[c]
MIP-1α	Aggregates at pH 7.2, reversibly dissociates to monomers[g]
MIP-1β	Aggregates at pH 7.2, is a dimer at pH 2.5[h], dissociates to monomers Kd 40 nM[h]
I-309	Monomer[a]

[a]Paolini et al. [24].
[b]Burrows et al. [25].
[c]Kim, K.-S., Rajarathnam, K., Clark-Lewis, I., Sykes, B.D., and Kay, C.M., unpublished data.
[d]LAPF4, low-affinity platelet factor 4, as with NAP-2, is a proteolytic product of platelet basic protein.
[e]Mayo [27].
[f]Mayo et al. [28].
[g]Patel et al. [29].
[h]Lodi et al. [17].

2.5) [17]. This dimer observed under these conditions dissociated with a K_d of 40 nM. At higher pH, it shows a strong tendency to aggregate. MIP-1α also shows a strong tendency to aggregate but under certain solvent conditions can form stable tetramers or monomers [29]. Equipotent mutants have been prepared that form tetramers, dimers, or monomers [30]. The results suggest that the aggregation of MIP-1α is reversible and that it dissociates into monomers under physiological conditions. We have found that MCP-1 dimerizes at high concentrations, but at pH 6.6 dissociation, as measured by sedimentation equilibrium studies, was apparent at K_d of 570 μM, suggesting that it functions as a monomer. Paolini et al. [24] found that MCP-1 has a K_d of 33 μM; the difference in values is likely to be due to the difference in conditions used for the analysis. The related chemokine MCP-2 was also a dimer and dissociated with a K_d of 58 μM. The truncated MCP-1 analogue, MCP-1 (10-76), was detected as a monomer at all concentrations tested, suggesting that the dimer interactions of native MCP-1 are located at the NH_2-terminal and it may have an end-on-end orientation similar to MIP-1β. Interestingly, if the dimer interface of MCP-1 is analogous to MIP-1β, then it includes a key receptor binding region (see below), raising the question as to whether it is possible for it to be active in the dimer form. It should be noted that both the aggregation states and the concentrations at which dissociation occurs varies considerably according to the conditions used.

However, not all C-C chemokines dimerize. MCP-3 was always a monomer by NMR and sedimentation equilibrium studies. This is the first chemokine to be described that has a monomeric three-dimensional structure in solution. Our finding that MCP-3 is functionally similar to MCP-2 [31], yet the latter forms dimers, suggests that dimerization is not correlated with function. I-309, a weak monocyte chemoattractant, was a monomer with no detectable tendency to dimerize, as determined by sedimentation and other techniques [24].

Does dimerization have a function?

Most of the above studies have been conducted in vitro and there are a number of possible roles for the dimer in vivo. Dimerization could be important for cellular secretion of the molecules, although the finding that some C-C chemokines are always monomers is an argument against this idea. Dimerization could protect the molecules from proteolysis at high concentrations. Several chemokines, particularly in the C-X-C class, have been shown to bind to sulfated glycans and it has been proposed that this generates an immobilized gradient of chemokine on tissue cells and matrix proteins [32]. Currently, the importance of this mechanism or whether dimerization is important for binding to sulfated glycans is unknown. A similar presentation role has been suggested for the Duffy antigen, a nonfunctional and multispecific chemokine receptor [33]. It is also a seven transmembrane receptor, therefore the arguments made for dimer-monomer binding to the functional chemokine receptors are likely to apply. Currently, none of the above arguments suggest a convincing functional role for dimerization.

Why do chemokines dimerize?

In biology, not everything that exists need have an explicit function. Thus, there is no *a priori* reason for dimerization. Even if it is not required for biological activity it is interesting to speculate as to the role of dimerization. The reasons could be purely structural rather than functional. For example, it could be simply an intrinsic tendency of the protein molecules to self-associate in an ordered and symmetrical manner. Thus, dimer formation could simply be thermodynamically favored and have physical but no biological relevance.

Summary

Chemokines are found in a range of aggregation states and this is highly dependent on the experimental conditions. Nevertheless, physical data indicate that all the chemokines are fully dissociated into monomers in their normal functional concentration range. The results of these studies are summarized in Table 1. In general, chemokines have a tendency to dimerize but there is no apparent correlation between dimerization or type of dimer and function. The available evidence indicates that the forms that bind and activate the functional receptors are monomers. Currently, there is no evidence for a biological role for higher order forms and it is possible that dimerization may simply be a thermodynamically favored form.

STRUCTURE-FUNCTION OF C-X-C CHEMOKINES

Background

The aim of our structure-function studies is to understand the ligand requirements for binding and functional activation of the specific cell surface receptors. All of the human C-X-C chemokines, except for PF-4 and IP10, bind

IL-8 receptors and attract and activate neutrophils [1]. IL-8 stimulates the highest maximal response and is the most potent of the C-X-C chemokines, thus our experiments have been performed with the IL-8 as the ligand and neutrophils as the targets.

The IL-8 monomer

The finding that IL-8 functions as a monomer discussed above has important implications for structure-activity relationships. If the dimer was required for activation, then it would be necessary for regions from both halves of the dimer to simultaneously bind the receptor. Thus, the binding surface, i.e., the surface area of ligand-receptor interaction, would be considerably larger and much more complex than if only one subunit was involved. However, because the monomer is sufficient for activity, all the structure-function studies can be interpreted in terms of the folded IL-8 monomer [21].

The ELR motif

All of the results we have obtained with approximately 250 analogues of IL-8 and other C-X-C chemokines point to the ELR motif as the most critical region for interaction with the IL-8R [22, 34, 35]. No other region is anywhere near as sensitive to modification (except for some key individual structural residues). The ELR motif is common in all the C-X-C chemokines that activate neutrophils and bind to IL-8R2 as well as IL-8R1. The ELR region can be modified such that receptor binding is retained but activity is lost. These antagonist analogues, e.g., IL-8 (6-72) and (*Ala4,5*) IL-8 (4-72), have much lower receptor affinity than IL-8, indicating that the ELR motif is both a binding and receptor-activation motif [36]. With the ELR replacements made thus far, loss of functional activity appears necessary for antagonist activity and is coincident with considerably reduced binding affinity [36].

Multiple substitutions showed that all three residues of the ELR motif were highly sensitive to modification, with the order of sensitivity being R>>E>L [35]. Substitution of nonnatural backbone-modified amino acids NMe-Leu and NMe-Arg lowered activity, suggesting that the ELR conformation and side chain integrity is critical. Single D-amino acid substitutions in the ELR motif greatly reduced activity, further suggesting that conformation is important. Adding "spacer" residues, either Gly or Ala, between the ELR and the cysteine at position 7 resulted in loss of activity with some residual binding. Thus, not only the integrity of the ELR was important, but its location relative to the rest of IL-8 was also critical. NMR analysis of several ELR-modified analogues, including some with antagonist activity, indicated that the well-defined regions of the protein structure are the same as native IL-8 [20].

In the IL-8 structure the ELR motif is not restrained in the protein structure and it can adopt multiple conformations [14]. However, it cannot be completely disordered. It is tethered to the first cysteine (*Cys7*) and its conformations clearly must be limited by the 7-34 disulfide and the adjacent 30-35 turn. Furthermore, the 9-50 disulfide increases the rigidity of the Cys-Gln-Cys region, which we predict will affect the possible conformation of the ELR motif and its relationship to the rest of the protein.

The loop region

The loop region, including the connecting loop, 10-17, and the 3:10 turn, 18-22, was generally not affected by single substitutions. However, experiments in which hybrid proteins were made between IL-8 and the inactive C-X-C protein IP10 were informative. The aim of these hybrid analogues was to determine the minimal IL-8 required to activate IP10 [22]. The hybrids demonstrated that this entire region was critical for IL-8 activity. The residues close to the NH_2-terminal end of the loop, i.e., close to cysteine 9, were the most critical. The major difference between the single substitution and hybrid strategies is that the hybrids had multiple replacements. Thus, only when several substitutions were made were significant effects observed. Taken together, the results suggest that the NH_2-terminal loop comprises a secondary binding site.

The 3:10 turn, however, does not appear to be essential, as multiple substitutions in this region failed to affect activity [22]. *Phe21* makes aromatic contacts with *Tyr13, Phe17,* and *Trp57* and may have a structural role. Nevertheless, the possibility that *Phe21* has hydrophobic or aromatic contacts with the receptor cannot be ruled out, but more experiments are required to test this.

In a study measuring changes in structure (chemical shifts) on binding of the IL-8 dimer to a receptor peptide corresponding to the NH_2-terminal of IL-8R1, changes involving many sites were observed [26] and it is instructive to compare the findings with our structure-activity studies. Peptide-IL-8 contacts were observed between *Thr12, Lys15, Phe17, His18, Lys20,* and *Phe21.* We have found that the individual substitution of Ala or Arg for *Lys15,* Leu for *Phe17,* and Phe for *His18* had little or no effect on activity. In the IL-8R1 peptide study interactions were observed between the loop region of IL-8 and also *Glu48, Leu49, Cys50, Ser44,* and *Val61.* Residues 44, 48, and 61 were replaced in hybrids (S44K, E48K, V61K) without loss of activity. *Leu49* shifts were prominent and are of interest because of the proximity of the side chain to the C-X-C region in the three-dimensional structure. To test the role of *Leu49* we synthesized L49A and no difference in activity compared with native was observed, thus suggesting that any hydrophobic contacts involving the receptor and this residue are not crucial for function. However, a L49R analogue was less active, probably due to the introduction of a positively charged group near the C-X-C and ELR motifs.

Overall, the observed IL-8R1 peptide–IL-8 interactions [26] do not correlate well with our structure-activity studies. As the authors indicate the interactions are weak and the NH_2-terminal receptor peptide may not be representative of the receptor. Nevertheless, our results indicating the importance of the NH_2-terminal loop region of IL-8 agree with the receptor peptide-induced chemical shift changes in that region. The latter is also consistent with receptor mutagenesis studies showing that the NH_2-terminal region of the receptor is the determinant of C-X-C chemokine selectivity [5].

The disulfides

When the cysteines that form each disulfide bridge were substituted in pairs with the cysteine isostere, α-aminobutyric acid (side chain CH_2-CH_3), both analogues were inactive and NMR studies showed significant structural perturbation, probably due to loss of the disulfide

[22]. Both disulfides are essential for function, indicated by lack of activity of the two analogues. These results demonstrate that the conformational restrictions imposed by the disulfides are critical for function.

The 30–35 turn

Some residues within the 30–35 turn could be substituted without loss of activity. For example, *His33* was analyzed extensively due to its interaction with the C-X-C region and proximity to the two disulfides and the ELR motif. Various substitutions for *His33* had no effect on activity [22]. NMR studies of the H33A analogue demonstrate that the structural changes were local and included *Cys34*, which is involved in the 7–34 disulfide. There was no difference in the well-ordered structure [20]. Further analogues showed that the *Gly31–Pro32* motif in the 30–35 turn was essential. This motif determines the structure of the 30–35 turn, and, most likely, also the 7–34 disulfide, which would be predicted to influence the conformation of the ELR motif.

Receptor interaction hypothesis

We hypothesize that the IL-8 protein structure, including the two disulfide bridges, acts as a scaffold that controls the conformation of two receptor binding regions: the ELR motif and a region in the 10–17 loop. According to the C5a receptor model [37], the ELR motif would bind site 2, which is buried in among the seven receptor helices, and the loop region would bind site 1 on the surface of the receptor. As ELR-containing peptides do not bind to the receptor, we speculate that binding to site 1 is required to expose the ELR binding site.

STRUCTURE-FUNCTION OF C-C CHEMOKINES

Based on the sequence relatedness of chemokines and our results with analogues, we hypothesized that there would be similarities in the way that C-X-C and C-C chemokines interact with their receptors. Specifically, we speculated that the NH_2-terminal region would be critical and that secondary sites would be necessary.

The role of the NH_2 terminal in MCP-1 activity was investigated by deletion and substitution analogues [38]. The results demonstrated that the NH_2-terminal region was essential for receptor binding and activity. However, instead of just three residues as in the C-X-C chemokines, the entire 10 residues that are NH_2-terminal to the first cysteines were important. A peptide corresponding to residues 1–10 lacked binding and activity, a finding that is consistent with C-X-C chemokine results.

Several unexpected findings were obtained with these analogues [38]. Deletion of the first residue (a pyroglutamate) of MCP-1 markedly decreased activity. This contrasts with the C-X-C chemokines, where the presence of ELRCXC is essential, but residues NH_2-terminal to the ELR motif vary and are not critical. For MCP-1, addition of a residue to the NH_2-terminal or acetylation of the NH_2-terminal glutamine resulted in loss of activity. Surprisingly, analogues with the NH_2-terminal residue converted to Asn (but not *N*-acetylated Asn), or residues with nonpolar side chains of varying size, had equivalent activity to native MCP-1. Thus, the cyclic pyroglutamate was not required. Nevertheless, the integrity of a residue at the NH_2-terminal position is required for full activity.

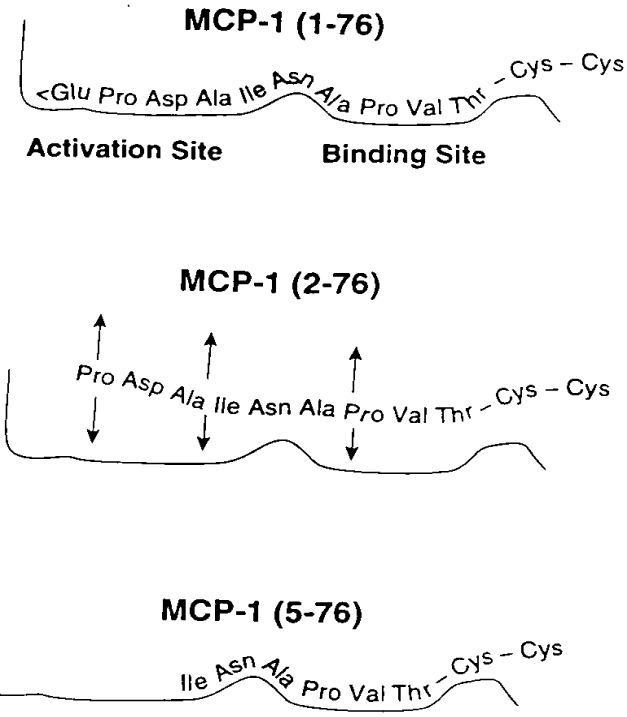

Fig. 4. Model for interaction of MCP-1 analogues with the receptor. An outline of part of the MCP-1 receptor binding pocket, showing activation and binding region. The binding interactions of three MCP-1 analogues: full-length MCP-1 (top), 2–76 (middle), and 5–76 (bottom) are indicated.

These observations suggest that the peptide backbone but not the side chain of residue 1 is critical and interacts with the receptor (**Fig. 4**) in a complementary manner and that the side chain is not involved.

It should be noted that the conversion of glutamine to pyroglutamate is spontaneous, with the equilibrium favoring the latter. Thus, it is not possible to determine whether the glutamine form is biologically active, because during isolation the pyroglutamyl form will be generated. Nevertheless, from our results we would predict that the glutamine form would be equivalent to the pyroglutamate form.

Analogues that had either one, two, or three residues deleted from the NH2-terminal had lower (~150-fold) binding affinity and activity than full-length native MCP-1. However, surprisingly, MCP-1, 5–76 had significant activity and bound to the MCP-1 receptor (K_d 8-fold lower than native MCP-1). The 6–76 analogue was the shortest NH_2-terminally truncated molecule with detectable biological activity. Further deletion resulted in analogues that had significant binding to the receptor but no functional activity. These results are interpreted according to the diagram shown in Figure 4. We propose the existence of an activation region and a receptor binding region that comprise residues 1–6 and 7–10, respectively. According to this model, deletion of NH_2-terminal residues 1–3 caused not only loss of some of the receptor contacts necessary for activation, but also inhibited binding of the 7–10 region. Presumably, the shortened NH_2-terminal region adopts conformations that reduce binding. However, once the NH_2-terminal residues 1–4 are removed, residue 5 from the activation region and residues 7–10 revert to a form that has significant binding and also

activates the receptor (Fig. 4). The results also suggest that *Ile5* is involved in receptor activation.

Several of the truncated analogues bind receptors but have no activity, suggesting that they may be competitive receptor antagonists. MCP-1, 7–76, 8–76, 9–76, 10–76, and 11–76 were all receptor antagonists, the most potent being MCP-1, 9–76, which had an IC_{50} of 20 nM when 5 nM of MCP-1 agonist was used as the stimulus [38]. The MCP-1 antagonists desensitized the calcium response to MCP-receptor ligands but not the response to RANTES, MIP-1α, or MIP-1β. Receptor binding studies confirmed the specificity of the MCP-1 antagonists.

Truncation of the NH_2-terminal region (up to the first cysteine) of MCP-1 resulted in MCP-1, 11–76, which had residual binding activity, suggesting that a second binding site is present elsewhere in the molecule, and this second region binds, although with low affinity, independently of residues 1–10 [38]. This contrasts with the C-X-C chemokines, where truncation of the ELR motif resulted in no receptor binding.

We attempted to transfer the potency and cellular activity of the closely related C-C chemokines MCP-1 and MCP-3 by swapping the NH_2-terminal regions. However, the activity and binding of the resulting hybrids was lower than expected, suggesting that the NH_2-terminal is not sufficient to determine activity, and that the NH_2-terminal binding site and secondary sites complement each other to give maximal binding and activity.

To begin to examine additional MCP-1 binding sites, we showed that *Tyr* 13 and *Tyr* 28 can be converted to phenylalanine without loss of activity. Furthermore, an analogue (Y28L, R30V) MCP-1 was shown to retain MCP-1 activity, although the potency was reduced compared with MCP-1. However, in contrast to published results [39], our analogue lacked activity on neutrophils, thus the reported conversion of MCP-1 from monocyte activity to neutrophil activity was not reproduced. The reasons for this difference are unknown. A more extensive report described MCP-1 NH_2-terminal mutants that had antagonist activity and also some mutants with internal substitutions [40]. The authors interpreted their functional results as supporting an earlier model proposed for IL-8 that involved receptor binding between the two α-helices of the dimer [14]. None of our data for any chemokine are consistent with this hypothesis.

The C-C chemokines were analyzed for the chemotactic activity on monocytes and THP-1 cells. The order of potency was MCP-1, MCP-3, MCP-2, RANTES, MIP-1α, and MIP-1β. Synthetic I-309 lacked detectable activity, in contrast to cell-derived I-309 [41]. It is possible that glycosylation or some other posttranslational modification is responsible for the difference.

We have found that both MCP-3 and MCP-2 stimulate chemotaxis, enzyme release, and intracellular calcium induction in monocytes and THP-1 cells and enzyme release in monocytes. MCP-3 is always the more potent of the two. MCP-3 and MCP-2 appear to be functionally similar and both stimulate basophils, eosinophils, and lymphocytes, as well as monocytes [31, 42]. Thus, in contrast to published findings suggesting a distinct mechanism of action for MCP-2 [43], our results indicate that it is simply a less potent ligand for MCP-3 receptors.

SUMMARY

Based on the close structural similarity of the C-X-C and C-C chemokines and our current knowledge of their structure-activity relationships, we propose that despite the differences noted above, the general mechanism of receptor binding will be similar for both. Thus, the chemokines function as monomers, the primary binding and activation site is located at the NH_2-terminal, and a secondary site is located in the flexible loop region that follows the second cysteine. The tertiary structure provides a scaffold that controls the conformations of these regions so that they can form complementary interactions with the receptor binding site.

ACKNOWLEDGMENTS

This work was supported by the Protein Engineering Network of Centres of Excellence (PENCE) (I.C.-L., K.R., K.-S.K., B.D.S.), The National Institutes of Health RO1 GM-50969 (I.C.-L.), The Arthritis Society (Canada) (I.C.-L.), The National Cancer Institute of Canada (I.C.-L.), and The Swiss National Science Foundation (M.B., B.D., B.M.). We thank Dr. Cyril Kay and his research group for their invaluable advice and assistance in the analytical ultracentrifugation studies. We thank Philip Owen, Peter Borowski, Luen Vo, Jennifer Anderson, and Andrea Blaser for excellent technical assistance and Catherine Davidson-Hall for assistance in preparation of the manuscript.

REFERENCES

1. Baggiolini, M., Dewald, B., Moser, B. (1994) Interleukin-8 and related chemotactic cytokines: CXC and CC chemokines. *Adv. Immunol.* **55,** 97–179.
2. Strieter, R.M., Koch, A.E., Antony, V.B., Fick, R.B., Jr., Standiford, T.J., Kunkel, S.L. (1994) The immunopathology of chemotactic cytokines: the role of interleukin-8 and monocyte chemoattractant protein-1. *J. Lab. Clin. Med.* **123,** 183–197.
3. Sekido, N., Mukaida, N., Harada, A., Nakanishi, I., Watanabe, Y., Matsushima, K. (1993) Prevention of lung reperfusion injury in rabbits by a monoclonal antibody against interleukin-8. *Nature,* **365,** 654–657.
4. Jones, M.L., Mulligan, M.S., Flory, C.M., Ward, P.A., Warren, J.S. (1992) Potential role of monocyte chemoattractant protein 1/JE in monocyte/macrophage dependent IgA immune complex alveolitis in the rat. *J. Immunol.* **149,** 2147–2154.
5. LaRosa, G.J., Thomas, K.M., Kaufmann, M.E., Mark, R., White, M., Taylor, L., Gray, G., Witt, D., Navarro, J. (1992) Amino terminus of the interleukin-8 receptor is a major determinant of receptor subtype specificity. *J. Biol. Chem.* **267,** 25402–25406.
6. Cerretti, D.P., Kozlosky, C.J., Vanden Bos, T., Nelson, N., Gearing, D.P., Beckmann, M.P. (1993) Molecular characterization of receptors for human interleukin-8, gro/melanoma growth-stimulatory activity and neutrophil activating peptide-2. *Mol. Immunol.* **30,** 359–367.
7. Moser, B., Barella, L., Mattei, S., Schumacher, C., Boulay, F., Colombo, M.P., Baggiolini, M. (1993) Expression of transcripts for two interleukin 8 receptors in human phagocytes, lymphocytes, and melanoma cells. *Biochem. J.* **294,** 285–292.
8. Loetscher, P., Seitz, M., Clark-Lewis, I., Baggiolini, M., Moser, B. (1994) Both interleukin-8 receptors independently mediate chemotaxis: Jurkat cells transfected with IL-8R1 or

IL-8R2 migrate in response to IL-8, GROα, and NAP-2. *FEBS Lett.* **341,** 187–192.
9. Gao, J.-L., Kuhns, D.B., Tiffany, H.L., McDermott, D., Li, X., Francke, U., Murphy, P.M. (1993) Structure and functional expression of the human macrophage inflammatory protein 1α/RANTES receptor. *J. Exp. Med.* **177,** 1421–1427.
10. Neote, K., DiGregorio, D., Mak, J.Y., Horuk, R., Schall, T.J. (1993) Molecular cloning, functional expression, and signaling characteristics of a C-C chemokine receptor. *Cell* **72,** 415–425.
11. Charo, I.F., Myers, S.J., Herman, A., Franci, C., Connolly, A.J., Coughlin, S.R. (1994) Molecular cloning and functional expression of two monocyte chemoattractant protein 1 receptors reveals alternative splicing of the carboxyl-terminal tails. *Proc. Natl. Acad. Sci. USA* **91,** 2752–2756.
12. Baggiolini, M., Dahinden, C.A. (1994) CC chemokines in allergic inflammation. *Immunol. Today* **15,** 127–133.
13. Ahuja, S.K., Gao, J.-L., Murphy, P.M. (1994) Chemokine receptors and molecular mimicry. *Immunol. Today* **15,** 281–287.
14. Clore, G.M., Appella, E., Yamada, M., Matsushima, K., Gronenborn, A.M. (1990) Three-dimensional structure of interleukin 8 in solution. *Biochemistry* **29,** 1689–1696.
15. Baldwin, E.T., Weber, I.T., St. Charles, R., Xuan, J.C., Appella, E., Yamada, M., Matsushima, K., Edwards, B.F.P., Clore, G.M., Gronenborn, A.M., Wlodawer, A. (1991) Crystal structure of interleukin 8: Symbiosis of NMR and crystallography. *Proc. Natl. Acad. Sci. USA* **88,** 502–506.
16. Zhang, X., Chen, L., Bancroft, D.P., Lai, C.K., Maione, T.E. (1994) Crystal structure of recombinant human platelet factor 4. *Biochemistry* **33,** 8361–8366.
17. Lodi, P.J., Garrett, D.S., Kuszewski, J., Tsang, M.L.S., Weatherbee, J.A., Leonard, W.J., Gronenborn, A.M., Clore, G.M. (1994) High-resolution solution structure of the β chemokine hMIP-1β by multidimensional NMR. *Science,* **263,** 1762–1767.
18. Kim, K.-S., Clark-Lewis, I., Sykes, B.D. (1994) Solution structure of GRO/MGSA determined by ^{1}H NMR spectroscopy. *J. Biol. Chem.* **269,** 32909–32915.
19. Fairbrother, W.J., Reily, D., Colby, T.J., Hesselgesser, J., Horuk, R. (1994) The solution structure of melanoma growth stimulating activity. *J. Mol. Biol.* **242,** 252–270.
20. Rajarathnam, K., Clark-Lewis, I., Sykes, B.D. (1994) ^{1}H NMR studies of interleukin-8 analogs: characterization of the domains essential for function. *Biochemistry* **33,** 6623–6630.
21. Rajarathnam, K., Sykes, B.D., Kay, C.M., Dewald, B., Geiser, T., Baggiolini, M., Clark-Lewis, I. (1994) Neutrophil activation by monomeric interleukin-8. *Science* **264,** 90–92.
22. Clark-Lewis, I., Dewald, B., Loetscher, M., Moser, B., Baggiolini, M. (1994) Structural requirements for interleukin-8 function identified by design of analogs and CXC chemokine hybrids. *J. Biol. Chem.* **269,** 16075–16081.
23. Schnitzel, W., Monschein, U., Besemer, J. (1994) Monomer-dimer equilibria of interleukin-8 and neutrophil-activating peptide 2. Evidence for IL-8 binding as a dimer and oligomer to IL-8 receptor B. *J. Leukoc. Biol.* **55,** 763–770.
24. Paolini, J.F., Willard, D., Consler, T., Luther, M., Krangel, M.S. (1994) The chemokines IL-8, monocyte chemoattractant protein-1, and I-309 are monomers at physiologically relevant concentrations. *J. Immunol.* **153,** 2704–2712.
25. Burrows, S.D., Doyle, M.L., Murphy, K.P., Franklin, S.G., White, J.R., Brooks, I., McNulty, D.E., Scott, M.O., Knutson, J.R., Porter, D., Young, P.R., Hensley, P. (1994) Determination of the monomer-dimer equilibrium of interleukin-8 reveals it is a monomer at physiological concentrations. *Biochemistry* **33,** 12741–12745.
26. Clubb, R.T., Omichinski, J.G., Clore, G.M., Gronenborn, A.M. (1994) Mapping the binding surface of interleukin-8 complexed with an N-terminal fragment of the Type 1 human interleukin-8 receptor. *FEBS Lett.* **338,** 93–97.
27. Mayo, K.H., Chen, M.-J. (1989) Human platelet factor 4 monomer-dimer-tetramer equilibria investigated by ^{1}H NMR spectroscopy. *Biochemistry* **28,** 9469–9478.
28. Mayo, K.H. (1991) Low affinity platelet factor 4 ^{1}H NMR derived aggregate equilibria indicate a physiologic preference for monomers over dimers and tetramers. *Biochemistry* **30,** 925–934.
29. Patel, S.R., Evans, S., Dunne, K., Knight, G.C., Morgan, P.J., Varley, P.G., Craig, S. (1993) Characterization of the quaternary structure and conformational properties of the human stem cell inhibitor protein I.D78 in solution. *Biochemistry* **32,** 5466–5471.
30. Graham, G.J., MacKenzie, J., Lowe, S., Tsang, M.L-S., Weatherbee, J.A., Issacson, A., Medicherla, J., Fang, F., Wilkinson, P.C., Pragnell, I.B. (1994) Aggregation of the chemokine MIP-1α is a dynamic and reversible phenomenon. *J. Biol. Chem.* **269,** 4974–4978.
31. Weber, M., Uguccioni, M., Ochensberger, B., Baggiolini, M., Clark-Lewis, I., Dahinden, C.A. The monocyte chemotactic protein MCP-2 activates human basophil and eosinophil leukocytes and has functional similarity to MCP-3. *J. Immunol.* In press.
32. Webb, L.M.C., Ehrengruber, M.U., Clark-Lewis, I., Baggiolini, M., Rot, A. (1993) Binding to heparan sulfate or heparin enhances neutrophil responses to interleukin 8. *Proc. Natl. Acad. Sci. USA* **90,** 7158.
33. Horuk, R., Zi-xuan, W., Peiper, S.C., and Hesselgesser, J. (1994) Identification and characterization of a promiscuous chemokine-binding protein in a human erythroleukemic cell line. *J. Biol. Chem.* **269,** 17730.
34. Clark-Lewis, I., Schumacher, C., Baggiolini, M., Moser, B. (1991) Structure-activity relationships of interleukin-8 determined using chemically synthesized analogs. *J. Biol. Chem.* **262,** 23128.
35. Clark-Lewis, I., Dewald, B., Geiser, T., Moser, B., Baggiolini, M. (1993) Platelet factor 4 binds to interleukin 8 receptors and activates neutrophils when its N terminus is modified with Glu-Leu-Arg. *Proc. Natl. Acad. Sci. USA* **90,** 3574.
36. Moser, B., Dewald, B., Barella, L., Schumacher, C., Baggiolini, M., Clark-Lewis, I. (1993) Interleukin-8 antagonists generated by N-terminal modification. *J. Biol. Chem.* **268,** 7125.
37. Siciliano, S.J., Rollins, T.E., DeMartino, J., Konteatis, Z., Malkowitz, L., Van Riper, G., Bondy, S., Rosen, H., Springer, M.S. (1994) Two-site binding of C5a by its receptor: an alternative binding paradigm for G protein-coupled receptors. *Proc. Natl. Acad. Sci. USA* **91,** 1214.
38. Gong, J.-H., Clark-Lewis, I. Antagonists of monocyte chemoattractant protein-1 identified by modification of functionally critical NH_2-terminal residues. *J. Exp. Med.* in press.
39. Beall, C.J., Mahajan, S., Kolattukudy, P.E. (1992) Conversion of monocyte chemoattractant protein-1 into a neutrophil attractant by substitution of two amino acids. *J. Biol. Chem.* **267,** 3455–3459.
40. Zhang, Y.J., Rutledge, B.J., Rollins, B.J. (1994) Structure/activity analysis of human monocyte chemoattractant protein-1 (MCP-1) by mutagenesis. *J. Biol. Chem.* **269,** 15918–15924.
41. Miller, M.D., Krangel, M.S. (1992) The human cytokine I-309 is a monocyte chemoattractant. *Proc. Natl. Acad. Sci. USA* **89,** 2950–2954.
42. Loetscher, P., Seitz, M., Clark-Lewis, I., Baggiolini, M., Moser, B. (1994) The monocyte chemotactic proteins, MCP-1, MCP-2 and MCP-3 are major attractants for human CD4;sp and CD8;sp T lymphocytes. *FASEB J.* **8,** 1055–1060.
43. Sozzani, S., Zhou, D., Locati, M., Rieppi, M., Proost, P., Magazin, M., Vita, N., Van Damme, J., Mantovani, A. (1994) Receptors and transduction pathways for monocyte chemotactic protein-2 and monocyte chemotactic protein-3: similarities and differences with MCP-1. *J. Immunol.* **152,** 3615–3622.

THE JOURNAL OF BIOLOGICAL CHEMISTRY
Vol 269 No 23, Issue of June 10, pp 16075-16081, 1994
Printed in U.S.A.

Structural Requirements for Interleukin-8 Function Identified by Design of Analogs and CXC Chemokine Hybrids*

(Received for publication, December 16, 1993, and in revised form, March 8, 1994)

Ian Clark-Lewis‡§, Beatrice Dewald¶, Marcel Loetscher¶, Bernhard Moser¶, and Marco Baggiolini¶

From the ‡Biomedical Research Centre and Biochemistry and Molecular Biology Department, University of British Columbia, 2222 Health Sciences Mall, Vancouver British Columbia V6T 1Z3, Canada and the ¶Theodor-Kocher Institute, University of Bern, Freiestrasse 1, Bern CH-3000, Switzerland

Structure-activity relationships of human interleukin-8 (IL-8) were probed using chemically synthesized analogs with single or double amino acid substitutions, as well as hybrids derived by substituting IL-8 regions into IP10, a related protein that lacks IL-8 activity. The analogs were tested for functional activity by measuring induction of elastase release from human neutrophils and competition for binding of radiolabeled IL-8. The hybrid studies indicated that Gly^{31} and Pro^{32}, as well as the NH_2-terminal region from IL-8 are required to convert IP10 into a fully functional protein, suggesting that these elements are critical for IL-8 activity. Both disulfide bridges, linking residue 7 to 34 and residue 9 to 50, were critical for function, as shown by substituting the cysteine pairs with α-aminobutyric acid. Single conservative substitutions were generally accepted into the 10–22 region of IL-8, which contrasts with the ELR motif (residues 4–6), previously shown to be essential for activity. The importance of residues within the 10–15 region and the 17–22 region was demonstrated with hybrids. In addition, some of the 4–22 residues have structural roles that may be important; for example, Tyr^{13}, Phe^{17}, and Phe^{21} are involved in aromatic interactions in the IL-8 structure, and are also moderately sensitive to modification. Except for Cys^{50}, the results argue against a role for the 36–72 region, including the COOH-terminal α-helix, in receptor binding. We conclude that the disulfide bridges and 30–35 turn provide a structural scaffold for the NH_2-terminal region which includes the primary receptor-binding site (the ELR motif) and secondary binding and conformational determinants between residues 10 and 22.

Human interleukin-8 (IL-8)[1] is the most studied member of a superfamily of proinflammatory cytokines, many of which are chemoattractants for leukocytes, and which have been termed chemokines (from chemotactic cytokine) (1–3). Chemokines are 70–80-residue proteins with 4 conserved cysteines and are subdivided into two families; one, which includes IL-8, in which the first 2 cysteines are separated by 1 amino acid (CXC chemokines), and the other, in which the first 2 cysteines are adjacent (CC chemokines). Other CXC chemokines are neutrophil-activating peptide-2 (4), the growth-related gene products GRO-α, -β, -γ (5, 6), ENA-78 (7), granulocyte chemotactic protein-2 (8), platelet factor 4 (PF4) (9), and IP10, the product of an interferon-γ-inducible gene (10). With the exception of PF4 and IP10, all the members of the IL-8 family have neutrophil activating properties and induce chemotaxis and granule release (exocytosis). There are two high affinity CXC chemokine receptors, IL-8R1 which has high affinity for IL-8 and low affinity for other family members, and IL-8R2, which has high affinity for IL-8 and other neutrophil-activating CXC chemokines (11–14). Both PF4 and IP10 lack significant IL-8 receptor binding (15, 16) and probably have unrelated functions (17, 18).

NMR studies of IL-8 have shown that it is a homodimer in solution (19). The monomeric unit in the three-dimensional structure reveals a highly flexible NH_2-terminal region followed by three antiparallel β strands and a COOH-terminal α-helix. The dimer is stabilized by formation of a six-stranded antiparallel β sheet (three from each monomer) and by hydrophobic interactions with the overlying helices (19, 20). The structure of IL-8 has also been determined by x-ray diffraction, and although the overall fold is very similar some differences are apparent (20, 21). For example, the NH_2 terminus is more ordered in the x-ray structure, and the two α-helices are closer by 3 Å. The strongest indication of structural relatedness within the IL-8 family comes from the PF4 x-ray structure which has a fold very similar to that of IL-8 (20, 22). PF4 crystallizes as a tetramer, although NMR studies indicate the existence of an equilibrium between monomers, dimers, and tetramers in solution (23). A preliminary NMR study of GROα also suggests structural similarities to IL-8 (24).

We have used chemically synthesized analogs to study structure activity relationships of IL-8 and other CXC chemokines. In an earlier study with truncated analogs, we showed that three NH_2-terminal residues, Glu^4-Leu^5-Arg^6 (ELR motif), of the 72-residue form of IL-8 are essential for activity and receptor binding (25). In contrast, the COOH-terminal α-helix is not essential, as it could be deleted without complete loss of activity (25). A parallel study using alanine mutagenesis also demonstrated the importance of the ELR motif (26). We also synthesized multiple analogs with single replacements in the ELR motif and found that all 3 residues were sensitive to modification (15). An alternative approach was to incorporate the ELR motif into chemokines that are not active on neutrophils. ELR modification conferred activity to PF4, but not to IP10, indicating that the ELR is necessary, but not sufficient for IL-8 receptor interaction and neutrophil activation (15). This conclusion is further supported by the findings that the ELR peptide, and several peptides containing the ELR motif, did not bind to IL-8

* This work was supported by the Protein Engineering Network of Centres of Excellence, National Cancer Institute of Canada and National Institutes of Health Grant R01 GM-50969-01, and Swiss National Science Foundation Grant 31-25700.88. The costs of publication of this article were defrayed in part by the payment of page charges. This article must therefore be hereby marked "*advertisement*" in accordance with 18 U.S.C. Section 1734 solely to indicate this fact.

§ Recipient of a Medical Research Council of Canada Scholarship. To whom correspondence should be addressed.

[1] The abbreviations used are: IL-8, interleukin 8; NAP, neutrophil activating protein; GRO, growth related protein; PF4, platelet factor 4; ELR motif, Glu-Leu-Arg sequence; Gly-Pro motif, IL-8 Gly^{31} and Pro^{32}; HPLC, high performance liquid chromatography; Aba, α-aminobutyric acid.

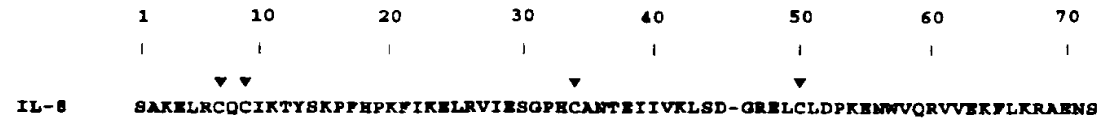

FIG. 1. **Sequences of IL-8 and IP10.** The aligned sequences of full-length IL-8 (1–72) and IP10 (1–74) are shown, with the cysteines highlighted with *arrowheads*.

receptors and lacked agonist or antagonist activity.

A recent study of the functional requirements for IL-8 dimerization showed that a monomeric form is fully active *in vitro*, suggesting that the biologically relevant form of IL-8 may be the monomer (27).

In this study we have used several strategies to define additional residues or structural regions as determinants of IL-8 activity. Substitutions of either a conservative or a nonconservative nature were made at various positions, focusing primarily on the NH_2-terminal 35 residues. In an alternative approach, hybrids between IL-8 and the inactive IP10 protein were designed to identify structural regions and residues required for IL-8 activity. The results presented indicate that residues 4–22 include all the essential receptor binding motifs and that the 30–35 turn is part of the scaffold that assures correct conformation of the NH_2-terminal region through the 7–34 disulfide bridge.

EXPERIMENTAL PROCEDURES

Chemical Synthesis Methods—All the IL-8 analogs and peptides were synthesized with *t*-butoxycarbonyl chemistry (28) and automated solid-phase methods (29) as described in detail elsewhere (25, 30). All the analogs were folded and purified by reverse-phase HPLC, as described (30). The fully folded products characteristically elute 3 min earlier than the unfolded forms. All analogs were tested for free thiols using Ellmans reagent as described (31).

Biological Assays—Human neutrophils were isolated from buffy coats of donor blood, and stimulus-dependent elastase release was determined after pretreatment of the cells with cytochalasin B, as described previously (32). Concentrations were determined by weighing of lyophilized material (0.5–2 mg), and the molar concentrations were based on the molecular weight of the monomer.

Receptor Binding Assays—IL-8 iodination, binding assays, and the calculation of binding parameters were performed as described (11).

Mass Spectrometry—Molecular masses were determined on a PE-SCIEX APIII spectrometer interfaced to an HPLC for ionspray sample delivery.

RESULTS AND DISCUSSION

The Synthetic Analogs—The rationale for the design of analogs is described below, in the appropriate sections. Each analog was chemically synthesized, folded, purified, and characterized. Almost all the analogs folded spontaneously to give molecules lacking detectable free thiols. An exception was the K23E analog, which gave two distinct peaks with identical mass. These two forms represent alternative stable conformations, but the structural basis for the two forms was not investigated. The analogs were purified by reverse-phase HPLC and each gave a discreet peak without shoulders (25, 30). The analogs were analyzed by isoelectric focusing and found to give single sharp bands with pI values between 7.5 and 9 (results not shown).

The analogs were subjected to electrospray mass spectrometry, and each determined mass corresponded to the calculated mass within experimental error. Although mass spectrometry does not provide the covalent structure, the data strongly support the contention that the molecule that was purified is the target protein. Mass spectrometry is one of the few physical techniques that analyzes the protein without fragmentation or chemical modification, and therefore is sensitive to most covalent modifications that can occur during synthesis. Amino acid analysis was performed on most analogs, and the results were consistent with the expected composition. For each analog, the average mass obtained, ± the error, and, in brackets, differences from the calculated average mass were: IL-8 (1–72), 8382.6 ± 0.9 (+0.8); IL-8 (3–72), 8223.2 ± 1.5 (-0.5); IL-8 (4–72), 8094.9 ± 0.8 (−0.6); Aba 4,34 (1–72), 8347.1 ± 1.1 (−0.8); Aba 9,50 (1–72), 8347.3 ± 0.6 (−0.6); Q8L (3–72), 8208.1 ± 0.8 (−0.6); Q8P (4–72), 8064.4 ± 0.7 (−0.1); I10V (4–72) 8081.2 ± 0.9 (−0.3); I10A (4–72), 8053 ± 1.3 (−0.4); K11R (3–72), 8251.5 ± 0.9 (−0.2); T12S (3–72), 8210.2 ± 0.6 (+0.6); Y13F (3–72), 8207.5 ± 0.7 (−0.2); Y13T (1–72), 8319.7 ± 1.1 (−0.1); S14T (3–72), 8237.1 ± 0.5 (−0.6); K15R (4–72), 8123.0 ± 1.3 (+0.5); P16G (4–72), 8055.9 ± 1.0 (+0.5); KP15,16G (3–72), 8054.3 ± 1.3 (−1.2); F17L (3–72), 8188.6 ± 1.4 (−1.0); H18F (3–72), 8232.8 ± 2.2 (−0.9); K20R (3–72), 8251.1 ± 0.9 (−0.6); K20E (3–72), 8223.6 ± 1.3 (−1.0); F21L (4–72), 8062.0 ± 1.3 (−0.5); K23E (3–72), 8224.6 ± 0.9 (0); K23E, E24K (3–72), 8223.5 ± 1.1 (−0.2); R26E (3–72), 8196.0 ± 1.1 (−0.6); E29K (3–72), 8221.9 ± 1.5 (−0.8); H33A (4–72), 8029.0 ± 0.6 (−0.2); H33F (1–72), 8391.9 ± 1.0 (0); H33L (1–72), 8358.1 ± 0.8 (+0.3); H33E (4–72), 8086.5 ± 1.1 (−1.0); H33Q (4–72), 8085.7 ± 1.2 (−0.8); H33S (4–72), 8044.7 ± 1.1 (−0.7); H33D (4–72), 8073.1 ± 1.0 (−0.3); G31S, P32Q (4–72), 8156.3 ± 0.4 (−0.3); G31P, P32G (4–72), 8096.2 ± 1.0 (+0.7); A35P (4–72), 8121.4 ± 0.2 (−0.1); IP10H-1, 7853.6 ± 1.5 (−0.7); IP10H-2, 8341 ± 1.3 (−1.2); IP10H-3, 8063.4 ± 1.1 (−0.3); IP10H-4, 8144.1 ± 0.6 (−0.7); IP10H-5, 8260.4 ± 0.8 (−0.6); IP10H-6, 8217.0 ± 1.5 (−1.0); IP10H-7, 8088.9 ± 0.9 (−0.8); IP10H-8, 8252.8 ± 0.9 (−0.3); IP10H-9, 8233.8 ± 0.8 (−0.2); IP10H-10, 7960.0 ± 0.8 (−1.4); IP10H-11, 7985.4 ± 0.6 (−0.1); IP10H-12, 8190.5 ± 0.8 (−0.4).

The purified analogs were assayed for functional activity by measuring their ability to induce the release of elastase from human neutrophils and for IL-8 receptor interaction by measuring competition for binding of radiolabeled IL-8. Previous studies (15, 25) have shown that elastase release is the most reliable assay for comparing the potency of IL-8 analogs. To enable evaluation of analogs with low activity, the concentration required to induce 30% of the maximum response (EC_{30}) obtained with IL-8 was chosen as the basis for comparison.

IL-8 analogs with single or double amino acid substitutions were synthesized as either the 1–72, 3–72, or 4–72 forms. The IL-8 (1–72) sequence is shown in Fig. 1. The 3–72 and 4–72 forms of IL-8 have significantly lower EC_{30} than the full-length form, IL-8 (1–72) (25, Table I). All three forms are found in IL-8 derived from mononuclear cells (33, 34). The IP10-IL-8 hybrids were synthesized with the NH_2-terminal sequence ELRC, as for IL-8 (4–72).

Role of the Disulfide Bridges—Previous studies with reduced and carboxymethylated IL-8 suggested that the disulfide bridges are critical for activity (32, 35). However, with this approach all cysteines are modified simultaneously, and secondary reactions cannot be ruled out. To assess the role of the individual disulfide bridges, we substituted the cysteine pairs for α-aminobutyric acid (Aba). This non-natural amino acid was chosen because on superimposition with cysteine its ethyl side chain is closer to being isosteric than any of the naturally

TABLE I

Neutrophil activation and binding of IL-8 substitution analogs

Chemically synthesized analogs were tested at concentrations ranging between 0.1 and 1000 nM for stimulation of elastase release from cytochalasin B-pretreated neutrophils. The concentration required for 30% (EC_{30}) of the maximal elastase release that was obtained with the corresponding IL-8 control was determined. EC_{30} values shown are the mean ± S.D. from three or four experiments performed with different neutrophil preparations. To allow quantitative comparison between different experiments, the EC_{30} values for the unknowns were normalized by a factor equivalent to the ratio of the appropriate control (IL-8 (1–72), (3–72) or (4–72)) value obtained in the same experiment and the corresponding mean control value obtained from multiple experiments. These mean control values were: IL-8, (1–72), 5.3 ± 3.6 (n = 25); IL-8 (3–72), 0.8 ± 1.0 (n = 17); and IL-8 (4–72), 1.6 ± 1.0 (n = 46). Fold increase designates the ratio of the EC_{30} of the analog to the EC_{30} of the appropriate IL-8 control. The binding dissociation constants (K_d values) were determined from competition curves obtained for ^{125}I-IL-8 binding to neutrophils in the presence of unlabeled analogs at concentrations ranging from 0.1 to 10,000 nM. Values are means from two independent experiments. The mean control K_d values (nM ± S.D.) were: IL-8 (1–72), 0.5 ± 0.1 (n = 5); IL-8 (3–72), 0.3 ± 0.07 (n = 4); and IL-8 (4–72), 0.35 ± 0.05 (n = 5). Fold increase is the ratio of the K_d of the analog to the K_d of the respective IL-8 control.

Substitution analog	Elastase release		Binding	
	EC_{30} ± S.D.	Fold increase	K_d	Fold increase
	nM		nM	
Controls				
IL-8 (1–72)	5.3 ± 3.6	1.0	0.5	1.0
IL-8 (3–72)	0.8 ± 1.0	1.0	0.3	1.0
IL-8 (4–72)	1.6 ± 1.0	1.0	0.35	1.0
Cysteine analogs				
C 7,34 Aba (1–72)	>10,000	>1,900	600	1,200
C 9,50 Aba (1–72)	Not detectable		4,000	8,000
8–16 loop analogs				
Q8L (3–72)	0.37 ± 0.17	0.5	0.07	0.2
Q8P (4–72)	3.3 ± 1.5	2.0	1.3	3.7
I10V (4–72)	3.5 ± 0.81	2.2	0.55	1.6
I10A (4–72)	35 ± 8.0	22	10	29
K11R (3–72)	0.72 ± 0.31	0.9	0.08	0.3
T12S (3–72)	0.80 ± 0.09	1.0	0.1	0.3
Y13F (3–72)	0.71 ± 0.33	0.9	0.07	0.2
Y13T (1–72)	33 ± 16	6.2	3.2	6.4
S14T (3–72)	0.67 ± 0.31	0.8	0.25	0.8
K15R (4–72)	1.4 ± 0.25	0.9	0.2	0.6
P16G (4–72)	2.2 ± 0.31	1.4	0.6	1.7
KP15,16G (3–72)*	22 ± 2.7	28	12	40
17–21 turn analogs				
F17L (3–72)	2.5 ± 1.8	3.1	0.3	1.0
H18F (3–72)	0.94 ± 0.24	1.2	0.4	1.3
K20E (3–72)	8.5 ± 3.4	11	2.0	6.7
K20R (3–72)	0.43 ± 0.24	0.5	0.15	0.5
F21L (4–72)	16 ± 4.3	10	3.0	8.6
Dimer interface analogs				
K23E (3–72)	1.2 ± 0.06	1.5	0.4	1.3
K23E, E24K (3–72)	1.0 ± 0.55	1.3	0.2	0.7
R26E (3–72)	1.0 ± 0.46	1.2	0.3	1.0
E29K (3–72)	1.1 ± 0.77	1.3	0.3	1.0
30–35 turn analogs				
H33A (4–72)	1.2 ± 0.55	0.7	0.35	1.0
H33D (4–72)	19 ± 5.9	12	15	43
H33E (4–72)	2.3 ± 0.31	1.4	1.6	4.6
H33F (1–72)	16 ± 11	3.0	1.2	2.4
H33L (1–72)	46 ± 21	8.7	8.0	16
H33Q (4–72)	1.1 ± 0.10	0.7	0.35	1.0
H33S (4–72)	1.6 ± 0.05	1.0	0.55	1.6
G31S, P32Q (4–72)	310 ± 250	190	60	170
G31P, P32G (4–72)	500 ± 330	300	16	46
A35P (4–72)	1.7 ± 0.26	1.1	0.4	1.1

* Pro^{16} converted to glycine and Lys^{15} deleted.

occurring nonpolar amino acids (36). As expected, both the Aba 7,34 and Aba 9,50 analogs formed the single disulfide bridge. However, Aba 7,34 lacked detectable activity, and Aba 9,50 had only marginal activity in both binding and elastase release assays, suggesting that both disulfides are required to maintain the biologically active conformation. Molecular dynamics of the Aba 7,34 model that was derived by modification of the NMR structure suggest that the molecule loses its compact structure, and the 7–17 and 29–37 regions in particular were displaced and exhibited increased mobility. Only the 7–17 region was apparently displaced in models of the Aba 9,50 analog (data not shown). These results suggest that the disulfide bridges maintain the structure in a compact form and retain the receptor binding regions in the appropriate conformation. Thus, even though earlier studies showed that the highly flexible ELR motif is essential for receptor binding (25, 26), the integrity of the folded compact tertiary structure is also necessary (19, 20, Fig. 2). It is not known whether the mobility of the structure prevents access of the ELR motif to the binding site, or whether it alters the three-dimensional relationship between multiple receptor binding regions.

The Loop Region Residues 8–16—In the flexible NH_2-termi-

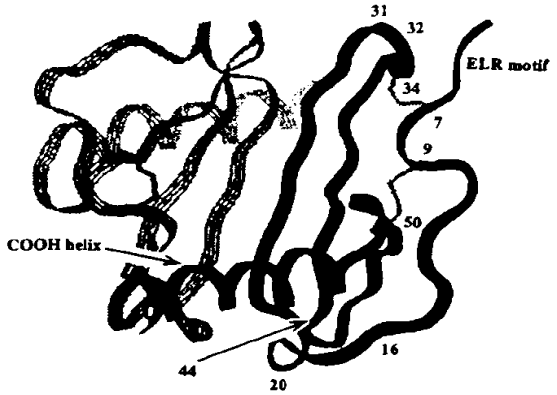

FIG. 2. **A ribbon diagram of IL-8.** Shown is the backbone fold of the IL-8 (4–72) dimer, with one monomer as a *solid ribbon* and the other as *ribbon strands*. The disulfide bridges and structural features and residues that are relevant to the described experiments are indicated.

nal region, conservative substitutions were made to test the importance of these residues. The rationale was that a conservative substitution of a residue that is directly involved in binding to the receptor would be poorly tolerated. This was the case for the ELR motif, where even conservative modifications had substantially reduced potency (15). These results were interpreted as indicating that the ELR motif is directly involved in receptor binding. Although the interpretation depends on the individual residues, small reductions in activity (less than 3-fold increase in EC_{30}) could be a consequence of conformational changes distant from the substituted amino acid.

Gln^8 is located between 2 critical cysteines (Fig. 2) although in CXC chemokines this position is not conserved (1–3). Surprisingly, replacement of this residue with leucine led to a 2-fold decrease in EC_{30} and a 5-fold decrease in K_d compared with IL-8 (4–72). When the more constrained proline residue was substituted for Gln^8, the EC_{30} increased 2-fold, and the K_d increased 4-fold. The results indicate that neither substitution had a major effect on activity, although the enhanced binding of Q8L is noteworthy. Minor changes were also observed when Ile^{10} was changed to valine (Table I). However, by alanine mutagenesis, Ile^{10} was identified as being critical, since the Ala^{10} mutant had a 30-fold lower affinity (26). We synthesized the Ala^{10} analog, and the assays showed a 22-fold increase in EC_{30} and a similar increase in K_d. (Table I). One interpretation of these results is that a β-branched amino acid is required for maintaining the conformation of the NH_2-terminal loop. Another interpretation is that receptor binding interactions involve the β-branched methyl of isoleucine or valine, but not the methyl of alanine.

As shown in Table I, the EC_{30} of the K11R, T12S, Y13F, S14T, and K15R analogs were not significantly different from wild type. The corresponding K_d values, however, were up to 5-fold lower, suggesting that receptor binding can be enhanced by modifying this region. Not all modifications were inert, as Y13T had about 6-fold increased K_d. However, this change is structurally more radical than the Y13F, as it is β branched and much smaller. Nevertheless, these results suggest that these 5 residues individually are not essential for function and do not directly influence receptor binding. The findings with the 10–16 region contrast with the conclusions from the hybrid approach discussed later.

With the exception of IP10, in all the other human CXC chemokines the 8–16 loop is 1 residue shorter, and proline is replaced by glycine. We replaced Lys^{15} and Pro^{16} with glycine to give a shortened loop that resembles these other CXC chemokines. The resulting analog had readily detectable activity, but its EC_{30} and receptor affinity were increased 28- and 40-fold respectively, compared with the control IL-8 (3–72). Although the other members of the CXC chemokine family are less potent than IL-8, their activities vary, and more data will be required to determine whether this is related to the shorter loop. IL-8 binds to both receptors (IL-8R1 and IL-8R2), whereas the other neutrophil-activating chemokines bind only to IL-8R2 with high affinity. It is possible that the larger loop of IL-8 determines binding to IL-8R1. Nevertheless, the differences observed with this analog compared with the single substitution analogs are probably due to the greater structural change involved with shortening the loop.

The 3:10 Turn Residues 17–21—Phe^{17} leads into the 3:10 turn and, when it was changed to leucine, the resulting analog, F17L, had an enhanced EC_{30}, but no significant difference in binding affinity compared with IL-8 (3–72) (Table I). The H18F analog had similar functional activity. For Lys^{20}, an arginine substitution was fully accepted; however, the non-conservatively substituted K20E analog had an 11-fold higher EC_{30} and a 7-fold higher K_d. Substitution of Phe^{21} for leucine resulted in an analog, F21L, that had about 10-fold higher EC_{30} and K_d value. Thus His^{18} and Lys^{20}, which are solvent exposed in the 3:10 turn, were not highly sensitive to modification. The 2 phenylalanines at positions 17 and 21 are bulky and buried in the structure, and form a number of hydrophobic contacts (19, 20). This suggests that modification of these residues could leave a hole and thus cause adjustments to the packing of the hydrophobic core. Furthermore, both residues are involved in aromatic interactions with Tyr^{13}, another residue that is sensitive to modification. It appears that the aromatic interactions between Tyr^{13}, Phe^{17}, and Phe^{21} are important for a fully functional molecule. It is noteworthy that these aromatic residues are not present in CXC chemokines other than IL-8.

β Strand Residues 23–29—This β strand stabilizes the dimer interface through hydrogen bonds with the corresponding antiparallel 23–29 β strand of the other subunit. To examine the role of this region, we maintained the hydrophobic residues that pack in the interior and converted the charged amino acids to oppositely charged amino acids.

The synthetic analogs synthesized were K23E, R26E, and E29K. In addition, a double modification analog was made with Lys^{23} converted to glutamic acid, and Glu^{24} changed to lysine to form the K23E, E24K analog. All of these proteins had EC_{30} and K_d values that were similar to the wild type form, indicating that the residues that were modified do not determine function and/or receptor binding. The role of Lys^{23} deserves further comment. In the x-ray structure, this lysine forms a salt bridge with Glu^4 of the second subunit of the dimer and results in ordering of the ELR region (20). This is of interest because of the critical role of Glu^4 in determining activity (25, 26). This was not observed in the solution structure (19, 21), but the x-ray structure represents a less solvated molecule that may be more analogous to the receptor-bound structure. Thus it is a theoretical possibility that the Glu^4 to Lys^{23} salt bridge forms on receptor binding. However, with Lys^{23} changed to glutamic acid, the configuration observed in the wild type x-ray structure is unlikely to form under any circumstances as the negatively charged residues would repel, rather than form a salt bridge. As K23E was fully active, we conclude that the salt bridge is not essential for activity or for stabilization of the receptor-bound form of IL-8.

Residues 30–35—The β strand of residues 23–29 is followed by an atypical β turn, consisting of residues 30–35, that leads into the second β strand. Three of the 6 amino acids can be considered structural: Gly^{31}, Pro^{32}, and Cys^{34}, with the latter forming a disulfide bridge with Cys^7. Much of our initial work

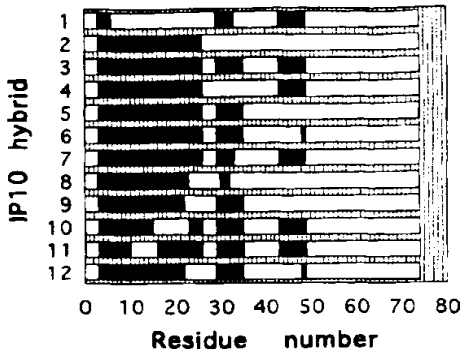

FIG. 3. **Comparison of sequences of IP10 hybrids.** Each hybrid (*numbered*) is represented by a *horizontal bar* with the IP10 region *open* and IL-8 region *closed*. For comparison with Figs. 1 and 2, residues are expressed in terms of the IL-8, 1–72 sequence. IP10 has an insertion at position 45 in the aligned sequences (Fig. 1), and to maintain sequence alignment of the hybrids, this residue was not included in the diagram. The NH_2-terminal sequence of all the hybrids is ELRC, corresponding to IL-8 (4–72).

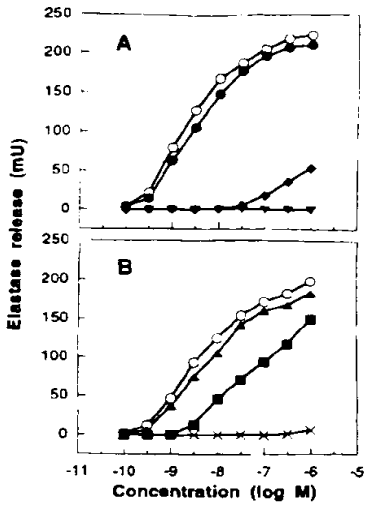

FIG. 4. **The 30–35 turn of IL-8 is required for function.** The activity of IP10 hybrids (Fig. 3) was determined in an assay measuring elastase activity (milliunits, *mU*) released from human neutrophils. *A* is IP10H-1 (▼), IP10H-2 (◆), IP10H-3 (●), and IL-8 (4–72) (○). *B* is IP10H-4 (×), IP10H-5 (■) and IP10H-6 (▲). IL-8 (4–72) was included in each set of measurements as a positive control. All the data shown were derived from the same experiment, and all the hybrids were assayed at least four times using different neutrophil preparations.

has focused on His^{33} because of its proximity to the ELR motif and to the 7 to 34 disulfide, and also because its NE2 imidazole nitrogen accepts a hydrogen bond from the main chain amide of Gln^6. In addition, His^{33} is conserved in most neutrophil-activating chemokines. Replacement of His^{33} with alanine, serine, or glutamine had no significant effect on function. Replacement with leucine, aspartic acid, glutamic acid, and phenylalanine caused a moderate increase in EC_{30} and K_d. Overall, these results demonstrate that His^{33} can be radically modified without affecting function. The basis for the decreased activity of some of the analogs is uncertain. Nevertheless, the hydrogen bonding to the backbone amide of Gln^6 that is observed in the IL-8 structure cannot be supported by H33A or the other fully active analogs, suggesting that this is not an essential structural feature.

Design of Hybrids—Overall, the findings with the single and double replacement analogs were quite surprising. With the exception of the cysteines and the ELR motif, no other residues were found to be essential and many could be modified without significantly affecting activity or receptor binding. To further investigate the structural requirements for function, we designed molecular hybrids between IL-8 and CXC proteins that lack IL-8-like activity. The aim was to convert the inactive molecule to an active hybrid and to identify the minimal IL-8 structure that is required for "activation" of the surrogate protein, the role of which is to provide a structural scaffold.

The first protein targeted for activation was PF4; however, we discovered that the ELR region alone was sufficient to confer activity upon PF4 (15). The two possible conclusions from this are that the ELR motif is the only receptor binding region, or that PF4 has recently evolved from a neutrophil-activating protein and has retained several structural motifs required for IL-8 receptor binding. In fact, evolutionary distance comparison indicates that PF4, GRO-α, and NAP-2 are closely related to each other. As IP10 is more distant from these chemokines and IL-8, it was chosen for hybrid studies.

The IP10 molecule is ideal for the hybrid study because, of the 17 residues which are identical in IP10 and IL-8 (Fig. 1), 9 could be considered structural (prolines, glycines, and cysteines) and 5 belong to the hydrophobic core. Moreover, incorporation of the ELR motif did not confer IL-8 activity upon IP10, suggesting that additional structural determinants are required (15). In designing hybrids, care was taken to maintain the hydrophobic core of the IP10 protein that was predicted from the IL-8 structure. Comparisons of the primary structures of the IP10 hybrids are shown diagrammatically in Fig. 3.

The 30–35 Turn Is Critical—We first focused on the NH_2-terminal region, 4–26, the 30–35 atypical β turn, and the 44–49 region that includes a type 1 β turn (Fig. 2). These IL-8 regions were chosen for initial incorporation into IP10 because of their proximity to the ELR motif and/or exposed surface location in the IL-8 structure.

IP10 hybrid-1 (IP10H-1), which contained only the ELR motif (residues 4–6) and residues 30–33 and 44–49 from IL-8, lacked detectable activity (Fig. 4*A*). Additionally, IP10H-2, which included NH_2-terminal residues 4–26, but not the 30–35 or 44–49 regions, also had only barely detectable activity. In contrast IP10H-3, which contained all three regions, 4–26, 30–35, and 44–49, was equivalent to IL-8 in potency (Fig. 4*A*) and receptor affinity (Table II). This demonstrated that elements from the NH_2-terminal region and the two turns are sufficient for full activity.

Hybrids were then designed to determine if both β turns are necessary for function. IP10H-5, which contains only the 4–26 and 30–35 regions, effectively stimulated elastase release, but was significantly less potent (9-fold) than IP10H-3 (Fig. 4*B*). Conversely, IP10H-4, which contained 4–26 and only the second β turn (44–49), had only barely detectable activity (Fig. 4*B*) and very high K_d (Table II). Together these results indicate that the 30–35 turn is critical for activity; however, potency was also affected by the 44–49 region. Examination of the IL-8 structure shows that Leu^{49} is close to the two disulfide bridges and the ELR motif (19, 20, Fig. 2). In IP10, this residue is an arginine. To test whether this non-conservative change is responsible for the functional difference between IP10H-3 and IP10H-5, we synthesized a hybrid, IP10H-6, which was identical to IP10H-5, except for Leu^{49}. Elastase release and receptor binding demonstrate that IP10H-6 is functionally similar to IP10H-3, thus indicating that the L49R difference was the basis for the lower activity of IP10H-5 (Fig. 4*B*; Table II). We can conclude from these results that residues essential for IL-8 activity are contained within the 30–35 turn.

Gly-Pro Is the Key Motif in the 30–35 Region—Another set of

TABLE II
Receptor binding of IP10 hybrids

Hybrid[a]	K_d[b]	Fold increase
	nM	
IL-8 (4–72)	0.35	1.0
IP10H-1	Undetectable	>10,000
IP10H-2	100	290
IP10H-3	0.7	2.0
IP10H-4	50	140
IP10H-5	8.0	23
IP10H-6	0.4	1.2
IP10H-7	1.3	3.7
IP10H-8	0.5/80[c]	1.4
IP10H-9	2.5	7.0
IP10H-10	35	100
IP10H-11	60	170
IP10H-12	0.45	1.3

[a] A schematic representation of the hybrids between IP10 and IL-8 is shown in Fig. 3.

[b] K_d values were obtained as in Table I. The mean K_d ± S.D. for IL-8 (4–72) was 0.35 ± 0.05 (n = 5). The binding data were consistent with either the one-site or two-site model.

[c] Two distinct binding sites were apparent, and both K_d values are given.

hybrids was designed to determine the relevant residues within the 30–35 region of IL-8. The single replacement experiments had shown that His^{33} could be modified without loss of activity (Table I). IP10H-7 was synthesized with 30–33 instead of 30–35 substitution, but otherwise was identical to IP10H-3 (Fig. 3). IP10H-7 had only slightly less activity than IP10H-3 (Fig. 5), indicating that Ala^{35} is not an important functional determinant. Similarly, the single substitution analog, IL-8, A35P, was only slightly less potent than IL-8 (4–72) (Table I), further suggesting that replacement of Ala^{35} with Pro is not significant for function.

Subsequently, two analogs were synthesized to address the role of the β strand residues 23–26 and the importance of the Gly-Pro motif. In these analogs, the IL-8 44–49 turn, which is not essential (Fig. 4*B*), was omitted. Comparison of IP10H-9 (Fig. 5) with IP10H-5 (Fig. 4*B*) indicates that side chains of residues 23–26 at the dimer interface are not functionally important. IP10H-8, which contains only residues 4–23 and Gly^{31} and Pro^{32} from IL-8, was only slightly less active (less than 2-fold difference in potency) than IP10H-9, which contains the complete 30–35 turn as well as residues 4–22 of IL-8 (Fig. 5). Interestingly, IP10H-8 had two receptor-binding sites, one with high affinity (K_d 0.5), and the other with a 160-fold higher K_d (Table II). The basis for the two-site binding is unknown, but it is unlikely to account for the 10-fold lower potency of IP10H-8, compared with IL-8 (4–72). This difference is probably due to the Arg^{49} of IP10, as previous experiments established that this substitution alone accounted for a 9-fold lower activity of IP10H-5, compared with IP10H-6 (Fig. 4*B*, see above).

The results with IP10H-8 and IP10H-9 suggested that the Gly-Pro motif within the 30–35 turn is the critical element. This hypothesis was examined by substitution of these 2 residues in IL-8. An IL-8 analog in which Gly^{31} and Pro^{32} were replaced by serine and glutamine, respectively, the corresponding residues in IP10, had a greatly increased EC_{30} (190-fold) and K_d (170-fold), providing further evidence for the importance of the Gly-Pro motif for function (Table I). Furthermore, when the glycine and proline of IL-8 were interconverted to form IL-8, Pro^{31}, Gly^{32}, the EC_{30} of the resulting analog was 300-fold higher (Table I). The results indicate that the Gly-Pro motif is the critical component of the 30–35 region.

Requirements in the NH_2-terminal Region—We have shown that, apart from the ELR motif and the cysteines, additional residues from the 10–26 region of IL-8 are also required for activity. Further hybrids were designed to identify the essential

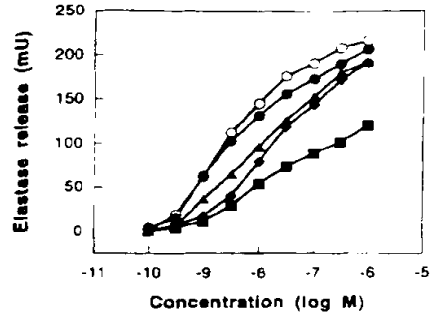

FIG. 5. **IL-8, Gly^{31}, Pro^{32} is an important structural motif.** The activity of IP10H-3 (●), IP10H-7 (▲), IP10H-8 (■), IP10H-9 (◆) and IL-8 (4–72) (○) was determined as described in Fig. 4.

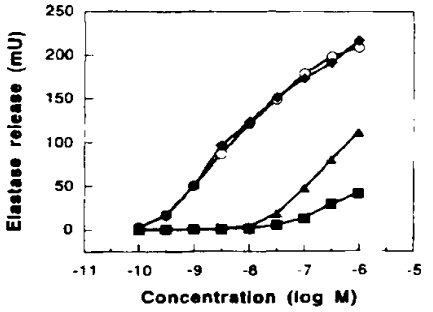

FIG. 6. **NH_2-terminal region 10–23 is critical for IL-8 function.** The activity of IP10H-10 (▲), IP10H-11 (■), IP10H-12 (◆), and IL-8 (4–72) (○) was determined as described in Fig. 4.

elements. IP10H-10, containing residues 4–15, 24–26, 30–35, and 44–49 from IL-8, and IP10H-11, containing 4–10, 17–26, 30–35, and 44–49 had only weak activity (90- and 440-fold decrease in potency, respectively, Fig. 6). The difference between the two hybrids was in the 11–24 region, and the results demonstrate that residues within both the 11–15 and the 17–24 regions are important. IP10H-12, which contains residues 4–22, 30–35 and residue 49, had activity equivalent to IL-8, thus further demonstrating that IL-8 residues 23–29 were not required (Fig. 6). Of all the IP10 hybrids with full activity, IP10H-12 contained the minimal IL-8 sequence.

CONCLUSIONS

The question being addressed in this paper is which structural features are critical for IL-8 receptor binding and functional activation? Within the limits of the structure-function approach used, many of the questions have been answered, and a clear picture of the determinants of IL-8 receptor binding and activity has been inferred. Broadly, two different strategies have been employed: generation of analogs with single residue replacements and design of hybrids of IP10 and IL-8. Consistent with previous studies showing the importance of the ELR motif (residues 4–6), the results clearly demonstrate that the NH_2-terminal region is the focus of the functional determinants. In particular, the two disulfide bridges, residues 10–22 and 30–35, were found to be critical using the hybrid approach. Furthermore, the results indicate that the major structural regions in the three β strands and the COOH-terminal α-helix are not directly involved in receptor binding. Lys^{23} analogs indicated that the ordering of the ELR motif observed in the x-ray structure (20) is not critical for function.

The 30–35 turn has a key structural role, and the disulfide bridge between Cys^{34} and Cys^{7} anchors the ELR region to the

30–35 turn (19, 20). It is possible that this turn provides the correct geometry for the 7–34 disulfide, and this controls the conformation of the ELR motif. Alternatively, the 30–35 region or the disulfide itself, which is relatively exposed, could directly interact with the receptor. Single substitutions demonstrate that His^{33} and Ala^{35} are not essential for receptor binding. The importance of the Gly-Pro motif suggests that the conformation of this region is critical and is likely to provide part of the framework for the receptor binding motifs.

Within the 10–23 region, residues between Lys^{11} and Lys^{15} are of particular interest. Although individual substitutions had no functional consequences, the hybrid experiments indicate that they are essential. This apparent contradiction is intriguing, but cannot be resolved with existing data. One possibility is that the residues corresponding to the IP10 11–15 sequence are not compatible with receptor binding. It is unlikely that this would be due purely to the steric bulk as the side chains of these IP10 residues are smaller. The low activity of IP10H-11 is also surprising because the 11–15 region is variable in the CXC chemokine family. Only Thr^{12} is invariant, but this residue can be substituted for serine without affecting function (Table I). Even though the other IL-8 family members are less active than IL-8 and bind with high affinity to only one of the two receptors, selectivity for receptors could not account for the difference in activity between IP10H-11 and IP10H-6.

Predicting the roles of the IL-8 10–23 region with higher resolution will require further analogs aimed at fine mapping of the contributions of the individual residues. The three-dimensional structures of the analogs will be necessary to determine the structural changes that have occurred as a consequence of the modifications. Ultimately, direct measurements of the binding to the receptor will be needed. Additional questions of IL-8 structure-activity relationships are the difference in requirements for binding to the two IL-8 receptors, and the difference in requirements for chemotactic and exocytosis activities.

Acknowledgments—We thank Peter Borowski, Philip Owen, and Luan Vo for expert technical assistance in the preparation and analysis of the analogs. Assistance with the mass spectrometry was provided by Dr. Ruedi Aebersold and Hamish Morrison. Andrea Blaser assisted with the functional studies. Cathy Davidson-Hall helped with preparation of the manuscript.

REFERENCES

1. Miller, M. D., and Krangel, M. S. (1992) *Crit. Rev. Immunol.* **12**, 17–46
2. Baggiolini, M., and Clark-Lewis, I. (1992) *FEBS Lett.* **307**, 97–101
3. Oppenheim, J. J., Zachariae, C. O. C., Mukaida, N., and Matsushima, K. (1991) *Annu. Rev. Immunol.* **9**, 617–648
4. Walz, A., and Baggiolini, M. (1989) *Biochem. Biophys. Res. Commun.* **159**, 969–975
5. Haskill, S., Peace, A., Morris, J., Sporn, S. A., Anisowicz, A., Lee, S. W., Smith, T., Martin, G., Ralph, P., and Sager, R. (1990) *Proc. Natl. Acad. Sci. U. S. A.* **87**, 7732–7736
6. Geiser, T., Dewald, B., Ehrengruber, M. U., Clark-Lewis, I., and Baggiolini, M. (1993) *J. Biol. Chem.* **268**, 15419–15424
7. Walz, A., Burgener, R., Car, B., Baggiolini, M., Kunkel, S. L., and Strieter, R. M. (1991) *J. Exp. Med.* **174**, 1355–1362
8. Proost, P., Wuyts, A., Conings, R., Lenaerts, J.-P., Billiau, A., Opdenakker, G., and Van Damme, J. (1993) *Biochemistry* **32**, 10170–10177
9. Holt, T. C., Harris, M. E., Holt, A. M., Lange, E., Henschen, A., and Niewiarowski, S. (1986) *Biochemistry* **25**, 1988–1996
10. Luster, A. D., Unkeless, J. C., and Ravetch, J. V. (1985) *Nature* **315**, 672–676
11. Moser, B., Schumacher, C., von Tscharner, V., Clark-Lewis, I., and Baggiolini, M. (1991) *J. Biol. Chem.* **266**, 10666–10671
12. Schumacher, C., Clark-Lewis, I., Baggiolini, M., and Moser, B. (1992) *Proc. Natl. Acad. Sci. U. S. A.* **89**, 10542–10546
13. Holmes, W. E., Lee, J., Kuang, W. J., Rice, G. C., and Wood, W. I. (1991) *Science* **253**, 1278–1280
14. Murphy, P. M., and Tiffany, H. L. (1991) *Science* **253**, 1280–1283
15. Clark-Lewis, I., Dewald, B., Geiser, T., Moser, B., and Baggiolini, M. (1993) *Proc. Natl. Acad. Sci. U. S. A.* **90**, 3574–3577
16. Dewald, B., Moser, B., Barella, L., Schumacher, C., Baggiolini, M., and Clark-Lewis, I. (1992) *Immunol. Lett.* **32**, 81–94
17. Zucker, M. B., and Katz, I. R. (1991) *Proc. Soc. Exp. Biol. Med.* **198**, 693–702
18. Luster, A. D., and Leder, P. (1993) *J. Exp. Med.* **178**, 1057–1065
19. Clore, G. M., Appella, E., Yamada, M., Matsushima, K., and Gronenborn, A. M. (1990) *Biochemistry* **29**, 1689–1696
20. Baldwin, E. T., Weber, I. T., St. Charles, R., Yuan, J. C., Appella, E., Yamada, M., Matsushima, K., Edwards, B. F. P., Clore, G. M., Gronenborn, A. M., and Wlodawer, A. (1991) *Proc. Natl. Acad. Sci. U. S. A.* **88**, 502–506
21. Clore, G. M., and Gronenborn, A. M. (1991) *J. Mol. Biol.* **217**, 611–620
22. St. Charles, R., Walz, D. A., and Edwards, B. F. P. (1989) *J. Biol. Chem.* **264**, 2092–2099
23. Mayo, K. H., and Chen, M. J. (1989) *Biochemistry* **28**, 9469–9478
24. Fairbrother, W. J., Reilly, D., Colby, T., and Horuk, R. (1993) *FEBS Lett.* **330**, 302–306
25. Clark-Lewis, I., Schumacher, C., Baggiolini, M., and Moser, B. (1991) *J. Biol. Chem.* **266**, 23128–23134
26. Hébert, C. A., Vitangcol, R. V., and Baker, J. B. (1991) *J. Biol. Chem.* **266**, 18989–18994
27. Rajarathnam, K., Sykes, B. D., Kay, C. M., Dewald, B., Geiser, T., Baggiolini, M., Clark-Lewis, I. (1994) *Science* **264**, 90–92
28. Merrifield, R. B. (1963) *J. Am. Chem. Soc.* **85**, 2149–2154
29. Clark-Lewis, I., and Kent, S. (1989) in *The Use of HPLC in Receptor Biochemistry* (Kerlavage, A. R., ed) pp. 43–75, AR Liss, New York
30. Clark-Lewis, I., Moser, B., Walz, A., Baggiolini, M., Scott, G. J., and Aebersold, R. (1991) *Biochemistry* **30**, 3128–3135
31. Clark-Lewis, I., Hood, L. E., and Kent, S. B. H. (1988) *Proc. Natl. Acad. Sci. U. S. A.* **85**, 7897–7902
32. Peveri, P., Walz, A., Dewald, B., and Baggiolini, M. (1988) *J. Exp. Med.* **167**, 1547–1559
33. Yoshimura, T., Robinson, E. A., Appella, E., Matsushima, K., Showalter, S. D., Skeel, A., and Leonard, E. J. (1989) *Mol. Immunol.* **26**, 87–93
34. Lindley, I., Aschauer, H., Seifert, J.-M., Lam, C., Brunowsky, W., Kownatzki, E., Thelen, M., Peveri, P., Dewald, B., von Tscharner, V., Walz, A., and Baggiolini, M. (1988) *Proc. Natl. Acad. Sci. U. S. A.* **85**, 9199–9203
35. Van Damme, J., Van Beeumen, J., Conings, R., Decock, B., and Billiau, A. (1989) *Eur. J. Biochem.* **181**, 337–344
36. Schneider, J., and Kent, S. B. H. (1988) *Cell* **54**, 363–368

THE JOURNAL OF BIOLOGICAL CHEMISTRY
Vol. 266, No. 16, Issue of June 5, pp. 10666-10671, 1991
Printed in U.S.A.

Neutrophil-activating Peptide 2 and *gro*/Melanoma Growth-stimulatory Activity Interact with Neutrophil-activating Peptide 1/Interleukin 8 Receptors on Human Neutrophils*

(Received for publication, January 9, 1990)

Bernhard Moser‡, Christoph Schumacher, Vinzenz von Tscharner, Ian Clark-Lewis§, and Marco Baggiolini

From the Theodor-Kocher Institute, University of Bern, P. O. Box 99, CH-3000 Bern, Switzerland and the §Biomedical Research Centre, University of British Columbia, Vancouver, British Columbia, Canada, V6T 1W5

Neutrophil-activating peptide 1/interleukin 8 (NAP-1/IL-8), neutrophil-activating peptide 2 (NAP-2), and *gro*/melanoma growth-stimulatory activity (*gro*/MGSA) are potent inflammatory cytokines with homologous structure and similar neutrophil-activating properties. Receptors on human neutrophils that interact with these peptides were studied. Analysis of ^{125}I-NAP-1/IL-8 binding at 0–4 °C revealed 64,500 ± 14,000 receptors/cell with an apparent K_d of 0.18 ± 0.07 nM (mean ± S.D. of six independent experiments). Unlabeled NAP-1/IL-8, NAP-2, and *gro*/MGSA competed with ^{125}I-NAP-1/IL-8 for binding to human neutrophils. Competition with increasing concentrations of unlabeled NAP-2 and *gro*/MGSA resolved two classes of NAP-1/IL-8 binding sites: about 70% of them bound NAP-2 and *gro*/MGSA with high affinity (K_d: 0.34 ± 0.2 and 0.14 ± 0.02), while 30% were of low affinity (K_d: 100 ± 20 and 130 ± 10 nM). Different binding sites, however, were not apparent upon competition with unlabeled NAP-1/IL-8, suggesting that both classes of receptors have similar affinities for NAP-1/IL-8. The existence of two receptors was also suggested by ligand cross-linking and cross-desensitization experiments. Two neutrophil membrane proteins with apparent M_r of 66,000–74,000 and 42,000–46,000 became cross-linked to ^{125}I-NAP-1/IL-8, and the labeling was decreased when excess NAP-1/IL-8, NAP-2, or *gro*/MGSA was present. Stimulation of neutrophils with NAP-1/IL-8 resulted in desensitization toward a subsequent challenge with NAP-2 or *gro*/MGSA as shown by the rise in cytosolic free calcium. By contrast, following primary stimulation with NAP-2 or *gro*/MGSA, responses to NAP-1/IL-8 were only moderately attenuated, supporting the existence of NAP-1/IL-8 receptors which bind NAP-2 or *gro*/MGSA with low affinity. In conclusion, our results demonstrate that NAP-2 and *gro*/MGSA act upon human neutrophils by directly interacting with two classes of receptors for NAP-1/IL-8.

Neutrophil-activating peptide 1/interleukin 8 (NAP-1/IL-8),[1] neutrophil-activating peptide 2 (NAP-2), and *gro*/melanoma growth-stimulatory activity (*gro*/MGSA) are structurally related human peptides which were recently identified, and which are thought to act as mediators of inflammation (1, 2). NAP-1/IL-8 was originally described as a product of stimulated human mononuclear phagocytes (3–5), and later found to be produced by a variety of stimulated tissue cells, including fibroblasts (6, 7), endothelial, and epithelial cells (8), keratinocytes (9), and alveolar macrophages (10). Several N-terminal variants were identified in the conditioned media of blood monocytes (11), suggesting the generation of various active forms of NAP-1/IL-8 through differential proteolytic processing. A nucleotide sequence corresponding to the major form, which consists of 72 amino acids, has been synthesized and expressed in *Escherichia coli* (11). NAP-2, a peptide of 70 amino acids, results from the N-terminal cleavage of platelet basic protein and its derivative, connective tissue-activating peptide III (CTAP-III) (12, 13). Upon stimulation, platelets release from their α-granules the precursor peptides which were shown to be processed into NAP-2 by monocyte proteases (12). *gro*/MGSA is a potent activator of human neutrophils (14) that was originally described as a mitogen for the human melanoma cell line Hs294T (15). This peptide of 73 amino acids corresponds to a cDNA (*gro*) isolated from a cDNA library prepared from a human bladder carcinoma explant (16). In addition to melanoma cells and *in vitro* transformed cell lines, *gro* expression has been demonstrated in human fibroblasts, endothelial and epithelial cells (17, 18). Recently, *gro*/MGSA was purified from conditioned media of lipopolysaccharide-stimulated human blood monocytes (19). NAP-1/IL-8, NAP-2, and *gro*/MGSA share a range of neutrophil-activating functions. They induce chemotaxis, release of enzymes from specific and azurophil granules, mobilization of cytosolic free calcium (13, 14, 20, 21), and cause exudation and massive neutrophil infiltration upon intradermal injection in rats and rabbits (14, 22, 23). A striking feature of these inflammatory cytokines is their extensive structural homology (Fig. 1). When aligned according to their 4 cysteine residues identity with NAP-1/IL-8 is 47% for *gro*/MGSA and 42% for NAP-2.

Several recent reports described receptors for NAP-1/IL-8

* This work was supported by a grant from the Swiss Federal Commission for Rheumatic Diseases and Grant 31-25700.88 from the Swiss National Science Foundation. The costs of publication of this article were defrayed in part by the payment of page charges. This article must therefore be hereby marked "*advertisement*" in accordance with 18 U.S.C. Section 1734 solely to indicate this fact.

‡ To whom correspondence should be addressed: Theodor-Kocher Institute, P. O. Box 99, CH-3000 Bern 9, Switzerland. Tel.: 41-31-654-141; Fax: 41-31-653-799.

[1] The abbreviations used are: NAP-1/IL-8, neutrophil-activating peptide 1/interleukin 8; NAP-2, neutrophil-activating peptide 2; *gro*/MGSA, *gro*/melanoma growth-stimulatory activity; CTAP-III, connective tissue-activating peptide III; fMLP, *N*-formylmethylleucylphenylalanine; TNF, tumor necrosis factor; BSA, bovine serum albumin; DFP, diisopropyl fluorophosphate; EGTA, [ethylenebis(oxyethylenenitrilo)tetraacetic acid; HEPES, 4-(2-hydroxethyl)-1-piperazineethanesulfonic acid; PMSF, phenylmethanesulfonyl fluoride.

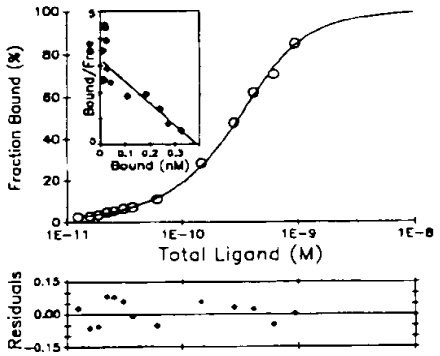

FIG. 2. **Steady-state binding of ^{125}I-NAP-1/IL-8 to human neutrophils.** The ratio of sites bound with iodinated ligand to the total number of binding sites per 10^6 neutrophils (% fraction bound) and the corresponding concentrations of total ligand were corrected for unspecific binding and binding capacity (33) after fitting of the experimental data with the program LIGAND (28). Values obtained from cells incubated with 1 μM unlabeled NAP-1/IL-8 and various concentrations of iodinated ligand are not represented in this diagram. The plot of residuals (fraction bound measured minus fraction bound calculated divided by the fraction bound calculated), corresponding to the binding data, illustrate the deviations from the fitted curve (one-binding site model). *Inset*, the same data represented by a Scatchard plot. The *straight line* corresponds to the fitted curve shown in the figure. Each value is the mean of duplicate measurements.

on human neutrophils and myeloid cell lines (24–27). For neutrophils these results are conflicting with respect to receptor species and numbers, and so far no information is available on receptors for NAP-2 and *gro*/MGSA. In this report, we show that NAP-2 and *gro*/MGSA compete with iodinated NAP-1/IL-8 for binding to two classes of binding sites on human neutrophils, and present evidence from cross-linkage and functional studies that all three chemotactic cytokines activate neutrophils through a common receptor system.

MATERIALS AND METHODS[2]

RESULTS

Binding of ^{125}I-NAP-1/IL-8 to Human Neutrophils—Iodinated NAP-1/IL-8 (0.2 nM) bound very rapidly to human neutrophils at 0–4 °C. Approximately 80% of maximal binding was reached after 5 min, and binding was at equilibrium after 45–60 min (data not shown). Consequently, the incubation time in all steady-state binding experiments was chosen to be 60 min or longer. Neutrophils were incubated at 0–4 °C for 90 min with increasing concentrations of iodinated NAP-1/IL-8, and number of binding sites, affinity constants (K_d values), and unspecific binding parameters were determined by nonlinear least squares fits of the measured binding data using the program LIGAND (28). Unspecific binding did not exceed 3% of the respective free ligand concentrations. The binding data of a typical experiment are shown in Fig. 2. The fitted line was drawn through the measured points according to the one-binding site model (28). The difference between the measured and the respective calculated points were too small to be seen and were thus plotted as residuals. A sign test (29) showed that the residuals were distributed randomly indicating that the fitting according to a one-binding site model was appropriate. The absence of a non-random distribution of the residuals excludes the existence of a sizable number of additional binding sites of higher or lower affinity. Further model calculations indicated that a second class of as little as 500 binding sites with a K_d of 1 order of magnitude lower than that indicated by the one-binding site model (see below) would be detectable as a systematic deviation in the plot of residuals. The Scatchard plot in the *inset* of Fig. 2 shows the linear behavior expected for the binding of ^{125}I-NAP-1/IL-8 to a single binding site. In six independent binding experiments with neutrophils from different donors, the data were best described by a one-binding site model with 64,500 ± 12,000 receptors/cell and a K_d of 0.18 ± 0.07 nM. As indicated above, however, our analysis does not rule out the existence of a low number (<500 sites/cell) of binding sites with a K_d smaller than 0.01 nM.

Competition Binding Assays—It has been shown previously that at 37 °C receptor-bound NAP-1/IL-8 is rapidly internalized by human neutrophils (25). Twenty min after addition of ^{125}I-NAP-1/IL-8 more than 95% of cell-associated radioactivity was resistant to acid washing. In contrast, bound ^{125}I-NAP-1/IL-8 could be recovered almost completely (>95%) from the cells by acid treatment following incubation for up to 3 h at 0–4 °C (data not shown). Under these conditions it was therefore possible to investigate whether preincubation of neutrophils with excess NAP-2 or *gro*/MGSA could interfere with ^{125}I-NAP-1/IL-8 binding. As shown in Fig. 3, neutrophils that had been preincubated with either NAP-2 or *gro*/MGSA still bound iodinated NAP-1/IL-8. The binding occurred at similar rates as with untreated cells, and reached steady-state conditions after 45–60 min. The total binding of iodinated NAP-1/IL-8, however, was decreased by approximately 75 and 60% for cells preincubated with NAP-2 or *gro*/MGSA, respectively, indicating that both peptides interacted with NAP-1/IL-8 receptors. Also, the residual binding of ^{125}I-NAP-1/IL-8 (approximately 25% and 40% for *gro*/MGSA and NAP-2 preincubated cells, respectively) suggests that a significant proportion of NAP-1/IL-8 receptors did not interact with NAP-2 or *gro*/MGSA with high affinity or that the two homologous ligands dissociated from these binding sites at a fast off-rate.

The ability of NAP-1/IL-8, NAP-2, or *gro*/MGSA to compete with ^{125}I-NAP-1/IL-8 for binding to human neutrophils was further investigated by cold ligand titration studies. Increasing concentrations of NAP-1/IL-8 competed with 1 nM iodinated ligand for binding and led to a sigmoidal decrease of the fraction of receptors occupied by ^{125}I-NAP-1/IL-8 (Fig. 4). As in Fig. 2, the data were best fitted to a one-binding site model (28). In three independent experiments using different preparations of ^{125}I-NAP-1/IL-8, the number of binding sites per cell (62,000 ± 14,000) and the K_d (0.24 ± 0.1 nM) obtained were in full agreement with the values from the ^{125}I-NAP-1/IL-8 binding studies (Fig. 2).

As expected from the data shown in Fig. 3, NAP-2 and *gro*/MGSA also competed with iodinated NAP-1/IL-8 for binding to neutrophils. However, in contrast to NAP-1/IL-8, the competition curves for the related peptides were not sigmoidal (Fig. 4). Already at concentrations as low as 30 pM NAP-2 and *gro*/MGSA were able to compete with iodinated NAP-1/IL-8 for binding, indicating that both ligands interacted with high affinity with part of the receptors for NAP-1/IL-8. With increasing concentrations the competition became less efficient, and even 1 μM NAP-2 or *gro*/MGSA, in contrast to NAP-1/IL-8, did not displace 1 nM ^{125}I-NAP-1/IL-8 completely. Apparently, a sizable fraction of the receptors for NAP-1/IL-8 bound NAP-2 and *gro*/MGSA with low affinity.

[2] Portions of this paper (including "Materials and Methods" and Figs. 1, 3, 5–7) are presented in miniprint at the end of this paper. Miniprint is easily read with the aid of a standard magnifying glass. Full size photocopies are included in the microfilm edition of the Journal that is available from Waverly Press.

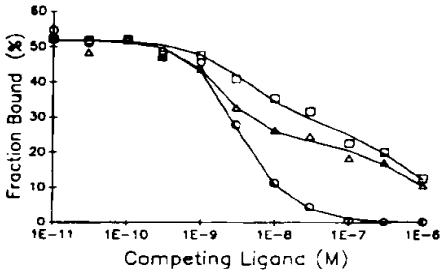

FIG. 4. **Cold ligand competition of ^{125}I-NAP-1/IL-8 binding to human neutrophils.** 2×10^6 cells were incubated at 0–4 °C for 90 min with 1 nM ^{125}I-NAP-1/IL-8 in the presence of increasing concentrations of unlabeled NAP-1/IL-8 (○), NAP-2 (□), or *gro*/MGSA (△) and further processed as described under "Materials and Methods." Fractions (%) of sites bound with iodinated NAP-1/IL-8 were determined, and the respective binding parameters calculated exactly as described in the legend to Fig. 2. Each point is the mean of duplicate measurements. The results are representative of three independent experiments.

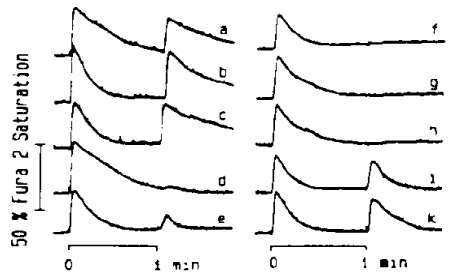

FIG. 8. **Desensitization of human neutrophils by NAP-1/IL-8, NAP-2, and *gro*/MGSA.** $[Ca^{2+}]_i$ changes, expressed as changes in percent Fura-2 saturation, were measured during sequential stimulations with agonists at 1-min time intervals. *a–c*), cells were first stimulated with NAP-1/IL-8 (*a*), NAP-2 (*b*), or *gro*/MGSA (*c*), followed by a second stimulation with fMLP; *d–f*), repeated stimulation with the same agonist, NAP-1/IL-8 (*d*), NAP-2 (*e*), or *gro*/MGSA (*f*); *g* and *h*, first stimulation with NAP-1/IL-8 and second stimulation with NAP-2 (*g*) or *gro*/MGSA (*h*); *i* and *k*, first stimulation with NAP-2 (*i*) or *gro*/MGSA (*k*) and second stimulation with NAP-1/IL-8.

In contrast to NAP-1/IL-8, the competition binding data for NAP-2 and *gro*/MGSA could not be fitted by a one-binding site model (28). These results suggest that the NAP-1/IL-8 receptors consist of two separate classes of binding sites, distinguishable by their different affinities for NAP-2 and *gro*/MGSA. Fitting of the data from three separate experiments to a two-binding site model revealed that 70 ± 5% of the NAP-1/IL-8 receptors had high affinity for NAP-2 (0.34 ± 0.20 nM) and *gro*/MGSA (0.14 ± 0.02 nM), while 30 ± 5% were of low affinity (100 ± 20 nM for NAP-2 and 130 ± 10 nM for *gro*/MGSA). CTAP-III, the precursor of NAP-2 (12, 13), platelet factor 4 (30), and the potent chemotactic peptide fMLP (31) were also tested for inhibition of ^{125}I-NAP-1/IL-8 binding to human neutrophils. As shown in Fig. 5, at 1000-fold molar excess CTAP-III inhibited the binding by approximately 30%, an effect that is most likely due to its structural similarity to NAP-2. By contrast, neither platelet factor 4 nor fMLP were inhibitory.

Cross-linking Studies—Cross-linking of ^{125}I-NAP-1/IL-8 to neutrophil cell surface proteins led to the labeling of two proteins with apparent molecular mass of 66–74 (p70) and 42–46 (p44) kDa, after deduction of 8 kDa for the mass of NAP-1/IL-8 (Fig. 6). Virtually identical results were obtained when the cross-linking agent disuccinimidyl suberate was substituted for glutaraldehyde (data not shown). Cross-linking of iodinated NAP-1/IL-8 to both proteins was diminished in the presence of an excess of unlabeled NAP-1/IL-8, NAP-2, or *gro*/MGSA. In contrast to NAP-1/IL-8, however, NAP-2 and *gro*/MGSA did not fully prevent the labeling of p70 and p44, as revealed by prolonged exposure of the autoradiograms (data not shown). This finding was confirmed by experiments using the unlabeled ligands at 4-, 16-, or 64-fold molar excess. At lower concentrations, NAP-2 or *gro*/MGSA were considerably less effective than NAP-1/IL-8 in preventing the cross-linking of ^{125}I-NAP-1/IL-8 to p70 and p44 (Fig. 7).

Cross-desensitization—A transient rise in cytosolic free calcium ($[Ca^{2+}]_i$) is an early event in signal transduction during activation of human neutrophils with chemotactic agonists including NAP-1/IL-8, NAP-2, and *gro*/MGSA (13, 14, 20, 32). As shown in Fig. 8, *a–c*, stimulation of the cells with maximum effective peptide concentrations (0.1 μM NAP-1/IL-8 and *gro*/MGSA, and 1.0 μM NAP-2) did not prevent responses to subsequent stimulation with the unrelated agonist, fMLP. By contrast, the second response was abolished or profoundly attenuated after repeated stimulation with the same agonist as shown for NAP-1/IL-8, NAP-2, and *gro*/MGSA (Fig. 8, *d–f*). The responses to NAP-2 and *gro*/MGSA were also abrogated after stimulation of the cells with NAP-1/IL-8, indicating that the latter agonist desensitized the cells toward NAP-2 and *gro*/MGSA (Fig. 8, *g–h*). In the reverse experiment, however, prestimulation with either NAP-2 or *gro*/MGSA merely led to a slight reduction in the response to NAP-1/IL-8 (Fig. 8, *i* and *k*). Even at 100-fold molar excess NAP-2 or *gro*/MGSA did not markedly desensitize the cells toward NAP-1/IL-8 (data not shown). Fig. 9 illustrates the concentration dependence of the desensitizing effect of NAP-1/IL-8. The response to 100 nM *gro*/MGSA was not affected after stimulation with 0.1 or 1 nM NAP-1/IL-8, but was reduced with 10 nM and abolished with 100 nM NAP-1/IL-8, respectively. Similar results were obtained using NAP-2 instead of *gro*/MGSA as the second stimulus (data not shown). Interestingly, the potency of NAP-1/IL-8 in desensitizing the cells to subsequent stimulations with NAP-2 or *gro*/MGSA (Fig. 9) seems to correlate with the degree of inhibition of receptor binding at higher competing ligand concentrations (Fig. 4). It should be noted, however, that a quantitative comparative analysis of the results from these two kinds of experiments is problematic since mobilization of cytosolic free calcium is not only a function of the number of free receptors, as determined under steady-state conditions, but also of the rate of ligand binding or (at high ligand concentrations) of rate-limiting steps in signal transduction.

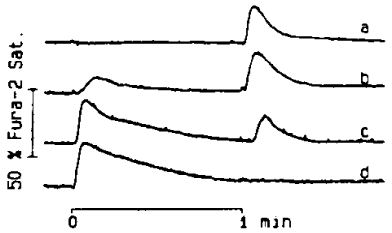

FIG. 9. **NAP-1/IL-8-induced desensitization of human neutrophils toward *gro*/MGSA.** The experiments were performed as described in the legend to Fig. 8. The cells were stimulated with 0.1, 1.0, 10, and 100 nM NAP-1/IL-8 (*a–d*), followed by second additions of 100 nM *gro*/MGSA.

DISCUSSION

In agreement with a recent report (27), our studies with iodinated NAP-1/IL-8 revealed a single class of binding sites

with approximately 64,000 sites/cell and an apparent K_d of approximately 0.2 nM. However, our binding data do not exclude with certainty the existence of a low number (<500) of additional high affinity NAP-1/IL-8 receptors. Especially at low ligand concentrations small errors (±5%) in the experimentally determined binding capacities (33) of iodinated ligand preparations drastically affect the analyses of binding data. Results showing a relatively large number of additional high affinity binding sites (5200 sites/cell), as previously reported (26), are probably a consequence of difficulties in interpreting binding data by Scatchard analysis (34).

NAP-2 and *gro*/MGSA (which do not contain tyrosine residues) were studied for competition with binding of iodinated NAP-1/IL-8 to human neutrophils. Both ligands interfered with ^{125}I-NAP-1/IL-8 binding, and analysis of the competition binding data indicated the existence of at least two classes of binding sites with high and low affinity for each of the two cytokines. These results suggest that NAP-1/IL-8 is also recognized by at least two distinct species of binding sites. And it must be assumed that the apparent K_d of approximately 0.2 nM, as determined by ^{125}I-NAP-1/IL-8 binding experiments, represents an intermediate value for two distinct populations of binding sites with similar affinities for NAP-1/IL-8. Based on the fact that these sites bound NAP-2 and *gro*/MGSA, in contrast to NAP-1/IL-8, with affinities differing by several orders of magnitude we postulate that they represent two distinct receptor species. Similar findings were recently obtained for TNFs. Binding studies indicated the presence of a single class of binding sites, and competition binding analysis revealed that TNFα and TNFβ, which share about 30% sequence homology, interact with the same cellular binding sites. Yet, two distinct receptor species were recently identified on monocytes and related cell lines which bind both TNFα and TNFβ (35–40).

Cross-linking experiments revealed two proteins (p44 and p70) that became labeled with ^{125}I-NAP-1/IL-8. Labeling was markedly reduced in the presence of excess NAP-2 or *gro*/MGSA, indicating that both peptides interacted with receptor(s) for NAP-1/IL-8. It is tempting to speculate that p44 and p70 represent the two distinct receptors for the three related cytokines. The observed difference in labeling intensity of the two proteins appears to correlate with the relative numbers of the two types of receptors. The occurrence of two ^{125}I-NAP-1/IL-8-labeled bands is in agreement with the results of Samanta *et al.* (24), but not with those of Grob *et al.* (27), who reported a single NAP-1/IL-8-binding protein of 58 kDa. Although several protease inhibitors were included during sample preparation, the generation of two binding species by partial proteolysis cannot be excluded, as documented by other studies (41).

Further evidence for the presence, on human neutrophils, of more than one receptor for NAP-2 and *gro*/MGSA with affinities differing by several orders of magnitude comes from functional studies. Stimulation with NAP-2 or *gro*/MGSA did not markedly affect the responsiveness of neutrophils to the subsequent stimulation with NAP-1/IL-8. It is possible that the receptors with low affinity for NAP-2 and *gro*/MGSA may not be saturated under these conditions, or that NAP-1/IL-8 can displace NAP-2 or *gro*/MGSA from those receptors to which they bind with low affinity. The converse experiment shows that prestimulation with NAP-1/IL-8 renders the cells unresponsive to either NAP-2 or *gro*/MGSA. Through its high affinity for both receptors, NAP-1/IL-8 could completely prevent the binding of subsequently added NAP-2 or *gro*/MGSA. Alternatively, desensitization could result from "cross-talk" between the two receptors. This type of inhibition has been described in Swiss 3T3 cells, where stimulation with platelet-derived growth factor resulted in decreased affinity of the epidermal growth factor receptor for its ligand (42). These effects were observed at low ligand concentrations, however, in contrast to the desensitization caused in neutrophils by NAP-1/IL-8.

The common receptor system proposed here suggests that in the recruitment of neutrophils at sites of inflammation and disturbed tissue homeostasis NAP-1/IL-8, NAP-2, and *gro*/MGSA may synergize with unrelated chemotactic agonists, but not with each other.

Acknowledgments—We wish to thank J. Blumenstein for technical assistance, Dr. A. Walz for providing purified CTAP-III, and Drs. A. D. Deranleau and B. Dewald for helpful discussions during the preparation of this manuscript.

REFERENCES

1. Baggiolini, M., Walz, A., and Kunkel, S. L. (1989) *J. Clin. Invest.* **84**, 1045–1049
2. Westwick, J., Li, S. W., and Camp, R. D. (1989) *Immunol. Today* **10**, 146–147
3. Walz, A., Peveri, P., Aschauer, H., and Baggiolini, M. (1987) *Biochem. Biophys. Res. Commun.* **149**, 755–761
4. Yoshimura, Z., Matsushima, K., Oppenheim, J. J., and Leonard, E. J. (1987) *J. Immunol.* **139**, 788–793
5. Gregory, H., Young, J., Schröder, J.-M., Mrowietz, U., and Christophers, E. (1988) *Biochem. Biophys. Res. Commun.* **151**, 883–890
6. Larsen, C. G., Zachariae, C. O. C., Oppenheim, J. J., and Matsushima, K. (1989) *Biochem. Biophys. Res. Commun.* **160**, 1403–1408
7. Strieter, R. M., Phan, S. H., Showell, H. J., Remick, D. G., Lynch, J. P., Genord, M., Raiford, C., Eskandari, M., Marks, R. M., and Kunkel, S. L. (1989) *J. Biol. Chem.* **264**, 10621–10626
8. Kunkel, S. L., Strieter, R. M., Chensue, S. W., and Remick, D. G. (1990) in *Respiratory Distress Syndrome: Molecular to Man* (Brigham, K., and Stahlmann, M., eds) pp. 204–224, Vanderbilt Press, Nashville, TN
9. Larsen, C. G., Anderson, A. O., Oppenheim, J. J., and Matsushima, K. (1989) *Immunology* **68**, 31–36
10. Sylvester, I., Rankin, J. A., Yoshimura, T., Tanaka, S., and Leonard, E. J. (1990) *Am. Rev. Respir. Dis.* **141**, 683–688
11. Lindley, I., Aschauer, H., Seifert, J. M., Lam, C., Brunowsky, W., Kownatzki, E., Thelen, M., Peveri, P., Dewald, B., von Tscharner, V., Walz, A., and Baggiolini, M. (1988) *Proc. Natl. Acad. Sci. U. S. A.* **85**, 9199–9203
12. Walz, A., and Baggiolini, M. (1990) *J. Exp. Med.* **170**, 449–454
13. Walz, A., Dewald, B., von Tscharner, V., and Baggiolini, M. (1989) *J. Exp. Med.* **170**, 1745–1750
14. Moser, B., Clark-Lewis, I., Zwahlen, R., and Baggiolini, M. (1990) *J. Exp. Med.* **171**, 1797–1802
15. Richmond, A., Balentien, E., Thomas, H. G., Flaggs, G., Barton, D. E., Spiess, J., Bordoni, R., Francke, U., and Derynck, R. (1988) *EMBO J.* **7**, 2025–2033
16. Anisowicz, A., Bardwell, L., and Sager, R. (1987) *Proc. Natl. Acad. Sci. U. S. A.* **84**, 7188–7192
17. Anisowicz, A., Zajchowski, D., Stenman, G., and Sager, R. (1988) *Proc. Natl. Acad. Sci. U. S. A.* **85**, 9645–9649
18. Wen, D., Rowland, A., and Derynck, R. (1989) *EMBO J.* **8**, 1761–1766
19. Schroeder, J. M., Persoon, N. L. M., and Christophers, E. (1990) *J. Exp. Med.* **171**, 1091–1100
20. Thelen, M., Peveri, P., Kernen, P., von Tscharner, V., Walz, A., and Baggiolini, M. (1988) *FASEB J.* **2**, 2702–2706
21. Peveri, P., Walz, A., Dewald, B., and Baggiolini, M. (1988) *J. Exp. Med.* **167**, 1547–1559
22. Colditz, I., Zwahlen, R., Dewald, B., and Baggiolini, M. (1989) *Am. J. Pathol.* **134**, 755–760
23. Walz, A., Zwahlen, R., and Baggiolini, M. (1991) in *Chemotactic Cytokines: Formation and Biological Properties of Neutrophil-Activating Peptide 2* (NAP-2) (Westwick, J., Kunkel, S. L., and Lindley, I. J. D., eds) Plenum Publishing Corp., in press
24. Samanta, A. K., Oppenheim, J. J., and Matsushima, J. (1989) *J. Exp. Med.* **169**, 1185–1189

25. Samanta, A. K., Oppenheim, J. J., and Matsushima, K. (1990) *J. Biol. Chem.* **265,** 183–189
26. Besemer, J., Hujber, A., and Kuhn, B. (1989) *J. Biol. Chem.* **264,** 17409–17415
27. Grob, P. M., David, E., Warren, T. C., DeLeon, R. P., Farina, P. R., and Homon, C. A. (1990) *J. Biol. Chem.* **265,** 8311–8316
28. Munson, P. J., and Rodbard, D. (1990) *A user's gude to LIGAND,* Laboratory of Theoretical and Physical Biology, National Institute of Child Health and Human Development, National Institute of Health, Bethesda, MD
29. Mannervik, B. (1982) *Methods Enzymol.* **87,** 370–390
30. Deuel, T. F., Keim, P. S., Farmer, M., and Heinrikson, R. L. (1977) *Proc. Natl. Acad. Sci. U. S. A.* **74,** 2256–2258
31. Schiffmann, E., Corcoran, B. A., and Wahl, S. M. (1975) *Proc. Natl. Acad. Sci. U. S. A.* **72,** 1059–1062
32. von Tscharner, V., Prod'hom, B., Baggiolini, M., and Reuter, H. (1986) *Nature* **324,** 369–372
33. Calvo, J. C., Radicella, J. P., and Charreau, E. H. (1983) *Biochem. J.* **212,** 259–264
34. Zieler, K. (1989) *Trends Biochem. Sci.* **14,** 314–317
35. Brockhaus, M., Schoenfeld, H. J., Schlaeger, E. J., Hunziker, W., Lesslauer, W., and Loetscher, H. (1990) *Proc. Natl. Acad. Sci. U. S. A.* **87,** 3127–3131
36. Hohmann, H.-P., Remy, R., Brockhaus, M., and van Loon, A. P. G. M. (1989) *J. Biol. Chem.* **264,** 14927–14934
37. Loetscher, H., Pan, Y. C. E., Lam, H. W., Gentz, R., Brockhaus, M., Tabuchi, H., and Lesslauer, W. (1990) *Cell* **61,** 251–359
38. Smith, C. A., Davis, T., Anderson, D., Solam, L., Beckmann, M. P., Jerzy, R., Dower, S. K., Cosman, D., and Goodwin, R. G. (1990) *Science* **248,** 1019–1023
39. Schall, T. J., Lewis, M., Koller, K. J., Lee, A., Rice, G. C., Wong, G. H. W., Gatanaga, T., Granger, G. A., Lentz, R., Raab, H., Kohr, W. J., and Goeddel, D. V. (1990) *Cell* **61,** 361–370
40. Aggarwal, B. B., Eessalu, T. E., and Hass, P. E. (1985) *Nature* **318,** 665–667
41. Fountoulakis, M., Kania, M., Ozmen, L., Loetscher, H., Garotta, G., and van Loon, A. P. G. M. (1989) *J. Immunol.* **143,** 3266–3276
42. Collins, M. K. L., Sinnett-Smith, J. W., and Rozengurt, E. (1983) *J. Biol. Chem.* **258,** 11689–11693
43. Laemmli, U. K. (1970) *Nature* **227,** 680–685

Supplementary Material to

Neutrophil-Activating Peptide 2 and gro/Melanoma Growth-Stimulatory Activity interact with Neutrophil-Activating Peptide 1/Interleukin 8 Receptors on Human Neutrophils

by

Bernhard Moser, Christoph Schumacher, Vinzenz von Tscharner, Ian Clark-Lewis, and Marco Baggiolini

MATERIALS AND METHODS

Reagents

Fura-2/AM, BSA, DFP, EGTA and leupeptin were purchased from Fluka AG. HEPES, PMSF and ionomycin were from Sigma, DBS was from Pierce and RPMI 1640 was from Gibco BRL AG. Na^{125}I was obtained from Amersham. NAP-1/IL-8[3], NAP-2 [3] and gro/MGSA (14) were prepared by stepwise chemical synthesis on an Applied Biosystems 430A peptide synthesizer. CTAP-III, isolated as described previously (15), was kindly provided to us by Dr. A. Walz. fMLP was purchased from Bachem AG, and human C5a was a gift of Dr. C. A. Dahinden, Department of Clinical Immunology, University of Bern, Bern, Switzerland.

Neutrophil isolation

Human neutrophils were isolated from buffy coats of donor blood as described previously (21). The final suspensions (10^8 cells/ml consisting of 95 - 98% neutrophils) was made up in 0.15 M NaCl supplemented with 0.05 mM $CaCl_2$ and kept at 10°C until use.

Iodination

NAP-1/IL-8 was iodinated with Enzymobead reagent (Bio-Rad) as instructed by the supplier. Briefly, 1 ug of peptide ligand was mixed with 50 ul rehydrated Enzymobead reagent, 50 ul 0.2 M phosphate buffer, pH 7.2, 1 - 2 mCi Na^{125}I and 25 ul 1% ß-D-glucose, and incubated for 30 min at 21°C. Iodinated NAP-1/IL-8 was separated from free ^{125}I by Bio-Gel P2 gel filtration. Routinely, ^{125}I-NAP-1/IL-8 preparations were analyzed by SDS-polyacrylamide gel electrophoresis (SDS-PAGE). Prior to use each freshly prepared ^{125}I-NAP-1/IL-8 sample was characterized experimentally according to Calvo *et al.* (33) to evaluate its binding capacity (30 - 40%) with human neutrophils and to determine its corrected specific activity (0.3 - 1.3 x 10^{16} dpm/mol unmodified NAP-1/IL-8 equivalents). In our hands enzymatic modifications were superior to chemical iodination procedures as assessed by the specific activities and the capacities of ^{125}I-NAP-1/IL-8 to bind to neutrophils, indicating that NAP-1/IL-8 was affected by harsh oxidative conditions.

^{125}I-NAP-1/IL-8 binding and cold ligand competition

0.5 - 2.0 x 10^6 neutrophils in 120 ul RPMI 1640 containing 20 mM Hepes, pH 7.4, and 10 mg/ml BSA (binding medium) were incubated on ice (0 - 4°C) for 60 - 90 min with 0.02 - 1.10 nM ^{125}I-NAP-1/IL-8 in the presence or absence of 300 nM cold ligand (NAP-1/IL-8, NAP-2 or gro/MGSA). Cells were separated from unbound radioactivity by centrifugation at approximately 8,000 g for 1 min through 350 ul phosphate-buffered saline (PBS) containing 60 mg/ml BSA (wash medium) in a Heitech Microliter centrifuge model 2020. The supernatant was aspirated and the cell sediment was sliced off and counted in a MR 480 automatic gamma counter (Kontron). For competition binding experiments, the cells that were preincubated at 0 - 4°C for the time indicated with 1 uM cold ligand (NAP-1/IL-8, NAP-2 or gro/MGSA), were washed twice by centrifugation through wash medium and then resuspended in binding medium containing ^{125}I-NAP-1/IL-8 as indicated and further processed as described above.

Cross-linking of ^{125}I-NAP-1/IL-8 to human neutrophils

6 x 10^6 neutrophils in 120 ul binding buffer were incubated at 0 - 4°C for 90 min with 18 nM ^{125}I-NAP-1/IL-8 in the presence or absence of increasing concentrations of cold agends (NAP-1/IL-8, NAP-2 or gro/MGSA). The cells were washed once as described above and the cell sediments were resuspended in 900 ul of ice-cold PBS. Bound radioactive peptides were cross-linked to the cells with 0.5 or 1.0 mM disuccinimidyl suberate (DSS) at 0 - 4°C for 15 min. After addition of 100 ul 1 M Tris-HCl, pH 7.4, the cells were washed as described above and resuspended in 450 ul ice-cold PBS. After treatment of the cells with 450 ul 5.5 mM DFP in PBS for 10 min at 0 - 4°C, the cells were washed as described and resuspended in 1 ml PBS containing 1 mM PMSF, 20 ug/ml leupeptin and 1 mM EGTA. The cells were disrupted on ice with a Sonifier Cell Disruptor B-30, Branson Sonic Power Co. (30 pulses at setting 6, 50% duty cycles), and the unbroken cells were separated by centrifugation at 450 g for 10 min in a Minifuge GL (Heraeus). The supernatants were centrifuged for 10 min at 230,000 g (TL-100, Beckman), and the pellets were analyzed under reducing conditions by SDS-PAGE (43). After staining and drying, the gels were exposed to Amersham Hyperfilm-MP films for 1 - 4 days at -70°C. Stained molecular weight markers were from Bio-Rad.

Sequential calcium mobilization

Cytosolic-free calcium ($[Ca^{2+}]_i$) measurements were performed essentially as described by von Tscharner *et al.* (32). Briefly, 10^6 neutrophils were loaded with 0.1 nmol Fura-2/AM in 0.4 ml of incubation medium (130 mM NaCl, 4.8 mM KCl, 1 mM $CaCl_2$, 5 mM glucose and 20 mM HEPES, pH 7.4) for 20 min at 37°C. Immediately after washing with incubation medium sequential stimulations of the cells at 37°C were performed by addition of the first agonist at time 0 and the second agonist 1 min later. Fluorescence intensities, a function of saturation of Fura-2 with free calcium, were measured with a purpose-built filter fluorimeter linked by an A/D converter to a personal computer. Fluorescence signals (excitation at 334 nm, and emission larger than 485 nm) were recorded at 0.1 sec time intervals. Each measurement was standardized by addition of 2 uM ionomycin (100% Fura-2 saturation) and subsequent quenching of the fluorescence with 1 mM $MnCl_2$.

[3] Clark-Lewis, I., Moser, B., Walz, A., Baggiolini, M., Scott, G. J., and Aebersold, R., manuscript in preparation.

Fig. 1. Amino acid sequences of NAP-1/IL-8, NAP-2 and GRO/MGSA. The sequences are aligned according to their four cysteine residues (arrow heads). Conserved amino acids are boxed.

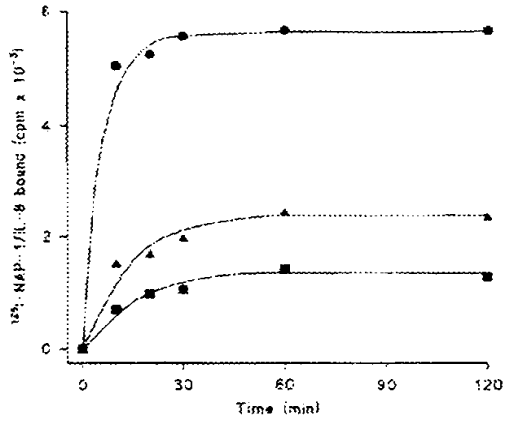

Fig. 3. Inhibition of ^{125}I-NAP-1/IL-8 binding to human neutrophils after pre-incubation with cold ligands. Aliquots of 2×10^6 cells in 100 µl were pre-incubated for 5 min at 0°C with 100 µl NAP-2 (○), gro/MGSA (△) or NAP-1/IL-8 (background, □, see Abbreviations). The cells were washed, resuspended in 100 µl, 10 nM ^{125}I-NAP-1/IL-8 and further incubated for 60 min at 0°C for the time intervals indicated. Radioactivity bound was corrected for background binding by subtracting the corresponding counts of radioactivity bound to cells pre-incubated with 1 µM NAP-1/IL-8. Data shown is the mean of duplicate measurements.

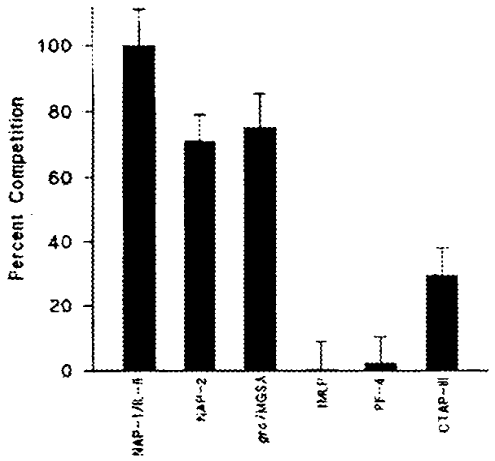

Fig. 5. Cold ligand competition for binding of ^{125}I-NAP-1/IL-8 to human neutrophils. 2×10^6 cells in 100 µl were incubated for 60 min at 0–4°C with 1 nM iodinated NAP-1/IL-8 and 1000-fold excess of unlabeled ligand (NAP-1/IL-8, NAP-2, gro/MGSA, ENA-78, PF-4, or CTAP-III). 100% competition corresponds to radioactivity displaced in the presence of 1000-fold molar excess of unlabeled NAP-1/IL-8. Error bars represent the standard deviation from the mean of three determinations.

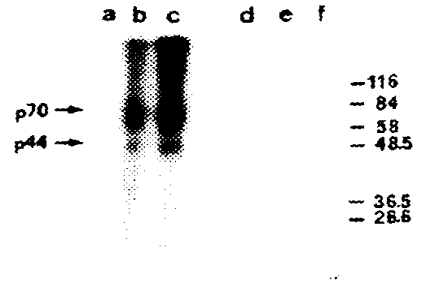

Fig. 6. Chemical cross-linking of ^{125}I-NAP-1/IL-8 to human neutrophil membranes. 6×10^6 cells in 120 µl were incubated for 30 min at 0–4°C with 5.0 nM ^{125}I-NAP-1/IL-8 in the absence (lanes a–c) or presence of 1000-fold molar excess of cold NAP-1/IL-8 (lane d), NAP-2 (lane e), or gro/MGSA (lane f). The cross-linking agent DSS was added (lane a) or absent (b–f) and incubated for 30 min (lanes b–f). The cells were further processed as described in the Methods, and the membrane proteins were analyzed by SDS-PAGE and autoradiography.

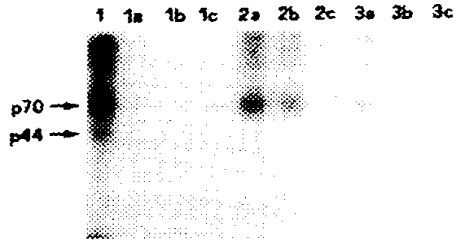

Fig. 7. Cold ligand competition during cross-linkage of ^{125}I-NAP-1/IL-8 to human neutrophil membranes. Cells were incubated at 0–4°C for 60 min with 5.0 nM ^{125}I-NAP-1/IL-8 in the absence (lanes 1) or presence of various concentrations of unlabeled NAP-1/IL-8 (lanes 1a–c), NAP-2 (lanes 2a–c) or gro/MGSA (lanes 3a–c). Concentrations of cold ligand additions were 2.5 nM (lanes 1a,2a,3a), 25 nM (lanes 1b,2b,3b) or 250 nM (lanes 1c,2c,3c). Bound ^{125}I-NAP-1/IL-8 was cross-linked with 1 mM of DSS, and the cells were further processed as described in Fig. 6.

THE JOURNAL OF BIOLOGICAL CHEMISTRY
Vol. 275, No. 10, Issue of March 3, pp. 6868–6875, 2000
Printed in U.S.A.

Chemokine Receptors CXCR-1/2 Activate Mitogen-activated Protein Kinase via the Epidermal Growth Factor Receptor in Ovarian Cancer Cells*

(Received for publication, September 8, 1999, and in revised form, November 30, 1999)

Gita Venkatakrishnan‡, Ravi Salgia§, and Jerome E. Groopman‡¶

From the ‡Divisions of Experimental Medicine and Hematology/Oncology, Beth Israel Deaconess Medical Center, Harvard Institutes of Medicine, Boston, Massachusetts 02115 and the §Department of Adult Oncology, Dana-Farber Cancer Institute and Division of Medicine, Brigham and Women's Hospital and Harvard Medical School, Dana 530C, Boston, Massachusetts 02115

Ovarian cancer typically disseminates widely in the abdomen, a characteristic that limits curative therapy. The mechanisms that promote ovarian cancer cell migration are incompletely understood. We studied model SK-OV-3 ovarian cancer cells and observed robust expression of the α chemokine receptors CXCR-1 and CXCR-2. Interleukin-8 (IL-8) treatment caused shape changes in the cells, with membrane ruffling and formation/retraction of thin actin-like projections, as detected by time-lapse microscopy. Stimulation of the CXCR-1/2 receptors by human interleukin 8 (IL-8) rapidly activated the p44/42 mitogen-activated protein (extracellular signal-regulated kinase (Erk1/2)) kinase pathway. Treatment of SK-OV-3 cells with the inhibitors genestein and herbimycin A indicated that tyrosine kinases were involved in the IL-8 activation of Erk1 and Erk2. Of note, IL-8 induced transient phosphorylation of the epidermal growth factor (EGF) receptor and its association with the adaptor molecules Shc and Grb2. This transactivation of the EGF receptor was dependent on intracellular Ca^{2+} mobilization. Furthermore AG1478, a specific inhibitor of the EGF receptor kinase, blocked Erk1 and Erk2 activation. c-Src kinase was not involved in the IL-8-mediated phosphorylation of the EGF receptor, but was critical for Shc phosphorylation and downstream Erk1/2 kinase activation. These results suggest important "cross-talk" between chemokine and growth factor pathways that may link signals of cell migration and proliferation in ovarian cancer.

The rapid spread of ovarian cancer to distant organs within the abdomen contributes to its morbidity and mortality in affected women. The movement and proliferation of the cancer cells may be regulated in an autocrine or paracrine fashion by protein factors present in the peritoneal fluid. Although the effects of growth factors like epidermal growth factor (EGF),[1] basic fibroblast growth factor, transforming growth factor α, hepatocyte growth factor, and platelet-derived growth factor on ovarian cancer cell migration and growth have been characterized (1–3), there is scant information on chemokine signaling mechanisms in this tumor type.

Chemokines have pleiotropic biological effects. They are well known to regulate the recruitment and trafficking of leukocytes to sites of inflammation. The α chemokine interleukin-8 (IL-8) also has been reported to promote tumor cell growth (4, 5). It can induce migration of melanoma and breast carcinoma cells (6, 7) and stimulate angiogenesis (8). Despite the prominent migratory behavior of ovarian cancer, no report to our knowledge has investigated which chemokine receptors and/or ligands may be involved in this phenomenon.

Chemotactic and growth signals initiated by chemokines belonging to α (-CXC), β (-CC), γ (-C), and δ (-CX_3C) subfamilies are all transduced by the activation of heptahelical G protein-coupled receptors (9). The heterotrimeric GTP-binding proteins involved are members of the pertussis toxin-sensitive G_i and -insensitive G_q families. Both the Gα subunits from the G_q class and the Gβγ subunit complex released from G_i are involved in chemokine-induced signaling (10). The activation of these G protein subunits by agonist-bound receptors triggers a typical signal transduction pathway involving activation of phospholipase C β isoforms. This results in the generation of diacylglycerol and inositol 1,4,5-trisphosphate with a subsequent increase in protein kinase C (PKC) activity and intracellular Ca^{2+} mobilization (10, 11). In addition, although chemokine receptors lack tyrosine kinase activity, they can stimulate the phosphorylation of cytoskeletal proteins, p130 Cas and paxillin (12), induce the activation of the related adhesion focal tyrosine kinase (also known as Pyk2 or CAKβ; 13), mitogen-activated protein kinases (Erk1/2, p38, and c-Jun kinase; 11, 13), phosphatidylinositol 3-kinase (11), and Janus kinase 2 (14).

p44/42 MAP kinases, also termed extracellular signal-regulated kinases (Erk1 and Erk2), are important mediators of growth and other signals from cell surface receptors to the nucleus (15, 16). Because most of the G protein-coupled receptors (GPCR) can activate a variety of effector pathways via various G protein subunits, considerable heterogeneity exists in the signaling pathways leading to Erk1/2 phosphorylation and the subsequent activation of transcription factors (17–22). An important step in the Ras/MAP kinase pathway is the

* This work was supported in part by National Institutes of Health Grants HL43510, CA77846, CA71375, HL55187, HL53745, HL61940 (to J. E. G.), and CA75348 (to R. S.). The costs of publication of this article were defrayed in part by the payment of page charges. This article must therefore be hereby marked "*advertisement*" in accordance with 18 U.S.C. Section 1734 solely to indicate this fact.

¶ To whom correspondence should be addressed: Div. of Experimental Medicine and Hematology/Oncology, 3rd Floor, 4 Blackfan Circ., Beth Israel Deaconess Medical Center, Harvard Institutes of Medicine, Boston, MA 02115. Tel.: (617) 667-0070; Fax: (617) 975-5244; E-mail: jgroopma@caregroup.harvard.edu.

[1] The abbreviations used are: EGF, epidermal growth factor; IL-8, interleukin-8; PKC, protein kinase C; MAP kinase, mitogen-activated protein kinase; Erk, extracellular signal-regulated kinase; GPCR, G protein-coupled receptors; LPA, lysophosphatidic acid; FBS, fetal bovine serum; PTX, pertussis toxin; MBP, myelin basic protein; TNF, tumor necrosis factor; GST, glutathione *S*-transferase; PE, phycoerythrin; EGFR, epidermal growth factor receptor; PBS, phosphate-buffered saline; G protein, GTP-binding protein; PP1, 4-amino-5-(4-methylphenyl)-7-(*t*-butyl) pyrazolo (3,4-d) pyrimidine.

formation of a Shc-Grb2.*son-of-sevenless* (23) or Grb2.*son-of-sevenless* (24) complex. Recently, several reports have shown that following GPCR ligation by agonists like lysophosphatidic acid (LPA), bradykinin, angiotensin II, and UTP, the formation of this complex is mediated by EGF and platelet-derived growth factor receptor kinases (25–30) as well as by cytoplasmic Pyk2/related adhesion focal tyrosine kinase and Src family kinases (31–34). However, no information on whether chemokines utilize similar mechanisms of cross-talk has been presented.

With this background, we examined ovarian cancer cells and found robust expression of the IL-8-specific receptors CXCR-1 and CXCR-2. Stimulation of these cells with recombinant human IL-8 resulted in the rapid activation of p44/42 MAP kinases (Erk1/2). Furthermore, we found that the EGF receptor and c-Src participated in the transduction of GPCR-mediated IL-8 signals, indicating a newly observed link between G protein-coupled chemokine receptor activation and tyrosine kinases believed important in ovarian cancer cell proliferation.

EXPERIMENTAL PROCEDURES

Chemicals and Reagents Were Obtained from the Following Sources—McCoy's 5A medium, fetal bovine serum (FBS), L-glutamine, and penicillin-streptomycin were from Life Technologies Inc.; protease inhibitors (phenylmethylsulfonyl fluoride, aprotinin, trypsin inhibitor, leupeptin), phorbol 12-myristate 13-acetate (PMA), and pertussis toxin (PTX) were from Sigma; genestein, herbimycin A, tyrphostin AG1478, Src family tyrosine kinase inhibitor PP1, and the calcium ionophore A23187 were from Calbiochem; myelin basic protein (MBP) was from Upstate Biotechnology (Lake Placid, NY); recombinant human IL-8, tumor necrosis factor (TNF-α), and EGF were from R & D Systems (Minneapolis, MN); glutathione *S*-transferase (GST) amino acid residues 1–218, full-length GST-Grb2 (amino acids 1–217) fusion protein, GST, normal rabbit and mouse IgG and mouse IgG conjugated with fluorescein isothiocyanate were all procured from Santa Cruz Biotechnology (Santa Cruz, CA). The Dc protein assay kit and nitrocellulose transfer membrane were from Bio-Rad, and the enhanced chemiluminescence (ECL) detection system, donkey anti-rabbit and sheep anti-mouse IgG conjugated to horseradish peroxidase, protein A and Gamma Bind plus Sepharose and Glutathione-Sepharose 4B were from Amersham Pharmacia Biotech.

Antibodies and Their Specificities—Mouse monoclonal antibody to human interleukin-8 receptor A (IL-8RA or CXCR-1) conjugated with phycoerythrin (PE) and PE-mouse IgG2b isotype control were from PharMingen (San Diego, CA), and monoclonal anti-IL-8RB (CXCR-2) was a gift from LeukoSite, Inc. (Cambridge, MA). Monoclonal antibody from Santa Cruz (sc-120, 528) raised against the cell surface epitope of the human EGF receptor (EGFR) was used for immunoprecipitations, and rabbit anti-EGFR (sc-03, 1005) with an epitope mapping at residues 1005–1016 of the precursor form of EGFR (human origin) was used for Western blotting. Rabbit polyclonal antibodies to Erk1 (sc-93, C-16) and Erk2 (sc-154, C-14) with epitopes corresponding to an amino acid sequence mapping at the carboxyl terminus of Erk1-encoded MAP kinase p44 and Erk2-encoded MAP kinase p42 of rat origin were used in the *in vitro* kinase assays. Rabbit polyclonal antibodies to human Shc (06–203; Upstate Biotechnology) corresponding to amino acids 366–473 and monoclonal anti-Shc antibody (sc-967) corresponding to amino acids 366–473 within the SH2 domain of Shc (human origin) were used for immunoprecipitation and Western blotting, respectively. For anti-phosphotyrosine Western blot analysis, a combination of PY99 (sc-7020, dilution 1:1000) and 4G10 (a gift from Dr. B. Druker, Oregon Health Sciences University, Portland, OR; dilution 1:3000) was used.

Cells, Culture Conditions, and Stimulation—SK-OV-3 cells (ATCC, TB-77), derived from the malignant ascites of a human ovary adenocarcinoma, were maintained in McCoy's 5A medium supplemented with 10% FBS, 1.5 mM L-glutamine, and 20 IU/ml penicillin-streptomycin at 37 °C in humidified 5% CO_2 atmosphere. Prior to stimulation, the cells were serum-starved for 24 h. Stimulation occurred at 37 °C with IL-8 (100 ng/ml) or EGF (10 ng/ml) as specified in the figures.

Flow Cytometric Analysis—Cells were detached from the substratum with 2 mM EDTA/Dulbecco's PBS (minus Ca^{2+} and Mg^{2+}). They were washed twice with D-PBS and resuspended at 3×10^6 cells/0.5 ml and then incubated on ice for 30 min with primary antibody (anti-human IL-8RA conjugated with PE or with PE-conjugated mouse IgG2b isotype control). Cells were screened for the expression of IL-8RB by incubation on ice for 30 min with monoclonal IL-8RB primary antibody, washed, and then incubated for another 30 min on ice with the secondary antibody (goat anti-mouse IgG labeled with fluorescein isothiocyanate). Normal mouse IgG was used as the control. After the final incubation, cells were washed twice with D-PBS and analyzed immediately on a Becton Dickinson FACSCAN driven by Cell Quest software (Beth Israel Deaconess Medical Center, Boston, MA).

Chemokine Secretion—Cells (4×10^5) plated in 12-well plates were allowed to grow to 80% confluency and then were serum-starved for 24 h. Quiescent cells were then incubated for 6 h in serum-free medium or medium containing fetal bovine serum or TNF-α. Culture medium was cleared by centrifugation at 2000 rpm and 4 °C to remove debris. IL-8 secreted into the culture medium was quantitated using the human IL-8 enzyme-linked immunosorbent assay kit obtained from Endogen (Woburn, MA).

Time-lapse Video Microscopy—The effect of IL-8 on the morphology of SK-OV-3 cells was monitored using time-lapse video microscopy. Cells were detached from the substratum with 2 mM EDTA/D-PBS (minus Ca^{2+} and Mg^{2+}), and washed twice with McCoy's 5A medium. Before the start of the experiment, cells (1×10^5) were cultured in 35×10 mm tissue culture plates (Becton Dickinson Labware) in serum-free McCoy's 5A medium for 18 h in a humidified 37 °C incubator with 5% CO_2. The cells were then observed via time-lapse video microscopy in a 37 °C and 5% CO_2 controlled chamber, and 12 h later they were stimulated with IL-8 (50 ng/ml). Changes in cell morphology were examined using an Olympus IX70 inverted microscope, Omega temperature control device, Optronics Engineering DE1-750 3CCD digital video camera, and Sony SVT-S3100 time-lapse S-VHS video recorder. For image presentation, video images were captured and printed with the Sony Color Video Printer UP-5600MD.

Immunoprecipitation and Immunoblotting—After stimulation, monolayers were washed with ice-cold D-PBS and lysed in chilled radioimmune precipitation buffer (50 mM Tris-HCl, pH 7.6, 150 mM NaCl, 1% Nonidet P-40, 1 mM Na_3VO_4, 1 mM NaF, 1 mM sodium pyrophosphate, 1 mM phenylmethylsulfonyl fluoride, 1 μg/ml aprotinin, 1 μg/ml leupeptin, 1 μg/ml trypsin inhibitor, 1 μg/ml pepstatin). Cell lysates were cleared by centrifugation at 13,000 rpm, and protein concentration was determined using a Dc protein assay kit (Bio-Rad). For immunoprecipitations, 1 ml of cell lysates (0.5 to 1.0 mg/ml protein) was incubated at 4 °C for 1–2 h with the appropriate primary antibodies. The immune complexes absorbed to protein A or Gamma Bind plus Sepharose were washed thrice with chilled lysis buffer, once with D-PBS, and then eluted with 2× Laemmli SDS sample buffer. When GST fusion proteins were used in immunoprecipitations, glutathione-Sepharose 4B was employed to adsorb the immune complexes. The immunoprecipitated proteins were resolved by SDS-polyacrylamide gel electrophoresis and transferred onto nitrocellulose membranes (Bio-Rad). The membranes were blocked for 1 h at room temperature in 5% milk prepared in Tris-buffered saline-T (10 mM Tris-HCl, pH 7.5, 150 mM NaCl, 0.1% Tween 20) and probed for 1–2 h at room temperature or overnight at 4 °C with the appropriate antibodies diluted in blocking buffer. The membranes were washed and incubated with the appropriate horseradish peroxidase-conjugated secondary antibody diluted in Tris-buffered saline-T for 1 h at room temperature. The immune complexes on the washed membranes were visualized using ECL reagents.

In Vitro Kinase Assay—MAP kinase activity was determined following immunoprecipitation using MBP as substrate. Serum-starved cells pretreated with vehicle or specific inhibitors were stimulated with IL-8 or EGF, as indicated in the figures. Cells were lysed in lysis buffer and clarified at 15,000 × *g* for 15 min, and then 100–500 μg of protein was immunoprecipitated with 1 μg each of anti-Erk1 and Erk2. After 4 h at 4 °C, the immune complexes were absorbed to protein A-Sepharose. After overnight rocking at 4 °C, the beads were washed thrice with lysis buffer containing protease inhibitors and twice with kinase buffer (20 mM Hepes, pH 7.4, 10 mM $MgCl_2$, 3 mM β-mercaptoethanol). Phosphorylation of MBP was carried out at room temperature for 30 min in a total volume of 25 μl by the addition of a mixture containing 5–7 μg of MBP, 5 μCi of [γ-^{32}P]ATP, and 20 μM ATP to the Erk1/2 immunoprecipitates. The reaction was terminated by the addition of 4× Laemmli SDS buffer. ^{32}P-labeled MBP was resolved on 14% SDS-polyacrylamide gel electrophoresis.

RESULTS

Cell Surface Expression of CXCR-1 and CXCR-2 Receptors—SK-OV-3 ovarian cancer cells were screened for cell surface expression of chemokine receptors by fluorescence-activated cell sorter analysis. Only cells incubated with monoclonal anti-

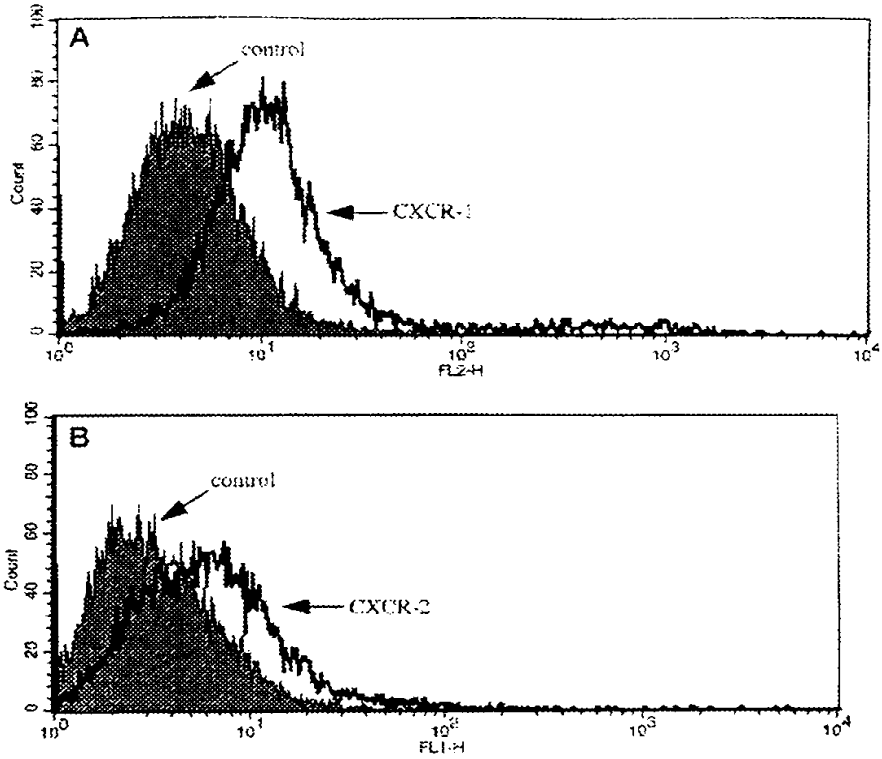

FIG. 1. **Analysis of cell surface expression of CXCR-1 (*A*) and CXCR-2 (*B*) by flow cytometry.** The results are shown as fluorescence histograms representing chemokine receptor expression (*line*) and isotype IgG control (*solid*).

human IL-8RA (CXCR-1) antibody conjugated with PE or anti-IL-8RB (CXCR-2) primary antibody followed by staining with fluorescein isothiocyanate-labeled secondary antibody displayed a shift in fluorescence intensity (Fig. 1). This confirmed the expression of α chemokine IL-8-specific receptors, CXCR-1 and CXCR-2.

Secretion of IL-8 Protein—Secretion of IL-8 protein by various cell lines in the absence or presence of cytokines like TNF-α, IL-1α, and -β has been reported (4, 35, 36). To determine if SK-OV-3 cells produced IL-8 protein, monolayers of quiescent cells were stimulated for 6 h with medium alone or medium containing varying concentrations of FBS or TNF-α (20 ng/ml). A dose-dependent increase in the release of IL-8 was detected in response to FBS by enzyme-linked immunosorbent assay. At 5% FBS, approximately 1 ng/ml of IL-8 was detected; controls without serum yielded 0.1 ng/ml, and TNF-α stimulation yielded 1.2 ng/ml (data not shown).

IL-8 Induces Morphological Changes in SK-OV-3 Cells—Chemotactically stimulated myeloid cells, neutrophils, and breast cancer carcinoma cell lines undergo transient cytoskeletal rearrangements that lead to morphological alterations, ultimately resulting in cell migration (7, 37, 38). Similarly, SK-OV-3 cells, as shown in Fig. 2, *E–H*, displayed increased membrane ruffling and altered membrane protrusions in response to IL-8 as determined by time-lapse video microscopy. As seen in Fig. 2, *A–D*, untreated SK-OV-3 cells had little membrane ruffling and minimal actin protrusions. When IL-8 was added to the cells, increased membrane ruffling and the formation/retraction of thin actin-like projections were readily apparent (Fig. 2, *E–H*). The formation/retraction of thin actin-like projections was observed in at least 75% of the cells over an 18-h time period.

Stimulation of CXCR-1 and CXCR-2 Receptors Leads to the Activation of MAP Kinase—IL-8 signals are transduced by the heterotrimeric G protein-coupled receptors CXCR-1 and CXCR-2. It is well documented that signals relayed by various GPCRs result in the activation of MAP kinases Erk1 and Erk2 (15, 18, 39). To examine the effect of IL-8 on MAP kinase activation, lysates from SK-OV-3 cells treated with IL-8 (100 ng/ml) were immunoprecipitated with anti-Erk1 and Erk2-specific antibodies and subjected to an *in vitro* kinase assay. The activation of these MAP kinases was assessed by the extent of phosphorylation of the substrate, MBP. Maximum activation was observed between 1 and 2 min, and leveled off by 10 min (Fig. 3*A*).

Depending on the G protein subunits involved, a variety of effectors can be activated that result in multiple signaling pathways. We therefore mapped pathways leading to Erk1/2 activation in SK-OV-3 cells in response to IL-8 stimulation. Pretreatment of cells with PTX (100 ng/ml) or tyrosine kinase-specific inhibitors genestein (20 μM) and herbimycin A (1 μM) or down-regulation of PKC by prolonged exposure to phorbol 12-myristate 13-acetate (100 nM) each had a significant effect on reducing enzyme activity (Fig. 3*B*). This suggested the involvement of tyrosine kinases in CXCR-1 and CXCR-2 mediated signaling in these cells.

IL-8 Induces Association of the Phosphorylated EGF Receptor with Shc and Grb2—Activation of the Ras-dependent MAP kinase signaling pathway by receptor tyrosine kinases involves the recruitment of a Grb2.*son-of-sevenless* complex to the plasma membrane, either directly or indirectly by its association with phosphorylated Shc (24, 25, 34, 40, 41). To address whether these cytosolic adaptor molecules participated in the transduction of IL-8 signals, interacting proteins from cell lysates treated with IL-8 (100 ng/ml) or EGF (10 ng/ml) were immunoprecipitated with a full-length GST-Grb2 fusion protein. IL-8 treatment induced phosphorylation of a number of cellular proteins and their association with GST-Grb2 (Fig. 4). Of these Grb2-associating proteins, the ~170-kDa molecule was identified as the EGF receptor and the 46-, 52-, and 66-kDa

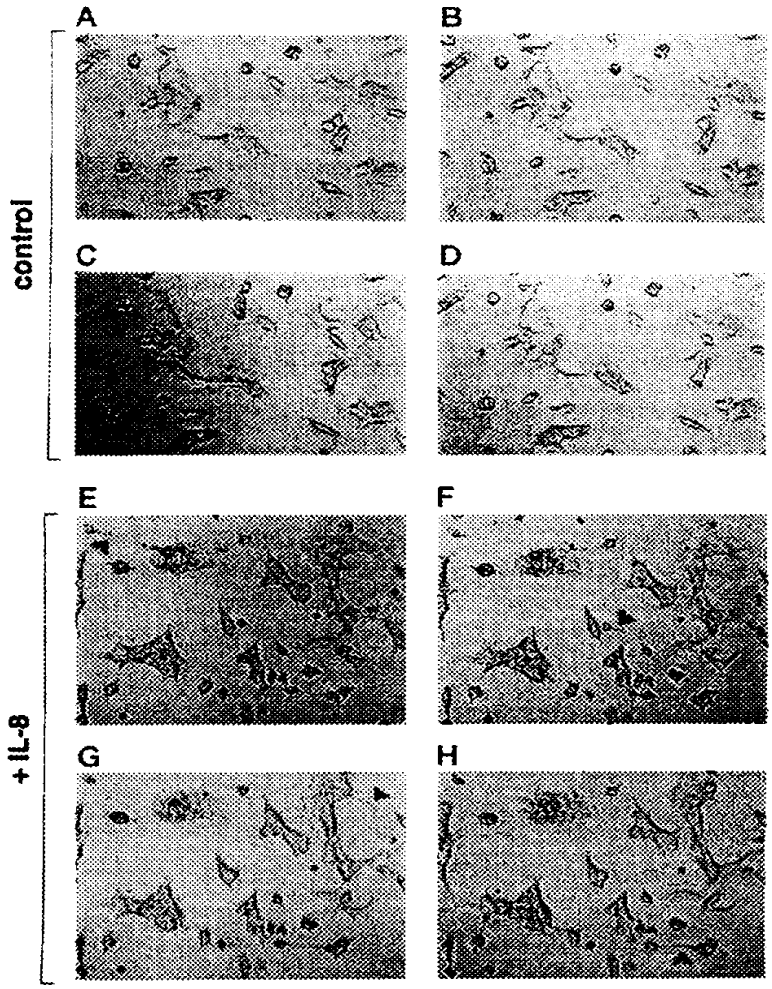

FIG. 2. **Time-lapse video microscopy of unstimulated and IL-8-stimulated SK-OV-3 cells.** As described under "Experimental Procedures," SK-OV-3 cells were observed over a 12-h period of time, and approximately 3-h time points are shown (*A–D*). Cells were later stimulated with IL-8 (50 ng/ml), and again 3-h time point intervals are shown (*E–H*). The long actin-like projections, which are readily formed and retracted in response to IL-8, are indicated by *arrowheads*.

proteins as the isoforms of Shc. Although the phosphorylation and association of the 46 and 52 kDa forms of Shc were transient, occurring as early as 1 min, the phosphorylation of p66 was much weaker and sustained over a 30-min period.

Inhibition of EGF Receptor Autophosphorylation Blocks CXCR-1/2-mediated Mitogen-activated Protein Kinase Activation—The EGF receptor is one of the protein-tyrosine kinases that has been implicated in transducing signals initiated by GPCR-specific agonists like angiotensin II, LPA, and bombesin (25–27). To determine if the EGF receptor plays a role in CXCR-1/2-mediated signaling in ovarian cancer cells, lysates from cells stimulated with IL-8 (100 ng/ml) or EGF (10 ng/ml) were immunoprecipitated with a monoclonal anti-EGFR antibody. Western blot analysis of the immunoprecipitated proteins clearly showed the phosphorylation of a 170-kDa protein. Transactivation of the EGFR was rapid, reaching a maximum by 2 min (Fig. 5). The specificity of this rapid phosphorylation was further confirmed by pretreating cells with the EGF receptor kinase-specific inhibitor, tyrphostin AG1478. Incubation of cells with AG1478 (250 nM) for 30 min prior to stimulation with IL-8 or EGF significantly reduced the activation of the EGF receptor (Fig. 5).

Tyrphostin AG1478, the inhibitor of EGF receptor autophosphorylation, was found to partially block IL-8 or EGF-induced downstream signals leading to the activation of MAP kinase (Fig. 6, *A* and *B*, and 9*A*). In the control cells, the maximum phosphorylation of the MBP substrate occurred at 1 min and tapered off by 10 min, whereas in the AG1478-treated cells there was a weak but gradual increase in phosphorylation, peaking by 10 min.

IL-8 Induces Calcium-dependent Phosphorylation of the EGF Receptor—CXCR-1 and CXCR-2 stimulation activate the phosphatidylinositol-phospholipase C pathway leading to increases in intracellular calcium levels (10, 42). We assessed the role of Ca^{2+} in the IL-8-induced transactivation of the EGF receptor by treating the cells with the calcium ionophore, A23187 (10 μM). A rapid increase in the tyrosyl phosphorylation of the EGF receptor kinase was observed (Fig. 7). The intracellular calcium chelator 1,2-bis(*o*-aminophenoxy) ethane-*N*,*N*,*N*′,*N*′-tetraacetic acid tetra (acetoxymethyl) ester (10 μM) blocked this phosphorylation, whereas the extracellular calcium chelator EGTA (5 mM) had no effect on the extent of phosphorylation (data not shown). This indicated that the transactivation of the receptor tyrosine kinase was mediated by intracellular calcium mobilization.

Role of c-Src Kinase in IL-8-induced EGFR Phosphorylation and MAP Kinase Activation—Recent studies indicate that nonreceptor tyrosine kinases of the c-Src family are involved in GPCR-mediated Ras/MAP kinase activation. Src kinases par-

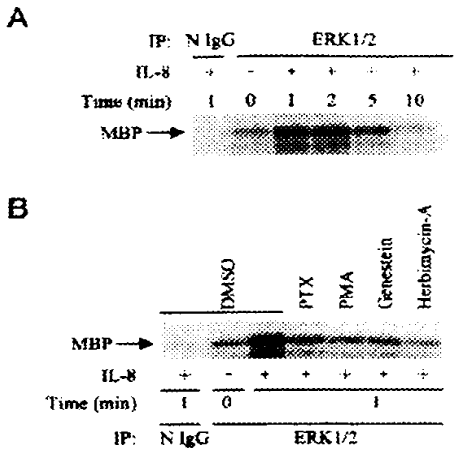

FIG. 3. *A*, IL-8-induced MAP kinase activation. Quiescent SK-OV-3 cells were stimulated with IL-8 (100 ng/ml) at 37 °C for the indicated periods of time. After lysis, endogenous Erk1 and Erk2 were immunoprecipitated (*IP*) with the indicated antibodies or with control antibody (*N IgG*). Immune complexes were analyzed for MAP kinase activity by *in vitro* kinase assay as described under "Experimental Procedures." *B*, effect of signaling inhibitors on IL-8-induced MAP kinase activation. Quiescent SK-OV-3 cells were treated at 37 °C with 100 ng/ml PTX (24 h), 100 nM PMA (24 h), 20 μM genestein (30 min), or 1 μM herbimycin A (20 h). After lysis, endogenous MAP kinases Erk1 and Erk2 were immunoprecipitated (*IP*) with the indicated antibodies or with control antibody (*N IgG*). Immune complexes were analyzed for MAP kinase activity by *in vitro* kinase assay as described under "Experimental Procedures." *DMSO*, Me_2SO.

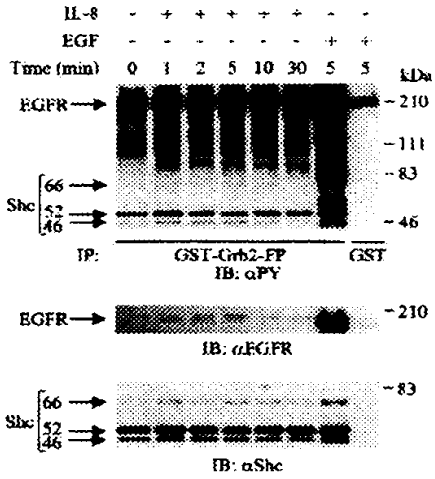

FIG. 4. **Phosphorylation and association of the EGF receptor and Shc to the GST-Grb2 fusion protein in response to IL-8 or EGF stimulation.** Quiescent SK-OV-3 cells were stimulated at 37 °C with IL-8 (100 ng/ml) or EGF (10 ng/ml) for the indicated periods of time. After lysis, Grb2-associated proteins were immunoprecipitated (*IP*) with 30 ng of full-length GST-Grb2 fusion protein or GST alone, and the immune complexes were adsorbed to glutathione-Sepharose 4B. The associated proteins were resolved by SDS-polyacrylamide gel electrophoresis and immunoblotted (*IB*) with a mixture of anti-phosphotyrosine monoclonal antibodies (*αPY*), anti-EGFR polyclonal, and anti-Shc monoclonal antibodies as indicated.

ticipate by phosphorylating two important substrates, Shc and EGFR (26, 34, 43, 44). We therefore treated cells with the Src kinase family inhibitor, PP1, prior to exposure to IL-8. We did not observe changes in the phosphorylation of EGFR in response to IL-8 under these conditions (Fig. 8). This result suggests another nonreceptor kinase may contribute to the

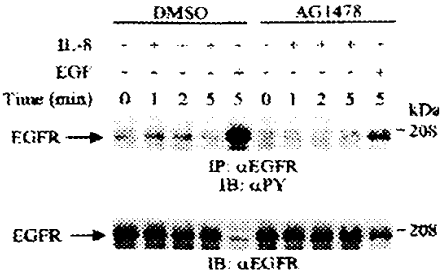

FIG. 5. **Effect of tyrphostin AG1478 on IL-8- or EGF-induced phosphorylation of the EGF receptor.** Quiescent SK-OV-3 cells were pretreated at 37 °C with Me_2SO (*DMSO*, vehicle) or 250 nM AG1478 for 30 min prior to stimulation with IL-8 (100 ng/ml) or EGF (10 ng/ml). EGFR was immunoprecipitated with monoclonal anti-EGFR antibody. Tyrosyl-phosphorylated EGFR was detected by immunoblotting (*IB*) with a mixture of anti-phosphotyrosine monoclonal antibodies (*αPY*). The amount of EGFR in the immunoprecipitates was assessed by reprobing the blot with anti-EGFR polyclonal antibody.

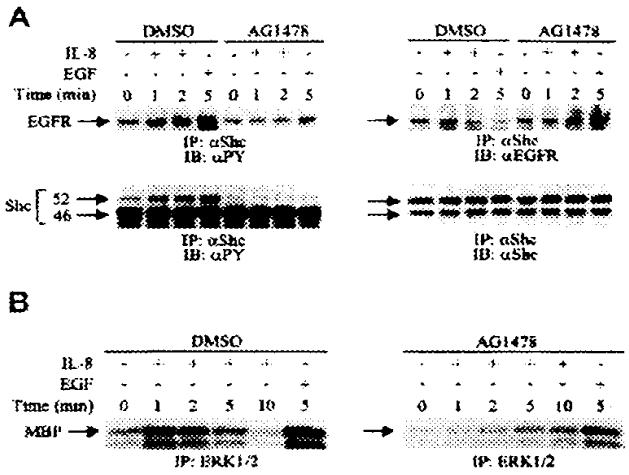

FIG. 6. *A*, effect of EGFR tyrosine kinase inhibitor AG1478 on IL-8 or EGF induced phosphorylation of Shc. Quiescent SK-OV-3 cells were treated at 37 °C with Me_2SO (*DMSO*, vehicle) or 250 nM AG1478 for 30 min prior to stimulation of cells with IL-8 (100 ng/ml) or EGF (10 ng/ml). Shc was immunoprecipitated (*IP*) from cell lysates with anti-Shc polyclonal antibody. Phosphorylated Shc and EGFR were detected by immunoblotting (*IB*) with a mixture of anti-phosphotyrosine monoclonal antibodies (*αPY*). The amounts of Shc and EGFR in the immunoprecipitates were assessed by reprobing the blot with anti-Shc monoclonal antibody and anti-EGFR polyclonal antibody. *B*, effect of tyrphostin AG1478 on IL-8- or EGF-induced MAP kinase activation. Quiescent SK-OV-3 cells were pretreated with Me_2SO (*DMSO*, vehicle) or 250 nM AG1478 for 30 min at 37 °C prior to stimulation with IL-8 (100 ng/ml) or EGF (10 ng/ml) for the indicated periods of time. After lysis, endogenous Erk1 and Erk2 were immunoprecipitated (*IP*) with the indicated polyclonal antibodies. Immune complexes were analyzed for MAP kinase activity by *in vitro* kinase assay as described under "Experimental Procedures."

transactivation of EGFR upon IL-8 stimulation in SK-OV-3 cells. PP1 did, however, have an inhibitory effect on the phosphorylation of Shc protein (Fig. 9*A*) and on the activation of Erk1/2 in response to both IL-8 and EGF (Fig. 9*B*).

DISCUSSION

IL-8 belongs to the α or CXC subfamily of proinflammatory chemokines and induces neutrophil chemotaxis, respiratory burst, granule release, and increased cell adhesion (45–48). It is also produced endogenously by nonhematopoietic cells like human melanoma and pancreatic cancer cells and exerts autocrine growth modulating effects (4, 5, 49). IL-8 mediates these

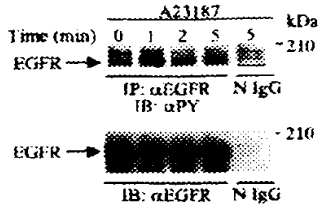

FIG. 7. **Ca^{2+} ionophore A23187-induced tyrosine phosphorylation of the EGFR.** Quiescent SK-OV-3 cells were stimulated at 37 °C with 10 μM A23187 for the indicated periods of time. EGFR was immunoprecipitated (*IP*) from cell lysates with monoclonal anti EGFR antibody. Normal mouse IgG (*N IgG*) was used as the control. Tyrosyl-phosphorylated EGFR was detected by immunoblotting (*IB*) with a mixture of anti-phosphotyrosine monoclonal antibodies (*αPY*). The amount of EGFR in the immunoprecipitates was assessed by reprobing the blot with anti-EGFR polyclonal antibody.

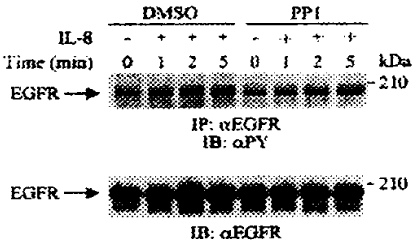

FIG. 8. **Effect of Src tyrosine kinase inhibitor PP1 on IL-8-induced tyrosine phosphorylation of EGFR.** Quiescent SK-OV-3 cells were treated at 37 °C with Me_2SO (*DMSO*, vehicle) or 10 μM PP1 for 15 min prior to stimulation of cells with IL-8 (100 ng/ml). EGFR was immunoprecipitated (*IP*) from cell lysates with monoclonal anti-EGFR antibody. Tyrosyl-phosphorylated EGFR was detected by immunoblotting (*IB*) with a mixture of anti-phosphotyrosine monoclonal antibodies (*αPY*). The amount of EGFR in the immunoprecipitates was assessed by reprobing the blot with anti-EGFR polyclonal antibody.

effects by binding to the G protein-coupled CXCR-1 and CXCR-2 receptors (50).

We observed robust expression of the CXCR-1 and CXCR-2 receptors on SK-OV-3 human ovarian cancer cells (Fig. 1). We also detected significant amounts of extracellular IL-8 protein in the culture medium. IL-8, a potent neutrophil chemoattractant, is known to induce migratory responses in non-hematopoietic cells such as human A2058 melanoma and MCF-7 and ZR-75-1 breast cancer cells (7). The mechanisms by which cells translocate in response to various factors are complex. The migratorial processes include dissolution of cell surface contacts, formation of lamellipodia, actin filament fragmentation and nucleation, and finally contraction of the actin filament network leading to cell movement (51). In the present study, exposure to IL-8 caused changes in the shape of the ovarian cancer cells with increased membrane ruffling and the formation/retraction of thin actin-like projections. This would indicate that IL-8 potentially may be involved in the cell motility of ovarian cancer cells and could contribute to the process of metastasis.

Erks are important mediators of signals from cell surface receptors to the nucleus (16, 20). Agonists like hormones, neuropeptides, and chemokines that activate heterotrimeric G proteins signal to these MAP kinases (15). It has been reported that the IL-8-specific receptors CXCR-1 and CXCR-2, in neutrophils, COS and Jurkat cells, couple to both PTX-sensitive G_i and -insensitive G_q (α14 and α16) family members and stimulate phosphatidylinositol hydrolysis with increases in intracellular calcium levels and PKC activity (10, 42, 52). PKC is known to mediate activation of MAP kinase both via Ras-dependent and -independent mechanisms (20, 53, 54). In SK-OV-3 cells, IL-8 induced activation of p44/42 MAP (Erk1/2) kinases (Fig. 3*A*). This effect was significantly reduced when cells were treated with PTX or after cellular depletion of PKC by prolonged exposure to phorbol 12-myristate 13-acetate (Fig. 3*B*). Several studies suggest that the potent mitogenic effects of GPCR-specific agonists (angiotensin II, LPA, and bombesin) in different cell types result from cooperative activation of multiple signal-transducing pathways involving G proteins and tyrosine kinases (26, 27, 30, 32, 34, 55, 56). This, to our knowledge, has not yet been investigated with chemokines. In SK-OV-3 cells, MAP kinase activity was attenuated when cells were pretreated with the tyrphostins genestein and herbimycin A prior to IL-8 stimulation (Fig. 3*B*). This clearly showed the involvement of tyrosine kinases in IL-8 signal transduction.

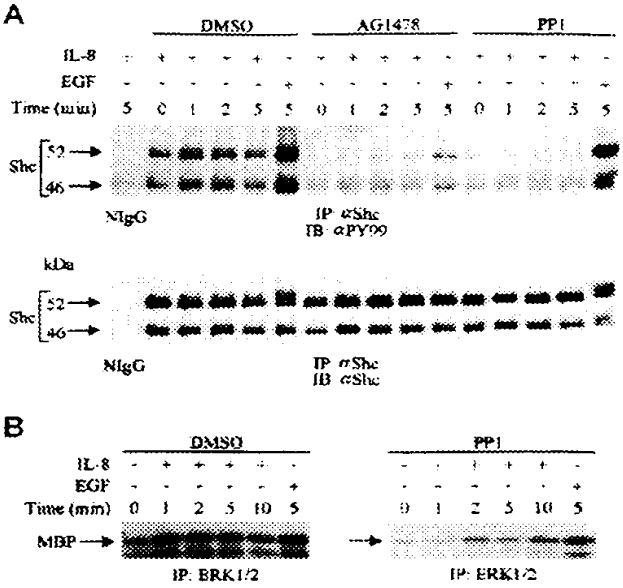

FIG. 9. *A*, effect of EGFR and Src tyrosine kinase inhibitors AG1478 and PP1, respectively, on IL-8- or EGF-induced phosphorylation of Shc. Quiescent SK-OV-3 cells were treated at 37 °C with Me_2SO (*DMSO*, vehicle) or 10 μM PP1 for 15 min prior to stimulation of cells with IL-8 (100 ng/ml) or EGF (10 ng/ml). Shc was immunoprecipitated (*IP*) from cell lysates with anti-Shc polyclonal antibody. Phosphorylated Shc was detected by immunoblotting (*IB*) with a mixture of anti-phosphotyrosine monoclonal antibodies (*αPY*). The amount of Shc in the immunoprecipitates was assessed by reprobing the blot with anti-Shc monoclonal antibody. *B*, effect of Src tyrosine kinase inhibitor PP1 on IL-8- or EGF-induced MAP kinase activation. Quiescent SK-OV-3 cells were pretreated with Me_2SO (*DMSO*, vehicle) or 10 μM PP1 for 15 min at 37 °C prior to stimulation with IL-8 (100 ng/ml) or EGF (10 ng/ml) for the indicated periods of time. After lysis, endogenous Erk1 and Erk2 were immunoprecipitated (*IP*) with the indicated polyclonal antibodies. Immune complexes were analyzed for MAP kinase activity by *in vitro* kinase assay as described under "Experimental Procedures."

An important feature in tyrosine kinase receptor-mediated activation of Ras-dependent MAP kinase activation is the phosphorylation of the receptor and its association with Grb2 either directly (24) or indirectly through the phosphorylated Shc adaptor protein (23, 41, 57, 58). There is also the recruitment of the Ras guanine nucleotide exchange factor to the plasma membrane where it activates Ras, thereby initiating a signaling cascade leading to the activation of MAP kinase. Several studies have demonstrated the involvement of EGFR in mitogenic signaling induced by GPCR agonists (25–29, 43). In the present study, we observed the phosphorylation of several cellular proteins upon IL-8 stimulation. Of these Grb2-associating proteins, 46-, 52-, and 66-kDa proteins were identified as isoforms of the Shc protein, and the high molecular mass (~170

kDa) protein was identified as EGFR (Fig. 4). It is possible that other members of the EGFR family like ErbB2 and ErbB3 are present in the Grb2 fusion protein complex. Using the specific inhibitor AG1478, we showed that the intrinsic kinase activity of EGFR was required for receptor autophosphorylation (Fig. 5) and for phosphorylation of downstream molecules like Shc (Fig. 6*A* and 9*A*), leading to MAP kinase activation (Fig. 6*B*). Intrinsic EGFR kinase activity was also required for Shc phosphorylation in studies of LPA, endothelin-1, and α-thrombin-induced signaling in Rat-1 cells, UTP signaling in PC12 neuronal cells, and angiotensin II-induced responses in vascular smooth muscle cells (25–28).

Previously reported GPCR agonists that are involved in EGFR transactivation act via the G_i and G_q class of G proteins (25, 26, 28, 43). The α subunit of the G_q family member and $\beta\gamma$ released from G_i activate various isoforms of phospholipase C-β, thereby increasing intracellular Ca^{2+} levels (59–61). In PC12 neuronal cells, membrane depolarization induced Ca^{2+} influx and treatment with bradykinin or calcium ionophore also triggered EGFR transactivation (29). Tyrosyl phosphorylation of the EGF receptor in SK-OV-3 cells (Fig. 7) was also initiated by the calcium ionophore A23187, which mimicks the G protein-mediated increase in Ca^{2+} flux. The intracellular calcium chelator 1,2-bis(*o*-aminophenoxy) ethane-*N*,*N*,*N*′,*N*′-tetraacetic acid tetra (acetoxymethyl) ester blocked this phosphorylation, although no such effect was observed when the influx of extracellular Ca^{2+} was blocked by EGTA (data not shown). We found that intracellular Ca^{2+} was both necessary and sufficient to trigger EGFR transactivation in a ligand-independent manner in ovarian cancer cells. It is possible that the Ca^{2+}-dependent transactivation of the EGF receptor in SK-OV-3 cells may result from the activation of a nonreceptor kinase, the involvement of phosphatidylinositol-phospholipase C-mediated activation of Ca^{2+}-dependent PKC isoforms, or the inhibition of a phosphotyrosine phosphatase. These possibilities will be addressed in future studies.

The Src family of protein-tyrosine kinases has been implicated in relaying responses of various mitogenic factors (56, 62, 63). However, there are conflicting reports on its role in GPCR-mediated signaling. Roche *et al.* (64) and Kranenburg *et al.* (65) reported that c-Src activity was not required for relaying the mitogenic effects of LPA, bombesin, and thrombin. Activation of $p60^{c\text{-}src}$ was required for the G_i-coupled LPA receptor-mediated $G\beta\gamma$ subunit-dependent activation of Erk1/2 in COS-7 cells (26, 34) and for the G_i and $G_{q/11}$-coupled (LPA, bradykinin, and thrombin) receptor stimulation of Erk1/2 in PC12 cells and growth-responsive fibroblasts (25, 30). Activated Src mediates Ras/MAP kinase activation through tyrosine phosphorylation of the adaptor protein Shc and its subsequent association and complex formation with Grb2 as demonstrated for the receptors for *N*-formyl peptides, LPA, UTP, angiotensin II, and the α2A adrenergic receptors (26–28, 43, 44). Another prominent substrate of Src is EGFR (63, 66). Using the specific inhibitor PP1, we showed that Src phosphorylated Shc protein and was required for MAP kinase activity (Fig. 9, *A* and *B*) but not for EGFR phosphorylation upon IL-8 stimulation in SK-OV-3 cells (Fig. 8). Similar results were reported by Daub *et al.* (26) on the effects of LPA in COS cells. Thus, additional signaling factors like tyrosine kinases may act downstream of EGFR in SK-OV-3 cells.

In these ovarian cancer cells, CXCR-1/2 receptors mediated the activation of p44/42 MAP kinase via multiple tyrosine kinase pathways (Fig. 3*B*). The increase in intracellular Ca^{2+} appeared responsible for the transactivation of the EGF receptor tyrosine kinase (Fig. 7). It is known that both the $G\beta\gamma$ subunit and the $G\alpha$ subunit of the G_q class of proteins contribute to increases in intracellular Ca^{2+} levels in response to IL-8 (10, 42, 52). Whereas MAP kinase activity was totally abolished by PTX, the extent of EGFR phosphorylation was unaffected (data not shown). These results suggest that a member of a PTX-insensitive G_q family regulates MAP kinase activity via an EGF receptor tyrosine kinase pathway in SK-OV-3 cells. The involvement of EGFR in the signaling of CXCR-1/2 suggests important cross-talk between chemokine and growth factor receptor signaling pathways in ovarian cancer.

Acknowledgments—We thank Nancy DesRosiers for preparation of the figures, Simone Jadusingh for typing, and Janet Delahanty for editing the manuscript.

REFERENCES

1. Corps, A. N., Sowter, H. M., and Smith, S. K. (1997) *Int. J. Cancer* **73,** 151–155
2. Ellerbrock, S. M., Hudson, L. G., and Stack, M. S. (1998) *Int. J. Cancer* **78,** 331–337
3. Westermann, A. M., Beijnen, J. H., Moolenaar, W. H., and Rodenhuis, S. (1997) *Cancer Treat. Rev.* **23,** 113–131
4. Schadendorf, D., Moller, A., Algermissen, B., Worm, M., Sticherling, M., and Czarnetzki, B. M. (1993) *J. Immunol.* **151,** 2667–2675
5. Miyamoto, M., Shimizu, Y., Okada, K., Kashii, Y., Higuchi, K., and Watanabe, A. (1998) *Cancer Immunol. Immunother.* **47,** 47–57
6. Wang, J. M., Taraboletti, G., Matsushima, K., Van Damme, J., and Mantovani, A. (1990) *Biochem. Biophys. Res. Commun.* **169,** 165–170
7. Youngs, S. J., Ali, S. A., Taub, D. D., and Rees, R. C. (1997) *Int. J. Cancer* **71,** 257–266
8. Koch, A. E., Polverini, P. J., Kunkel, S. L., Harlow, L. A., DiPietro, L. A., Elner, V. M., Elner, S. G., and Strieter, R. M. (1992) *Science* **258,** 1798–1801
9. Rollins, B. J. (1997) *Blood* **90,** 909–928
10. Wu, D., LaRosa, G. J., and Simon, M. I. (1993) *Science* **261,** 101–103
11. Ganju, R. K., Brubaker, S. A., Meyer, J., Dutt, P., Yang, Y., Qin, S., Newman, W., and Groopman, J. E. (1998) *J. Biol. Chem.* **273,** 23169–23175
12. Dutt, P., Wang, J. F., and Groopman, J. E. (1998) *J. Immunol.* **161,** 3652–3658
13. Ganju, R. K., Dutt, P., Wu, L., Newman, W., Avraham, H., Avraham, S., and Groopman, J. E. (1998) *Blood* **91,** 791–797
14. Mellado, M., Rodriguez-Frade, J. M., Aragay, A., del Real, G., Martin, A. M., Vila-Coro, A. J., Serrano, A., Mayor, F., Jr., and Martinez, A. C. (1998) *J. Immunol.* **161,** 805–813
15. Gutkind, J. S. (1998) *J. Biol. Chem.* **273,** 1839–1842
16. Cobb, M. H., and Goldsmith, E. J. (1995) *J. Biol. Chem.* **270,** 14843–14846
17. Crespo, P., Xu, N., Simonds, W. F., and Gutkind, J. S. (1994) *Nature* **369,** 418–420
18. Della Rocca, G. J., van Biesen, T., Daaka, Y., Luttrell, D. K., Luttrell, L. M., and Lefkowitz, R. J. (1997) *J. Biol. Chem.* **272,** 19125–19132
19. Hawes, B. E., Luttrell, L. M., van Biesen, T., and Lefkowitz, R. J. (1996) *J. Biol. Chem.* **271,** 12133–12136
20. Hawes, B. E., van Biesen, T., Koch, W. J., Luttrell, L. M., and Lefkowitz, R. J. (1995) *J. Biol. Chem.* **270,** 17148–17153
21. Lopez-Ilasaca, M., Crespo, P., Pellici, P. G., Gutkind, J. S., and Wetzker, R. (1997) *Science* **275,** 394–397
22. Richardson, R. M., Ali, H., Pridgen, B. C., Haribabu, B., and Snyderman, R. (1998) *J. Biol. Chem.* **273,** 10690–10695
23. van Biesen, T., Hawes, B. E., Luttrell, D. K., Krueger, K. M., Touhara, K., Porfiri, E., Sakaue, M., Luttrell, L. M., and Lefkowitz, R. J. (1995) *Nature* **376,** 781–784
24. Buday, L., and Downward, J. (1993) *Cell* **73,** 611–620
25. Daub, H., Weiss, F. U., Wallasch, C., and Ullrich, A. (1996) *Nature* **379,** 557–560
26. Daub, H., Wallasch, C., Lankenau, A., Herrlich, A., and Ullrich, A. (1997) *EMBO J.* **16,** 7032–7044
27. Eguchi, S., Numaguchi, K., Iwasaki, H., Matsumoto, T., Yamakawa, T., Utsunomiya, H., Motley, E. D., Kawakatsu, H., Owada, K. M., Hirata, Y., Marumo, F., and Inagami, T. (1998) *J. Biol. Chem.* **273,** 8890–8896
28. Soltoff, S. P. (1998) *J. Biol. Chem.* **273,** 2311[illegible]–23117
29. Zwick, E., Daub, H., Aoki, N., Yamaguchi-Aoki, Y., Tinhofer, I., Maly, K., and Ullrich, A. (1997) *J. Biol. Chem.* **272,** 24767–24770
30. Linseman, D. A., Benjamin, C. W., and Jones, D. A. (1995) *J. Biol. Chem.* **270,** 12563–12568
31. Dikic, I., Tokiwa, G., Lev, S., Courtneidge, S. A., and Schlessinger, J. (1996) *Nature* **383,** 547–550
32. Eguchi, S., Iwasaki, H., Inagami, T., Numaguchi, K., Yamakawa, T., Motley, E. D., Owada, K. M., Marumo, F., and Hirata, Y. (1999) *Hypertension* **33,** 201–206
33. Soltoff, S. P., Avraham, H., Avraham, S., and Cantley, L. C. (1998) *J. Biol. Chem.* **273,** 2653–2660
34. Luttrell, L. M., Hawes, B. E., van Biesen, T., Luttrell, D. K., Lansing, T. J., and Lefkowitz, R. J. (1996) *J. Biol. Chem.* **271,** 19443–19450
35. Singh, R. K., and Varney, M. L. (1998) *Cancer Res.* **58,** 1532–1537
36. Standiford, T. J., Kunkel, S. L., Basha, M. A., Chensue, S. W., Lynch, J. P., III, Toews, G. B., Westwick, J., and Strieter, R. M. (1990) *J. Clin. Invest.* **86,** 1945–1953
37. Salgia, R., Quackenbush, E., Lin, J., Souchkova, N., Sattler, M., Ewaniuk, D. S., Klucher, K. M., Daley, G. Q., Kraeft, S. K., Sackstein, R., Alves, E. P., ven Andrian, U. H., Chen, L. B., Gutierrez-Ramos, J.-C., Pendergast, A. M., and Griffin, J. D. (1999) *Blood* **94,** 4232–4246
38. Ehrengruber, M. U., Coates, T. D., and Deranleau, D. A. (1995) *FEBS Lett.* **359,** 229–232

39. Eguchi, S., Matsumoto, T., Motley, E. D., Utsunomiya, H., and Inagami, T. (1996) *J. Biol. Chem.* **271,** 14169–14175
40. Chen, Y., Grall, D., Sulcini, A. E., Pelicci, P. G., Pouyssegur, J., and Van Obberghen-Schilling, E. (1996) *EMBO J.* **15,** 3037–3044
41. Ohmichi, M., Matuoka, K., Takenawa, T., and Saltiel, A. R. (1994) *J. Biol. Chem.* **269,** 1143–1148
42. Jones, S. A., Moser, B., and Thelen, M. (1995) *FEBS Lett.* **364,** 211–214
43. Luttrell, L. M., Della Rocca, G. J., van Biesen, T., Luttrell, D. K., and Lefkowitz, R. J. (1997) *J. Biol. Chem.* **272,** 4637–4644
44. Ptasznik, A., Traynor-Kaplan, A., and Bokoch, G. M. (1995) *J. Biol. Chem.* **270,** 19969–19973
45. Loetscher, P., Seitz, M., Clark-Lewis, I., Baggiolini, M., and Moser, B. (1994) *FEBS Lett.* **341,** 187–192
46. Detmers, P. A., Powell, D. E., Walz, A., Clark-Lewis, I., Baggiolini, M., and Cohn, Z. A. (1991) *J. Immunol.* **147,** 4211–4217
47. Jones, S. A., Dewald, B., Clark-Lewis, I., and Baggiolini, M. (1997) *J. Biol. Chem.* **272,** 16166–16169
48. Rainger, G. E., Rowley, A. F., and Nash, G. B. (1998) *Blood* **92,** 4819–4827
49. Bar-Eli, M. (1999) *Pathobiology* **67,** 12–18
50. Murphy, P. M. (1997) *Semin. Hematol.* **34,** 311–318
51. Stossel, T. P. (1993) *Science* **260,** 1086–1094
52. L'Heureux, G. P., Bourgoin, S., Jean, N., McColl, S. R., and Naccache, P. H. (1995) *Blood* **85,** 522–531
53. Watanabe, T., Waga, I., Honda, Z., Kurokawa, K., and Shimizu, T. (1995) *J. Biol. Chem.* **270,** 8984–8990
54. Zou, Y., Komuro, I., Yamazaki, T., Aikawa, R., Kudoh, S., Shiojima, I., Hiroi, Y., Mizuno, T., and Yazaki, Y. (1996) *J. Biol. Chem.* **271,** 33592–33597
55. Marrero, M. B., Schieffer, B., Li, B., Sun, J., Harp, J. B., and Ling, B. N. (1997) *J. Biol. Chem.* **272,** 24684–24690
56. Rodriguez-Fernandez, J. L., and Rozengurt, E. (1998) *J. Biol. Chem.* **271,** 27895–27901
57. Okada, S., Yamauchi, K., and Pessin, J. E. (1995) *J. Biol. Chem.* **270,** 26737–26741
58. Lee, C. H., Park, D., Wu, D., Rhee, S. G., and Simon, M. I. (1992) *J. Biol. Chem.* **267,** 16044–16047
59. Katz, A., Wu, D., and Simon, M. I. (1992) *Nature* **360,** 686–689
60. Hepler, J. R., Kozasa, T., Smrcka, A. V., Simon, M. I., Rhee, S. G., Sternweis, P. C., and Gilman, A. G. (1993) *J. Biol. Chem.* **268,** 14367–14375
61. Wu, D., Katz, A., and Simon, M. I. (1993) *Proc. Natl. Acad. Sci. U. S. A.* **90,** 5297–5301
62. Gelderloos, J. A., Rosenkranz, S., Bazenet, C., and Kazlauskas, A. (1998) *J. Biol. Chem.* **273,** 5908–5915
63. Wasilenko, W. J., Payne, D. M., Fitzgerald, D. J., and Weber, M. J. (1991) *Mol. Cell. Biol.* **11,** 309–321
64. Roche, S., Koegl, M., Barone, M. V., Roussel, M. F., and Courtneidge, S. A. (1995) *Mol. Cell. Biol.* **15,** 1102–1109
65. Kranenburg, O., Verlaan, I., Hordijk, P. L., and Moolenaar, W. H. (1997) *EMBO J.* **16,** 3097–3105
66. Stover, D. R., Becker, M., Liebetanz, J., and Lydon, N. B. (1995) *J. Biol. Chem.* **270,** 15591–15597

THE JOURNAL OF BIOLOGICAL CHEMISTRY
Vol. 269, No. 52, Issue of December 30, pp. 32909–32916, 1994
Printed in U.S.A.

Solution Structure of GRO/Melanoma Growth Stimulatory Activity Determined by ^{1}H NMR Spectroscopy*

(Received for publication, June 21, 1994, and in revised form, October 4, 1994)

Key-Sun Kim‡§, Ian Clark-Lewis¶, and Brian D. Sykes‡‖

From the ‡Protein Engineering Network of Centres of Excellence (PENCE) and Dept. of Biochemistry, University of Alberta, Edmonton, Alberta T6G 2S2, Canada and the ¶PENCE, The Biomedical Research Centre and Dept. of Biochemistry and Molecular Biology, University of British Columbia, Vancouver, British Columbia V6T 1Z3, Canada

The three-dimensional solution structure of the growth-related protein-α/melanoma growth stimulatory activity (GRO/MGSA) has been solved by two-dimensional ^{1}H nuclear magnetic resonance spectroscopy. The GRO/MGSA monomer consists of an NH_2-terminal loop, a three-stranded antiparallel β-sheet, and a COOH-terminal α-helix. Dimerization, which is apparent under the experimental conditions used (2 mM, pH 5.10, 30 °C), results in a six-stranded antiparallel β-sheet and a pair of helices with 2-fold symmetry. While the basic fold is similar to that seen for interleukin-8 (IL-8) (Clore, G. M., Appella, E., Yamada, M., Matsushima, K., and Gronenborn, A. M. (1990) *Biochemistry*, 29, 1689–1696), there are differences in the ELR motif (residues 6–8), the turn involving residues 31–36, which is linked to the NH_2-terminal region through the 9–35 disulfide bond. The most significant differences are in the NH_2-terminal loop (residues 12–23). In IL-8, all the corresponding regions have been shown to be required for receptor binding (Clark-Lewis, I., Dewald, B., Loetscher, M., Moser, B., and Baggiolini, M. (1994) *J. Biol. Chem.* 269, 16075–16081). The structural differences thus have been identified between GRO/MGSA and IL-8 could contribute to their different receptor binding specificities.

Melanoma growth stimulatory activity (MGSA)[1] was originally identified as an autocrine growth factor for the human melanoma cell line Hs294T (Richmond *et al.*, 1988). The amino acid sequence revealed that MGSA is similar to interleukin-8 (IL-8), and functional studies showed that MGSA is a potent neutrophil-activating protein like IL-8 (Moser *et al.*, 1990). MGSA expression is induced in a wide range of tissues by interleukin 1 or tumor necrosis factor α (Richmond *et al.*, 1988; Haskill *et al.*, 1990; Wen *et al.*, 1989) and may have an important role in inflammation as well as melanoma transformation. The sequence of MGSA shows that it is the product of a gene termed the growth-related gene α (*groα*), which is induced in fibroblasts (Anisowicz *et al.*, 1987). Two additional closely related genes, *groβ* and *groγ*, have also been identified (Haskill *et al.*, 1990, Tekamp-Olson *et al.*, 1990). Herein, the GROα or MGSA protein will be termed GRO/MGSA.

GRO/MGSA is a member of a family of chemokines (CXC chemokines), which have the first two cysteines separated by 1 amino acid (Miller and Krangel, 1992; Baggiolini and Clark-Lewis, 1992). Many of these CXC chemokines, including GRO/MGSA, GROβ, GROγ, IL-8, granulocyte chemotactic protein-2 (Proost *et al.*, 1993), ENA78 (Walz *et al.*, 1991), and neutrophil activating protein-2 (Walz and Baggiolini, 1989), are chemoattractants and activators of neutrophils.

Among CXC chemokines, IL-8 is the best characterized, and the three-dimensional structure of the dimer has been solved by both NMR (Clore *et al.*, 1990) and x-ray crystallography (Baldwin *et al.*, 1991). The three-dimensional structure of IL-8 monomer consists of an NH_2-terminal loop, a three-stranded antiparallel β-sheet, and a COOH-terminal α-helix. The dimer is stabilized by the formation of a six-stranded antiparallel β-sheet and interactions between the two α-helices and the β-sheet. Structure-function studies of IL-8 have shown that the NH_2-terminal ELR motif (residues 4–6, see Fig. 1) is critical for receptor binding and function (Clark-Lewis *et al.*, 1991b, 1993; Hébert *et al.*, 1991). In addition, both disulfide bridges (Cys-7 to Cys-34, Cys-9 to Cys-50), the NH_2-terminal loop (residues 10–22), and the β-turn (residues 30–35) between the first and second β-strands are also important for function (Clark-Lewis *et al.*, 1994). GRO/MGSA has 43% sequence identity with IL-8 (Fig. 1).

Two receptors for IL-8 have been identified on human neutrophils: IL-8 receptor 1 and IL-8 receptor 2 (Holmes *et al.*, 1991; Murphy and Tiffany, 1991). IL-8 receptor 1 has high affinity for IL-8 but low affinity for GRO/MGSA and neutrophil-activating protein 2, whereas IL-8 receptor 2 has high affinity for all three chemokines (Cerretti *et al.*, 1993; Moser *et al.*, 1991; Schumacher *et al.*, 1992). Recently, a separate GRO/MGSA receptor was detected in human melanoma cells (Horuk *et al.*, 1993). Compared with IL-8 receptor 2, this receptor is specific for GRO/MGSA in that binding sites cannot be displaced by IL-8. In addition, a promiscuous receptor that binds to GRO/MGSA and other chemokines has been discovered on erythrocytes (Neote *et al.*, 1993).

Many questions remain concerning GRO/MGSA structure and function. The structural basis for discrimination between the two IL-8 receptors by CXC chemokines remains to be determined. The role of GRO/MGSA in cell growth and transformation (Balentien *et al.*, 1991) has not been defined. The basis for binding to the unique growth-inducing receptor on melanoma cells or to the Duffy antigen receptor is unknown. The role of dimerization in chemokine function is controversial.

* This work is supported by the Protein Engineering Network of Centres of Excellence (PENCE), the National Cancer Institute of Canada, and National Institutes of Health Grant R01 GM50969-01 (to I. C.-L.). The costs of publication of this article were defrayed in part by the payment of page charges. This article must therefore be hereby marked "*advertisement*" in accordance with 18 U.S.C. Section 1734 solely to indicate this fact.

§ A PENCE postdoctoral fellow.

‖ To whom correspondence should be addressed. Tel.: 403-492-6540; Fax: 403-492-1473; E-mail: bds@polaris.biochem.ualberta.ca.

[1] The abbreviations use are: MGSA, melanoma growth stimulatory activity; GRO, growth-related protein; IL-8, interleukin-8; DQF-COSY, two-dimensional double quantum filtered correlation spectroscopy; HOHAHA, two-dimensional homonuclear Hartmann-Hahn spectroscopy; PE-COSY, primitive exclusive two-dimensional correlation spectroscopy; ROESY, two-dimensional rotating frame nuclear Overhauser spectroscopy; NOE, nuclear Overhauser effect; NOESY, two-dimensional nuclear Overhauser spectroscopy; r.m.s., root-mean-square; H-bond, hydrogen bond; HPLC, high pressure liquid chromatography.

TABLE I
Proton resonance assignments of GRO/MGSA at 30 °C at pH 5.1

*, stereospecifically assigned protons; for the C^{β}, C^{γ}, and C^{δ}, the asterisk indicates protons of the $C^{\beta 2}H$, $C^{\gamma 2}H_3$, and $C^{\delta 2}H_3$, respectively. Degenerate chemical shifts are separated by a slash (/). All chemical shifts are from 2,2-dimethyl-2-silapentane 5-sulfonate.

Residue	NH	$C^{\alpha}H$	$C^{\beta}H$	Others
Ala-1		4.15	1.54	
Ser-2	8.65	4.57	3.85/3.85	
Val-3	8.27	4.13	2.06	$C^{\gamma}H_3$ 0.91/0.91
Ala-4	8.40	4.29	1.37	
Thr-5	7.99	4.14	4.18	$C^{\gamma}H_3$ 1.19
Glu-6	8.38	4.27	1.93, 2.03	$C^{\gamma}H$ 2.24, 2.18
Leu-7	8.05	4.26	1.57, 1.45*	$C^{\gamma}H$ 1.54; $C^{\delta}H_3$ 0.84, 0.70*
Arg-8	7.78	4.77	1.81, 2.06*	$C^{\gamma}H$ 1.56/1.56; $C^{\delta}H$ 3.18/3.18; $N^{\epsilon}H$ 7.18
Cys-9	8.52	4.67	2.70, 3.81*	
Gln-10	11.22	4.28	2.00, 2.12*	$C^{\gamma}H$ 2.37/2.37; $N^{\epsilon}H_2$ 6.80, 7.48
Cys-11	9.45	4.90	3.17, 2.77*	
Leu-12	8.70	4.36	1.67/1.67	$C^{\gamma}H$ 1.64; $C^{\delta}H_3$ 0.92, 0.84*
Gln-13	7.78	4.62	2.02, 2.14*	$C^{\gamma}H$ 2.33/2.33
Thr-14	8.49	4.54	3.94	$C^{\gamma}H_3$ 1.03
Leu-15	8.60	4.67	1.65/1.65	$C^{\gamma}H$ 1.81; $C^{\delta}H_3$ 0.92/0.92
Gln-16	8.75	4.46	2.02, 2.20*	$C^{\gamma}H$ 2.47/2.47; $N^{\epsilon}H_2$ 6.87, 7.54
Gly-17	7.74	3.93, 3.76		
Ile-18	7.08	4.21	1.67	$C^{\gamma}H$ 1.08, 1.36; $C^{\gamma}H_3$ 0.74; $C^{\delta}H_3$ 0.75
His-19	8.48	4.77	3.08/3.08	$C^{\delta 2}H$ 7.14; $C^{\epsilon 1}H$ 7.98
Pro-20		4.10	2.20/2.20	$C^{\gamma}H$ 2.01, 1.82; $C^{\delta}H$ 3.78, 3.27
Lys-21	9.65	4.26	1.84/1.84	$C^{\gamma}H$ 1.35/1.35; $C^{\delta}H$ 1.57/1.57; $C^{\epsilon}H$ 2.84/2.84
Asn-22	8.14	4.87	2.77, 3.12*	$N^{\delta}H_2$ 7.10, 7.50
[illegible]	[illegible]	[illegible]	[illegible]	[illegible]
Ser-25	8.21	5.36	4.01, 3.96	
Val-26	9.28	4.75	1.76	$C^{\gamma}H_3$ 0.78, 0.82*
Asn-27	8.80	5.68	2.88, 2.59*	$N^{\delta}H_2$ 6.62, 7.18
Val-28	9.37	4.57	2.18	$C^{\gamma}H_3$ 0.87, 0.82*
Lys-29	9.37	4.70	1.96/1.96	$C^{\gamma}H$ 1.51/1.51; $C^{\delta}H$ 1.69/1.69; $C^{\epsilon}H$ 2.95/2.95
Ser-30	7.94	4.75	4.04/4.04	
Pro-31		4.49	1.78, 2.11	$C^{\gamma}H$ 2.00, 1.69; $C^{\delta}H$ 3.59, 4.10
Gly-32	8.58	4.43, 4.02		
Pro-33		4.15	2.22, 1.40	$C^{\gamma}H$ 1.97, 1.89; $C^{\delta}H$ 3.65, 3.57
His-34	8.42	4.77	3.22,2.90	$C^{\delta 2}H$ 7.16; $C^{\epsilon 1}H$ 8.32
Cys-35	7.26	4.77	2.95/2.95	
Ala-36	8.88	4.49	1.46	
Gln-37	7.46	4.81	1.96, 2.16	$C^{\gamma}H$ 2.42, 2.27; $N^{\epsilon}H_2$; 6.71, 7.79
Thr-38	8.66	4.53	3.93	$C^{\gamma}H_3$ 1.12
Glu-39	8.60	4.90	1.93, 1.99	$C^{\gamma}H$ 2.41/2.41
Val-40	9.56	4.91	2.28	$C^{\gamma}H_3$ 0.82, 0.72*
Ile-41	9.15	4.72	1.81	$C^{\gamma}H$ 1.52, 1.13; $C^{\gamma}H^3$ 0.79; $C^{\delta}H_3$ 0.84
Ala-42	9.89	5.27	1.35	
Thr-43	9.17	4.77	4.20	$C^{\gamma}H_3$ 1.20
Leu-44	9.42	5.04	2.14, 1.78*	$C^{\gamma}H$ 1.67; $C^{\delta}H_3$ 0.85, 0.71*
Lys-45	8.47	3.99	1.81, 1.97*	$C^{\gamma}H$ 1.36/1.36; $C^{\delta}H$ 1.72/1.72; $C^{\epsilon}H$ 2.90/2.90
Asn-46	7.70	4.63	3.28, 2.79*	$N^{\delta}H_2$ 6.56, 7.41
Gly-47	8.13	4.32, 3.56		
Arg-48	7.74	4.33	1.90, 1.82	$C^{\gamma}H$ 1.62/1.62; $C^{\delta}H$ 3.19/3.19; $N^{\epsilon}H$ 7.21
Lys-49	8.30	5.46	1.70, 1.57*	$C^{\gamma}H$ 1.47/1.47; $C^{\delta}H$ 1.57/1.57; $C^{\epsilon}H$ 2.96/2.96
Ala-50	9.12	4.67	1.25	
Cys-51	9.00	5.54	3.89, 3.12*	
Leu-52	8.99	4.96	1.45/1.45	$C^{\gamma}H$ 1.65; $C^{\delta}H_3$ 0.71, 0.77*
Asn-53	8.85	4.79	2.98, 2.82	$N^{\delta}H_2$ 7.13, 7.93
Pro-54			1.99/1.99	$C^{\gamma}H$ 2.08, 2.29; $C^{\delta}H$ 4.30, 4.09
Ala-55	7.52	4.38	1.43	
Ser-56	7.65	4.89	4.21/4.21	$O^{\gamma}H$ 6.38
Pro-57		4.36	2.47, 2.03	$C^{\gamma}H$ 2.16/2.16; $C^{\delta}H$ 4.18, 4.06
Ile-58	7.65	3.86	1.93	$C^{\gamma}H$ 1.53, 1.30; $C^{\gamma}H_3$ 0.95; $C^{\delta}H_3$ 0.86
Val-59	7.22	3.43	2.35	$C^{\gamma}H_3$ 1.12, 0.82*
Lys-60	7.24	3.74	1.88/1.88	$C^{\gamma}H$ 1.50, 1.32; $C^{\delta}H$ 1.66, 1.71; $C^{\epsilon}H$ 2.93/2.93
Lys-61	7.31	4.08	1.95/1.95	$C^{\gamma}H$ 1.47, 1.58; $C^{\delta}H$ 1.68/1.68; $C^{\epsilon}H$ 2.94/2.94
Ile-62	8.35	3.58	1.98	$C^{\gamma}H$ 1.94, 0.94; $C^{\gamma}H_3$ 0.80; $C^{\delta}H_3$ 0.78
Ile-63	7.90	3.58	1.88	$C^{\gamma}H$ 1.00, 1.76; $C^{\gamma}H_3$ 0.86; $C^{\delta}H_3$ 0.72
Glu-64	8.20	3.82	2.17, 2.09	$C^{\gamma}H$ 2.71, 2.48
Lys-65	8.04	4.11	1.94/1.94	$C^{\gamma}H$ 1.50/1.50; $C^{\delta}H$ 1.59, 1.66; $C^{\epsilon}H$ 2.94/2.94
Met-66	8.01	4.07	2.20, 1.94	$C^{\gamma}H$ 2.84, 2.42; $C^{\epsilon}H_3$ 1.90
Leu-67	7.92	4.02	1.85, 1.68*	$C^{\gamma}H$ 1.95; $C^{\delta}H_3$ 0.85, 0.77*
Asn-68	7.54	4.75	2.76, 2.96	$N^{\delta}H_2$ 6.90, 7.60
Ser-69	8.06	4.32	3.99/3.99	
Asp-70	8.35	4.59	2.76, 2.67	
Lys-71	8.23	4.40	1.77, 1.94	$C^{\gamma}H$ 1.47/1.47; $C^{\delta}H$ 1.69/1.69; $C^{\epsilon}H$ 3.03/3.03
Ser-72	8.01	4.23	3.86/3.86	

Dimerization of IL-8 is not essential for receptor binding (Rajarathnam *et al.*, 1994a), although an *in vivo* role has not been ruled out. On the other hand, an alternative dimer form for CC chemokines (Lodi *et al.*, 1994) has been described, leading to speculation of the functional significance of dimerization. Knowledge of the three-dimensional structure of GRO/MGSA would greatly enhance our ability to resolve these structure-function questions by comparison with known structures. Here, we present the solution structure of GRO/MGSA solved by ^1H NMR spectroscopy and compare it with IL-8. A preliminary report of NMR assignments and secondary structure of GRO/MGSA has appeared (Fairbrother *et al.*, 1993).

MATERIALS AND METHODS

Sample Preparation—The 72-residue GRO/MGSA protein was synthesized by automated solid phase synthesis (Applied Biosystems model 430A) using the tertiary butyloxycarbonyl and benzyl protection strategy. After deprotection with hydrogen fluoride, the material was folded by air oxidation and purified by reverse-phase HPLC. Purity was assessed by reverse-phase HPLC and isoelectric focusing. The final amino acid composition was determined by amino acid analysis. The sources of reagents were as previously described (Clark-Lewis *et al.*, 1991a). The last amino acid (Asn) was truncated to avoid peptide by-products that were initially thought to be due to impurities in the Asn acyl-resin used for synthesis. The resin was later shown not to be a problem. Truncated GRO/MGSA had the same activity as the full-length protein. An NMR sample was prepared by dissolving lyophilized protein in either 90% H_2O, 10% D_2O or 99.9% D_2O, and the pH was adjusted to 5.10 ± 0.05 (glass electrode, uncorrected) with concentrated NaOD. For hydrogen exchange rate measurements, the sample was adjusted to pH 4.6.

NMR Spectroscopy—The DQF-COSY (Ernst *et al.*, 1986), HOHAHA (Bax, 1889), ROESY (Bothner-By *et al.*, 1984), and NOESY (Ernst *et al.*, 1986) spectra were acquired in both H_2O and D_2O solutions, and PE-COSY (Mueller, 1987) spectrum was acquired in D_2O (HOHAHA, with mixing times of 45 and 55 ms and with 1.5 ms trim pulse; NOESY, with mixing times of 50, 100, 150, and 200 ms; ROESY, with mixing time of 30 ms; and PE-COSY, with a 36° mixing pulse). The spectral width of 8500 Hz was used for H_2O, and a narrower spectral width (4000 Hz) was used for D_2O. All NMR spectra were recorded in the phase-sensitive mode using the States *et al.* (1982) method on a Varian Unity 600 NMR spectrometer. For amide proton exchange measurements, hydrogen exchange was started by dissolving the lyophilized sample in D_2O. A COSY spectrum was acquired every 3 h, and the hydrogen exchange rates were derived from cross-peak volumes.

Sequential Assignments—The sequential assignment of the residues in the ^1H NMR spectrum was achieved by identifying spin systems using HOHAHA spectra and establishing through-space connectivities using NOESY spectra. The direct scalar connectivities were unambiguously identified in DQF-COSY and PE-COSY recorded in H_2O and D_2O, respectively. Despite the severe spectral overlap due to low numbers of aromatic residues (2 histidines) and the resulting ring current effect of on the ^1H NMR chemical shift of neighboring residues in the protein, the assignments of all overlapped peaks could be accomplished by observing NOE connectivities to neighboring residues.

Interproton Distance Restraints—NOE intensities measured by volume integration were converted into distances referenced to the long range β-sheet NOE between C$^\alpha$H and backbone NH as 3.2 Å (Wüthrich, 1986) and were divided into four groups with distance ranges of 1.8–2.7, 1.8–3.5, 2.3–5.0, and 2.8–6.0 Å (Clore *et al.*, 1990). The NOE intensities for distance restraints were derived from the 150-ms NOESY spectra. In the case of distances involving methyl or methylene protons, an additional 0.5 Å was added to the upper distance limit to account for the higher apparent intensity of multiple protons. If NOEs were observed from a proton to both methylene protons, which were not stereospecifically assigned, the weaker NOE was explicitly used for the restraints of the two NOEs. A total of 366 long range ($|i-j| \geq 5$) NOEs, 204 medium range ($2 \leq |i-j| \leq 4$) NOEs, 518 sequential NOEs, 974 intraresidue NOEs, and 42 dimeric NOEs were used for structure calculations.

Stereospecific Assignments and Torsion Angle Restraints—Stereospecific assignments were made based on $^3J_{\alpha\beta}$ coupling constants, intraresidue, and sequential NOEs (Wagner *et al.*, 1987). The $^3J_{\alpha\beta}$ coupling constants were measured from PE-COSY spectrum recorded in D_2O at 30 °C. Due to spectral overlap, only a portion of methylene protons were stereospecifically assigned. Some of the protons could not be stereospecifically assigned because they are in the rapid conformational exchange. The χ_1 angles were restrained approximately based on three major conformations, and a deviation of ±60° was allowed for χ_1 torsion angle restraints. The stereospecific assignments of methyl groups of leucine and valine were made from the intraresidue NOEs (Zuiderweg *et al.*, 1985; Powers *et al.*, 1993). A total of 30 χ_1 angle restraints were used for structure calculations.

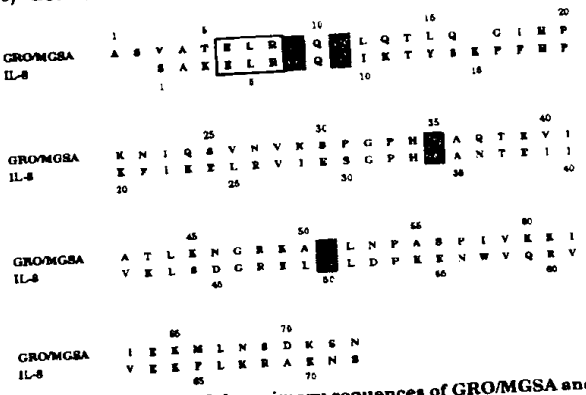

FIG. 1. **Alignment of the primary sequences of GRO/MGSA and IL-8.** The residue numbers of GRO/MGSA are shown on the *top*. The ELR motif is *boxed*, and the conserved cysteines are *hatched*.

Hydrogen Bonding Restraints—Backbone hydrogen bonds were initially assigned from NOE connectivities and hydrogen exchange rate measurements. An amide proton with a measurable exchange rate under the experimental conditions of 30 °C, pH 4.6 (~2 mM protein), was considered as a possible hydrogen bond donor. Only hydrogen bonds that satisfied both NOE connectivities and hydrogen exchange rates were used for structure calculations. A total of 20 intra-subunit hydrogen bonds for the dimer were assigned. Two of the inter-subunit hydrogen bonds used for structure calculations (26 NH-28′ O, 26′ NH-28 O) did not satisfy hydrogen exchange rate criteria; however, NOE connectivities and initial structure showed the existence of these hydrogen bonds. For each hydrogen bond, two restraints ($r_{NH\text{-}O}$, 1.8–2.3 Å; $r_{N\text{-}O}$, 2.4–3.3 Å) were used resulting in 80 intra-subunit hydrogen bond restraints and 8 inter-subunit hydrogen bond restraints.

Structure Calculations—Structure calculations were carried out by a hybrid distance geometry-dynamical simulated annealing protocols using the program X-PLOR (Brünger, 1992). The protocols were slightly modified to take into account the dimeric structure. The dimeric symmetry was achieved by the combinatorial use of distance symmetry restraints and non-crystallographic symmetry restraints. The distance symmetry restraints symmetrically arrange the monomers by keeping a pair of distances the same (*e.g.* C$^\alpha$:1:subunit A to C$^\alpha$:72:subunit B and C$^\alpha$:72:subunit B to C$^\alpha$:1:subunit A), whereas non-crystallographic symmetry restraints minimize the atomic root-mean-square (r.m.s.) difference between the two monomers (Brünger, 1992; Nilges, 1993). The structure calculations were carried out in an iterative manner by adding more NOEs to each cycle of calculations to resolve the ambiguous assignments (Kraulis *et al.*, 1989).

RESULTS AND DISCUSSION

NMR Resonance Assignments and NOE Connectivities—A complete list of assignments of the proton NMR resonances of GRO/MGSA at 30 °C, pH 5.1, is given in Table I. The assignments are very similar to the 73-residue GRO/MGSA at 30 °C, pH 5.7, reported by Fairbrother *et al.* (1993).

The ^1H NMR resonance of the backbone amide proton of Gln-10, the residue between the first 2 cysteines in the CXC motif, has a large downfield chemical shift (11.22 ppm). The amide proton of Lys-21 (9.65 ppm) also had a large downfield chemical shift. This was also found in IL-8 (Clore *et al.*, 1989), where the amide protons of Gln-8 and Lys-20 (see Fig. 1 for sequence alignment) have large downfield shifts (11.94 and 11.53 ppm, respectively). In the case of IL-8, both amide protons have H-bonds to the imidazole ring nitrogens of histidines in the NMR structure. Clore *et al.* (1990) suggested that the

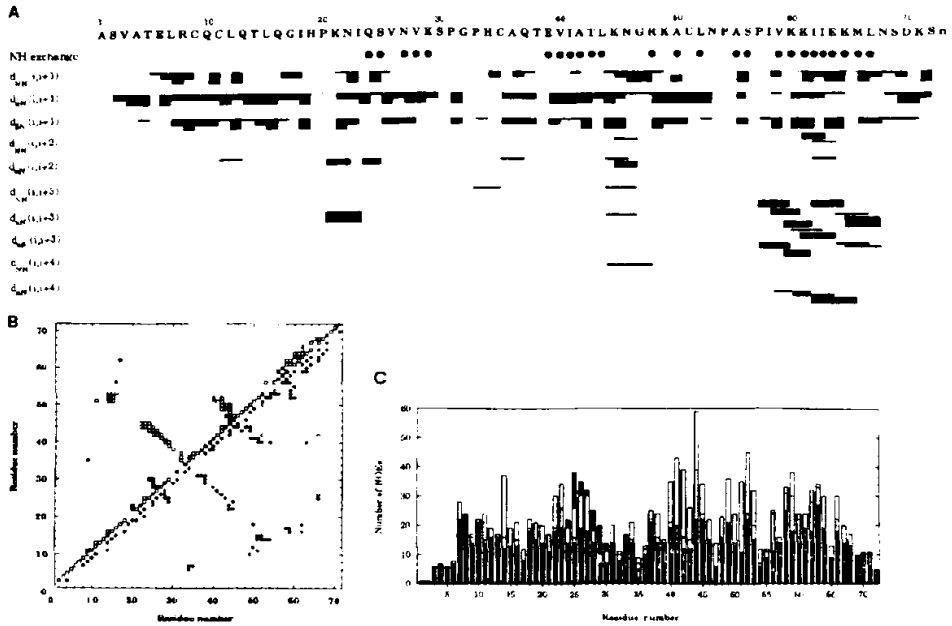

FIG. 2. **Summary of the NOE connectivities.** *a*, sequential NOEs. The relative strengths of the NOEs are indicated by the *thickness* of the *lines*. The $C^{\alpha}H$ protons of proline are treated as backbone NH protons. NOEs involving the $C^{\alpha}H$ protons of proline are given by the *hatched box* in $d_{\alpha N}$ connectivity. The degenerate neighboring amide protons are shown by the *dotted line* in d_{NN} connectivity. Slowly exchanging amide proton is indicated by a *solid circle* (●). *b*, medium to long range NOEs. *Upper triangles* are for the NOE connectivities between backbone protons including $C^{\beta}H$ protons (□). The *lower triangles* are for the NOE connectivities between the side chain protons (○). The *filled symbols* (■, ●) are for the dimeric NOEs. *c*, the number of NOEs used for structure calculations for each residue. The *column* from the *bottom* (■) to the top (■) indicates the number of NOEs for intraresidue, sequential, medium, long, and dimeric NOEs.

alignment of the imidazole ring and the NH proton induced by H-bonding was the cause of the large downfield shift. In GRO/MGSA structure, the corresponding amide protons (Gln-10, Lys-21) do not have H-bonds to the imidazole ring nitrogens of histidines (His-19, His-34). The lack of the ring current effect may explain the reduced downfield shift of Lys-21 but cannot explain the chemical shift of Gln-10. To investigate this, we synthesized an analog of GRO/MGSA in which both His-19 and His-34 were substituted by Asn (H19N, H34N) so that polypeptide had no aromatic residues. A large downfield ^1H NMR chemical shift was also observed for Gln-10 (11.15 ppm) in the double mutant. This suggests that factors other than a ring current effect influence the chemical shift of the Gln-10 amide proton.

A summary of short-range ^1H NMR NOE connectivities involving the NH, $C^{\alpha}H$, and $C^{\beta}H$ protons, together with an indication of the slowly exchanging amide protons, is shown in Fig. 2*a*, and a summary of medium and long range NOE connectivities is shown in Fig. 2*b*. Central β-strands and a COOH-terminal helix are evident in Fig. 2*b*. Fig. 2*b* also shows that the dimer interface (*filled symbols*) forms across β-strands of two subunits. A difference from the 73-residue GRO/MGSA (Fairbrother *et al.*, 1993) can be found in the COOH-terminal helix in sequential NOE connectivity diagram. In the 73-residue GRO/MGSA, the helical NOEs (i, i + 3) can be observed up to residue 69. However in the 72-residue GRO/MGSA, NOEs extend only up to residue 68. The NOE connectivities shown in Fig. 2*a* are similar to the corresponding connectivities in IL-8, but the number of backbone NOEs between two subunits in GRO/MGSA is fewer than in IL-8. The secondary structures identified in the sequential medium and long range NOE connectivity diagrams (Fig. 2, *a* and *b*) are consistent with the number of NOEs for each residue (Fig. 2*c*). More medium range NOEs are found in the helix, whereas long range NOEs are more abundant in β-strands.

Hydrogen exchange rate measurements were used for the identification of H-bonds. Since amide protons simultaneously exchange by both unfolding and local fluctuations of the protein, fast exchange of a proton does not necessarily indicate that no hydrogen bond is made to that proton, and slow exchange of a proton also does not guarantee the existence of a hydrogen bond to that proton, as other factors can protect a proton from exchange (Kim *et al.*, 1993). In particular, most of amide protons in GRO/MGSA exchange within 24 h at 30 °C, pH 4.6. Therefore, a H-bond was assigned only if the NOE connectivities around a visible amide proton in the freshly prepared sample in D_2O were consistent with a H-bond geometry.

Solution Structure of GRO/MGSA—The solution structure of the GRO/MGSA monomer consists of a NH_2-terminal loop, 3-stranded β-sheet (residues 25–29, 39–44, and 48–51), a COOH-terminal α-helix (57–68), and turns between them. The NH_2-terminal loop is linked by disulfide bonds to one of the turns (Cys-9–Cys-35) and the third strand of β-sheet (Cys-11–Cys-51) as shown in Fig. 3. Under the experimental conditions used (2 mM, pH 5.10), GRO/MGSA forms a dimer resulting in 6-stranded antiparallel β-sheet and a pair of helices with 2-fold symmetry. The statistics of the 30 converged hybrid distance geometry-simulated annealing structures are shown in Table II. All ranges of NOEs are equally well satisfied, and the covalent geometries of the converged structures are close to ideal. The r.m.s. difference of the ensemble of structures to the average is 0.51 Å for the backbone atoms and 0.81 Å for all heavy atoms for residues 9–68. The r.m.s. difference to the minimized (minimized with NOE restraints) average structure is 0.58 Å for the backbone atoms and 0.94 Å for all heavy atoms. The inclusion of $^3J_{NH_{\alpha}}$ coupling constants in structure calculations for torsion angle constraints improved r.m.s. difference of backbone atoms by 0.1 Å, but they were not included in structure calculations reported here. Although the $^3J_{NH_{\alpha}}$ coupling con-

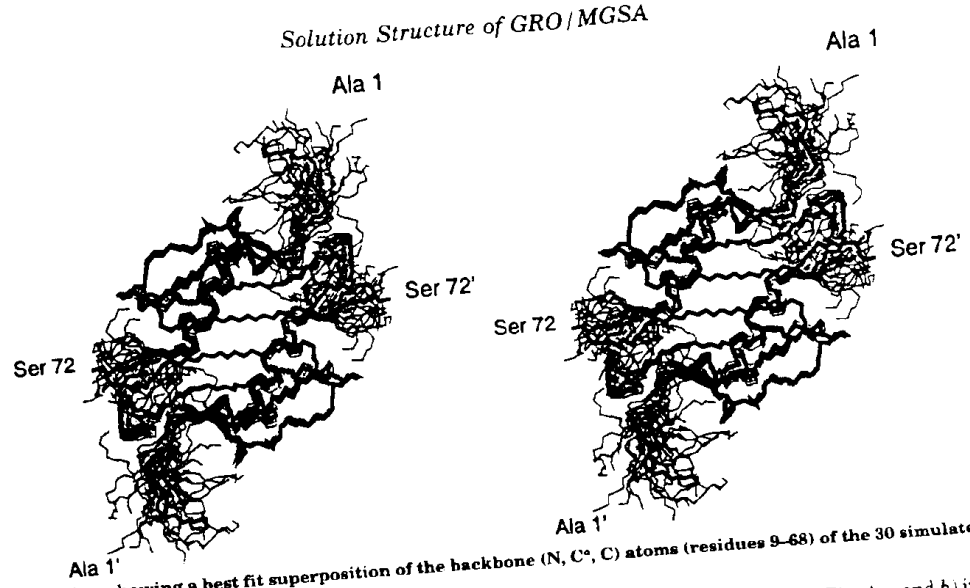

FIG. 3. **Stereoview showing a best fit superposition of the backbone (N, C^{α}, C) atoms (residues 9–68) of the 30 simulated annealing structures.**

TABLE II

Structural statistics and atomic r.m.s. differences

The notation of the structures is as follows: ⟨SA⟩ is the 30 final dynamical simulated annealing structures, $\overline{SA}$ is the mean structure of 30 individual SA dimer structures best fitted to each other (excluding residues 1–8 and 69–72), and $(\overline{SA})_r$ is the restrained minimized mean structure obtained by restrained minimization of SA.

	Structural statistics	
	⟨SA⟩	$(\overline{SA})_r$
r.m.s. deviations from experimental distance restraints (Å)		
All (2192)	0.080 ± 0.001	0.081
Interresidue long range ($\|i-j\| \geq 5$) (366)	0.096 ± 0.007	0.090
Interresidue medium range ($2 \leq \|i-j\| \leq 4$) (204)	0.130 ± 0.009	0.125
Sequential ($\|i-j\| = 1$) (518)	0.088 ± 0.005	0.085
Intraresidue (974)	0.066 ± 0.004	0.061
H-bonds (80)	0.097 ± 0.023	0.071
Dimer (42 NOEs, 8 H-bonds)	0.123 ± 0.026	0.122
r.m.s. deviation from experimental dihedral restraints (°) (30)	1.630 ± 0.160	1.435
Deviations from idealized covalent geometry		
Bonds (Å)	0.0073 ± 0.0001	0.0074
Angles (°)	1.103 ± 0.012	1.096
Improper (°)	0.859 ± 0.020	0.837
	Atomic r.m.s. differences of ordered residues (9–68)	
	Backbone atoms	Heavy atoms
	(Å)	
⟨SA⟩ *versus* $\overline{SA}$	0.51 ± 0.15	0.81 ± 0.15
⟨SA⟩ *versus* $(\overline{SA})_r$	0.58 ± 0.15	0.94 ± 0.16

stants are higher in β-sheet and lower in α-helix, it was difficult to distinguish useful $^3J_{NH\alpha}$ coupling constants from conformationally averaged $^3J_{NH\alpha}$ values. However, χ_1 torsion angles were used in structure calculations since the intensity of COSY cross-peaks and $^3J_{\alpha\beta}$ coupling constants measured from PE-COSY were consistent with observed NOEs. Structures calculated by an alternate template-based simulated annealing protocol using IL-8 as a template were essentially the same as those presented in Fig. 3. The plot of the r.m.s. difference of atomic positions for each residue (Fig. 4, *a* and *b*) indicates that NH_2 and COOH termini are poorly defined, but the rest of protein is well ordered. A large r.m.s. difference is also observed for the loop comprising residues 31–37. Fig. 4*c* shows the fractional accessible surface area of each residue in the monomer and dimer forms (Lee and Richards, 1971). The reduction of accessible surface area by dimerization is basically confined to the interfacial β-strands, indicating that dimer is stabilized by the interactions between the interfacial strands. The residues Ile-23, Cys-35, Val-40, Ile-41, Ala-42, Ala-50, Cys-51, Leu-52, Val-59, and Ile-62 are completely buried in both monomer and dimer forms. These hydrophobic residues, with the exception of Cys-35 and Cys-51, form a hydrophobic stretch to stabilize the tertiary interaction between the β-sheet and the overlapping helix. This hydrophobic stretch also forms protein folding core, which is responsible for protein folding and stability, defined by the hydrogen exchange rates (Kim *et al.*, 1993). The slowest hydrogen exchange rates were observed among the amide protons of residues Val-40, Ala-42, Leu-52, and Ile-63. The loss of activity observed in a truncation mutant of COOH-terminal helix in IL-8 (Clark-Lewis *et al.*, 1991b) may be explained by the destabilization of protein folding core by analogy with GRO/MGSA.

While the overall fold of GRO/MGSA monomer is very similar to that of IL-8, several notable differences are evident (Fig. 5). First, the NH_2-terminal region including the ELR motif is more restrained in GRO/MGSA. This is supported by NOEs between sequential amide protons (d_{NN} NOEs) involving residues 5–9 (Fig. 2*a*) and NOEs between Leu-7 and the $C^{\alpha 2}H$ proton of His-34 (Fig. 2*b*). Sequential d_{NN} NOEs involving residues 5–9 were also observed in the H19N,H34N double mutant showing that the side chain of His-34 does not affect the ELR motif conformation.[2] The corresponding residues in IL-8 do not have d_{NN} NOEs. Second, the turn involving residues 31–36, which is connected to the NH_2-terminal ELR motif by the disulfide bond, is also different from IL-8. The kink at Pro-31 and Ala-36 is less severe in GRO/MGSA than in IL-8. Third, the loop between Leu-12 and Asn-23 is clearly different from IL-8. The size of loop is smaller, and the 3–10 helical turn observed in IL-8 (Clore *et al.*, 1990) is not defined in GRO/MGSA. This loop is 1 residue shorter in GRO/MGSA (see Fig. 1). Fourth, the α-helix is shorter in GRO/MGSA, which contributes to a weaker

[2] K. S. Kim, I. Clark-Lewis, and B. D. Sykes, unpublished results

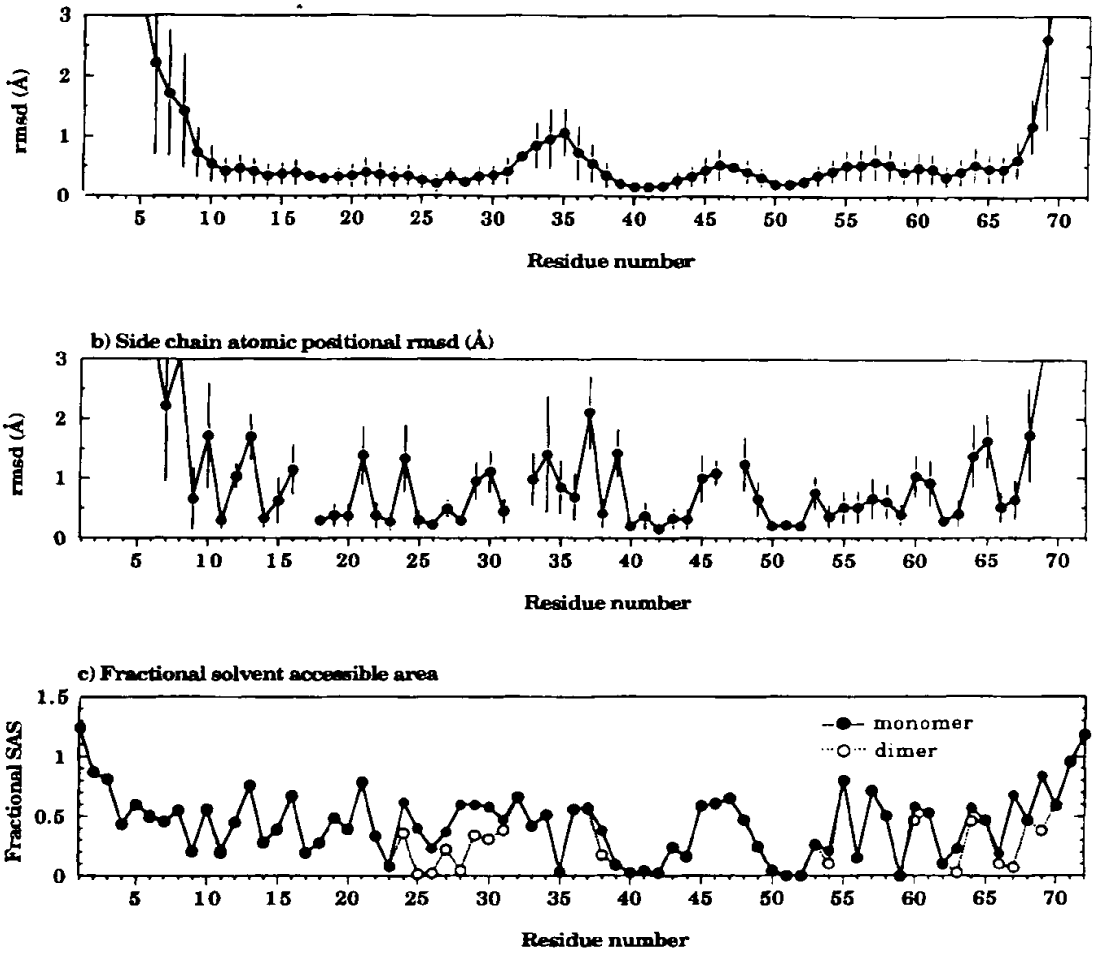

FIG. 4. The average r.m.s. distribution of the 30 simulated annealing structures about the average structure best fitted to the backbone atoms of residues 9–68 (*a*, *b*) and fractional accessible surface area of minimized average structure (*c*). The standard deviations are shown by the *vertical bars*, and accessible surface area is calculated as a single subunit (-○-) and dimer (-●-).

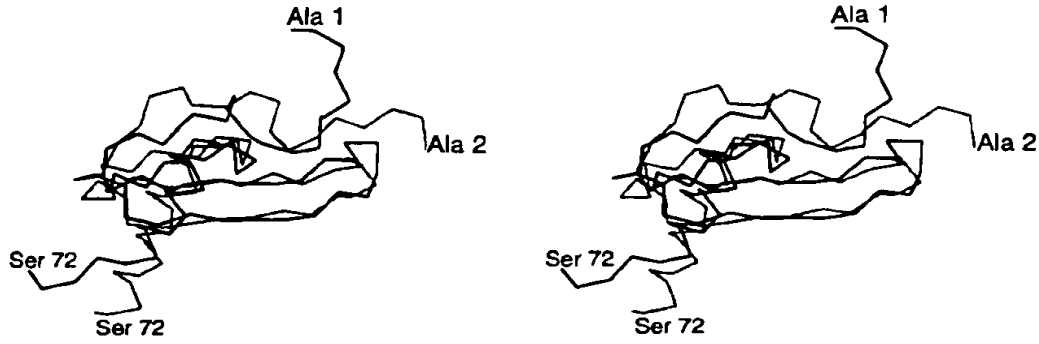

FIG. 5. **Comparison of GRO/MGSA and IL-8.** The best fit superposition was obtained by fitting C$^{\alpha}$ atoms of residues 9–68 of GRO/MGSA (*thick line*) and the corresponding residues (see Fig. 1) of the IL-8 NMR structure (*gray line*).

dimer interface. In GRO/MGSA, there are no inter-subunit interactions between the COOH-terminal helix and β-strands of the other subunit. Dimeric NOEs between subunits in GRO/MGSA reside only in the strands (residues 23–30), whereas in IL-8 the COOH-terminal helix and the β-sheet of the other subunit interact, and the dimer is additionally stabilized by salt bridges across the β-sheet interface. No such inter-subunit salt bridges were found in GRO/MGSA. Hydrogen exchange rate measurements and ultracentrifugation studies also indicate that dimeric interactions are much weaker than in IL-8. It is also of interest that the α-helix separation in the dimer is narrower in GRO/MGSA (~10 Å) compared with the NMR structure of IL-8 (~15 Å) (Clore *et al.*, 1990), but it is closer to the x-ray structure of IL-8 (~11 Å) (Baldwin *et al.*, 1990; Clore

and Gronenborn, 1991). The r.m.s. difference of C^{α} atoms of the ordered polypeptide (residues 9–68) between GRO/MGSA and IL-8 NMR structure (see Fig. 1 for sequence alignment) is 2.06 Å (secondary structure regions (residues 25–29, 39–44, 48–51), 1.18 Å; residues 12–23, 2.98 Å; residues 32–37, 2.2 Å).

Structure and Function—The protein fold of GRO/MGSA is essentially the same as that of IL-8, but the less restrained regions are different from IL-8. Differences in the COOH-terminal helix and the dimeric interactions are apparent, but these are not considered to be important for receptor binding by analogy with IL-8 (Clark-Lewis *et al.*, 1991b; Rajarathnam *et al.*, 1994a). The ELR motif is more restrained and has helical propensity that is not apparent in IL-8, the NH_2-terminal loop (residues 12–23) is smaller, and the kink at Pro-31 and Ala-36 is less severe than in IL-8. Since these regions of IL-8 have been shown to be important for receptor binding (Clark-Lewis *et al.*, 1994), the structural differences in these regions could contribute to the differences in receptor binding and selectivity. Structure-function analysis of IL-8 and NMR studies of IL-8 analogs suggests that the protein core provides a scaffold for presentation of the NH_2-terminal to the receptor (Rajarathnam *et al.*, 1994b). The GRO/MGSA and IL-8 structures suggest that the similarity of the protein fold enables these chemokines to be cross-reactive, but differences in the flexible regions are likely to determine the receptor selectivity.

Acknowledgments—We are indebted to Dr. Cyril Kay for ultracentrifuge work, Dr. A. Wlodawer for providing the coordinates of IL-8, Dr. M. Nilges for making available his paper before publication, and Philip Owen, Peter Browski, and Luen Vo for assistance with the synthesis, purification, and characterization of the proteins. We are also thankful to Drs. Krishna Rajarathnam, Patricia Campbell, and Jian-Jun Wang for critical reading of the manuscript and helpful discussions, Gerry McQuaid for spectrometer maintenance, and Les Hicks for ultracentrifuge run.

REFERENCES

Anisowicz, A., Bardwell, L., and Sager, R. (1987) *Proc. Natl. Acad. Sci. U. S. A* **84**, 7188–7192
Baggiolini, M., and Clark-Lewis, I. (1992) *FEBS Lett.* **307**, 97–101
Baldwin, E. T., Weber, I. T., Charles, R. S., Xuan, J.-C., Appella, E., Yamada, M., Matsushima, K., Edwards, B. F. P., Clore, G. M., Gronenborn, A. M., and Wlodawer, A. (1991) *Proc. Natl. Acad. Sci. U. S. A.* **88**, 502–506
Balentien, E., Mufson, B. E., Shattuck, R. L., Derynck, R., and Richmond, A. (1991) *Oncogene* **6**, 1115–1124
Bax, A. (1989) *Methods Enzymol.* **176**, 151–158
Bothner-By, A. A., Stephens, R. L., Lee, J. T., Warren, C. D., and Teanloz, R. W. (1984) *J. Am. Chem. Soc.* **106**, 811–813
Brünger, A. T. (1992) *X-PLOR: A System for X-ray Crystallography and NMR*, Yale University Press, New Haven, CT
Cerretti, D. P., Kozlosky, C. J., Vanden Bos, T., Nelson, N., Gearing, D. P., and Bechmann, M. P. (1993) *Mol. Immunol.* **30**, 359–367
Clark-Lewis, I., Moser, B., Walz, A., Baggiolini, M., Scott, G. J., and Aebersold, R. (1991a) *Biochemistry* **30**, 3128–3135
Clark-Lewis, I., Schumacher, C., Baggiolini, M., and Moser, B. (1991b) *J. Biol. Chem.* **266**, 23128–23134
Clark-Lewis, I., Dewald, B., Geiser, T., Moser, B., and Baggiolini, M. (1993) *Proc. Natl. Acad. Sci. U. S. A.* **90**, 3574–3577
Clark-Lewis, I., Dewald, B., Loetscher, M., Moser, B., and Baggiolini, M. (1994) *J. Biol. Chem.* **269**, 16075–16081
Clore, G. M., and Gronenborn, A. M. (1991) *J. Mol. Biol.* **217**, 611–620
Clore, G. M., Appella, E., Yamada, M., Matsushima, K., and Gronenborn, A. M. (1989) *J. Biol. Chem.* **264**, 18907–18911
Clore, G. M., Appella, E., Yamada, M., Matsushima, K., and Gronenborn, A. M. (1990) *Biochemistry* **29**, 1689–1696
Ernst, R. R., Bodenhausen, G., and Wokaun, A. (1986) *Principles of Nuclear Magnetic Resonance in One and Two Dimensions*, Clarendon Press, Oxford
Fairbrother, W. J., Reilly, D., Colby, T., and Horuk, R. (1993) *FEBS Lett.* **330**, 302–306
Haskill, S., Peace, A., Morris, J., Sporn, S. A., Anisowicz, A., Lee, S. W., Smith, T., Martin, G., Ralph, P., and Sager, R. (1990) *Proc. Natl. Acad. Sci. U. S. A.* **87**, 7732–7736
Hébert, C. A., Vitangcol, R. V., and Baker, J. B. (1991) *J. Biol. Chem.* **266**, 18989–18994
Holmes, W. E., Lee, J., Kuang, W. J., Rice, G. C., and Wood, W. I. (1991) *Science* **253**, 1278–1280
Horuk, R., Yansura, D. G., Reilly, D., Spencer, S., Bourell, J., Henzel, W., Rice, G., and Unemori, E. (1993) *J. Biol. Chem.* **268**, 541–546
Kim, K.-S., Fuchs, J. A., and Woodward, C. K. (1993) *Biochemistry* **32**, 9600–9608
Kraulis, P. J., Clore, G. M., Nilges, M., Jones, T. A., Petterson, G., Knowles, J., and Gronenborn, A. M. (1989) *Biochemistry* **28**, 7241–7257
Lee, B., and Richards, F. M. (1971) *J. Mol. Biol.* **55**, 379–400
Lodi, P. J., Garret, D. S., Kuszewski, J., Tsang, M. L.-S., Weatherbee, J. A., Leonard, W. J., Gronenborn, A. M., and Clore, G. M. (1994) *Science* **263**, 1762–1767
Miller, M. D., and Krangel, M. S. (1992) *Crit. Rev. Immunol.* **12**, 17–46
Moser, B., Clark-Lewis, I., Zwahlen, R., and Baggiolini, M. (1990) *J. Exp. Med.* **171**, 1797–1802
Moser, B., Schumacher, C., von Tscharner, V., Clark-Lewis, I., and Baggiolini, M. (1991) *J. Biol. Chem.* **266**, 10666–10671
Mueller, L. (1987) *J. Magn. Reson.* **72**, 191–196
Murphy, P. M., and Tiffany, H. L. (1991) *Science* **253**, 1280–1283
Neote, K., Darbonne, W., Ogez, J., Horuk, R., and Schall, T. J. (1993) *J. Biol. Chem* **268**, 12247–12249
Nilges, M. (1993) *Proteins Struct. Funct. Genet.* **17**, 297–309
Powers, R., Garrett, D. S., March, C. J., Frieden, E. A., Gronenborn, A. M., and Clore, G. M. (1993) *Biochemistry* **32**, 6744–6762
Proost, P., Wuyts, A., Connings, R., Lenaerts, J.-P., Billiau, A., Opdenakker, G., and Van Damme, J. (1993) *Biochemistry* **32**, 10170–10177
Rajarathnam, K., Sykes, B. D., Kay, C. M., Dewald, B., Geiser, T., Baggiolini, M., and Clark-Lewis, I. (1994a) *Science* **264**, 90–92
Rajarathnam, K., Clark-Lewis, I., and Sykes, B. D. (1994b) *Biochemistry* **33**, 6623–6630
Richmond, A., Balentien, E., Thomas, H. G., Flaggs, G., Barton, D. E., Spiess, J., Bordoni, R., Francke, U., and Derynck, R. (1988) *EMBO J.* **7**, 2025–2033
Schumacher, C., Clark-Lewis, I., Baggiolini, M., and Moser, B. (1992) *Proc. Natl. Acad. Sci. U. S. A.* **89**, 10542–10546
States, D. J., Haberkorn, R. A., and Ruben, D. J. (1982) *J. Magn. Reson.* **48**, 286–292
Tekamp-Olson, P., Gallegos, C., Bauer, D., McClain, J., Sherry, B., Fabre, M., van Deventer, S., and Cerami, A. (1990) *J. Exp. Med.* **172**, 911–919
Wagner, G., Braun, W., Havel, T. F., Schaumann, T., Gō, N., and Wüthrich, K. (1987) *J. Mol. Biol.* **196**, 611–639
Walz, A., and Baggiolini, M. (1989) *Biochem. Biophys. Res. Commun.* **159**, 969–975
Walz, A., Burgener, R., Car, B., Baggiolini, M., Kunkel, S. L., and Strieter, R. M. (1991) *J. Exp. Med.* **174**, 1355–1362
Wen, D., Rowland, A., and Derynck, R. (1989) *EMBO J.* **8**, 1761–1766
Wüthrich, K. (1986) *NMR of Protein and Nucleic Acids*, John Wiley & Sons, Inc., New York
Zuiderweg, E. R. P., Boelens, R., and Kaptein, R. (1985) *Biopolymers* **24**, 601–611

Liposome encapsulated daunorubicin doubles anthracycline toxicity in cell lines showing a non-PGP related multidrug resistance

Sir,

DaunoXome (DNX) is a liposomal formulation of daunorubicin (DNR) developed by NeXstar with the aim of targeting the drug to tumors since liposomes have a better chance of penetrating the leaky vasculature of neoplastic tissues than the vasculature of normal tissues.[1] In a previous work it was observed that in cell lines showing PGP overexpression, DNX produced more DNR accumulation and higher toxicity than the conventional drug (free DNR) suggesting that liposomal anthracyclines could be suitable for treatment of PGP-positive leukemias.[2] In order to test the capacity of DNX to counteract DNR-resistance mechanisms associated with defects in cellular anthracycline accumulation other than PGP overexpression, a couple of drug-selected cell lines showing a multidrug resistance (MDR) and multidrug resistance protein (MRP) (GLC4-ADR150) or lung resistance-associated protein (LRP) (SW1573/2R120) overexpression were tested. The cellular time- and dose-related accumulation of DNX against free DNR were assayed by flow cytometry while the drugs' toxicity was tested by a MTT-microcultured tetrazolium colorimetric assay.[2] After 7 days of continuous exposure to the drugs, the toxicity of DNX was about 2.5 fold higher than that of the free DNR in both the drug-selected lines (Table 1 and Figure 1 A and B). In contrast to data observed in PGP-overexpressing cell lines,[2] cellular accumulation of the anthracycline was comparable when the LRP-overexpressing line SW1573/2R120 was treated with DNX or with free DNR. The MRP-overexpressing GLC4-ADR150 showed only a trend towards a greater DNR accumulation when exposed to DNX compared to free DNR (Figure 1 C and D). According to data reported by Forssen *et al.*, it could be hypothesized that the mechanism of the higher toxicity of DNX in cell lines with non-PGP related MDR could be a shift in nucle-

Table 1. Inhibition dose 50 (ID_{50}, ng/mL, mean ± 2SD of at least three tests) for liposomal DNR (DNX) and conventional (free DNR) daunorubicin. The cells' growth was assayed by the MTT tetrazolium colorimetric test after a 7-day culture in the presence of increasing doses of the anticancer drug with or without the addition of MDR modifiers. The ID_{50} was calculated from the dose-response curves. The resistance index (RI) was calculated by dividing the ID_{50} of the MDR sublines SW1573/2R120 and GLC4-ADR150 by the ID_{50} of the respective non -MDR lines SW1573 and GLC4.

	GLC4 ADR 150	*GLC4*	*RI*	*SW1573/ 2R120*	*SW 1573*	*RI*
Free DNR	708.9±12.3	7.1±1.0	100	98.6±6.9	5.1±0.4	19
+DVP	556.3±20.6	7.3±0.6	76	75.4±8.6	5.7±1.0	13
+PSC	520.8±13.9	6.8±1.6	72	74.1±7.6	4.9±0.9	15
DNX	265.1±9.8	5.6±0.8	47	40.1±4.3	5.0±0.7	8
+DVP	248.3±11.2	5.4±0.9	46	34.0±3.9	4.8±0.9	7
+PSC	227.5±14.5	5.1±1.2	45	38.6±4.9	4.8±0.7	8

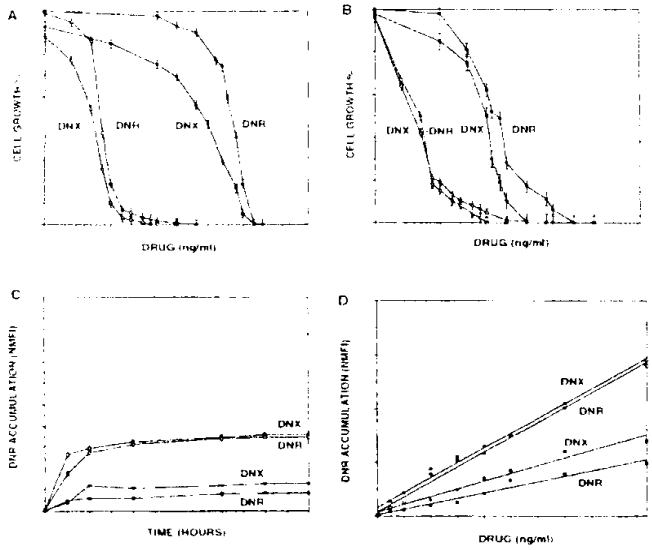

Figure 1. Dose-response curves for the two cell lines GLC4 ADR 150/ GLC4 (panel A) and SW1573/2R120/ SW1573 (panel B). In the two non-MDR lines GLC4 and SW1573 (open squares) the toxicity of daunoxome (DNX) parallels that of free DNR. In the two MDR variants GLC4-ADR 150 and SW1573/2R120 (closed squares) DNX is about 2.5 fold more toxic than the free drug (DNR). Panels C and D show the time- and dose-dependent cellular drug accumulation in the MRP overexpressing GLC4-ADR150 (closed squares) and in its parental non-MDR GLC4 cell line (open squares) assayed by flow cytometry. To test the relationship between the time of exposure to the drug and its accumulation, the cells were exposed for 24 hours to a fixed dose (300 ng/mL) of free DNR or DNX and the DNR-associated fluorescence was assayed at intervals (panel C). To test the relationship between exposure to the drug and its accumulation, the cells were exposed to increasing concentrations of free or liposomal DNR and the anthracycline-associated fluorescence was assayed after 24 hours of incubation (panel D).

us /cytoplasm distribution.[3] In fact, differently from PGP, LRP is primarily located in the cytoplasm[4] whereas MRP has been found both at the surface of the cellular plasma membrane, in the cytoplasm and in the Golgi region.[5,6] An additional part of this study was to compare the toxicity of DNX to that of a combination of free DNR plus MDR modifiers. In cell lines showing a non-PGP related MDR. In these MDR cell lines, the addition of MDR modifiers, such as D-verapamil or SDZPSC833, to free DNR only marginally increased the drug's toxicity. Moreover, this increase was smaller than that observed by substituting free DNR with DNX (Table 1). In conclusion, this work shows that the liposomal formulation of DNX doubles DNR toxicity in cell lines with an MDR associated overexpression of MRP or LRP. The increase in DNR toxicity due to the liposome encapsulation is higher than that produced by adding SDZPSC833 or D-verapamil to free anthracycline. These data support the ongoing research into the use of liposomal anthracyclines for the treatment of acute non-lymphocytic leukemia, considering that, even at disease onset, myeloid blast cells often show defects in drugs accumulation associated with co-overexpression of both PGP and LRP.[7-10]

Mariagrazia Michieli, Daniela Damiani, Anna Ermacora, Paola Masolini, Angela Michelutti, Michele Baccarani

Division of Hematology, Department of Medical and Morphological Research, Udine University Hospital, Italy

Key words

LRP, MRP, lung resistance-associated protein, multidrug resistance related protein, acute leukemia, liposome, daunorubicin, multi drug resistance.

Acknowledgments

This work was supported by the AIRC Milan and by MURST 1998 grant "Biological and molecular bases of therapy of acute non-lymphoid leukaemia and pharmacology and toxicology of anticancer anthracyclines: mechanisms and molecular basis for novel therapeutical strategy". We are grateful to Dr. MJ Broxterman (Dept. of Medical Oncology, Free University Hospital, Amsterdam, The Netherlands) and to Dr. EGE de Vries (Dept. of Internal Medicine, University Hospital, Groningen, The Netherlands) for supplying us with the LRP (SW-1573/2R120) and MRP (GLC4-ADR150) overexpressing cell lines.

Correspondence

Mariagrazia Michieli, M.D., Division of Hematology, University Hospital, p.le S. Maria della Misericordia, 33100 Udine, Italy. Phone: international +39-0432-559662-4 – Fax: international +39-0432-559661.

References

1. Chew T, Jacobs M. Pharmacology of liposomal daunorubicin and its use in Kaposi's sarcoma. Oncology 1996; 10:29-33.
2. Michieli M, Damiani D, Ermacora A, et al. Liposome encapsulated daunorubicin for PGP-related multidrug resistance. Br J Haematol 1999; 106:92-9.
3. Forssen EA, Male-Brune R, Adler-Moore JP, et al. Fluorescence imaging studies for the disposition of daunorubicin liposomes (daunoxome) within tumor tissue. Cancer Res 1996; 56:2066-75.
4. Scheffer GL, Wijngaard PJJ, Flens MJ, et al. The drug resistance related protein LRP is the human major vault protein. Nature Med 1995; 6:578-82.
5. Cole SPC, Bhardwaj G, Gerlach JH, et al. Overexpression of a transporter gene in a multidrug-resistant human lung cancer cell line. Science 1992; 258:1650-4.
6. De Vries EGE, Van Luyn MJA, Renes J, et al. Glutathione conjugate transport in intracellular vesicles in the doxorubicin resistant human lung carcinoma cell line GLC4-Adr is MRP mediated. Proc Am Ass Cancer Res 1996; 37:306-12.
7. Michieli M, Damiani D, Ermacora A, et al. P-glycoprotein, lung resistance related protein and multidrug resistance associated protein in de novo acute non-lymphocytic leukaemias: biological and clinical implications. Br J Haematol 1999; 104:328-35.
8. Willman CL. The prognostic significance of the expression and function of multidrug resistance transporter proteins in acute myeloid leukemia: studies of the southwest oncology group leukemia research program. Semin Hematol 1997; 34:25-33.
9. Damiani D, Michieli M, Ermacora A, et al. P-glycoprotein (PGP) and not lung resistance-related protein (LRP), is a negative prognostic factor in secondary leukemias. Haematologica 1998; 83:290-7.
10. Filipitis M, Pohl G, Stranzl T, et al. Expression of the lung resistance protein predicts poor outcome in de novo acute myeloid leukemia. Blood 1998; 91:1508-13.

Chronic myeloid leukemia in chronic phase with a partial trisomy 9 mosaicism

Sir,

We report a case of CML in chronic phase in a 72-year old woman with a previous history of heart disease and atrial fibrillation. She had a pronounced leukocytosis with a WBC count of 254×10^9/L, 1% of blasts and 10% of basophils. Her hematocrit was 33% and platelet count 370×10^9/L. Neutrophil alkaline phosphatase (NAF) activity was absent. Bone marow cellularity was increased and the myeloid/erythroid ratio was 1/2. The marrow contained 1% of blast cells.

Cytogenetic study, applying G-band techniques, of the bone marrow revealed the presence of two different cell lines: 60% of the metaphases analyzed were 46,XX,Ph while the remaining 40% had 47 chromosomes and Ph, the excess chromosome being a chromosome 9 with an interstitial deletion in its long arms.

Fluorescence *in situ* hybridization (FISH) was performed on chromosome preparations with two differently labeled bcr/abl translocation DNA probes (Vysis LSI bcr/abl tp). A total of 100-150 cells (metaphase and interphase) were counted. The existence of three signals was proved by the ABL probe, one hybridized to chromosome 9, another to the deleted 9 and the classic ABL/BCR fusion, in its nor-

original paper
Haematologica 1996; 81:295-301

OVERCOMING PGP-RELATED MULTIDRUG RESISTANCE. THE CYCLOSPORINE DERIVATIVE SDZ PSC 833 CAN ABOLISH THE RESISTANCE TO METHOXY-MORPHOLYNIL-DOXORUBICIN

Mariagrazia Michieli, Daniela Damiani, Angela Michelutti, Cristina Melli, Anna Ermacora, Antonella Geromin, Renato Fanin, Domenico Russo, Michele Baccarani

Division of Hematology, Department of Clinical and Morphological Research and Department for Bone Marrow Transplantation, University Hospital, Udine, Italy

ABSTRACT

Background. The results obtained so far in studies designed to neutralize P glycoprotein (PGP)-related multidrug resistance (MDR) by using MDR reversal agents, have not yet fulfilled the promise of the experiments which were performed *in vitro*. In order to improve PGP-related MDR neutralization, we tested *in vitro* the activity of the cyclosporine derivative SDZ PSC 833 (PSC) together with doxorubicin (DOX) and with two new DOX derivatives named 4' iodo 4' deoxy-doxorubicin (IODODOX) and methoxy-morpholynil-doxorubicin (MMDOX, FCE 23762) using four different human cell lines and their multi-drug resistant variants.

Methods. Anthracycline toxicity was evaluated by using the MTT method after a 7-day culture with continuous exposure to the antitumor drugs with or without the addition of PSC.

Results. PSC significantly downmodulated the toxicity of all three anthracyclines in all the four cell systems. However, despite the great increase caused by PSC in the toxicity of DOX and a more modest effect on the toxicity of the two DOX derivatives, this MDR reversal agent could only completely block the PGP mediated MMDOX resistance whereas DOX refractoriness was only decreased.

Conclusions. The combination of MMDOX or IODODOX with PSC 1.6 μM is more efficient than the combination of DOX plus PSC for the full reversion of PGP-mediated drug resistance. Careful clinical studies are required to evaluate if these associations can also effectively and safely neutralize MDR *in vivo*.

Keywords: multidrug resistance, P-glycoprotein, reversal agents, anthracyclines

A number of experimental studies showed that the multi drug resistance (MDR) caused by the overexpression of the P-glycoprotein (PGP), can be successfully blocked *in vitro* by several different methods including the use of a wide range of drugs named MDR reversal agents.[1-5] However, the results of the pilot clinical trials designed to overcome MDR *in vivo* did not fulfill the promise of previous *in vitro* observations.[6-11] While this could reflect a limited clinical relevance of the MDR phenomenon, the scarce results obtained in these clinical trials could also be explained by the use of inappropriate MDR reversal agents or by an inappropriate association with antitumor drugs. In fact, in these first studies drugs as verapamil, quinidine or cyclosporine A were used as MDR reversal agents. It should be noticed that these drugs were not originally designed for the neutralization of the MDR phenomenon. Thus, in the majority of the studies the doses of these modulators were below those required to achieve effective inhibition of PGP function *in vitro*, because of their dose-limiting toxicity. Moreover, all the studies that were performed up to now tried to downmodulate the resistance to drugs that, like doxorubicin, daunorubicin, etoposide or vincristine, are quickly captured and efficiently pumped out by the PGP.[6-16] In the past 20 years, many efforts

Correspondence: Dr.ssa M. Michieli, Division of Hematology, University Hospital, p.le S. Maria della Misericordia, 33100 Udine, Italy. Tel. international +39.432.559662. Fax. international +39.432.559661.
Received February 6, 1996; accepted June 4, 1996.

were devoted to select new reversal agents lacking the dose limiting toxicities and to synthesize new antitumor derivatives that are not transported by the P-glycoprotein.[17,27] With the aim of optimizing the neutralization of PGP-MDR through the use of reversal agents, we tested two lyphofilic doxorubicin (DOX) derivatives that are more toxic than the parent compound against MDR cells, namely 4'iodo 4'deoxy DOX (IODODOX) and methoxy-morpholynil DOX (MMDOX) together with the cyclosporine derivative SDZ PSC 833 (PSC). This is one of the most efficient MDR reversal agents developed and tested so far.[28,33] In comparison with DOX, it was found that the combination of both compounds with PSC was highly efficient and could abolish PGP-related resistance.

Materials and Methods

Drugs

Doxorubicin (DOX) was purchased from Pharmacia S.p.A. Milano, Italy. The two DOX-derivatives 4'iodo4'deoxyDOX (IODODOX) and methoxy-morpholynil-DOX (MMDOX, FCE 23762) were a gift from Pharmacia S.p.A. SDZ PSC 833 was a gift from Sandoz, Basel. DOX and IODODOX were dissolved in water at 100 μg/mL. MMDOX and PSC were dissolved in ethanol at 1 and 5 mg/mL, respectively. All the drugs were stored at −20° and were immediately thawed and diluted before use.

Cell lines

Four systems of human cell lines were used. Each system included a parental, drug sensitive, line without the amplification of the mdr-1 gene and PGP overexpression, and one drug-selected MDR variant with mdr-1 gene amplification and PGP overexpression. The first cell system included the acute myeloid leukemia HL60 cell line and its daunorubicin-selected variant HL60DNR.[34] The second system included the acute lymphocytic leukemia cell line CCRFCEM and its vinblastine-selected variant CEMVLB300.[23] The third system included the colon adenocarcinoma cell line LOVO109 and its DOX-selected variant LOVODOX[23] The fourth system included the breast cancer cell line MCF7 and its DOX-selected variant MCF7DOX.[34] All cell lines were cultured at 37°C in a humidified atmosphere of 5% CO_2 and maintained in an exponential growth in RPMI 1640 (Biochem KG Seromed) with 10% heat-inactivated foetal calf serum (Biochem KG Seromed), 2 mM glutamine solution, 100 U/mL penicillin and 100 μg/mL streptomycin (Biochem KG Seromed). A selected pressure of the appropriate antiblastic drug (HL60DNR, daunorubicin 0.4 μg/mL; CEMVLB300, vinblastine 0.3 μg/mL; LOVODOX, DOX 0.2 μg/mL; MCF7DOX, DOX 0.2 μg/mL) was constantly maintained just for the MDR cell lines. Before each drug sensitivity assay the PGP expression and the expression of other MDR-associated proteins (*lung resistance protein* or LRP, *multidrug resistance-associated protein* or MRP) and of the GSTπ enzyme were evaluated by a flow cytometry assay by using the MRK-16 (Kamiya), the LRP56 (Kamiya), the MRPm6 (Kamiya) and the GSTπ (Dako) monoclonal antibodies. PGP was evaluated as described further on.[35,36] The LRP56, the MRPm6 and the GSTπ monoclonal antibodies were used following the company guidelines. To quantitate the expression of these MDR associated proteins, the number of the MoAbs bound sites per cell was evaluated by using the Quantum Simply Cellular Kit (Sigma). The results were expressed in units of *antibody binding capacity* (ABC) as required for this method. Before the experiments the non MDR parental cell lines had an ABC of 177×10^3 (HL60), 98×10^3 (CCRFCEM), 65×10^3 (LOVO 109) and 38×10^3 (MCF7). The respective MDR cell lines had an ABC of 3650×10^3 (HL60DNR), 1477×10^3 (CEMVLB300), 6903×10^3 (LOVODOX), and 7517×10^3 (MCF7DOX). No drug selected cell line variants overexpressed LRP, MRP or GSTπ in comparison with the respective parental sensitive cell lines, except LOVODOX, whose reactivity to LRP56 was about three times more than in LOVO109.

Drug sensitivity assay

Cell growth in presence or absence of drugs was determined by using the MTT-microcultured tetrazolium colorimetric assay, as described elsewhere.[24,25] Briefly, exponential

growing cells were harvested, washed twice in RPMI 1640 (Biochrom KG Seromed), checked for their vitality through the tripan blue exclusion test, and plated into 96 well microtiter plates at the required concentration in 200 µL of a complete culture medium (RPMI 1640 plus 10% fetal calf serum, 2 mM glutamine solution, penicillin and streptomicin). After a 24-hour incubation, ever increasing doses of anthracyclines (0.5-3000 ng/mL) with or without PSC 1.6 µM were added. Cell growth was evaluated after a 7-day incubation at 37°C and 5% CO_2, by using 50 µL per well of the MTT solution (5 mg/mL). Formazan crystals were dissolved in DMSO and their optical density (OD) was read at 540 nm. As required, wells containing no drugs or containing PSC were used to control cell viability. Wells containing no cells were used to blank the spectrophotometer (Novapath Microplate Reader, BioRad). The inhibition dose (ID) was calculated according to Pieters *et al.*[37] by the following equation, where ID=(mean OD treated wells/mean OD control wells) ×100. Every point of the dose-response curves was the mean of three tests at least. The ID_{50} was defined as the drug dose that inhibited the cell growth to 50% of the control. The resistance index (RI) was calculated by dividing the ID_{50} of the MDR cell line with the ID_{50} of the respective non MDR cell line.

Results

For all the MDR and non MDR cell lines the dose response curves obtained by testing the toxicity of all the anthracyclines in presence or in absence of PSC, were drawn to calculate the inhibition dose 50 (ID_{50}) and the resistance index (RI). Table 1 summarizes all the ID_{50} obtained testing DOX. As expected DOX was several times less toxic in the MDR cell lines than in the parental ones. In the parental cell lines PSC was inactive, whereas in resistant cells PSC the resistance to DOX was substantially decreased. In fact, in the MDR cell lines the ID50 fell from 433 to 27 ng/mL (CEMVLB300), from 1477 to 30 ng/mL (HL60DNR), from 718 to 15 ng/mL (LOVODOX) and from 1230 to 48 ng/mL (MCF7DOX) (Table 1). However, despite the impressive reductions of the ID_{50} caused by PSC, in the MDR cell lines the sensitivity to DOX never reached the level of the respective parental lines. A possible exception was LOVODOX. Table 2 reports the toxicity of IODODOX alone or in presence of PSC in the MDR and non MDR cell lines. In the MDR cell lines, IODODOX was by itself more toxic than the parental agent DOX. In fact, as shown in Table 2, the RI was 9.4 for the CEM system (CEMVLB300/CCRFCEM), 17.7 for the HL60 system (HL60DNR/HL60), 4 for the LOVO system (LOVODOX/LOVO109) and 3 for the MCF7 system (MCF7DOX/MCF7). Once again the addition of PSC increased the anthracycline toxicity only in the MDR cell lines. Thus, the ID_{50}s of IODODOX fell from 18 to 7.7 ng/mL in CEMVLB300, from 55 to 6.8 ng/mL in HL60DNR, from 26 to 9.9 in LOVODOX and from 57 to 26 ng/mL in MCF7DOX. Therefore, for IODODOX an almost complete neutraliza-

MDR/non MDR cell lines	Doxorubicin		Doxorubicin Plus PSC 1.6 µM	
	Inhibition Dose 50 (ng/mL)	Resistance Index	Inhibition Dose 50 (ng/mL)	Resistance Index
CEM VLB300/CCRF CEM	433/5.5	79	27.0/5.4	5.0
HL60 DNR/HL60	1477/7.6	194	30.0/7.2	4.2
LOVO DOX/LOVO109	718/8.6	83	15.0/8.0	1.8
MCF7 DOX/MCF7	1230/10	123	48.0/9.2	5.2

Table 1. Inhibition dose$_{50}$ (ID_{50}) and resistance index (RI) obtained testing doxorubicin with or without PSC 1.6 µM in the MDR and non MDR cell lines. In all the MDR cell lines PSC significantly increased doxorubicin toxicity. However this MDR reversal agent could not neutralize completely the resistance to doxorubicin, with a possible exception for the LOVODOX/LOVO109 system, where the RI became close to 1.

MDR/non MDR cell lines	Iodo-doxorubicin		Iodo-doxorubicin Plus PSC 1.6 μM	
	Inhibition Dose 50 (ng/mL)	Resistance Index	Inhibition Dose 50 (ng/mL)	Resistance Index
CEM VLB300/CCRF CEM	18.0/1.9	9.4	7.7/1.3	5.9
HL60 DNR/HL60	55.0/3.1	17.7	6.8/2.8	2.4
LOVO DOX/LOVO109	26.0/6.5	4.0	9.9/6.2	1.6
MCF7 DOX/MCF7	57.0/19	3.0	26.0/19.0	1.4

Table 2. Inhibition dose$_{50}$ (ID_{50}) and resistance index (RI) obtained testing iodo-doxorubicin with or without the addition of PSC 1.6 μM in the MDR and non MDR cell lines. The addition of PSC decreased all the ID_{50} in all the MDR cell lines. A RI closed to one was obtained in LOVODOX/LOVO109 and MCF7DOX/MCF7 systems.

MDR/non MDR cell lines	Methoxy-morpholynil doxorubicin		Methoxy-morpholynil doxorubicin plus PSC 1.6 μM	
	Inhibition Dose 50 (ng/mL)	Resistance Index	Inhibition Dose 50 (ng/mL)	Resistance Index
CEM VLB300/CCRF CEM	7.8/4.4	1.7	2.8/4.4	0.6
HL60 DNR/HL60	27.2/3.4	8.0	6.8/3.6	1.9
LOVO DOX/LOVO109	21.6/6.8	3.1	8.4/6.4	1.3
MCF7 DOX/MCF7	17.0/13.0	1.3	15.3/13.3	1.2

Table 3. Inhibition dose$_{50}$ (ID_{50}) and resistance index (RI) obtained testing methoxy-morpholynil doxorubicin in presence or in absence of PSC 1.6 μM in the MDR and non MDR cell lines. MMDoxorubicin was very toxic against MDR cells also when it was used alone. When it was used together with PSC, the RI become close to 1 in all four cell systems, showing that this combination had the potential of abolishing PGP-related resistance.

tion of PGP activity, that means a RI close to 1, was obtained in LOVODOX/LOVO109 (RI = 1.6) and in MCF7DOX/MCF7 (RI = 1.4) cell lines. Table 3 summarizes the results obtained with MMDOX. In the drug resistant cell lines MMDOX itself was highly toxic. Its power was particularly evident in MCF7DOX and in CEMVLB300 where the dose response curves of MMDOX alone were very close to the curves obtained in the respective parental cell lines (Figure 1). The coincubation of this anthracycline derivative with PSC further increased MMDOX toxicity in the MDR cell lines so that the addition of PSC could almost completely neutralize the residual resistance to MMDOX (Table 3 and Figure 1).

Discussion

SDZ PSC 833 (PSC) is a novel non immunosuppressive analog of cyclosporine. It was recently completed phase-1 trials which show that at the maximum tolerated dose plasma levels ranged between 2 and 4 μg/mL (1.6-3.2 μM).[19,28,29] Laboratory studies showed that at these concentration ranges PSC can provide highly efficient chemosensitization, but also that a complete MDR elimination may be compromised by a high overexpression of the mdr-1 gene.[19,24,30-33] The new anthracyclines IODODOX and MMDOX where shown to be very powerful DOX derivatives.[38-41] Compared to their drug parent, they are characterized by a higher lipophilicity which seems to be the basis of their rapid spreading through the cell membrane and also by their higher intracellular accumulation in MDR cells.[39,40,42,43] With the aim of optimizing the neutralization of PGP-related MDR through the use of reversal agents we selected the two best available DOX derivatives (IODODOX and MMDOX). We tested their toxicity in comparison with DOX, with or without the addition of PSC in an experimental model of four different human cell line systems, including a sensitive line and a PGP-overexpressing MDR variant. Our findings confirmed prior reports, showing that both DOX derivatives alone were more toxic than DOX in the MDR cell lines.[25,26,42-48] However,

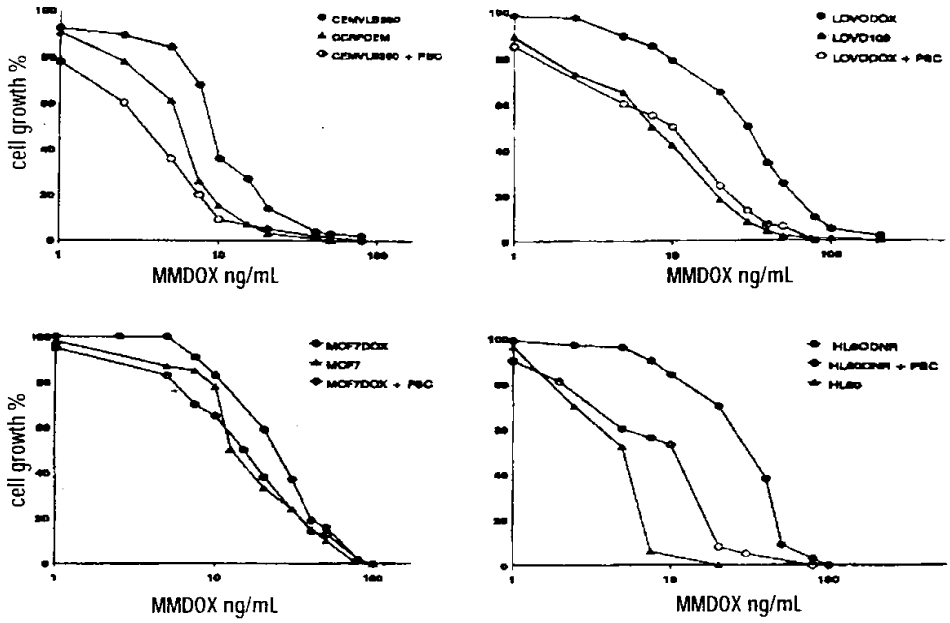

Figure 1. Dose response curves of methoxy-morpholynil doxorubicin (MMDOX) with (open symbols) or without (closed symbols) SDZ PSC 833 (PSC) 1.6 μM in the four cell systems which were composed of parental, drug sensitive, line (CCRFCEM, LOVO109, MCF7, HL60) and its drug-selected MDR variant (CEMVLB300, LOVODOX, MCF7DOX, HL60DNR). In the drug-resistant cell lines (closed circles), MMDOX was less toxic than in the parental cell lines (closed triangles). In all the four MDR-resistant cell lines the addition of MMDOX increased the toxicity of MMDOX and almost completely neutralized PGP-related resistance.

to completely remove the anthracycline resistance caused by PGP in an experimental model based on MDR positive and negative cells, it is necessary that in the presence of the reversal agent, the ID_{50} of the MDR positive cell line variant must equal the ID_{50} of the parental line. In other words, the RI must fall close to 1. In our example, PSC at 1.6 μM which was shown to be a safely achievable concentration also *in vivo*, was inactive in the non MDR cell lines, while it influenced the toxicity of all the anthracyclines in the MDR cell lines. The power of PSC in blocking PGP was particularly evident when it was used in combination with DOX. In fact this association could reduce DOX ID_{50} more than 15 fold, while the ID_{50} of IODODOX and MMDOX was only reduced by 2-5 folds. However, despite the great effect in sensitizing DOX and the apparently modest effect in sensitizing DOX derivatives, when the toxicity of the anthracyclines plus PSC in the MDR cell lines was compared with the toxicity in the non MDR cell lines, it emerged that only MMDOX resistance could be almost completely abolished. On the contrary, resistance to DOX only decreased.

A possible exception was LOVODOX; in this cell line, PSC was highly efficient in blocking PGP, and in the case of DOX it could reduce the RI to almost 1. The discrepant effect of reversal agents in counteracting the drug resistance to different drugs in different cell lines has already been described.[49] A possible explanation could be that cell lines selected with a positive drug pressure can simultaneously develop different mechanisms of resistance. In our cell lines, an amplification of the mdr-1 gene has already been described and a high PGP overexpression was confirmed in our laboratory by using the MRK-16 MoAb and functional assays.[23,33] To better define the mechanisms of MDR in our cell lines, other possible MDR factors were investigated. This screening included the evaluation of the

expression of two other drug transporter proteins which belong to the ATP binding cassette superfamily, called the *lung resistance protein* (LRP)[50] and the *multidrug resistance-associated protein* (MRP),[51] as well as the study of the expression of the enzyme GSTπ.[52] We found that only LOVODOX displayed a modest increase of the LRP. Therefore, the results that were obtained in this study can apply specifically only to PGP-related MDR. Our observations show that PGP-related MDR can be almost completely removed by using PSC, even when tested cells have a very high PGP expression, if the parent drug DOX is substituted by its more lipophilic derivatives. This suggests that PSC is more efficient when it is used in association with drugs which by themselves can partially avoid the P-glycoprotein transport. Concerning the possible clinical application of these data, preliminary studies have already described the toxic, metabolic and pharmacokinetic properties of IODODOX, MMDOX and PSC respectively.[28,29,53-56] However, it must be pointed out that *in vitro* studies can describe and clarify the antitumor effect of a single drug or of a combination of drugs, but they can not predict therapeutic results and *in vivo* side-effects. Moreover, from the preclinical studies with reversal agents, including PSC, performed until now, we have learnt that the introduction of agents blocking the PGP-mediated drug efflux can also alter the antitumor drug metabolism, its delivery to the tumor and the pharmacokinetic.[12,16,29]

We conclude that the association of PSC and lipophilic anthracyclines like IODODOX and MMDOX is worth evaluating for antitumor effect and for toxicity in experimental models that is in high risk, primary chemoresistant human tumors.

References

1. Kaye SB. Reversal of multidrug resistance. Cancer Treat Rev 1990; 17:37-43.
2. Ramu A, Ramu N. Reversal of multidrug resistance by phenothiazines and structurally related compounds. Cancer Chemother Pharmacol 1992; 30:165-73.
3. Cano-Gauci DF, Riordan JR. Action of calcium antagonists on multidrug resistant cells. Biochem Pharmacol 1987; 36: 2115-23.
4. Merlin JL, Guerci A, Marchal S, et al. Comparative evaluation of S9788, verapamil, and cyclosporine A in K562 human leukemia cell lines and in P-glycoprotein-expressing samples from patients with hematologic malignancies. Blood 1994; 84:262-9.
5. Friche E, Skovsgaard T, Danø K. Multidrug resistance: drug extrusion and its counteraction by chemosensitizers. Eur J Haematol 1989; 42 (suppl. 48):59-67.
6. Raderer M, Scheithauer W. Clinical trials of agents that reverse multidrug resistance. Cancer 1993; 72:3553-63.
7. Gottesman MM, Pastan I. Clinical trials of agents that reverse multidrug-resistance. J Clin Oncol 1989; 7:409-11.
8. Yahanda AM, Adler KM, Fisher GA, et al. Phase I trial of etoposide with cyclosporine as a modulator of multidrug resistance. J Clin Oncol 1992; 10:1624-34.
9. Berman E, McBride M, Lin S, Menedez-Botet C, Tong W. Phase I trial of high-dose tamoxifen as a modulator of drug resistance in combination with daunorubicin in patients with relapsed or refractory acute leukemia. Leukemia 1995; 9: 1631-7.
10. Trump DL, Smith DC, Ellis PG, et al. High-dose oral tamoxifen, a potential multidrug-resistance-reversal agent: phase I trial in combination with vinblastine. J Natl Cancer Inst 1992; 84:1811-6.
11. Figueredo A, Arnold A, Goodyear M, et al. Addition of verapamil and tamoxifen to the initial chemotherapy of small cell lung cancer. Cancer 1990; 65:1895-902.
12. Sonneveld P, Durie BGM, Lokhurst HM, et al. Modulation of multidrug-resistant multiple myeloma by cyclosporin. Lancet 1992; 340:255-9.
13. Cairo MS, Siegel S, Anas N, Sender L. Clinical trial of continuous infusion verapamil, bolus vinblastine, and continuous infusion VP-16 in drug-resistant pediatric tumors. Cancer Res 1989; 49:1063-6.
14. Ozols RF, Cunnion RE, Klecker RW, et al. Verapamil and adriamycin in the treatment of drug-resistant ovarian cancer patients. J Clin Oncol 1987; 5:641-7.
15. Dalton WS, Grogan TM, Meltzer PS, et al. Drug-resistance in multiple myeloma and non-Hodgkin's lymphoma: detection of P-glycoprotein and potential circumvention by addition of verapamil to chemotherapy. J Clin Oncol 1989; 7:415-24.
16. List AF, Spier C, Greer J, et al. Phase I/II trial of cyclosporine as a chemotherapy-resistance modifier in acute leukemia. J Clin Oncol 1993; 11:1652-60.
17. Jachez B, Boesch D, Grassberger MA, Loor F. Reversion of the P-glycoprotein-mediated multidrug resistance of cancer cells by FK-506 derivatives. Anti Cancer Drugs 1993; 4:223-9.
18. Twentyman PR. Modification of cytotoxic drug resistance by non-immuno-suppressive cyclosporins. Br J Cancer 1988; 57: 254-8.
19. Gaveriaux C, Boesch D, Jachez B, Bollinger P, Payne T, Loor F. SDZ PSC 833, a non-immunosuppressive cyclosporin analog, is a very potent multidrug-resistance modifier. J Cell Pharmacol 1991; 2:225-34.
20. Shudo N, Mizoguchi T, Kiyosue T, et al. Two pyridine analogoues with more effective ability to reverse multidrug resistance and with lower calcium channel blocking activity than their dihydropyridine counterparts. Cancer Res 1990; 20: 3055-61.
21. Hyafil F, Vergely C, Du Vignaud P, Grand-Perret T. *In vitro* and in vivo reversal of multidrug resistance by GF120918, an acridonecarboxamide derivative. Cancer Res 1993; 53:4595-602.
22. Eliason JF, Ramuz H, Kaufmann F. Human multi-drug-resistant cancer cells exhibit a high degree of selectivity for stereoisomers of verapamil and quinidine. Int J Cancer 1990; 46:113-7.
23. Damiani D, Michieli M, Michelutti A, Melli C, Cerno M, Baccarani M. D-verapamil downmodulated P170-associated

resistance to doxorubicin, daunorubicin and idarubicin. Anti-Cancer Drugs 1993; 4:173-80.
24. Michieli M, Damiani D, Michelutti A, Melli C, Russo D, Fanin R, Baccarani M. P170-dependent multidrug resistance. Restoring full sensitivity to idarubicin with verapamil and cyclosporin A derivatives. Haematologica 1994; 79:119-26.
25. Michieli M, Michelutti A, Damiani D, et al. A comparative analysis of the sensitivity of multidrug resistant (MDR) and non-MDR cells to different anthracycline derivatives. Leuk Lymphoma 1993; 9:255-64.
26. Grandi M, Pezzoni G, Ballinari G, et al. Novel anthracycline analogs. Cancer Treat Rev 1990; 17:133-8.
27. Twentyman PR, Fox NE, Wright KA, et al. The *in vitro* effects and cross-resistance patterns of some novel anthracyclines. Br J Cancer 1986; 53:585-94.
28. Boesch D, Gaveriaux C, Jachez B, Pourtier-Manzanedo A, Bollinger P, Loor F. In vivo circumvention of P-glycoprotein-mediated multidrug resistance of tumor cells with SDZ PSC 833. Cancer Res 1991; 51:4226-33.
29. Keller RP, Altermatt HJ, Donatsch P, Zihlmann H, Laissue JA, Hiestand PC. Pharmacologic interactions between the resistance-modifying cyclosporine SDZ PSC 833 and etoposide (VP16-213) enhance *in vivo* cytostatic activity and toxicity. Int J Cancer 1992; 51:433-8.
30. Keller RP, Altermatt HJ, Nooter K, et al. SDZ PSC 833, a non-immunosuppressive cyclosporine: its potency in overcoming P-glycoprotein-mediated multidrug resistance of murine leukemia. Int J Cancer 1992; 50:593-7.
31. Loor F, Boesch D, Gavériaux C, Jachez B, Pourtier-Manazado A, Emmer G. SDZ 280-446, a novel semi-synthetic cyclopeptolide: in vitro and in vivo circumvention of the P-glycoprotein-mediated tumour cell multidrug resistance. Br J Cancer 1992; 65:11-8.
32. Boesch D, Muller K, Pourtier-Manzanedo A, Loor F. Restoration of daunomycin retention in multidrug-resistant P388 cells by submicromolar concentrations of SDZ PSC 833, a nonimmunosuppressive cyclosporin derivative. Exp Cell Res 1991; 196:26-32.
33. Michieli M, Damiani D, Michelutti A, et al. Restoring uptake and retention of daunorubicin and idarubicin in P170-related multidrug resistance cells by low concentration D-verapamil, cyclosporin-A and SDZ PSC 833. Haematologica 1994; 79:500-7.
34. Russo D, Marie JP, Zhou DC, et al. Evaluation of the clinical relevance of the anionic glutathione-S-transferase (GSTπ) and multidrug resistnace (mdr-1) gene coexpression in leukemias and lymphomas. Leuk Lymphoma 1994; 15:453-68.
35. Michieli M, Damiani D, Michelutti A, et al. Screening of multidrug resistance in leukemia: cell reactivity to MRK-16 correlates with anthracycline retention and sensitivity of leukemic cells. Leuk Lymphoma 1995; in press.
36. Michelutti A, Michieli M, Damiani D, et al. Overexpression of MDR-related p170 glycoprotein in chronic myeloid leukemia. Haematologica 1994; 79:200-4.
37. Pieters R, Huismans DR, Leyva A, Veerman AJP. Comparison of a rapid automated tetrazolium based (MTT)-assay with a dye exclusion assay for chemosensitivity testing in childhood leukemia. Br J Cancer 1989; 59:217-20.
38. Kuhl JS, Duran GE, Chao NJ, Sikic BI. Effects of the methoxymorpholino derivative of doxorubicin and its bioactivated form versus doxorubicin on human leukemia and lymphoma cell lines and normal bone marrow. Cancer Chemother Pharmacol 1993; 33:10-6.
39. Danesi R, Agen C, Grandi M, Nardini V, Bevilacqua G, Del Tacca M. 3'-deamino-3'-(2-methoxy-4-morpholinyl)-doxorubicin (FCE 23762), a new anthracycline derivative with enhanced cytotoxicity and reduced cardiotoxicity. Eur J Cancer 1993; 29:1560-5.
40. Barbieri B, Giuliani FC, Bordoni T, et al. Chemical and biological characterization of 4'-iodo-4'-deoxydoxorubicin. Cancer Res 1987; 47:4001-7.
41. Schott B, Vrignaud P, Ries C, Robert J, Londos-Gagliardi D. Cellular pharmacology of 4-iodo-4-deoxydoxorubicin. Br J Cancer 1990; 61:543-7.
42. Watanabe M, Komeshima N, Naito M, Isoe T, Otake N, Tsuruo T. Cellular pharmacology of MX2, a new morpholino anthracycline, in human pleiotropic drug-resistant cells. Cancer Res 1991; 51:157-61.
43. Streeter DG, Johl JS, Gordon GR, Peters JH. Uptake and retention of morpholinyl anthracyclines by adriamycin-sensitive and -resistant P388 cells. Cancer Chemother Pharmacol 1986; 16:247-52.
44. Coley HM, Twentyman PR, Workman P. 9-alkyl, morpholinyl anthracyclines in the circumvention of multidrug resistance. Eur J Cancer 1990; 26:665-7.
45. Ripamonti M, Pezzoni G, Pesenti E, et al. In vivo anti-tumor activity of FCE 23762, a methoxymorpholinyl derivative od doxorubicin active on doxorubicin-resistant tumor cells. Br J Cancer 1992; 65:703-7.
46. de Vries EGE, Zijlstra JG. Morpholinyl anthracyclines: option for reversal of anthracycline resistance. Eur J Cancer 1990; 26:659-60.
47. Capranico G, Supino R, Binaschi M, et al. Influence of structural modifications at 3' and 4' positions of doxorubicin on the drug ability to trap topoisomrase II and to overcome multidrug resistance. Mol Pharmacol 1994; 45:908-15.
48. Mariani M, Capolongo L, Suarato A, et al. Growth-inhibitory properties of novel anthracyclines in human leukemic cell lines expressing either Pgp-MDR or at-MDR. Invest New Drugs 1994; 12:93-7.
49. Krishan A, Sridhar KS, Davila E, Vogel C, Sternheim W. Patterns of anthracycline modulation in human tumor cells. Cytometry 1987; 8:306-14.
50. Scheffer GL, Wijngaard PLJ, Flens MJ, et al. The drug resistance-related protein LRP is the human major vault protein. Nature Medicine 1995; 1:578-83.
51. Cole SPC, Bhardwaj G, Gerlach JH, et al. Overexpression of a transporter gene in a multidrug-resistant human lung cancer cell line. Science 1992; 258:1650-6.
52. Ozols RF, O'Dwyer PJ, Hamilton TC, Young RC. The role of glutathione in drug resistance. Cancer Treat Rev 1990; 17:45-50.
53. Mross K, Mayer U, Langenbuch T, Hamm K, Burk K, Hossfeld D. Toxicity, pharmacokinetics and metabolism of iodoxorubicin in cancer patients. Eur J Cancer 1990; 26:1156-62.
54. Gianni L, Viganò L, Surbone A, et al. Pharmacology and clinical toxicity of 4'-iodo-4'-deoxydoxorubicin: an example of successful application of pharmacokinetics to dose escalation in phase I trials. J Natl Cancer Inst 1990; 82:469-77.
55. Vasey PA, Bissett D, Strolin-Benedetti M, et al. Phase I clinical and pharmacokinetic study of 3'-deamino-3'-(2-methoxy-4-morpholinyl) doxorubicin (FCE 23762). Cancer Res 1995; 55:2090-6.
56. Pacciarini MA, Grandi M, Geroni C, et al. Methoxymorpholino doxorubicin (FCE 23762): preclinical characteristics and first clinical experience. In: M. Gonzales Baron, Advances in Oncology. Noesis ed. 207-213, 1995.

The Anthracyclines: Will We Ever Find a Better Doxorubicin?

Raymond B. Weiss

The anthracyclines are the class of antitumor drugs with the widest spectrum of activity in human cancers, and only a few cancers (eg, colon cancer) are unresponsive to them. The first two anthracyclines were developed in the 1960s. Doxorubicin (DOX) differs from daunorubicin (DNR) only by a single hydroxyl group. This fact has spurred researchers worldwide to find analogs of DOX that have less acute toxicity, cause less cardiomyopathy, can be administered orally, and/or have different, or greater, antitumor efficacy. Five DOX/DNR analogs are marketed in other countries, and one (idarubicin) is available in the United States. None of these analogs have stronger antitumor efficacy than the original two anthracyclines, but there are some differences in toxicity. Methods have been fashioned to keep the peak plasma level of DOX muted to minimize cardiotoxicity, but the only apparently effective method available so far (prolonged drug infusion) is cumbersome. The bisoxopiperazine class of drugs (especially dexrazoxane) provides protection against anthracycline-induced cardiomyopathy and has much promise for helping mitigate this major obstacle to prolonged use of the anthracyclines. The DOX analogs being evaluated in the 1990s have been selected for their ability to overcome multidrug resistance in cancer cells. Thirty years after discovery of the anticancer activity of the first anthracycline, some means of reducing anthracycline toxicity have been devised. Current studies are evaluating increased doses of epirubicin to improve anthracycline cytotoxicity, while limiting cardiotoxicity, but at present DOX still reigns in this drug class as the one having the most proven cancerocidal effect.

THE BIFUNCTIONAL alkylating agents were the first drugs proven to have clinical anticancer activity. One of them, cyclophosphamide, remains one of the most widely used drugs today, even though it was synthesized nearly 40 years ago. The other most widely used class of antitumor agents today is the anthracyclines, and few patients with malignancies do not receive one of the anthracyclines at some point in their clinical course. The history of these drugs also goes back to the 1950s.

Farmitalia Research Laboratories of Milan, Italy (now part of the Montedison Group conglomerate) began an organized effort in the mid-1950s to find anticancer compounds produced by soil microbes. In 1958, a Farmitalia employee collected a random soil sample from the grounds of the Castel del Monte, a 12th-century castle that is a local tourist attraction near Andria in southeastern Italy. From this soil sample was grown a newly recognized species of *Streptomyces*, which produced a bright red pigment. Di Marco isolated an antibiotic from this fungus[1] that had striking activity against a wide spectrum of murine cancers.[2] It also had antifungal and antibacterial properties, but it was selected for clinical development because of its antitumor effects. Di Marco et al named this antibiotic daunomycin, using the name (Daunii) of a pre-Roman tribe that once resided in the Andria region.

Also in the early 1960s, Dubost et al at the laboratories of Rhône-Poulenc in suburban Paris independently isolated a new antibiotic from a different species of *Streptomyces* that also produced a red pigment.[3] They named their new antibiotic rubidomycin, using the French word rubis, for ruby. On public presentation of their new discoveries, both groups of researchers recognized that they had identified the same substance. The term daunorubicin (DNR) was later coined and adopted as the international nonproprietary name (INN) to give equal credit to both discoverers. By accepted convention, all new anthracyclines are given the suffix of "rubicin" in the INN system. The name anthracycline was created by Brockman in the late 1950s based on the presence of an anthraquinone chromophore and the polycyclic ring system in the chemical structure, which is similar to that of tetracycline.

Clinical trials of DNR began in 1964 in the respective countries of origin and at the Memo-

From the Departments of Medicine, Walter Reed Army Medical Center, Washington, DC; and the Uniformed Services University of the Health Sciences, Bethesda, MD.

Address reprint requests to Raymond B. Weiss, MD, Section of Medical Oncology, Walter Reed Army Medical Center, Washington, DC 20307.

The opinions expressed in this article are solely those of the author and are not necessarily those of any government agency.

0093-7754/92/1906-0007$0.00/0

rial Sloan-Kettering Cancer Center in the United States. At this time, hematologists treating leukemia and lymphoma were usually the only physicians who used drugs for cancer, and DNR was tested mostly in patients with these diseases. This circumstance was actually serendipitous because DNR was found by Tan to have high activity for acute leukemia,[4] and this cancer is still the only one for which it is effective. By 1967, French and American investigators recognized that DNR could produce fatal cardiac toxicity,[4,5] which is still the major obstacle for prolonged use of anthracyclines.

Comparison of the structure of DNR to an anthracycline predecessor of DNR (rhodomycin) showed the Farmitalia investigators that minor changes in the chemical structure could alter the biological activity of this drug class. A colleague and collaborator of Di Marco, Arcamone, then began an effort to develop analogs of DNR that might also have antitumor effects. Arcamone et al subjected the *Streptomyces* that produced DNR to the mutagenic effects of N-nitroso-N-methyl urethane and derived a strain that produced a different red-colored antibiotic.[6] Arcamone named this substance Adriamycin after the Adriatic Sea, which is only a few kilometers from the Castel del Monte. Because Adriamycin was a registered trade name, the INN doxorubicin (DOX) was later coined for this new agent. Di Marco et al showed that DOX had greater activity than DNR against some murine cancers and a better therapeutic index.[7]

DiMarco, who had moved to the Istituto Nazionale Tumori in Milan, then took a purified supply of Adriamycin for study to his clinical colleague, Bonadonna. Serendipity again played a strong role because the first patient treated with this new drug by Bonadonna had a metastatic fibrosarcoma.[8] After one dose of the drug this patient's pulmonary metastases regressed. Twenty-five years later, DOX is still the most active drug available for treatment of sarcomas. The subsequent high antitumor activity of DOX observed by Bonadonna et al[9] was confirmed by Tan et al[10] and many others in the United States. In 1974, only 6 years after the first patient received this drug, DOX was approved for marketing in the United States. DOX remains today the antitumor agent with the widest spectrum of antitumor activity. The world of oncology owes a large debt of gratitude to the Italian investigators, Di Marco, Arcamone, and Bonadonna, who led the research with these two anthracyclines in the 1960s.

There is a difference of only a single hydroxyl group between the chemical structures of DNR and DOX, in otherwise complex molecules. Despite the minor difference in structure, there is a great difference in clinical antitumor activity. DNR has little activity in carcinomas and sarcomas,[11] whereas DOX is one of the most effective drugs for these cancers. However, there are a few cancers where DOX is ineffective (eg, colon cancer, melanoma, chronic leukemias, and renal cancer). In addition, the cumulative cardiotoxicity limits the duration of DOX use to approximately 9 months at usual doses, and most cancers will develop resistance to it.

The singular success in developing DOX and its limitations in clinical use have been the basis for investigators worldwide trying to develop a better DOX. This research has followed three major pathways. One has been the creation of new anthracycline analogs, in hopes of emulating the success of Arcamone. This process has continued from the 1960s to the present, and will into the future. No one has kept count of the new anthracycline analogs synthesized over the past 25 years, but it probably numbers well in excess of 2,000, and more are reported every month. Over 400 analogs have been synthesized in one group (the AD series) alone (personal communication, Mervyn Israel, July 1992), and 553 had been evaluated in the screening program at the National Cancer Institute (NCI) by 1991 (personal communication, Edward Acton, September 1991). Another method has been to administer some agent in conjunction with DOX, either to protect against cardiotoxicity or to overcome drug resistance by the cancer. Finally, DOX has been modified "mechanically" (eg, by the use of liposomes) to minimize heart exposure to the drug while maintaining antitumor efficacy. The major question to be addressed in this article is, have (or will) any of these methods really given us a better DOX. Although there have been many failures in the attempts to improve on DOX, in the past few years some of

the developments allow a qualified "yes" to this question.

DOXORUBICIN (DOX) ANALOGS

The scientific and commercial success of Arcamone in adding a single hydroxyl group to an active drug and turning it into DOX has been the driving force for developing other new anthracycline analogs. Analogs have been obtained from fungi isolated from soil samples or rationally synthesized based on known structure-activity relationships. A variation of the fungal isolation method is to subject the parent *Streptomyces* organism to mutagens so that new compounds are created from genetic code modifications. Most of this work has been done in Europe and Japan, and the only clinically successful analogs developed so far have come from Italy and Japan. The focus of such analog development has been to find an anthracycline that is less cardiotoxic, is more able to be absorbed orally, has less acute toxicity, or has activity in cancers resistant to DOX. In the past 23 years, such a search has led to creation of several dozen anthracyclines with promise for clinical advantages that unfortunately were not borne out in clinical studies. Table 1 lists some of these agents and the reasons why they are no longer in clinical trial. There are other anthracycline analogs that either are marketed or in current trials and have promise for advantages over DOX. These will be discussed individually.

Table 1. Some Anthracyclines Tested Clinically and Found to Have No Advantages Over DOX

Name	Findings in Clinical Studies
Carminomycin	Antitumor activity appears inferior to DOX.
Detorubicin	Synthesis difficult. No advantages over DOX.
Esorubicin	Antitumor activity appears inferior to DOX. No less cardiotoxic than DOX.
Marcellomycin	Myelosuppression erratic in phase I trials. No phase II trials performed.
Quelamycin	Phase I trials showed both acute and chronic iron overloading toxicity resulting in hemachromotosis. No phase II trials performed.
Rodorubicin	Phase I trials showed both cardiotoxicity and nephrotoxicity. No phase II trials performed.

NOTE. None of these anthracyclines are in current clinical use.

Abbreviation: DOX, doxorubicin.

Idarubicin

The only anthracycline marketed in the United States besides DNR and DOX is idarubicin (IDA). This agent was synthesized by Arcamone[12] in 1976 and is actually a DNR analog because its only difference from DNR is the deletion of the methoxyl group at the C-4 position on Ring D. The INN was derived from its Italian name, 4-demetoss*ida*unon*ubicin*a. Animal tumor studies were conducted to compare IDA with its parent, DNR, and they showed that IDA had greater antitumor activity at lower drug concentrations.[12] IDA was found to have higher affinity for lipids than other anthracyclines, which suggested that good oral absorption was possible. Because both DNR and DOX are poorly absorbed orally and must be administered intravenously, oral administration of IDA might provide a distinct advantage.

Phase I trials of IDA in both intravenous and oral formulations showed that an approximately 3.5 × greater dose of IDA orally was necessary to produce an equivalent myelotoxic effect to that of the intravenous drug. Phase II trials with both formulations indicated that IDA was active in acute leukemias (both myeloid and lymphatic) and some carcinomas, notably breast cancer.[13] As might be expected, the response rates were highest in patients who had not previously received an anthracycline.[14]

Although oral IDA has been studied in patients with acute leukemia, there is no advantage to this administration route in a disease where insertion of a central venous access device is standard procedure as soon as the diagnosis is made. However, the activity of intravenous IDA in acute myeloid leukemia (AML) naturally raised the question, is it any better than the parent compound? Only prospective randomized trials comparing IDA with DNR, both in conjunction with cytarabine, could answer this question. There have been four such major randomized trials comparing these drugs vis-à-vis, each in a slightly different dose and/or age population.[15,16] The results in these studies are not consistent. Two of the four studies showed a statistically significant advantage for IDA in complete remission rate and two did not. In the three studies where the data were provided, none showed any difference in median duration of response. Finally, two of the

four studies showed no difference in survival.[15,16] What is puzzling about these trials is that the outcomes (response rate, response duration, and overall survival) for the IDA-treated groups are not really superior to those achieved in a large cooperative study using DNR plus cytarabine for induction therapy.[17] Moreover, the results of the DNR-treated patients in the randomized trials are inferior to those in this cooperative study.[15-17] On the other hand, when there is any difference in the results of the randomized trials, IDA is always superior, so the clinician is left with uncertainty about the question supposedly to be solved by these studies: does IDA have a greater efficacy than DNR, or is it a more expensive "me too" drug? The one conclusive point in these comparisons is that there is no meaningful toxicity difference between the two analogs.

DNR is an essential component of therapy for acute lymphocytic leukemia (ALL), as it is in AML. IDA has activity in ALL at a rate equivalent to that of DNR,[15] but no randomized comparisons of the two analogs have been performed in this disease.

Oral IDA appears to have efficacy in breast cancer,[14] in contrast with DNR, although DNR has had only cursory study in this disease.[11] If an oral anthracycline is effective as a palliative therapy for breast cancer, it would have a clearcut advantage over DOX. Does oral IDA represent the hoped-for "better doxorubicin"? Unfortunately, the answer seems to be no.

A randomized comparison of oral IDA versus intravenous DOX in 76 patients has shown a statistically significant, inferior response rate for the oral IDA.[18] In patients who had received no prior chemotherapy, the response rate was 60% for DOX versus 29% for IDA; in patients previously treated, the response figures were 29% versus 12%, respectively. This low response rate of oral IDA has been observed in single-arm studies also.[19,20]

A major problem with oral IDA is the variation in bioavailability. Stewart et al[21] showed that the oral bioavailability ranged from a low of 12% to a high of 49% in a series of nine patients. These data indicate that there can be up to a fourfold difference in ability to absorb the drug, with commensurate variations in toxicity (especially hematologic) and antitumor efficacy. This oral bioavailability issue could be the explanation for the response rates in breast cancer being lower than DOX.[18-20]

There are some advantages to oral IDA that could make it attractive for use in selected patients. IDA has activity in indolent lymphomas,[22] which is a disease where a convenient oral palliative drug could be useful as treatment for patients not responding to alkylator therapy. Myelodysplastic syndrome is another indolent disease that could be treated with oral IDA. IDA might be useful as part of outpatient treatment for chronic myelogenous leukemia or as maintenance therapy for AML. The apparent lower degree of alopecia associated with oral IDA[18-20] is also a worthy attribute. There also may be a somewhat smaller risk of cardiotoxicity, but a dose limit for heightened risk of such toxicity has not been established. However, before such oral therapy becomes recommended, it would be worthwhile to study the bioavailability problem in more depth. There may be phenotypic metabolic variations that could be determined before treatment, with commensurate adjustments in drug dose to minimize toxicity and maximize antitumor efficacy. The IDA patent is held by Farmitalia Carlo Erba, and Adria Laboratories, the American subsidiary of Farmitalia, does not have plans at present to pursue marketing of oral IDA in the United States but is interested in trials that might find oral IDA a niche in cancer treatment.

Epirubicin (EPI)

In their ongoing search for anthracycline analogs in the 1970s, Arcamone et al[23] modified the aminosugar moiety of DOX and created an epimer of the C-4′ hydroxyl group on the aminosugar (Table 2). The positional change in this hydroxyl group is the sole difference from DOX. It was selected for further development because its murine and human xenograft antitumor activity was equivalent to DOX, but it had less cardiotoxicity.[24] These features suggested an improved therapeutic index over DOX.

When phase I testing of epirubicin (EPI) was begun in Milan,[25] the same every 3-week schedule used with DOX was also used for this analog. However, the tolerable dose range established was 70 to 90 mg/m^2, which is equimyelo-

Table 2. Anthracyclines Marketed in the United States and/or Other Countries

Name	Chemical Structure	Where Marketed	Disease Indication
Daunorubicin	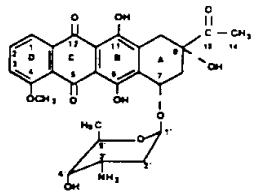	Worldwide	Acute leukemias
Doxorubicin	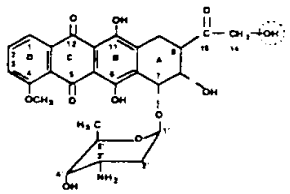	Worldwide	A wide cross-section of carcinomas, lymphomas, and sarcomas
Idarubicin	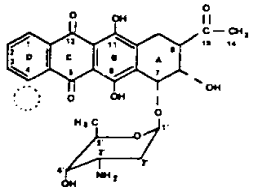	Worldwide (intravenous only)	Acute leukemias
Epirubicin	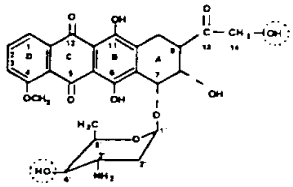	Worldwide (except U.S.)	A wide cross-section of carcinomas, lymphomas, and sarcomas
Pirarubicin	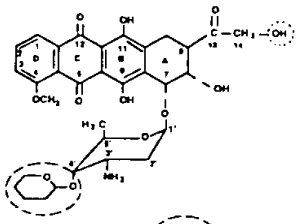	Japan, France	Carcinomas, lymphomas, and sarcomas
Aclarubicin	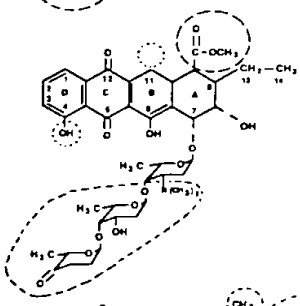	Japan, France	Acute leukemias and non-Hodgkin's lymphomas
Zorubicin	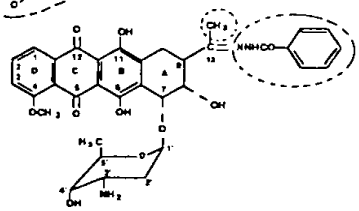	France	Acute leukemias

NOTE. The dotted line in each chemical structure encircles the point where a difference from daunorubicin exists. The carbon atoms are numbered and the rings are lettered in each structure configuration.

toxic to the 60 to 75 mg/m^2 dose range of DOX. Identical to DOX, nadir blood counts occurred 10 to 12 days after each dose with recovery by 21 days. Pharmacokinetic studies[26] showed that EPI is more rapidly and extensively metabolized than DOX with its alcohol metabolite (epirubicinol) being formed to a greater degree. In addition, EPI forms more glucuronides than DOX because of the positional change of the C-4′ hydroxyl group. This glucuronidation facilitates the excretion process.[26] As a result, the terminal elimination phase of EPI is shorter than DOX by an average of 10 hours, thus producing a higher plasma clearance. These features of EPI pharmacokinetics are important clinically because they may explain the toxicity advantage that EPI has.

Phase II trials of EPI conducted in the 1980s have established the fact that EPI has activity in the human cancers for which DOX is active and is inactive in the same tumors.[27,28] Because DOX is rarely used as a single agent, EPI also was evaluated in combination regimens, particularly for breast cancer. In two large prospective, randomized trials comparing EPI with DOX as part of combination therapy for metastatic breast cancer (both groups received cyclophosphamide and 5-fluorouracil to make CAF or CEF), there was no difference in response rate, response duration, or survival.[29,30] Therefore, it is clear that EPI has not proved to have an antitumor efficacy advantage over DOX and is disappointing in this regard.

EPI was selected for clinical development because it appeared to be less cardiotoxic than DOX. Does EPI have any toxicity advantages over DOX? In considering this point one must keep in mind the drug doses used in any randomized comparison of these two anthracyclines. Are the doses equimolar or equimyelotoxic (a 15 to 20 mg/m^2 greater dose for EPI)? This point is very important because if equimolar doses are compared, EPI will always show lower toxicity, both acute and chronic. Such an outcome was evident in the two studies comparing CEF with CAF.[29,30] Both used equimolar doses of EPI and DOX, and both showed less acute toxicity and cardiotoxicity for EPI. When the drugs are compared at equimyelotoxic doses, there is little difference in noncardiac toxicity.[31]

EPI clearly produces cardiomyopathy that can even be fatal sometimes.[32,33] The morphological features of EPI-induced cardiomyopathy are identical to those induced by DOX.[33] The total dose range in which the cardiotoxicity risk increases precipitously (akin to the 550 mg/m^2 cumulative dose limit of DOX) is 900 to 1,000 mg/m^2.[32-34] This total dose is ideally reached with approximately 11 doses of EPI administered over some 9 months, if 85 mg/m^2 are administered at an every 3-weeks schedule.[34] If a lower dose of EPI is used (eg, 50 mg/m^2) when it is incorporated into a combination regimen such as CEF,[29,30] then it will ideally take 17 doses administered over some 12 months to reach the toxic range. When one considers that the median duration of response to CAF or CEF regimens in breast cancer is 8 to 10 months,[29,30,35] one can see that most patients will have tumor progression and require a change in therapy before they have a serious cardiotoxicity risk from EPI.

CEF with a dose of EPI equimolar to that of DOX in CAF also produces less acute nausea and vomiting,[29,30] an important factor in patient compliance with therapy and quality of life, apparently without compromising therapeutic efficacy. Therefore, EPI seems to provide a marginal toxicity advantage over DOX.

EPI is now widely marketed in Canada, Japan, Australia, and Europe, but not in the United States, and has largely supplanted DOX in clinical use. A New Drug Application (NDA) was submitted to the Food and Drug Administration (FDA) in 1985 but was not approved, probably because the cardiotoxicity advantage of EPI was modest and applied to only a minority of patients whose cancer still had not progressed after approximately 10 months of therapy. The emesis induced by chemotherapy is very distressing to patients. If a CEF regimen has equivalent efficacy to CAF, but induces less vomiting, EPI should be available for clinical use in the United States, even if its therapeutic spectrum is not different from DOX.

DOX is usually administered in doses of 60 to 75 mg/m^2 when it is used alone and at 45 to 50 mg/m^2 when used in combination. Increasing the DOX dose to 90 to 135 mg/m^2 results in more total, and more complete, responses in breast cancer.[36] However, the cumulative dose limit for cardiotoxicity is reached more quickly

with such doses, and congestive heart failure can result.[36] Symptomatic acute mucositis is also a problem.

The maximum tolerated dose (MTD) of EPI in the phase I trials conducted 13 years ago[25] was 70 to 90 mg/m^2. Drug dose escalation has become a topic of intense research interest in oncology in the 1980s, and attempts have been made to increase EPI doses. These efforts are based on the premise that the moderate acute and chronic toxicity advantages of EPI over DOX might allow escalation of EPI doses with commensurate enhanced therapeutic efficacy at more moderate toxicity cost than similar studies[36] with DOX. Moreover, the concomitant use of bone marrow protective agents (such as filgrastim) and cardiotoxicity protectors (such as dexrazoxane [DXZ]) may allow even further dose escalations of EPI.

Initial studies of EPI dose escalation increased the dose to 120 mg/m^2, with which mucositis became dose-limiting, whereas myelosuppression was not.[37] Subsequent studies have increased the dose to 180 mg/m^2, in which myelosuppression did become dose-limiting and caused neutropenic fevers in 23% of 27 patients.[38] Complete or partial tumor responses occurred in 85% of the patients. A study by Bastholt et al[39] comparing four EPI doses in prospective randomized fashion for breast cancer has been preliminarily reported. The response rate was improved by increasing the EPI dose from 40 to 60 mg/m^2 to 90 mg/m^2, but not when it was increased to 135 mg/m^2. In addition, some patients had their dose increased after achieving no tumor regression at a lower EPI dose, and about 25% then had a response.[39]

The higher number of responses achieved with both DOX and EPI administered at heightened doses are encouraging, but they will not necessarily achieve better survival in patients with stage IV breast cancer. On the other hand, they could be advantageous for patients with locally advanced disease. Further work with EPI dose escalation using the toxicity protectants is ongoing.

Pirarubicin (PRA)

Umezawa, at the Institute of Microbial Chemistry in Tokyo, spent a long, illustrious career searching for antibiotics, particularly those with antitumor activity. In 1966 he isolated bleomycin, and in the 1970s he turned his attention to finding new anthracyclines. One of the anthracyclines he discovered was a tetrahydropyranyl derivative of DOX, which was initially labeled THP-Adriamycin.[40] The INN now is pirarubicin (PRA; the pronunciation of the "pyra" segment was internationalized with different spelling). Development of this analog has occurred primarily in Japan and France.

Preclinical tumor efficacy studies of PRA by Tsuruo et al[41] showed general equivalence or superiority to DOX. Cardiotoxicity studies performed in France[42] indicated a lesser degree of cardiotoxicity than DOX in experimental animals, and thus PRA was brought to clinical trial.

The dose and schedule for this analog used in phase II trials has been 50 to 70 mg/m^2, administered at 3-week intervals. Granulocytopenia is dose-limiting. PRA has undergone study in acute leukemia, lymphoma, sarcoma, and breast cancer, and the response rates have been equivalent to those achieved from DOX.[43-45] The spectrum and degree of its antitumor efficacy appear similar to DOX. When used in a combination regimen for breast cancer,[46] the response rate is equivalent to that of CAF.

Preclinical studies suggested a lesser degree of cardiotoxicity with PRA, but clinical studies have not been performed to establish this point. In particular, no randomized prospective comparisons of PRA with any other anthracycline (such as has been done with EPI[31,34]) have been reported. Also, the cumulative dose at which the cardiotoxicity risk becomes significant is poorly characterized.

The one attribute of PRA that could incite clinical interest is the lower rate of total alopecia. When PRA is used as a single agent, total alopecia is uncommon, and it does not develop as a cumulative toxicity.[43-45] Even when PRA is administered in combination with 5-fluorouracil and cyclophosphamide,[46] total alopecia occurred in only about half of the patients. DOX is well known to produce total alopecia in nearly every patient treated. Most oncologists have encountered patients (especially women) who are extremely reluctant to accept any chemotherapy that might cause total alopecia. PRA could

be an acceptable substitute for DOX or EPI (with equivalent antitumor activity) that would enhance quality of life.

The patent on PRA is owned by Meiji Seika Kiasha, Ltd. of Tokyo, Japan. It is marketed in Japan and, under licensing agreements, in Europe. No American company has developed any interest in pursuing the clinical trials necessary to establish a toxicity superiority of PRA over DOX. The one attractive feature of causing less alopecia may not be commercially promising enough to invest the necessary effort and resources for seeking marketing approval in the United States.

Zorubicin and Aclarubicin

Zorubicin (rubidazone) was isolated by Rhône-Poulenc investigators in France in 1969 and was found to have activity in acute leukemia.[47] This analog is marketed in France (Table 2). It was studied by American investigators and found to have no advantage over DNR or DOX, so no further development for marketing in the United States has been done.

Aclarubicin (aclacinomycin) is another analog found by Umezawa in the mid-1970s. It also has activity in acute leukemias and is marketed (Table 2) for this cancer in France and Japan. Studies in the United States did not show any advantages over DNR or DOX, so all clinical trials have been closed.

Iododoxorubicin (IODO)

This anthracycline is an analog of DOX synthesized by Arcamone and colleagues in the mid-1980s.[48] It was selected for clinical development because it had activity against DOX-resistant P388 leukemia, had greater activity than DOX in some preclinical tumor lines, and had more rapid cellular uptake than DOX. It also had less cardiotoxicity in preclinical testing.[49] The sole structural difference from DOX is the presence of an iodine atom at the C-4' position, instead of a hydroxyl group.

Phase I trials were performed in Europe in the late 1980s, and some phase II trials have now been completed. A clinically promising feature of the toxicity profile, established in phase I testing, was the fact that the sole dose-limiting acute toxicity was granulocytopenia, which was rapidly reversible.[50] DOX causes severe stomatitis at high doses, and during dose escalation. This toxicity feature of iododoxorubicin (IODO) favors the combining of the anthracycline with hematologic growth factors, such as filgrastim or sargramostim, thus allowing further dose escalation with perhaps greater antitumor activity.[51] This analog might even be useful as part of a preparatory regimen for marrow transplant.

Only a few phase II studies of IODO have been published, and they have not been full of promise for this agent.[51,52] In a trial of patients with advanced breast cancer receiving a 70 mg/m^2 dose, the response rate was only 10%, and there was negligible activity in colon and lung cancer.[52] Another trial[51] using a dose of 80 mg/m^2 gave a 35% response rate in advanced breast cancer, but this rate was achieved at the expense of a 34% incidence of grade 4 granulocytopenia. This hematologic toxicity was also more common with repeated treatment. DOX can produce a similar response rate as a single agent in breast cancer but without such severe hematologic toxicity.

At this point, IODO appears not to provide any clearcut advantage over DOX, although testing in a variety of cancers has not been performed yet. The only promising path for further development may be as a constituent of marrow ablative therapy.

AD-32

A series of DOX analogs have been synthesized by Israel et al, first at Dana-Farber Cancer Institute, and subsequently at the University of Tennessee. One of the early compounds in this series, AD-32, was created in 1973 and had greater antitumor activity, less cardiotoxicity, and less toxicity in general than DOX in preclinical testing.[53] A phase I trial of intravenously administered AD-32 was then performed,[54] but drug formulation and solubility problems prevented further clinical development.

AD-32 has recently been resurrected as an intravesical treatment for bladder cancer because it appears not to cause local tissue injury if extravasated and is poorly absorbed systemically when administered in the bladder.[55] Phase I trials have been performed,[55] and phase II

trials are underway through sponsorship of Anthra Pharmaceuticals, Inc. (Princeton, NJ), the holder of commercial rights to the AD series of compounds. Administration of AD-32 via the intraperitoneal route is also being studied.

ANTHRACYCLINE ANALOGS—THE NEXT GENERATION

The direction for development of new anthracycline analogs in the 1970s and early 1980s was to expand the antitumor spectrum of DOX, reduce cardiotoxicity and acute toxicity, and/or develop an orally absorbed compound. The fruits of this research have given us a few analogs with only marginal clinical advantages, if any. Research in antitumor drugs in the 1980s moved towards finding ways of overcoming tumor cell resistance to drugs. The ability of cancer cells to develop resistance to a variety of structurally unrelated compounds is called multidrug resistance (Mdr).[56] As the direction of oncology research turned to overcoming Mdr, so did research in anthracycline analog development.

Table 3[57-65] outlines some of the more prominent anthracycline analogs that have been entered, or soon will be entered in initial clinical trials. All have only laboratory code names so far. These analogs have been created by chemical synthesis or by biosynthesis through exposing *Streptomyces* species to mutagens. Most of these have been developed in Japan and Italy, in particular at the Institute of Microbial Chemistry in Tokyo and Farmitalia Carlo Erba Research Laboratories in Milan. Most were selected because of activity in preclinical murine and human tumor lines that were DOX-resistant. Another potential advantage is that some of these analogs (eg, FCE 23762 and MX-2) have greater antitumor potency than DOX (and possibly a different mechanism of action) while having no greater cardiotoxicity.

It is uncertain when, or if, any of these analogs will be clinically tested in the United States, but they would probably have to show real promise for an advantage over DOX before United States investigators would be interested. One advantage would have to be antitumor activity in patients previously exposed to DOX, because oncologists are now surfeited with analogs that have marginal toxicity advantages over DOX. They could even repeat the history of

Table 3. New Anthracyclines in Current Early Development

Code Name (Commercial Sponsor)	Country of Origin	Preclinical Study Advantages	Current Status	Reference No.
F 860191 (Hoechst)	France	Possible topoisomerase II inhibitor. More active than DNR and DOX in leukemia cell lines.	Preclinical development	57
FCE 21424 (Farmitalia Carlo Erba)	Italy	Increased potency against leukemia in preclinical testing.	Chemical stability problems	58
AD-198 (Anthra)	United States	Significantly less cardiotoxicity. Active against DOX-resistant cell lines. Cytotoxicity is potentiated by liver microsomes. Mechanism of action appears greatly different from that of DOX.	Preclinical development	59
FCE 23762 (Farmitalia Carlo Erba)	Italy	11-fold more potent than DOX against in vitro tumor cell lines. Active against DOX-resistant cell lines.	Phase I trials	60
SM-5887 (Sumitomo)	Japan	More active in preclinical carcinomas than DOX (especially gastric). Less cardiotoxic.	Phase II trials	61
ME 2303 (previously FAD-104) (Meiji Seika Kaisha)	Japan	A fluorinated anthracycline. Greater activity than DOX in P388 and L1210 leukemias. Active against DOX-resistant cell lines.	Phase II trials	62, 63
MX-2 (previously KRN-8602) (Kirin Brewing)	Japan	Active against DOX-resistant and multidrug resistant cell lines. Less cardiotoxic than DOX.	Phase II trials	64, 65

other promising analogs such as rodorubicin. This analog had a greater antitumor spectrum of activity and was active in DOX-resistant tumors in preclinical testing. However, when studied in phase I trials,[66] it not only caused cardiotoxicity, but added nephrotoxicity (in the form of proteinuria) to the spectrum of anthracycline clinical toxicity. Moreover, the cardiotoxicity was not only a cardiomyopathy, but also damage to the endothelium of endocardial veins. Rodorubicin has not been heard of since!

"MECHANICAL" MODIFICATIONS OF DOX

If 25 years of intensive research in creating anthracycline analogs has not provided us with a "better DOX," perhaps DOX itself can be modified by some means that will reduce cardiotoxicity and make the drug safer. Such methods would include using prodrugs and encasing DOX in liposomes or changing the drug administration method to retard the height of peak plasma levels of DOX. High peak plasma levels are thought to be related to DOX cardiotoxicity.

A prodrug of DOX (called leurubicin) was created by binding L-leucine to the nitrogen atom at the 3′ position on the amino sugar. This was work performed in the early 1980s by Belgian investigators. The L-leucine is hydrolyzed in blood and at cell surfaces, and active DOX is released. Not only is the peak plasma level thus moderated, but active drug is theoretically released at the cancer cell surface where it can have the most effect. Preclinical studies[67] showed that equitoxic doses of leurubicin were equivalent in antitumor activity to DOX while less cardiotoxic. A phase I trial[68] showed that about 37% of administered leurubicin is converted to DOX, and a threefold greater dose (210 mg/m^2) was the MTD.

The company involved in developing this prodrug (Megenix Group, Brussels, Belgium) has had financial problems, so the future of leurubicin is uncertain. The concept behind the drug is certainly worthy, but much work would be necessary in the form of phase II and III trials to establish its clinical efficacy and putative lesser cardiotoxicity.

Another means of reducing the peak plasma level of DOX is to administer it in a continuous infusion. Investigators at M.D. Anderson Hospital were the originators of this technique. Legha et al[69] showed that 96-hour infusions of DOX could maintain therapeutic efficacy while reducing cardiotoxicity. These investigators reported seven patients who each received cumulative DOX doses of >550 mg/m^2 (one patient received 1,500 mg/m^2) and had no cardiotoxicity, nor even severe pathological changes on endomyocardial biopsy.[69]

A randomized prospective comparison of the 96-hour infusion versus bolus administration of DOX did confirm that antitumor tumor efficacy is similar, whereas the cardiac toxicity of infused drug is significantly reduced.[70] The infusion group of patients also had less vomiting, but more stomatitis, than the group receiving bolus DOX.

This method of DOX administration does provide an advantage in ability to give higher cumulative doses of DOX without causing severe cardiac injury. However, one must keep in mind that few patients still have responding cancers by the time they reach the dose limit range of bolus DOX. In addition, such infusional therapy requires 4 days of hospitalization every 3 weeks, and a central venous catheter must be inserted to obviate the risk of inadvertent DOX extravasation. Infusional DOX administration is costly and cumbersome and, therefore, has not achieved widespread acceptance.

Another proposed solution to the cardiotoxicity problem is to incorporate DOX into phospholipid carrier systems (liposomes).[71] Both DOX- and DNR-containing liposome systems have been developed and clinically tested.[72,73] The rationale for encapsulating anthracyclines in liposomes is also based on the theory that high peak plasma levels of drug are more cardiotoxic. Therefore, if the drug could be administered in a bolus, but only slowly released into the blood, cardiotoxicity might be reduced or avoided. Laboratory work testing this concept was performed more than 10 years ago. Studies in both mice and dogs[74,75] indicated that whereas free DOX produced the expected cardiac abnormalities histologically, liposomal DOX did not. In addition, the antitumor efficacy of DOX was maintained despite the encapsulation of DOX within the liposomes.[74]

Although the concept of DOX liposomes was

proven of potential value for clinical trials in the early 1980s, major obstacles of chemical stability and drug formulation had to be solved before such trials could begin. A liposome that did not leak the drug had to be perfected. In the later 1980s, new drug loading techniques were developed that allowed the trials to start. Several commercial concerns have formulated anthracycline liposomes used for clinical trials. The Liposome Co. (Princeton, NJ) has one for DOX (called TLC-D99), and Vestar, Inc. (San Dimas, CA) has one for DNR. Another such DOX formulation was developed by investigators at Georgetown University. Phase I trials have been completed for DOX-liposomes, and phase II trials have been initiated. The formulation used by the Liposome Co. consists of egg phosphatidylcholine and cholesterol, whereas the one produced at Georgetown comprises phosphatidylcholine, cholesterol, cardiolipin, and stearylamine.[71]

The phase I trials with TLC-D99 have shown that the MTD is 75 mg/m^2 administered every 3 weeks or 30 mg/m^2 administered weekly.[76,77] The MTD used for the Georgetown product was 90 mg/m^2.[72] All these doses exceed those used for free DOX, although not to a large degree. Some observations from these preliminary studies that have clinical importance are that granulocytopenia was the dose-limiting toxicity, antitumor responses occurred in traditionally DOX-sensitive cancers (such as breast cancer), stomatitis was usually mild, and cardiac toxicity was generally mild, even in a few patients who received cumulative DOX doses of >500 mg/m^2.[72,76,77]

These findings support further studies using DOX-liposomes to verify antitumor efficacy in phase II trials[78] and then performing a randomized, prospective comparison (phase III trial) with free DOX. In addition, the fact that granulocytopenia is the dose-limiting toxicity of liposomal DOX, while other acute toxicity and cardiotoxicity are moderate, provides a rationale for testing liposomal DOX with filgrastim or sargramostim to overcome granulocytopenia and allow DOX dose escalation. Studies of these types are ongoing.

DOX or DNR liposomes are theoretically an answer to the practical problem of trying to deliver an anthracycline in a fashion that moderates the peak plasma level and, in turn, moderates the cardiotoxicity. The drug can be administered conveniently in a bolus, instead of a 96-hour infusion. It might even be possible to increase the individual DOX dose and heighten therapeutic efficacy. Free DOX doses have been increased in patients with breast cancer with resultant higher rates of both total remission and complete remission.[36] It is too early to state whether liposomal DOX represents a "better DOX." The results so far suggest only a marginally improved therapeutic index and a gain only for the occasional patient who is still responding to DOX after receiving a cumulative dose of 500 mg/m^2 and who could receive more drug without suffering cardiotoxicity.

CARDIOPROTECTIVE AGENTS

Researchers worldwide have attempted to modify the DOX structure and create a less toxic analog. Another line of research has been to administer DOX in conjunction with another substance that will mitigate cardiotoxicity. Such an approach is feasible because the cardiotoxicity appears to be mediated by free radical production by anthracyclines,[79] whereas the cytotoxicity to cancer cells is not.[80] The protector substance that has undergone the most evaluation is DXZ.

The development of DXZ extends back to the 1960s when British investigators at the Imperial Cancer Research Fund Laboratories in London began looking at chelating agents as potential antitumor agents.[81] A series of derivatives of ethylenediamine tetra-acetic acid (EDTA) were synthesized and tested for antitumor activity in murine cancers. One of these compounds was code named ICRF-187. It was the dextro form of the racemic compound ICRF-159. The INN of ICRF-187 is now dexrazoxane (DXZ), whereas that of ICRF-159 is razoxane. DXZ was more water soluble than razoxane and could be formulated for clinical trials. Phase I testing of DXZ, performed in the late 1970s, showed that the MTD was 3,000 mg/m^2 administered over 3 days, and the dose-limiting toxicity was primarily granulocytopenia.[82] This study also showed that DXZ enhanced the urinary excretion of iron, a point of possible importance in the mechanism of action for cardioprotection.

Unfortunately, DXZ produced few tumor responses in phase II trials and would have headed into oblivion but for the work of Herman et al, begun over 20 years ago. These investigators were working with an isolated dog heart model for anthracycline cardiotoxicity in the early 1970s and were attempting to find agents that might protect against heart damage. The chelating agent EDTA, and then its analog razoxane, were tested for ability to attenuate the acute cardiac effects of DNR and DOX, and both were successful.[83] Similar studies in intact animals later confirmed the fact that razoxane diminished acute anthracycline cardiotoxicity.[84] When the more water soluble EDTA analog, DXZ, became available to Herman et al in the mid-1970s, it also proved protective against anthracycline cardiotoxicity, both acute[85] and chronic.[86] This cardioprotective effect appears to be mediated by DXZ chelation of iron, which in turn limits the ability of anthracyclines to complex with intracellular iron and produce free radicals that damage cardiac myocytes.

This series of experiments and others[87-90] have confirmed that EDTA and its analogs can be useful in preventing anthracycline (DNR, DOX, or EPI) cardiotoxicity in a variety of experimental animals, while not compromising the antitumor efficacy of anthracyclines. Moreover, they showed that the anthracycline and an EDTA analog could be administered together safely and that the best timing was to administer them 30 minutes apart, with the anthracycline being administered second. The compound found to be most suitable for the cardioprotective effect was DXZ. The original code name for DXZ was ICRF-187, but Adria Laboratories (Columbus, OH) now holds the rights to this drug in the United States and has code named it ADR-529. The trade name in Europe is Cardioxane, and the proposed trade name for marketing in the United States is Zinecard.

With a solid record of cardioprotective efficacy in at least seven animal species, DXZ was next evaluated in a randomized clinical trial by Speyer et al.[91,92] These investigators based their dose and schedule of DXZ on the work of Herman and used a 20:1 ratio of DXZ to DOX. They chose the widely used regimen of cyclophosphamide, DOX, and 5-fluorouracil (CAF) and treated a disease (metastatic breast cancer) with the expectation that a large minority of patients would receive total DOX doses of 550 mg/m^2 or more. Patients were randomized to receive CAF or CAF + DXZ until either disease progression or evidence of cardiotoxicity occurred.

The results of this study of 150 patients showed that the DXZ group received a significantly higher total dose of DOX, had a much lower incidence of clinical congestive heart failure, and had a lower rate of removal from treatment because of cardiac changes from baseline.[92] In addition, 26 patients in the DXZ group received cumulative DOX doses of >700 mg/m^2, including 11 who were even able to tolerate $>1{,}000$ mg/m^2. At the same time, the tumor response rate was similar in the two groups. The DXZ group did have a slightly greater rate of grade 2 neutropenia, but there was no difference in rates of sepsis. Because DXZ produced granulocytopenia in the phase I trials[82] (although at higher doses), such effects in this trial would not be unexpected. A surprising result was that, despite the more total DOX cycles administered, there was no difference in the time to tumor progression or in overall survival.

Adria Laboratories set up similar randomized trials to confirm the results of Speyer et al but used a double-blind, placebo-controlled technique to obviate any possible biases in assessing either cardiotoxicity or tumor responses. Preliminary results of this work have been published.[93,94] Again, significant DXZ protection against DOX cardiotoxicity was shown by all measurements. Also, similar to the work of Speyer et al,[91,92] there were no differences in either disease-free survival or overall survival.[93]

These randomized trials were the basis for application to the FDA for marketing approval of Zinecard. DXZ is already marketed in Italy and Denmark and approval is pending in other countries. FDA approval was denied in June 1992 primarily because one trial[95] (and unpublished data) showed a statistically significant reduction in response rate for the patients receiving DXZ, although all studies are consistent that DXZ does serve effectively as a cardioprotectant. At this time it is uncertain when, and if, DXZ will receive approval for marketing in the United States.

What advantages does DXZ provide in making a "better DOX"? The randomized studies reported so far[91-95] document that a larger cumulative dose of DOX can be administered when DXZ is administered concurrently. However, the ability to administer a larger total dose has not translated into better progression-free or overall survival. This ability to administer several more months of an anthracycline with DXZ is akin to the ability to do the same thing using EPI, but a clear therapeutic efficacy advantage is lacking.

There are some probable advantages to use of DXZ as a cardioprotectant, although no clinical studies have yet been completed that establish these points. One situation is the patient whose cardiac status is of a borderline degree to tolerate DOX. Concurrent administration of DXZ can allow safe use of DOX for a patient to whom most oncologists would be reluctant to administer such therapy. Another is the patient who is to receive DOX as adjuvant therapy. Concomitant use of DXZ may be protective enough that DOX could be safely reused when, and if, metastatic disease occurs later.

The final and probably most important situation is in the pediatric age group. Children who received an anthracycline 5 to 20 years previously (and are cured of their cancer) are now being recognized to have severe cardiac function impairment as they have reached maturity.[96,97] Some patients have died,[96] and an occasional patient has undergone cardiac transplantation.[98] Some of these patients had received a cumulative dose of only 300 mg/m^2. These patients probably have death of myocytes during anthracycline therapy that remains asymptomatic until full growth or some stress, such as pregnancy, occurs in adulthood. If DXZ had been used in conjunction with the anthracycline years earlier, these late events were perhaps preventable. Before DXZ can be recommended for this age group, studies would have to be performed to establish no diminution of therapeutic efficacy in the curable childhood malignancies. One such study is presently ongoing in pediatric sarcomas at the NCI.

DXZ is the cardioprotectant that has had widest testing in animals and humans so far, but investigators at the Imperial Cancer Research Fund in London continue to evaluate the bisdioxopiperazines for cardioprotectant activity. They are currently studying ICRF-197, a transcyclobutane analog of DXZ, in animals for DOX-protectant efficacy.[99]

ANTHRACYCLINE AND MULTIDRUG RESISTANCE (MDR)

Most of the discussion in this article has focused on results of decreasing toxicity of anthracyclines. This is true because despite years of research and synthesis of hundreds of analogs, no DOX analog clearly kills human cancer cells more effectively, or for longer durations, than DOX. It is certainly worthwhile to investigate means of reducing cardiomyopathy or acute toxicity (especially the kind that causes patient distress such as alopecia or stomatitis), but the real obstacle to more effective use of DOX is cancer cell resistance to it, either native or acquired. In the late 1980s anthracycline analog research turned to finding structures capable of overcoming the Mdr phenomenon. However, these efforts are in their infancy, and it will be some years before it is known whether such research will bear fruit. In the meantime, investigators have tried to make a "better DOX" by administering other drugs concurrently with DOX that might overcome Mdr.

The drug that has had the most clinical study as a means of overcoming Mdr to DOX is verapamil. Preclinical studies 10 years ago showed that calcium channel blockers could aid DOX intracellular accumulation in DOX-resistant cell lines.[100,101] Such studies were promising enough to test the concept in clinical trials. A pilot study performed at the NCI found that the verapamil dose required to achieve plasma levels high enough to affect DOX Mdr caused too much acute cardiotoxicity.[102] Another pilot study at the University of Arizona using verapamil in conjunction with a DOX combination regimen was able to show partial reversal of tumor resistance to chemotherapy, whereas acute verapamil cardiotoxicity was manageable and reversible on stopping verapamil.[103] A current study at the NCI is evaluating the addition of verapamil to a DOX-containing regimen for refractory lymphomas, and again the verapamil has provided partial reversal of chemotherapy

resistance in a heavily pretreated group of patients.[104]

Attempts to modulate DOX Mdr are not limited to verapamil. Another calcium antagonist, bepridil, is being studied clinically by Dutch investigators.[105] This drug also has in vitro ability to reverse DOX resistance but may be less cardiotoxic acutely than verapamil at doses required to overcome Mdr.

Modulation of Mdr by various drugs is a concept worthy of continued study in clinical trials. However, use of the calcium channel blockers is subject to the danger of severe hypotension and cardiac arrhythmias. Therefore, it is often necessary to monitor cardiovascular parameters in an intensive care unit while the calcium channel blocker is being infused. This necessity makes implementation of this technique problematic for routine patient care when administering an anthracycline, so verapamil use as a DOX adjuvant is unlikely to become an accepted technique. Also, it is yet unclear this treatment will produce meaningful remissions of DOX-resistant cancers.

FUTURE DIRECTIONS

DNR and DOX were the first anthracyclines to be found clinically useful and were developed in the 1960s. Despite years of intense research by investigators in Japan, Europe, and the United States, a truly better DOX has not been found. There are several analogs that have some modestly reduced acute and/or chronic toxicity. In addition, there is a compound (DXZ) that is protective against cardiotoxicity when used in conjunction with the anthracyclines and an administration schedule (continuous infusion) that also can be cardioprotective. If DXZ is proven not to hinder the antitumor efficacy of DOX, further research to find less cardiotoxic analogs may be unrewarding and unnecessary.

Unfortunately, anthracyclines more effective at killing human tumor cells than DNR and DOX have not been found. Research ventures in the 1990s must begin with this fact (Table 3). It would be ironic if the best anthracyclines ever found are the first two discovered, but a parallel situation exists with the vinca alkaloids. Both vinblastine and vincristine were discovered in the mid-1950s. Some 35 years later, no other compound in this drug class has yet supplanted them.

ACKNOWLEDGMENT

The author thanks Dr. Luca Gianni of the Istituto Nazionale Tumori in Milan, Italy for his critical review of the manuscript.

REFERENCES

1. Di Marco A, Gaetani M, Orezzi P, et al: "Daunomycin," a new antibiotic of the rhodomycin group. Nature 201:706-707, 1964

2. Di Marco A, Gaetani M, Dorigotti L, et al: Studi sperimentale sull'attività antineoplastica del nuovo antibiotico daunomicina. Tumori 49:203-217, 1963

3. Dubost M, Ganter P, Maral R, et al: Rubidomycin: A new antibiotic with cytostatic properties. Cancer Chemother Rep 41:35-36, 1964

4. Tan C, Tasaka H, Kou-Ping Y, et al: Daunomycin, an antitumor antibiotic, in the treatment of neoplastic disease. Clinical evaluation with special reference to childhood leukemia. Cancer 20:333-353, 1967

5. Macrez C, Marneffe-Lebrequier H, Ripault J, et al: Accidents cardiaques observés au cours des traitements par la rubidomycine. Pathol Biol (Paris) 15:949-953, 1967

6. Arcamone F, Cassinelli G, Fantini G, et al: Adriamycin, 14-hydroxydaunomycin, a new antitumor antibiotic from *S. peucetius* var. *caesius*. Biotechnol Bioeng 11:1101-1110, 1969

7. Di Marco A, Gaetani M, Scarpinato B: Adriamycin (NSC-123,127): A new antibiotic with antitumor activity. Cancer Chemother Rep 53:33-37, 1969

8. Bonadonna G: Foreward, in Bonadonna G (ed): Advances in Anthracycline Chemotherapy: Epirubicin. Milan, Italy, Masson, 1984

9. Bonadonna G, Monfardini S, de Lena M, et al: Clinical evaluation of adriamycin, a new antitumour antibiotic. Br Med J 3:503-506, 1969

10. Tan C, Etcubanas E, Wollner N, et al: Adriamycin —An antitumor antibiotic in the treatment of neoplastic diseases. Cancer 32:9-17, 1973

11. Weiss RB, Bruno S: Daunorubicin treatment of adult solid tumors. Cancer Treat Rep 65:25-28, 1981 (suppl 4)

12. Arcamone F, Bermardi L, Giardino P, et al: Synthesis and antitumor activity of 4-demethoxydaunorubicin, 4-demethoxy-7,9-diepidaunorubicin, and their β anomers. Cancer Treat Rep 60:829-834, 1976

13. Ganzina F, Pacciarini MA, Di Pietro N: Idarubicin (4-demethoxydaunorubicin). A preliminary overview of preclinical and clinical studies. Invest New Drugs 4:85-105, 1986

14. Bastholt L, Dalmark M: Phase II study of idarubicin given orally in the treatment of anthracycline-naive advanced breast cancer patients. Cancer Treat Rep 71:451-454, 1987

15. Weiss RB: A third anthracycline for acute leukemia. Contemp Oncol 2:30-39, 1992

16. Wiernik PH, Banks PLC, Case DC, et al: Cytarabine

plus idarubicin or daunorubicin as induction and consolidation therapy for previously untreated adult patients with acute myeloid leukemia. Blood 79:313-319, 1992

17. Mayer RJ, Davis RB, Schiffer CA, et al: Comparative evaluation of intensive post-remission therapy with different dose schedules of ara-C in adults with acute myeloid leukemia (AML). Initial reports of a CALGB phase III study. Proc Am Soc Clin Oncol 11:261, 1992 (abstr)

18. Lopez M, Contegiacomo A, Vici P, et al: A prospective randomized trial of doxorubicin versus idarubicin in the treatment of advanced breast cancer. Cancer 64:2431-2436, 1989

19. Stuart NSA, Cullen MH, Priestman TJ, et al: A phase II study of oral idarubicin (4-demethoxydaunorubicin) in advanced breast cancer. Cancer Chemother Pharmacol 21:351-354, 1988

20. Hurteloup P, Armand JP, Schneider M, et al: Phase II trial of idarubicin (4-demethoxydaunorubicin) in advanced breast cancer. Eur J Cancer Clin Oncol 25:423-428, 1989

21. Stewart DJ, Grewaal D, Green RM, et al: Bioavailability and pharmacology of oral idarubicin. Cancer Chemother Pharmacol 27:308-314, 1991

22. Case DC, Hayes DM, Gerber M, et al: Phase II study of oral idarubicin in favorable histology non-Hodgkin's lymphoma. Cancer Res 50:6833-6835, 1990

23. Arcamone F, Penco S, Vigevani A: Adriamycin (NSC-123127): New chemical developments and analogs. Cancer Chemother Rep (part 3) 6:123-129, 1975

24. Goldin A, Venditti JM, Geran R: The effectiveness of the anthracycline analog 4′-epidoxorubicin in the treatment of experimental tumors: A review. Invest New Drugs 3:3-21, 1985

25. Bonfante V, Bonadonna G, Villani F, et al: Preliminary phase I study of 4′-epiadriamycin. Cancer Treat Rep 63:915-918, 1979

26. Weenen H, Van Maanen JMS, De Planque MM, et al: Metabolism of 4′-modified analogs of doxorubicin. Unique glucuronidation pathway for 4′-epidoxorubicin. Eur J Cancer Clin Oncol 20:919-926, 1984

27. Cersosimo R, Hong WK: Epirubicin: A review of the pharmacology, clinical activity, and adverse effects of an adriamycin analogue. J Clin Oncol 4:425-439, 1986

28. Mouridsen HT, Alfthan C, Basholt L, et al: Current status of epirubicin (Farmorubicin) in the treatment of solid tumors. Acta Oncol 29:257-285, 1990

29. French Epirubicin Study Group: A prospective randomized phase III trial comparing combination chemotherapy with cyclophosphamide, fluorouracil, and either doxorubicin or epirubicin. J Clin Oncol 6:679-688, 1988

30. The Italian Multicentre Breast Study with Epirubicin: Phase III randomized study of fluorouracil, epirubicin, and cyclophosphamide v. fluorouracil, doxorubicin, and cyclophosphamide in advanced breast cancer: An Italian multicentre trial. J Clin Oncol 6:976-982, 1988

31. Perez DJ, Harvey VJ, Robinson BA, et al: A randomized comparison of single-agent doxorubicin and epirubicin as first-line cytotoxic therapy in advanced breast cancer. J Clin Oncol 9:2148-2152, 1991

32. Nielsen D, Jensen JB, Dombernowsky P, et al: Epirubicin cardiotoxicity: A study of 135 patients with advanced breast cancer. J Clin Oncol 8:1806-1810, 1990

33. Dardir MD, Ferrans VJ, Mikhael YS, et al: Cardiac morphologic and functional changes induced by epirubicin chemotherapy. J Clin Oncol 7:947-958, 1989

34. Jain KK, Casper ES, Geller NL, et al: A prospective randomized comparison of epirubicin and doxorubicin in patients with advanced breast cancer. J Clin Oncol 3:818-826, 1985

35. Brincker H: Distant recurrence in breast cancer. Survival expectations and first choice of chemotherapy regimen. Acta Oncol 27:729-732, 1988

36. Jones RB, Holland JF, Bhardwaj S, et al: A phase I-II study of intensive-dose adriamycin for advanced breast cancer. J Clin Oncol 5:172-177, 1987

37. Hickish T, Cunningham D, Haydock A, et al: Experience with intermediate-dose (110-120 mg/m^2) epirubicin. Cancer Chemother Pharmacol 24:61-64, 1989

38. Sledge GW, Roth BJ, Munshi N, et al: High-dose epirubicin (EPI) as initial therapy for advanced breast cancer. Proc Am Soc Clin Oncol 11:85, 1992 (abstr)

39. Basholt L, Dalmark M, Gjedde S, et al: Epirubicin at four different dose levels in metastatic breast cancer. A randomized trial. Proc Am Soc Clin Oncol 11:56, 1992 (abstr)

40. Umezawa H, Takahashi Y, Kinoshita M, et al: Tetrahydropyranyl derivatives of daunomycin and adriamycin. J Antibiot (Tokyo) 32:1082-1084, 1979

41. Tsuruo T, Iida H, Tsukagoshi S, et al: 4′-O-tetrahydropyranyl-adriamycin as a potential new antitumor agent. Cancer Res 42:1462-1467, 1982

42. Dantchev D, Paintrand M, Hayat M, et al: Low heart and skin toxicity of tetrahydropyranyl derivative of adriamycin (THP-ADM) as observed by electron and light microscopy. J Antibiot (Tokyo) 32:1085-1086, 1979

43. Takagi T, Oguro M: (2″-R)-4′-O-tetra-hydropyranyladriamycin, a new anthracycline derivative; its effectiveness in lymphoid malignancies. Cancer Chemother Pharmacol 20:151-154, 1987

44. Spielmann M, Kerbrat P, Delozier T, et al: Pirarubicin in advanced breast cancer: A French cooperative phase II study. Eur J Cancer 26:821-823, 1990

45. Salem PA, Steiger S, Benjamin RS: Phase II study of THP-adriamycin (pirarubicin) and DTIC in advanced soft tissue sarcomas. Proc Am Soc Clin Oncol 10:351, 1991 (abstr)

46. Hortobagyi GN, Theriault RL, Frye D, et al: Pirarubicin in combination chemotherapy for metastatic breast cancer. Am J Clin Oncol (CCT) 13:S54-S56, 1990 (suppl 1)

47. Jacquillat C, Weil M, Gemon-Auclerc MF, et al: Clinical study of rubidazone (22 050 R.P.), a new daunorubicin-derived compound, in 170 patients with acute leukemia and other malignancies. Cancer 37:653-659, 1976

48. Barbieri B, Giuliani FC, Bordoni T, et al: Chemical and biological characterization of 4′-iodo-4′-deoxydoxorubicin. Cancer Res 47:4001-4006, 1987

49. Villani F, Galimberti M, Lanza E, et al: Evaluation of cardiotoxicity of a new anthracycline derivative: 4′-deoxy-4′-iodo-doxorubicin. Invest New Drugs 6:173-178, 1988

50. Gianni L, Vigano L, Surbone A, et al: Pharmacology

and clinical toxicity of 4'-iodo-4'-deoxydoxorubicin: An example of successful application of pharmacokinetics to dose escalation in phase I trials. J Natl Cancer Inst 82:469-477, 1990

51. Gianni L, Capri G, Greco M, et al: Activity and toxicity of 4'-iodo-4'deoxydoxorubicin in patients with advanced breast cancer. Ann Oncol 2:719-725, 1991

52. Sessa C, Calabresi F, Cavelli F, et al: Phase II studies of 4'-iodo-4'-deoxydoxorubicin in advanced non-small cell lung, colon and breast cancers. Ann Oncol 2:727-731, 1991

53. Israel M, Modest EJ, Frei E: *N*-trifluoroacetyladriamycin-14-valerate, an analog with greater experimental antitumor activity and less toxicity than adriamycin. Cancer Res 35:1365-1368, 1975

54. Blum RH, Garnick MB, Israel M, et al: Initial clinical evaluation of *N*-trifluoroacetyladriamycin-14-valerate (AD-32), an adriamycin analog. Cancer Treat Rep 63:919-923, 1979

55. Israel M, Sweatman TW, Soloway MS, et al: Initial clinical pharmacology of intravesical (ive) AD 32. Proc Am Assoc Cancer Res 33:445, 1992 (abstr)

56. Moscow JA, Cowan KH: Multidrug resistance. J Natl Cancer Inst 80:14-20, 1988

57. Nafziger J, Auclair C, Florent J-C, et al: Pharmacological and physiochemical properties of a new anthracycline with potent antileukemic activity. Leukemia Res 15:709-713, 1991

58. Cassinelli G, Arlandini E, Ballabio M, et al: New biosynthetic anthracyclines related to barminomycins incorporating barbituates in their moiety. J Antibiot (Toyko) 43:19-28, 1990

59. Israel M, Koseki Y, Jenkins JJ: Murine cardiotoxicity assay of the mechanistically novel adriamycin analog, N-benzyladriamycin-14-valerate (AD-198). Proc Am Assoc Cancer Res 32:423, 1991 (abstr)

60. Lau DHM, Lewis AD, Duran GE, et al: The cellular and biochemical pharmacology of the methoxymorpholino derivative of doxorubicin, FCE 23762. Proc Am Assoc Cancer Res 32:332, 1991 (abstr)

61. Inoue K, Ogawa M, Horikoshi N, et al: Phase I and pharmacokinetic study of SM-5887, a new anthracycline derivative. Invest New Drugs 7:213-218, 1989

62. Tsuruo T, Yusa K, Sudo Y, et al: A fluorine-containing anthracycline (ME 2303) as a new antitumor agent against murine and human tumors and their multidrug-resistant sublines. Cancer Res 49:5537-5542, 1989

63. Ariyoshi Y, Ota K, Wakui M, et al: Phase I clinical and pharmacokinetic study of ME 2303, a fluorine-containing anthracycline. Proc Am Soc Clin Oncol 10:121, 1991 (abstr)

64. Watanabe M, Komeshima N, Nakajima N, et al: MX2, a morpholino anthracycline, as a new antitumor agent against drug-sensitive and multidrug-resistant human and murine tumor cells. Cancer Res 48:6653-6657, 1988

65. Majima H: Phase I clinical study of MX2 (KRN 8602). Gan To Kagaku Ryoho 17:359-364, 1990

66. Verweij J, Van der Burg MEL, Van Putten WL, et al: Phase I studies of rodorubicin single bolus and daily times five, once every three weeks in patients with advanced solid tumors. Eur J Cancer Clin Oncol 25:627-632, 1989

67. de Jong J, Klein I, Snabilie AM, et al: Estimation of the cardiotoxicity of N-l-leucyldoxorubicin from *in vivo* and *ex vivo* data in mice. Ann Oncol 3:112, 1992 (suppl 1)

68. Tresca P, Canal P, Coupier J, et al: Leurubicin (LEU-DOX), a prodrug of doxorubicin (DOX): Results of an ARTAC phase I clinical and pharmacokinetic study. Ann Oncol 3:140, 1992 (suppl 1)

69. Legha SS, Benjamin RS, Mackay B, et al: Adriamycin therapy by continuous intravenous infusion in patients with metastatic breast cancer. Cancer 49:1762-1766, 1982

70. Zalupski M, Metch B, Balcerzak S, et al: Phase III comparison of doxorubicin and dacarbazine given by bolus versus infusion in patients with soft-tissue sarcomas: A Southwest Oncology Group study. J Natl Cancer Inst 83:926-932, 1991

71. Perez-Soler R: Liposomes as carriers of antitumor agents: Toward a clinical reality. Cancer Treat Rev 16:67-82, 1989

72. Treat J, Greenspan A, Forst D, et al: Antitumor activity of liposome-encapsulated doxorubicin in advanced breast cancer: Phase II study. J Natl Cancer Inst 82:1706-1710, 1990

73. Guaglianone P, Chan K, Hanisch R, et al: Phase I clinical trial of liposomal daunorubicin (daunoxome) in advanced malignancies. Proc Am Soc Clin Oncol 11:135, 1992 (abstr)

74. Forssen EA, Tokes Z: Use of anionic liposomes for the reduction of chronic doxorubicin-induced cardiotoxicity. Proc Natl Acad Sci U S A 78:1873-1877, 1981

75. Herman EH, Rahman A, Ferrans VJ, et al: Prevention of chronic doxorubicin cardiotoxicity in beagles by liposomal encapsulation. Cancer Res 43:5427-5432, 1983

76. Lohri A, Gelmon KA, Embree L, et al: Phase I/II study of liposome encapsulated doxorubicin (TLC-D99) in non small cell lung (NSCLC). Proc Am Soc Clin Oncol 10:106, 1991 (abstr)

77. Conley BA, Egorin MJ, Zubowski EG, et al: Phase I and comparative pharmacokinetic study of liposome-encapsulated doxorubicin. Proc Am Soc Clin Oncol 10:92, 1991 (abstr)

78. Batist G, Ahlgren P, Panasci L, et al: Phase II study of liposomal doxorubicin (TLCD99) in metastatic breast cancer. Proc Am Soc Clin Oncol 11:82, 1992 (abstr)

79. Rajagopalan S, Politi PM, Sinha BK, et al: Adriamycin-induced free radical formation in the perfused rat heart: Implications for cardiotoxicity. Cancer Res 48:4766-4769, 1988

80. Keizer HG, Pinedo HM, Schuurhuis GJ, et al: Doxorubicin (Adriamycin): A critical review of free radical-dependent mechanisms of cytotoxicity. Pharmacol Ther 47:219-231, 1990

81. Creighton AM, Hellman K, Whitecross S: Antitumour activity in a series of *bis*diketopiperazines. Nature 222:384-385, 1969

82. Von Hoff DD, Howser D, Lewis BJ, et al: Phase I study of ICRF-187 using a daily for 3 days schedule. Cancer Treat Rep 65:249-252, 1981

83. Herman EH, Mhatre RM, Lee IP, et al: Prevention of the cardiotoxic effects of adriamycin and daunomycin in the

isolated dog heart. Proc Soc Exp Biol Med 140:234-239, 1972

84. Herman EH, Mhatre RM, Chadwick DP: Modification of some of the toxic effects of daunomycin (NSC-82,151) by pretreatment with the antineoplastic agent ICRF 159 (NSC-129,943). Toxicol Appl Pharmacol 27:517-526, 1974

85. Herman E, Ardalan B, Bier C, et al: Reduction of daunorubicin lethality and myocardial cellular alterations by pretreatment with ICRF-187 in Syrian golden hamsters. Cancer Treat Rep 63:89-92, 1979

86. Herman EH, Ferrans VJ: Reduction of chronic doxorubicin cardiotoxicity in dogs by pretreatment with (±)-1,2, bis(3,5-dioxopiperazinyl-1-yl) propane (ICRF-187). Cancer Res 41:3436-3440, 1981

87. Agen C, Bernardini N, Danesi R, et al: Reducing doxorubicin cardiotoxicity in the rat using deferred treatment with ADR-529. Cancer Chemother Pharmacol 30:95-99, 1992

88. Yeung TK, Jaenke RS, Wilding D, et al: The protective activity of ICRF-187 against doxorubicin-induced cardiotoxicity in the rat. Cancer Chemother Pharmacol 30:58-64, 1992

89. Dardir M, Herman EH, Ferrans VJ: Effects of ICRF-187 on the cardiac and renal toxicity of epirubicin in spontaneously hypertensive rats. Cancer Chemother Pharmacol 23:269-275, 1989

90. Wadler S, Green MD, Muggia FM: Synergistic activity of doxorubicin and the bis-dioxopiperazine (+)-1,2 bis (3,5-dioxopiperazinyl-1-yl) propane (ICRF 187) against the murine sarcoma S180 cell line. Cancer Res 46:1176-1181, 1986

91. Speyer JL, Green MD, Kramer E, et al: Protective effect of the bispiperazinedione ICRF-187 against doxorubicin-induced cardiac toxicity in women with advanced breast cancer. N Engl J Med 319:745-752, 1988

92. Speyer JL, Green MD, Zeleniuch-Jacquotte A, et al: ICRF-187 permits longer treatment with doxorubicin in women with breast cancer. J Clin Oncol 10:117-127, 1992

93. Rosenfeld CS, Weisberg SR, York RM, et al: Prevention of adriamycin cardiomyopathy with dexrazoxane (ADR-529, ICRF-187). Proc Am Soc Clin Oncol 11:62, 1992 (abstr)

94. Maillard JA, Speyer JL, Hanson K, et al: Prevention of chronic adriamycin cardiotoxicity with the bisdioxopiperazine dexrazoxane (ICRF-187, ADR-529, Zinecard) in patients with advanced or metastatic breast carcinoma. Proc Am Soc Clin Oncol 11:91, 1992 (abstr)

95. Feldman JE, Jones SE, Weisberg SR, et al: Advanced small cell lung cancer treated with CAV (cyclophosphamide + adriamycin + vincristine) chemotherapy and the cardioprotective agent dexrazoxane (ADR-529). ICRF-187, Zinecard). Proc Am Soc Clin Oncol 11:296, 1992 (abstr)

96. Steinherz L, Steinherz P: Delayed cardiac toxicity from anthracycline therapy. Pediatrician 18:49-52, 1991

97. Lipshultz SE, Colan SD, Gelber RD, et al: Late effects of doxorubicin therapy for acute lymphoblastic leukemia in childhood. N Engl J Med 324:808-815, 1991

98. Jenney MEM, Morris Jones PH: Long term survival after heart transplantation for doxorubicin induced cardiomyopathy. Arch Dis Child 67:153, 1992 (letter)

99. Yeung TK, Jeffrey WA, Long J, et al: ICRF 197: A new agent for protecting against drug-induced cardiotoxicity. Ann Oncol 3:114, 1992 (abstr) (suppl 1)

100. Tsuruo T, Iida H, Tsukagoshi S, et al: Increased accumulation of vincristine and adriamycin in drug-resistant P388 tumor cells following incubation with calcium antagonists and calmodulin inhibitors. Cancer Res 42:4730-4733, 1982

101. Rogan AM, Hamilton TC, Young RC, et al: Reversal of adriamycin resistance by verapamil in human ovarian cancer. Science 229:994-996, 1984

102. Ozols RF, Cunnion RE, Klecker RW, et al: Verapamil and adriamycin in the treatment of drug-resistant ovarian cancer patients. J Clin Oncol 5:641-647, 1987

103. Dalton WS, Grogan TS, Meltzer PS, et al: Drug-resistance in multiple myeloma and non-Hodgkin's lymphoma: Detection of P-glycoprotein and potential circumvention by addition of verapamil to chemotherapy. J Clin Oncol 7:415-424, 1989

104. Chabner BA, Bates S, Fojo T, et al: Drug resistance in malignant lymphoma: Experience with EPOCH chemotherapy. Ann Oncol 3:63, 1992 (abstr) (suppl 1)

105. van Kalken CK, van der Hoeven JJM, de Jong J, et al: Bepridil in combination with anthracyclines to reverse anthracycline resistance in cancer patients. Eur J Cancer 27:739-744, 1991

Communication

THE JOURNAL OF BIOLOGICAL CHEMISTRY
Vol. 272, No. 15, Issue of April 11, pp. 9617–9620, 1997

Receptor-mediated Endocytosis of CC-chemokines*

(Received for publication, January 15, 1997, and in revised form, February 11, 1997)

Roberto Solari‡§, Robin E. Offord¶, Sandrine Remy¶, Jean-Pierre Aubry‖, Timothy N. C. Wells‖, Erik Whitehorn, Thim Oung**, and Amanda E. I. Proudfoot‖‡‡**

*From the ‡Cell Biology Unit, Glaxo Wellcome Medicines Research Centre, Gunnels Wood Road, Stevenage, Hertfordshire SG1 2NY, United Kingdom, the ¶Departement de Biochimie Medicale, Centre Medicale Universitaire, 1224 Champel, Geneva 1224, Switzerland, ‖Geneva Biomedical Research Institute, Glaxo Wellcome Research and Development, 14 Chemin des Aulx, 1228 Plan les Ouates, Geneva 1228, Switzerland, and **Affymax Research Institute, Palo Alto, California 94304*

Chemokines are chemotactic proteins which play a central role in immune and inflammatory responses. Chemokine receptors are members of the seven transmembrane G-protein coupled family and have recently been shown to be involved in the entry of human immunodeficiency virus (HIV) into target cells. To study chemokine endocytosis in detail we have used novel site-specific chemistry to make a fluorescently labeled CC-chemokine agonist (rhodamine-MIP-1α) and antagonist (NBD-RANTES). We have also generated a CHO cell line stably expressing a hemagglutinin-tagged version of the CC-chemokine receptor 1 (CCR1), and using these reagents we have examined the receptor-mediated endocytosis of CC-chemokines by confocal microscopy. Our studies reveal that the agonist was internalized and accumulated in transferrin receptor-positive endosomes whereas the antagonist failed to internalize. However, receptor-bound antagonist could be induced to internalize by co-administration of agonist. Analysis of receptor redistribution following chemokine addition confirmed that sequestration was induced by agonists but not by antagonists.

Chemokines are a large family of chemotactic proteins which regulate leukocyte activation and recruitment to sites of inflammation. They can be divided into two main classes, the C*X*C- and the CC-chemokines based on the spacing of the first two cysteine residues. Both C*X*C- and CC-chemokines bind to seven transmembrane G-protein coupled receptors (GPCRs)[1] which in most cases are promiscuous in that they will bind more than one ligand with high affinity (1). Although receptor-mediated endocytosis of certain GPCRs such as the β_2-adrenergic receptor has been well documented, the endocytic pathways utilized by most GPCRs are still uncharacterized. Following stimulation by agonist, the β_2-adrenergic receptor is rapidly phosphorylated by a specific GPCR kinase. This uncouples the interaction between the receptor and the G-protein and allows binding of β-arrestin which acts as an adapter to recruit the receptor into clathrin-coated vesicles (2). Several studies have shown that GPCRs are internalized via clathrin-coated vesicles, although this may not be a universal mechanism as alternative endocytic pathways have been described for a number of different ligands (3–10).

Chemokines such as RANTES (regulated on activation normal T cell expressed and secreted), MIP-1α, and MIP-1β have been shown to be the major HIV-suppressive factors produced by $CD8^+$ T cells (11), and a number of recent studies have gone on to show that chemokine receptors are co-receptors along with CD4 for the entry of HIV into cells (12–21). This has raised the possibility of using chemokines therapeutically to block HIV entry. Receptor-mediated endocytosis of chemokines has not been studied in detail, but an understanding of this process is clearly important if we are to develop selective therapeutic agents which block HIV entry into cells. To this end we have studied the receptor-mediated endocytosis of CC-chemokines by CCR1 as a prototype for the CC-chemokine receptor family.

EXPERIMENTAL PROCEDURES

Fluorescent Chemokines—Recombinant chemokines were expressed and purified from a bacterial expression system as described (22). Fluorescent chromophores were conjugated by chemically coupling to the amino terminus according to the procedures described (23). The formation of rhodamine-MIP-1 necessitated certain modifications of this technology.[2]

Receptor Expression—The full length cDNA encoding CCR1 was cloned by reverse transcriptase-PCR from the human eosinophilic cell line EOL-3 using specific primers based on the published sequence (24). The cDNA was subcloned into a pcDNAneo1-based mammalian cell expression vector (p12ca5) after the addition of the HA epitope tag (YPYDVPYASLRS) to the 5′ end of the receptor cDNA by PCR. The sequence of the receptor cDNA was verified prior to transfection into CHO-K1 cells. The CHO-K1 cells were maintained in Dulbecco's modified Eagle's medium-F12 medium containing 10% heat-inactivated fetal calf serum, 2 mM glutamine, and 100 units/ml penicillin/streptomycin (complete medium) and were harvested by trypsinization and resuspended at 2×10^7 cells/ml in 20 mM HEPES buffer pH 7.3 containing 150 mM NaCl. Five hundred-microliter aliquots of cells were electroporated with 30 μg of p12ca5 plasmids containing the receptor cDNA at 260 V, 960 μF, using a Bio-Rad Gene Pulser. After electroporation, cells were transferred to fresh medium and allowed to recover for 48 h before addition of 600 μg/ml geneticin (G418). Fourteen days after electroporation, individual G418-resistant colonies were isolated by ring cloning and maintained in complete medium containing G418. Individual clones were then tested for binding to the anti-HA monoclonal antibody 12CA5 (Boehringer), and cells expressing high levels of receptor were selected by a fluorescence-activated cell sorter using an anti-mouse fluorescein isothiocyanate conjugate. The resultant cell population was designated CHO-CCR1 and was subsequently maintained in complete medium.

Chemotaxis Assays—Biological activity of the chemokines or modified chemokines was assessed by their ability to induce monocyte chemotaxis in micro-Boyden chambers as described previously (22, 25). Assays were performed either on the THP-1 cell line or on human peripheral blood monocytes.

* The costs of publication of this article were defrayed in part by the payment of page charges. This article must therefore be hereby marked "*advertisement*" in accordance with 18 U.S.C. Section 1734 solely to indicate this fact.

§ To whom correspondence may be addressed. Fax: 44-01438-763232; E-mail: RCES4402@ggr.co.uk.

‡‡ To whom correspondence may be addressed. Fax: 41-22-794-6965.

[1] The abbreviations used are: GPCR, G-protein coupled receptor; PCR, polymerase chain reaction; HIV, human immunodeficiency virus; HA, hemagglutinin; NBD, 7-nitrobenz-2-oxa-1,3-diazole-4-yl; MIP, macrophage inflammatory polypeptide; CHO, Chinese hamster ovary.

[2] R. E. Offord and S. Remy, manuscript in preparation.

Immunofluorescence Confocal Microscopy—All experiments were performed on CHO-CCR1 cells grown overnight on chamber slides (Nunc). For chemokine endocytosis experiments the cells were washed twice with ice-cold buffer (phosphate-buffered saline with 1% bovine serum albumin). Fluorescent chemokines (500 nM) were incubated with the cells for 4 h on ice followed by three washes in ice cold buffer to remove unbound ligand. Fresh medium was added, and the cells were either kept at 4 °C or incubated at 37 °C for 15 or 30 min. At the end of this incubation cells were fixed, permeabilized, and processed for confocal microscopy by standard procedures. For immunofluorescence studies following incubation with chemokines the fixed cells were permeabilized and incubated with an anti-transferrin receptor monoclonal antibody (H68.4, a kind gift from Professor Colin Hopkins, Laboratory for Molecular Cell Biology, University College London) or with the anti-HA antibody 12CA5 (Boehringer). All slides were examined with a Leica TCS4 confocal scanning laser microscope.

RESULTS AND DISCUSSION

To study CC-chemokine endocytosis we generated fluorescently labeled RANTES and MIP-1α using site-specific chemistry to attach the fluorophore specifically to the terminal amino group of the polypeptide chain (23, 26). Using this technique we conjugated rhodamine to MIP-1α and 7-nitrobenz-2-oxa-1,3-diazole-4-yl (NBD) to RANTES. These fluorescently labeled CC-chemokines retained their ability to bind specifically to CCR1 although the binding affinity was slightly reduced compared with the unmodified agonist (23, 26). Prior to using these ligands to study endocytosis we assessed their biological activity in chemotaxis assays. Rhodamine-MIP-1α acted as a full agonist and induced maximal chemotaxis at a concentration of 100 nM (Fig. 1*A*). However, NBD-RANTES had no biological activity in a chemotaxis assay. We have previously shown that modification of the amino terminus of RANTES has a profound influence on its biological properties (25). Failure to cleave the initiating methionine from bacterially expressed RANTES (Met-RANTES) produced a protein which was devoid of agonist activity but was a potent antagonist. Similarly, conjugation of the fluorophore NBD to the amino terminus of RANTES also converted it from an agonist to an antagonist. As shown in Fig. 1*B* both Met-RANTES and NBD-RANTES can fully antagonize the chemotactic activity of RANTES on THP-1 cells.

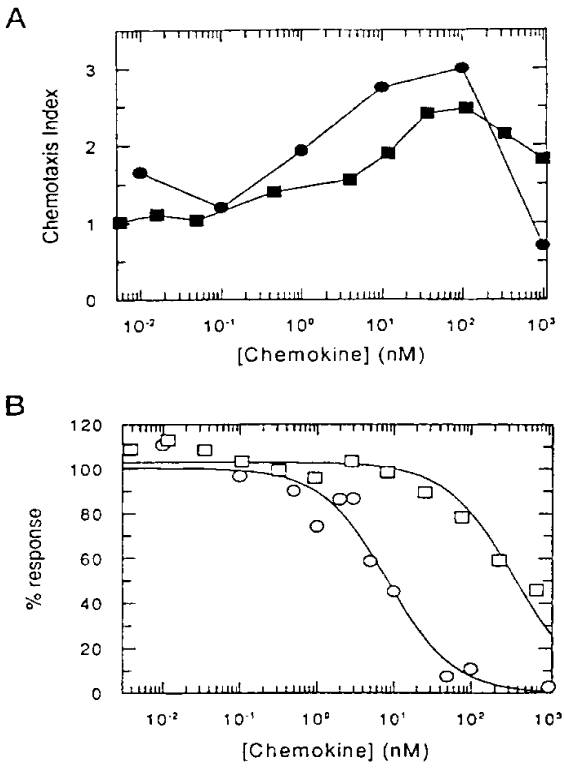

FIG. 1. *A*, chemotaxis of human peripheral blood monocytes in response to increasing concentrations of MIP-1α (●) and rhodamine-MIP-1α (■). Assays were performed in 48-well micro-Boyden chambers. Each point represents the mean of triplicate determinations. *B*, antagonism of RANTES-induced chemotaxis of THP-1 by Met-RANTES (○) and NBD-RANTES (□). The assays were performed in 96-well micro-Boyden chambers by measuring the chemotactic response of cells to a 3.5 nM concentration of RANTES mixed with increasing concentrations of antagonists. Each point represents the mean of triplicate determinations.

For endocytosis studies the human CCR1 cDNA was cloned by reverse transcriptase-PCR, and an HA epitope tag was placed at the extreme amino terminus. The tagged receptor was transfected into CHO cells, and lines stably expressing the receptor were cloned. Radioligand binding assays confirmed that the tagged CCR1 expressed in CHO cells (CHO-CCR1) retained high affinity ligand binding and ligand specificity (data not shown). In the initial experiments the fluorescent rhodamine-MIP-1α and NBD-RANTES were bound to CHO-CCR1 cells for 4 h at 4 °C at a final concentration of 500 nM. Unbound ligand was washed off with ice-cold buffer prior to warming the cells to 37 °C for timed periods up to 30 min (Fig. 2). The agonist, rhodamine-MIP-1α, was effectively internalized and accumulated in perinuclear vesicles (*panels A–C*) whereas the antagonist, NBD-RANTES, remained almost entirely on the cell surface (*panels D–F*). This is consistent with other GPCRs for which it has been shown that receptor internalization is dependent upon agonist stimulation and is inhibited by antagonists (4, 6, 9, 10). However, since we have made NBD-RANTES we were able to perform the experiment to study the effect of agonist stimulation upon the receptor-mediated endocytosis of a fluorescent antagonist. Binding of NBD-RANTES in the presence of an equimolar concentration of RANTES showed that the antagonist could be induced to cluster and internalize in the presence of agonist (*panels G–I*). Although the internalized antagonist appeared in more peripheral endosomes rather than in the perinuclear structures in which the agonist accumulated, this observation nonetheless demonstrated that agonist-bound receptor could induce the sequestration of antagonist-occupied receptor. These findings suggest that activation of the GPCR kinase by agonist will induce phosphorylation, and consequently sequestration, of receptors occupied by agonists or antagonists. The significance of this relates to how a virus uses a GPCR to gain entry to a cell. These findings suggest that HIV would not have to act as an agonist to be internalized via CC-chemokine receptors provided there is sufficient chemokine agonist present to induce receptor internalization. This is consistent with recent findings, using chimeric receptors, that the regions of CCR5 required for viral entry and for chemokine signal transduction are distinct (27). It may also explain the observation that in certain macrophage cultures addition of CC-chemokines actually enhances rather than inhibits HIV replication (28).

To define the endocytic compartment into which rhodamine-MIP-1α was being delivered we performed dual-labeling studies with the transferrin receptor. Rhodamine-MIP-1α was bound to CHO-CCR1 cells at 4 °C, and receptor-bound ligand was subsequently allowed to internalize for 30 min at 37 °C. Cells were fixed, permeabilized, and stained using an antibody to the transferrin receptor (Fig. 3). Analysis of the cells by confocal microscopy revealed that at 4 °C, the rhodamine-MIP-1α decorated the plasma membrane (*panel B*) whereas the transferrin receptor staining was both on the plasma mem-

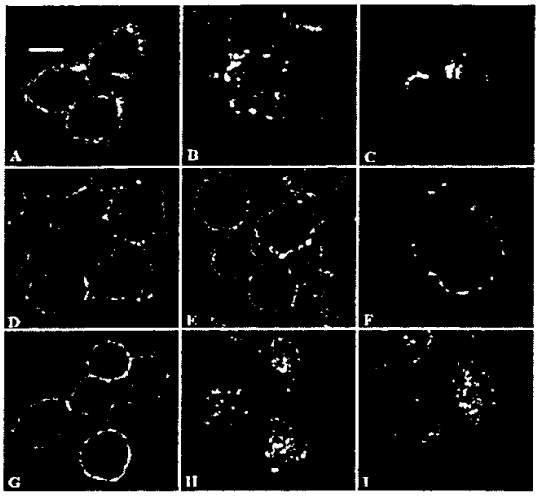

FIG. 2. **Receptor-mediated endocytosis of fluorescent chemokines.** Chemokines were bound to the surface of CHO-CCR1 cells at 4 °C. Unbound chemokine was washed off, and cells were either fixed immediately or rapidly warmed to 37 °C for 15 or 30 min prior to fixation. Following fixation the cells were examined by confocal microscopy. *Panels A, D,* and *G* show chemokine distribution with no warmup, *panels B, E,* and *H* show distribution after a 15-min warmup, and *panels C, F,* and *I* show distribution after a 30-min warmup. Rhodamine-MIP-1α (*panels A, B,* and *C*), NBD-RANTES (*panels D, E,* and *F*), and NBD-RANTES plus RANTES (*panels G, H,* and *I*). (*Bar* = 10 μm).

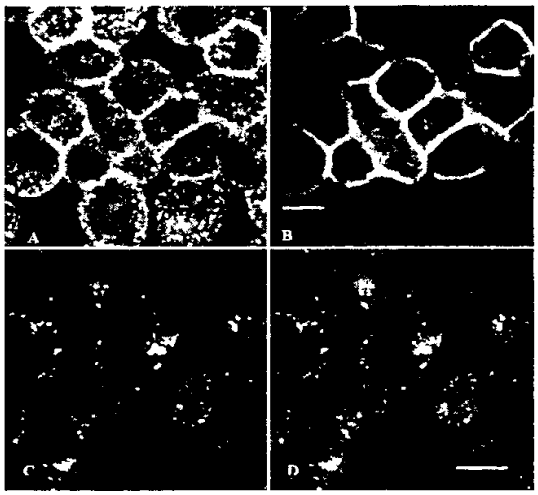

FIG. 3. **Co-localization of rhodamine-MIP-1α with the transferrin receptor.** Rhodamine-MIP-1α was bound to CHO-CCR1 cells at 4 °C. Unbound chemokine was washed off, and the cells were either fixed immediately or warmed to 37 °C for 30 min prior to fixation. Fixed cells were permeabilized and stained with a monoclonal antibody to the transferrin receptor (H68.4) followed by a goat anti-mouse-fluorescein isothiocyanate antibody. Dual staining of the transferrin receptor (*panels A* and *C*) and rhodamine-MIP-1α (*panels B* and *D*) were analyzed by confocal microscopy. *Panels A* and *B* show distribution at 4 °C, and *panels C* and *D* after a 30-min warmup to 37 °C. (*Bar* = 10 μm).

brane and in numerous endocytic vesicles (*panel A*). Following a 30-min warm up the rhodamine-MIP-1α was internalized into perinuclear endosomal vesicles (*panel D*) and showed an exact co-localization with the transferrin receptor (*panel C*). Since it is well documented that the transferrin receptor is a marker for the clathrin-coated pit endocytic pathway it is reasonable to conclude that the CCR1 is also internalized via this mechanism.

As a final study we decided to examine the receptor redistribution following addition of agonist or antagonist. For these experiments various chemokines were added to CHO-CCR1 cells at 37 °C for 30 min after which time the cells were washed, fixed, and permeabilized, and the CCR1 receptor was visualized by staining with the anti-HA monoclonal antibody (Fig. 4). The various chemokines were added at a concentration of either 50 nM or at 1 μM. Without chemokine addition the receptor was predominantly seen on the plasma membrane (*panel A*) and addition of the antagonists NBD-RANTES (*panels B* and *C*) or Met-RANTES (*panels D* and *E*) did not induce any significant receptor redistribution. However the agonists MIP-1α (*panels F* and *G*) and RANTES (*panels H* and *I*) both induced receptor sequestration, although MIP-1α appeared more effective in this respect than RANTES. Even at 50 nM, MIP-1α induced most of the CCR1 to redistribute from the plasma membrane to perinuclear vesicles, and at 1 μM receptor down-regulation was almost complete.

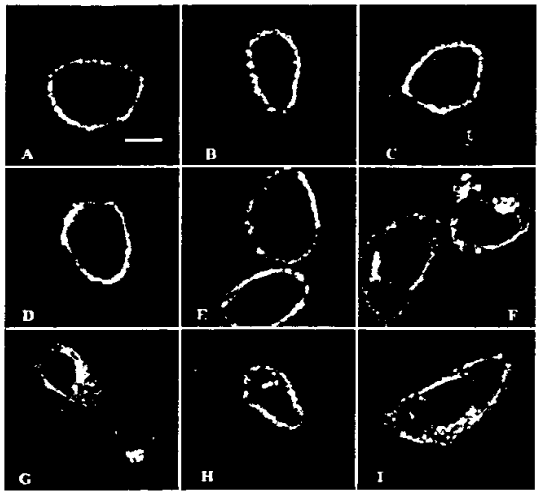

FIG. 4. **CC-chemokine receptor 1 redistribution following addition of chemokine agonists and antagonists.** CHO-CCR1 cells were incubated for 30 min at 37 °C with a range of CC-chemokines. Following this period the cells were fixed and permeabilized, and the HA-tagged receptor was detected with the anti-HA antibody 12CA5 followed a biotinylated rabbit anti-mouse antibody and a streptavidin-Texas Red conjugate. *Panel A*, no chemokine addition; *panel B*, 50 nM NBD-RANTES; *panel C*, 1 μM NBD-RANTES; *panel D*, 50 nM Met-RANTES; *panel E*, 1 μM Met-RANTES; *panel F*, 50 nM MIP-1α; *panel G*, 1 μM MIP-1α; *panel H*, 50 nM RANTES; *panel I*, 1 μM RANTES.

These observations are the first detailed description of chemokine and chemokine receptor endocytosis, and they show that CCR1 is likely to be internalized via clathrin-coated pits. We demonstrate that both ligand and receptor accumulate in perinuclear endosomes and that receptor internalization is dependent upon agonist stimulation. Provided that all CC chemokine receptors behave like CCR1, does this give us any insight into how we might use chemokines as therapeutic agents to prevent HIV entry into cells? The protective effects of chemokines may be due to two factors. The chemokine may act as a competitive inhibitor preventing binding of the virus to the receptor or it may down-regulate surface receptors so that there are no receptors available for the virus. If the second explanation were true then antagonists, which do not induce receptor sequestration, would not be expected to block HIV entry. Recently published data (29) and our own studies[3] confirm that chemokine antagonists are effective at inhibiting HIV

[3] Simmons, G., Clapham, P. R., Picard, L., Offord, R. E., Rosenkilde, M. M., Schwartz, T. W., Buser, R., Wells, T. N. C., and Proudfoot, A. E. I. (1997) *Science*, in press.

entry into target cells. Consequently our study strongly suggests that the observed HIV suppressive effects of chemokines are due to competitive inhibition for receptor binding and not due to receptor down-regulation. These findings have significant implications for the design and discovery of novel therapeutic agents targeted at blocking HIV entry into cells.

Acknowledgments—We thank Emily Tate, Frederic Borlat, Raphaelle Buser, and Marc-Olivier Montjovent for technical assistance.

REFERENCES

1. Power, C. A., and Wells, T. N. C. (1996) *Trends Pharmacol. Sci.* **17,** 209–213
2. Goodman, O. B., Krupnick, J. G., Santini, F., Gurevich, V. V., Penn, R. B., Gagnon, A. W., Keen, J. H., and Benovic, J. L. (1996) *Nature* **383,** 447–450
3. Raposo, G., Dunia, I., Delavier-Klutchko, C., Kaveri, S., Strosberg, A. D., and Benedetti, E. L. (1989) *Eur. J. Cell Biol.* **50,** 340–352
4. von Zastrow, M., and Kobilka, B. K. (1992) *J. Biol. Chem.* **267,** 3530–3538
5. Grady, E. F., Slice, L. W., Brant, W. O., Walsh, J. H., Payan, D. G., and Bunnett, N. W. (1995) *J. Biol. Chem.* **270,** 4603–4611
6. Fonseca, M. I., Button, D. C., and Brown, R. D. (1995) *J. Biol. Chem.* **270,** 8902–8909
7. Zhang, J., Ferguson, S. S.G., Barak, L. S., Menard, L., and Caron, M. G. (1996) *J. Biol. Chem.* **271,** 18302–18305
8. Garland, A. M., Grady, E. F., Lovett, M., Vigna, S. R., Frucht, M. M., Krause, J. E., and Bunnett, N. W. (1996) *Mol. Pharmacol.* **49,** 438–446
9. Tolbert, L. M., and Lameh, J. (1996) *J. Biol. Chem.* **271,** 17335–17342
10. Berry, S. A., Shah, M. C., Khan, N., and Roth, B. L. (1996) *Mol. Pharmacol.* **50,** 306–313
11. Cocchi, F., DeVico, A. L., Garzino-Demo, A., Arya, S. K., Gallo, R. C., and Lusso, P. (1995) *Science* **270,** 1811–1815
12. Feng, Y., Broder, C. C., Kennedy, P. E., and Berger, E. A. (1996) *Science* **272,** 872–877
13. Deng, H., Liu, R., Ellmeier, W., Choe, S., Unutmaz, D., Burkhart, M., Di Marzio, P., Marmon, S., Sutton, R. E., Hill, C. M., Davis, C. B., Peiper, S. C., Schall, T. J., Littman, D. R., and Landau, N. R. (1996) *Nature* **381,** 661–666
14. Dragic, T., Litwin, V., Allaway, G. P., Martin, S. R., Huang, Y., Nagashima, K. A., Cayanan, C., Maddon, P. J., Koup, R. A., Moore, J. P., and Paxton, W. A. (1996) *Nature* **381,** 667–673
15. Choe, H., Farzan, M., Sun, Y., Sullivan, N., Rollins, B., Ponath, P. D., Wu, L., Mackay, C. R., LaRosa, G., Newman, W., Gerard, N., Gerard, C., and Sodroski, J. (1996) *Cell* **85,** 1135–1148
16. Doranz, B. J., Rucker, J., Yi, Y., Smyth, R. J., Samson, M., Peiper, S. C., Parmentier, M., Collman, R. G., and Doms, R. W. (1996) *Cell* **85,** 1149–1158
17. Bleul, C. C, Farzan, M., Choe, H., Parolin, C., Clark-Lewis, I., Sodroski, J., and Springer, T. (1996) *Nature* **382,** 829–833
18. Oberlin, E., Amara, A., Bachelerie, F., Bessia, C., Virelizier, J-L., Arenzana-Seisdedos, F., Schwartz, O., Heard, J-M., Clark-Lewis, I., Legler, D. F., Loetscher, M., Baggiolini, M., and Moser, B. (1996) *Nature* **382,** 833–835
19. Berson, J. F., Long, D., Doranz, B. J., Rucker, J., Jirik, F. R., and Doms, R. W. (1996) *J. Virol.* **70,** 6288–6295
20. D'Souza, P. M., and Harden, V. A. (1996) *Nature Med.* **2,** 1293–1300
21. Fauci, A. S. (1996) *Nature* **384,** 529–534
22. Proudfoot, A. E. I., Power, C. A., Hoogewerf, A., Montjovent, M-O., Borlat, F., and Wells, T. N. C. (1995) *FEBS Lett.* **376,** 19–23
23. Offord, R. E., Gartner, H., Wells, T. N. C., and Proudfoot, A. E. I. (1997) *Methods Enzymol.*, in press
24. Neote, K., Darbonne, W., Ogez, J., Horuk, R., and Schall, T. J. (1993) *J. Biol. Chem* **263,** 12247–12249
25. Proudfoot, A. E. I., Power, C. A., Hoogewerf, A. J., Montjovent, M-O., Borlat, F., Offord, R. E., and Wells, T. N. C. (1996) *J. Biol. Chem.* **271,** 2599–2603
26. Alouani, S., Gaertner, H. F., Mermod, J-J., Power, C. A., Bacon, K., Wells, T. N. C., and Proudfoot, A. E. I. (1995) *Eur. J. Biochem.* **227,** 328–334
27. Atchison, R. E., Gosling, J., Montecarlo, F. S., Franci, C., Digilio, L., Charo, I. F., and Goldsmith, M. A. (1996) *Science* **274,** 1924–1926
28. Schmidtmayerova, H., Sherry, B., and Bukrinsky, M. (1996) *Nature* **382,** 767
29. Arenzana-Seisdedos, F., Virelizier, J-L., Rousset, D., Clark-Lewis, I., Loetscher, P., Moser, B., and Baggiolini, M. (1996) *Nature* **383,** 400

THE JOURNAL OF BIOLOGICAL CHEMISTRY Vol. 274, No. 16, Issue of April 16, pp. 11328–11333, 1999
Printed in U.S.A.

Role of Clathrin-mediated Endocytosis in CXCR2 Sequestration, Resensitization, and Signal Transduction*

(Received for publication, October 5, 1998, and in revised form, January 5, 1999)

Wei Yang‡, Dingzhi Wang‡, and Ann Richmond‡§¶

From the ‡Department of Cell Biology, Vanderbilt University School of Medicine, Nashville, Tennessee 37232-2175 and the §Veterans Affairs Medical Center, Nashville, Tennessee 37212-2637

CXCR2 is a seven-transmembrane receptor that transduces intracellular signals in response to the chemokines interleukin-8, melanoma growth-stimulatory activity/growth-regulatory protein, and other ELR motif-containing CXC chemokines by coupling to heterotrimeric GTP-binding proteins. In this study, we explored the mechanism responsible for ligand-induced CXCR2 endocytosis. Here, we demonstrate that dynamin, a component of clathrin-mediated endocytosis, is essential for CXCR2 endocytosis and resensitization. In HEK293 cells, dynamin I K44A, a dominant-negative mutant of dynamin that inhibits the clathrin-mediated endocytosis, blocks the ligand-stimulated CXCR2 sequestration. Furthermore, co-expression of dynamin I K44A significantly delays dephosphorylation of CXCR2 after ligand stimulation, suggesting that clathrin-mediated endocytosis plays an important role in receptor dephosphorylation and resensitization. In addition, ligand-mediated receptor down-regulation is attenuated when receptor internalization is inhibited by dynamin I K44A. Interestingly, inhibition of receptor endocytosis by dynamin I K44A does not affect the CXCR2-mediated stimulation of mitogen-activated protein kinase. Most significantly, our data indicate that the ligand-stimulated receptor endocytosis is required for CXCR2-mediated chemotaxis in HEK293 cells. Taken together, our findings suggest that clathrin-mediated CXCR2 internalization is crucial for receptor endocytosis, resensitization, and chemotaxis.

Melanoma growth-stimulatory activity (MGSA)[1]/growth-regulatory protein (GRO), interleukin-8 (IL-8), neutrophil-activating peptide-2, epithelial derived neutrophil-activating peptide 78, and granulocyte chemotactic protein-2 are members of a family of structurally related cytokines that induce chemotaxis and respiratory burst in neutrophils (1–3). These chemokines belong to the CXC chemokine subfamily in which the first two conserved cysteine residues are separated by an intervening amino acid (4). Several chemokine receptors have been cloned that bind MGSA: CXCR2 (formerly called IL-8 RB) (5), Duffy antigen receptor for chemokine, and two herpesvirus-encoded receptors: the herpesvirus saimiri ECRF-3 and the human herpesvirus-8 G protein-coupled receptor (6). IL-8 binds to these four receptors as well as CXCR1 (formerly called IL-8 RA) (7), which is a receptor for IL-8 and granulocyte chemotactic protein-2. CXCR2 is a shared receptor that binds to IL-8, MGSA, neutrophil-activating peptide-2, epithelial derived neutrophil-activating peptide 78, and granulocyte chemotactic protein-2 (8).

Like all of the chemokine receptors cloned to date, CXCR2 is a member of a superfamily of G protein-coupled receptors (GPCRs) that transduce signals to the interior of the cell through heterotrimeric guanine nucleotide-binding proteins (G proteins). These receptors share a common putative structural topology composed of seven-transmembrane domains separated by three extracellular and three intracellular loops. Upon agonist binding, CXCR2 activates G protein-mediated phosphoinositide hydrolysis to generate diacylglycerol and inositol 1,4,5-trisphosphate, thereby activating protein kinase C and mobilizing Ca^{2+} to initiate a variety of cellular responses (9). Receptor activation is followed by receptor phosphorylation on multiple serine residues and subsequent desensitization of the receptor to further stimulations. These events are usually accompanied by receptor endocytosis and/or recycling of the receptor (10).

A large body of evidence suggests that the major route of sequestration of GPCRs is via clathrin-coated pits and into early endosomes (11). The β_2-adrenergic receptor (β_2-AR), a prototypical GPCR, becomes phosphorylated upon ligand binding and then exhibits an increased binding affinity for the adaptor molecules (either β-arrestin or arrestin 3), which prevent further coupling between the receptor and G proteins (12, 13). The arrestins are subsequently involved in β_2-AR sequestration by specifically binding to clathrin, a major component of clathrin-coated pits (14, 15). It has been suggested that sequestration of GPCRs to early endosomes and lysosomes might be responsible for receptor down-regulation and resensitization (16, 17). Within the acidic environment of the endosomes and lysosomes, the receptors either undergo dephosphorylation and recycle back to the cell surface and thus are resensitized or are degraded and down-regulated (11).

At present, much of the information concerning the molecular mechanisms for GPCR sequestration and down-regulation is derived from the studies of β_2-AR. Due to the enormous number of GPCRs and the diverse cellular function evoked by each individual receptor, it is conceivable that multiple mechanisms may be employed for receptor sequestration, down-regulation, and resensitization. This is exemplified by the finding that while clathrin-coated pits are essential for agonist-promoted β_2-AR sequestration, sequestration of the angiotensin II type 1A receptor does not require intact function of clathrin-coated pits (18).

In contrast to the β_2-AR, little is known regarding the se-

* This research was supported by National Institutes of Health Grant CA34590 (to A. R.), Vanderbilt Cancer Center Support Grant CA68485, and a Department of Veterans Affairs Associate Career Scientist Award (A. R.). The costs of publication of this article were defrayed in part by the payment of page charges. This article must therefore be hereby marked "*advertisement*" in accordance with 18 U.S.C. Section 1734 solely to indicate this fact.

¶ To whom correspondence should be addressed.

[1] The abbreviations used are: MGSA/GRO, melanoma growth-stimulatory activity/growth-regulated protein; CXC chemokine, chemokine with the first two conserved cysteine residues separated by an intervening amino acid; HEK-293 cells, human embryonic kidney cell line; IL-8, interleukin-8; MAP, mitogen-activated protein; GPCR, G protein-coupled receptor; β_2-AR, β_2-adrenergic receptor; RIPA, radioimmune precipitation assay; ERK, extracellular signal-regulated kinase.

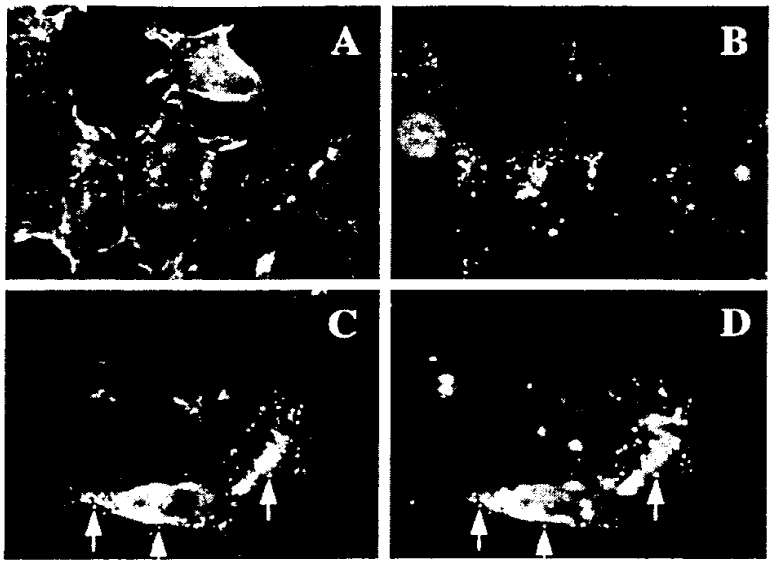

FIG. 1. **Colocalization of CXCR2 with the transferrin receptor.** HEK293 cells expressing CXCR2 were incubated with fluorescein isothiocyanate-conjugated transferrin for 2 h, washed, and chased for 30 min. The cells were treated with 100 ng/ml MGSA/GRO for 0 min (*A*, *B*) or 3 h (*C*, *D*). The cells were then fixed, permeablized, and stained for CXCR2 with a rabbit anti-CXCR2 antibody followed by rhodamine-conjugated goat anti-rabbit antibody (*A*, *C*). The emission of fluorescein isothiocyanate-transferrin is shown in *B* and *D*. The *arrows* indicate the examples of co-localization of CXCR2 and transferrin receptor. Images were processed using Photoshop software.

questration, down-regulation, and resensitization mechanisms of chemokine receptors and their roles in mediating cell chemotaxis, which is a distinct function for chemokine receptors. In order to chemotax along a gradient of chemotactic cytokine, the cells may employ an *on-off* mechanism in which the chemokine receptors undergo a continuous desensitization and resensitization process. The present studies were focused to delineate the sequestration and down-regulation mechanism of CXCR2. To accomplish this, we transiently expressed the CXCR2 in HEK293 cells and examined the effects of co-expression of the dynamin I K44A mutant on receptor sequestration, down-regulation, and resensitization. We also used ligand-mediated MAP kinase activation and chemotaxis as functional assays to examine the effects of blocking the endocytosis of CXCR2 on its signal transduction events. The results demonstrate that clathrin-coated pits are primary routes for CXCR2 sequestration and down-regulation. Blocking the endocytosis of CXCR2 does not affect downstream MAP kinase activation. However, it does severely attenuate ligand-mediated chemotaxis.

EXPERIMENTAL PROCEDURES

Cell Culture and Transfections—293 human embryonic kidney cells (HEK293) were cultured in Dulbecco's modified Eagle's medium supplemented with 10% fetal bovine serum. HEK293 cells cultured to 80% confluence were transfected with the CXCR2 cDNA in the pRc/cytomegalovirus vector and the dynamin I wild-type or K44A mutant in the pBJ vector using the LipofectAMINE PLUS reagent (Life Technologies, Inc.) according to the manufacturer's recommendation. Before each experiment, an indirect immunfluorescence assay was used to assess the transfection efficiency. The transfection efficiency was approximately 80% in each experiment.

Receptor Internalization Assay—The acid/buffer wash technique (19) was used to determine the kinetics of MGSA/GRO-induced internalization of CXCR2.

In Vivo Phosporylation and Western Blot Analysis—Receptor phosphorylation assays were performed as described previously (20). In brief, the transfected cells were plated on six-well plates 1 day after the transfection. On the following day, after incubating in serum- and phosphate-free medium for 1 h, cells were then labeled by incubating in [^{32}P]orthophosphate (100 μCi/ml) in the same medium at 37 °C for 2 h. Cells were then stimulated with or without 100 ng/ml MGSA/GRO for 10 min. Dephosphorylation was performed by allowing cells to recover in fresh serum-free media without ligand at 37 °C for 1 h. The cells were then lysed in RIPA buffer containing 0.1% SDS, 0.5% sodium deoxycholate, 1% Triton X-100, 10 mM Tris, pH 7.5, 150 mM NaCl, 1 mM EDTA, 1 mM phenylmethylsulfonyl fluoride, 10 μg/ml aprotinin, and 10 μg/ml leupeptin. CXCR2 was immunoprecipitated with a polyclonal rabbit anti-CXCR2 antibody (20) from cleared supernatants containing approximately 300 μg of protein (estimated by the BCA method; Pierce). The immunoprecipitates were electrophoresed through a 10% SDS-polyacrylamide gel and transferred to a nitrocellulose membrane (Bio-Rad). The phosphorylated receptors were then detected by autoradiography, and the total amount of receptor was determined by Western blotting using a monoclonal antibody against CXCR2 to ensure equal loading.

Indirect Immunofluorescence—HEK293 cells stably expressing CXCR2 (10) were grown on 10-mm coverslips (Fisher). To compare the distribution of CXCR2 and the transferrin receptor, cells were washed once with serum-free medium and then incubated at 37 °C with the same medium containing 100 μg/ml of fluorescein isothiocyanate-conjugated transferrin (Molecular Probes, Inc., Eugene, OR) for 2 h. The cells were washed and then chased for 30 min. Following MGSA/GRO or IL-8 (100 ng/ml) treatment for the indicated time periods, cells were processed for indirect immunofluorescence to detect the subcellular localization of CXCR2 (19).

Receptor Down-regulation Assay—Cells were collected by trypsinization 24 h after transfection and plated onto 12-well plates. The next day, the cells were treated with or without 100 ng/ml MGSA/GRO for 0.5–8 h. Cells were lysed in 0.5 ml/well RIPA buffer with proteinase and phosphatase inhibitors described as above. Aliquots of lysates containing 30 μg of protein were subjected to electrophoresis (10% SDS-polyacrylamide gel electrophoresis) and then transferred to nitrocellulose membrane. The amount of CXCR2 was detected by Western blot using the previously described rabbit anti-CXCR2 antibody.

MAP Kinase Assay—Agonist-treated cells were lysed by RIPA buffer. Lysates containing equal amounts of protein were subjected to SDS-polyacrylamide gel electrophoresis. Phosphorylated MAP kinase (ERK1/ERK2) was detected by a phosphospecific MAP kinase antibody (Santa Cruz Biotechnology, Inc., Santa Cruz, CA).

Chemotaxis Assay—Chemotaxis assays were performed on transiently transfected HEK293 cells as described previously (10) using a 96-well chemotaxis chamber (Neuroprobe Inc.).

RESULTS

Redistribution of CXCR2 to Endosomes following MGSA/GRO Treatment—Immunofluoresence microscopy was used to define the subcellular distribution of CXCR2 in stably transfected HEK293 cells using rabbit anti-CXCR2 polyclonal antibody. The localization of endosomes was detected using the transferrin-fluorescein isothiocyanate complex as described previously. The majority of CXCR2 was targeted to the plasma membrane in untreated cells (Fig. 1*A*). A small portion of CXCR2 was located intracellularly as punctate structures that colocalized with the transferrin receptor (Fig. 1, *A* and *B*). Following MGSA/GRO (100 ng/ml) treatment for 3 h, agonist

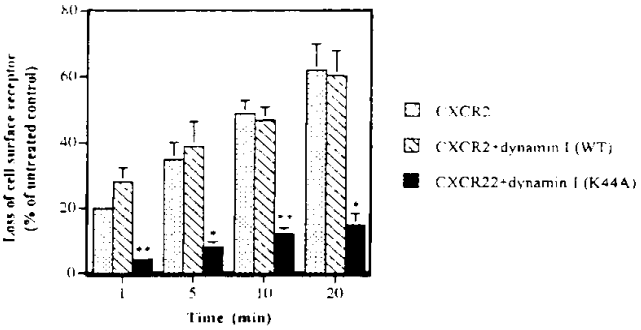

FIG. 2. **The effect of the wild-type and K44A mutant dynamin I on the MGSA/GRO-stimulated CXCR2 internalization.** HEK293 cells were transiently transfected with plasmids expressing CXCR2 with pBluescript (control) (*dotted bars*), rat dynamin I (*striped bars*), or rat dynamin I K44A (*black bars*). Two days after transfection, the cells were preincubated with binding buffer containing the ^{125}I-MGSA/GRO for 30 min at 4 °C. Unbound ^{125}I-MGSA/GRO was removed by washing at 4 °C. The cells were warmed to 37 °C for the indicated time period (also see "Expermental Procedures"). ^{125}I-MGSA/GRO remaining at the cell surface was removed with acetic acid (0.2 M, pH 2.5) containing 0.5 M NaCl, and the internalized ^{125}I-MGSA/GRO was then quantitated on a γ-counter. Data are presented as mean ± S.E. from three independent experiments. Binding to duplicate samples varied generally by less than 10%. The data were analyzed using Student's paired *t* test (*, $p < 0.05$; **, $p < 0.005$ (compared with control cells transfected with CXCR2 only)).

stimulation resulted in sequestration of CXCR2, observable as a loss of cell surface immunofluorescence with a concomitant increase in the number of intracellular punctate structures. The distribution of the punctate structures overlapped extensively with those of the transferrin receptor (Fig. 1, *C* and *D*), suggesting that agonist stimulation enhances CXCR2 redistribution into endosomes. This phenomenon was observable as early as 10 min with MGSA/GRO treatment (data not shown). IL-8 treatment induced a similar redistribution of CXCR2 to the endosomes (data not shown).

Effect of Dynamin I K44A on CXCR2 Endocytosis—It has been shown previously that CXCR2 undergoes a rapid endocytosis within minutes in response to either MGSA/GRO or IL-8 stimulation. To determine whether the agonist-promoted CXCR2 endocytosis is a clathrin-mediated process, HEK293 cells were transiently co-transfected with cDNAs encoding CXCR2 and dynamin I K44A. Agonist-promoted endocytosis was determined and compared with that observed in cells transfected only with CXCR2 or cells co-transfected with CXCR2 and wild-type dynamin I. Cells expressing only CXCR2 showed rapid receptor internalization after MGSA/GRO treatment (Fig. 2). The MGSA/GRO-stimulated sequestration of CXCR2 occurred in a time-dependent manner. The percentage of endocytosed receptor increased progressively from 20% at 1 min to approximately 60% at 20 min. Co-expression of wild-type dynamin I with CXCR2 seemed neither to promote nor inhibit the rate of CXCR2 endocytosis. In contrast, in cells co-expressing CXCR2 and dynamin I K44A, there was a profound inhibition of the MGSA/GRO-promoted CXCR2 endocytosis, with less than 15% of receptor endocytosed at 20 min. These data clearly indicate that agonist-promoted endocytosis of CXCR2 depends on functional expression of dynamin I and thus is a clathrin-mediated process. This is further supported by the fact that internalized CXCR2 colocalized with the transferrin receptor. Based on ligand binding data, we observed similar CXCR2 cell surface expression level in cells transfected with CXCR2 and dynamin I K44A as compared with those transfected with only CXCR2. We also observed a similar effect on receptor endocytosis when the cells were treated with IL-8 (data not shown).

The Effect of Dynamin K44A on CXCR2 Phosphorylation and Dephosphorylation—We have previously shown that CXCR2 undergoes a rapid phosphorylation and desensitization after MGSA/GRO treatment (10). To further investigate the effects of the inhibition of receptor endocytosis on CXCR2 dephosphorylation and resensitization, transiently transfected 293 cells were metabolically labeled with [^{32}P]orthophosphate, treated with MGSA/GRO, and allowed to recover from ligand. In the absence of dynamin I K44A expression, phosphorylation of CXCR2 was detected after 10-min treatment of 100 ng/ml MGSA. After a 1-h recovery period following removal of ligand, CXCR2 underwent dephosphorylation to 44% of the stimulated level. However, the dephosphorylation of CXCR2 in dynamin I K44A co-transfected cells was greatly attenuated. After the same recovery period, about 80% of receptor still remained in the phosphorylated form as compared with ligand-stimulated cells without recovery (Fig. 3, *A* and *D*). The equal loading of CXCR2 and expression of dynamin I K44A were confirmed by Western blots using antibodies against CXCR2 (Fig. 3*B*) and dynamin I (Fig. 3*C*). The rate of CXCR2 dephosphorylation with co-expression of wild-type dynamin is comparable with that which occurred in cells transfected with CXCR2 alone.

Effect of Dynamin K44A on CXCR2 Down-regulation—Previously, we have observed that MGSA/GRO treatment resulted in a concentration-dependent decrease in the level of CXCR2 in stably transfected 3ASubE P-3 and HEK293 T2 cells (10, 20). Based on information from a β_2-AR down-regulation experiment (16), we hypothesized that a portion of the internalized CXCR2 may be subject to proteolytic degradation in the endosome or lysosome following receptor endocytosis. Moreover, reducing this portion of receptors by blocking endocytosis should have a concomitant effect on receptor degradation and down-regulation. To test this hypothesis, we determined the effect of the dynamin I K44A mutant on CXCR2 degradation and down-regulation in HEK293 cells. Transiently transfected cells were stimulated with MGSA/GRO for various time periods and lysed. The relative amount of CXCR2 was assessed by Western blot using whole cell lysates. As demonstrated in Fig. 4, MGSA/GRO treatment promoted progressive CXCR2 degradation in a time-dependent fashion. After 2 h of treatment, cells lost 14% of receptor. The percentage of CXCR2 loss was increased to 49% following 8 h MGSA/GRO incubation. In contrast, the dynamin I K44A mutant effectively reduced the agonist-promoted CXCR2 degradation, with only 15% of CXCR2 being degraded after 8 h of MGSA/GRO treatment (Fig. 4). These data suggest that a portion of endocytosed CXCR2 undergoes degradation and down-regulation via a clathrin-mediated event.

Effect of Dynamin K44A on CXCR2-mediated MAP Kinase Activation—Previous studies demonstrated that IL-8 stimulation on its receptors in neutrophils resulted in activation of MAP kinase pathway (21). We also confirmed the activation of MAP kinase following MGSA/GRO stimulation in HEK293 T2 cells. To study the downstream CXCR2 signal transduction pathway, we next examined the effect of dynamin I K44A expression on MAP kinase activation. The MGSA/GRO-dependent activation of MAP kinase in cells expressing both CXCR2 and dynamin I K44A was compared with that of cells expressing only CXCR2 by using a phosphospecific ERK1/ERK2 antibody. As demonstrated in Fig. 5, *A* and *C*, dynamin I K44A cells exhibited an identical MAP kinase activation response following 5 min of MGSA/GRO or IL-8 (100 ng/ml) stimulation. Equal loading was confirmed by immunoblotting with an antibody against ERK-2.

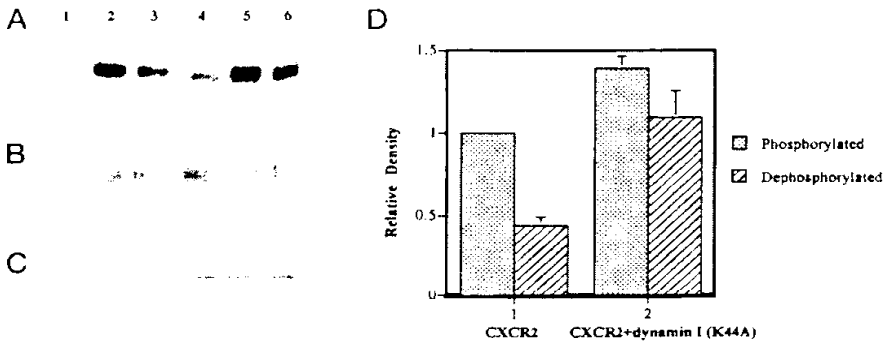

FIG. 3. **The effect of the dynamin I K44A mutant on CXCR2 phosphorylation and dephosphorylation.** HEK293 cells were transiently transfected with plasmids expressing CXCR2 with or without rat dynamin I K44A. *A*, a representative autoradiograph from two independent experiments showing the phosphorylation and dephosphorylation of CXCR2 in the whole cell lysates. Cells were treated with 100 ng/ml MGSA/GRO for 0 min (*lanes 1* and *4*) or 10 min (*lanes 2*, *3*, *5*, and *6*). Cells were then washed, incubated in fresh medium without ligand for 1 h (*lanes 3* and *6*), or kept on ice (*lanes 2* and *5*). *B*, the equal amount of receptor loading was confirmed by Western blot using a monoclonal anti-CXCR2 antibody. *C*, the expression of dynamin I K44A on the transfected cell lysates was detected by Western blot using anti-dynamin antibody. *D*, quantification of the mean ± S.E. of two different experiments performed in duplicate. The data were normalized to MGSA-stimulated CXCR2 phosphorylation. *Dotted bars*, phosphorylated; *striped bars*, dephosphorylated.

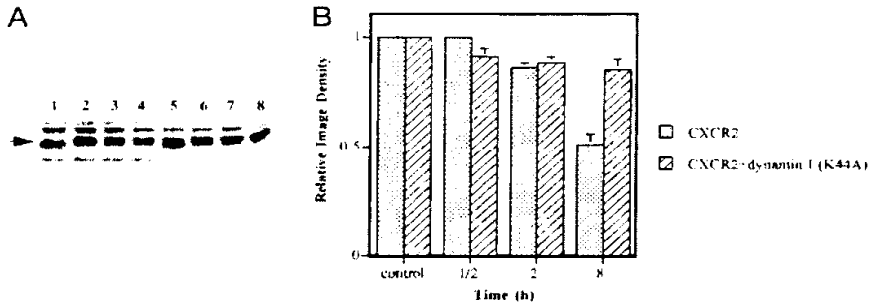

FIG. 4. **The effect of dynamin I K44A mutant on MGSA-stimulated CXCR2 degradation and down-regulation.** *A*, HEK293 cells were transiently transfected with plasmids expressing CXCR2 with (*lanes 5–8*) or without (*lanes 1–4*) rat dynamin I K44A. The cells were harvested and plated equally onto 12-well plates. The cells were then treated with 100 ng/ml MGSA/GRO for 0 min (*lanes 1* and *5*), 0.5 h (*lanes 2* and *6*), 2 h (*lanes 3* and *7*), and 8 h (*lanes 4* and *8*). 30 μg of protein from clarified RIPA lysates were loaded per lane, and Western blot analysis was performed with rabbit anti-CXCR2 polyclonal antibody and visualized by horseradish peroxidase-conjugated secondary antibody. The *arrow* indicates CXCR2 epitope. *B*, the density of the bands (mean ± S.E.) representing CXCR2 was determined by densitometric scanning. The results represent one of two experiments performed in duplicate. *Dotted bars*, CXCR2; *striped bars*, CXCR2 plus dynamin I K44A.

Effect of Dynamin K44A on CXCR2-mediated Chemotaxis—Ligand-stimulated CXCR2-mediated chemotaxis is a direct and effective functional test to access chemokine receptor signal transduction. We used chemotaxis assays to determine if blocking of receptor endocytosis by co-expression of dynamin I K44A could abolish the CXCR2-mediated chemotaxis toward a gradient of IL-8 (Fig. 6) or MGSA/GRO (data not shown). We observed an IL-8 concentration-dependent chemotactic response in cells expressing wild-type receptor, with a peak migration occurring at a concentration around 25–50 ng/ml IL-8. Also, the cellular migration response followed a typical bell-shaped curve in which the chemotaxis was inhibited at higher concentrations of IL-8 (Fig. 6). Strikingly, overexpression of dynamin I K44A resulted in marked attenuation of CXCR2-mediated chemotaxis. These data suggest that agonist-mediated endocytosis and resensitization are crucial for CXCR2-mediated chemotaxis.

DISCUSSION

CXCR2 is internalized into vesicular compartments following agonist stimulation and phosphorylation at multiple serine residues in the carboxyl-terminal domain in a manner similar to that observed for several other GPCRs. However, the mechanisms responsible for receptor endocytosis and the functional significance of this event regarding receptor signal transduction are largely unknown. Our studies provide direct biochemical evidence for the requirement of a dynamin-mediated formation of clathrin-coated pits in CXCR2 sequestration, resensitization, and down-regulation. More importantly, our data suggest that endocytosis of receptor is prerequisite to its ability to continuously sense the agonist stimulation that is unique for chemokine receptor-mediated chemotaxis.

Previous studies have identified dynamin as a major component of clathrin-mediated endocytosis (22). Dynamin associates with the adaptor protein AP2 complex (23). Once localized to the clathrin-coated pits, dynamin promotes endocytosis by catalyzing the pinching off process of coated vesicles (24, 25). Dynamin GTPase activity is essential for the formation of clathrin-coated pits. This is confirmed by the observation that expression of a GTPase-defective dynamin mutant prevents formation of the endocytic clathrin-coated vesicles (25, 26).

Using a dominant-negative mutant of dynamin I (K44A), we have demonstrated inhibition of ligand-induced CXCR2 endocytosis. This observation suggests that CXCR2 internalization is mediated by a highly conserved mechanism that is dynamin- and clathrin-dependent. Our immunofluorescence experiments revealed that CXCR2 internalization in HEK293 cells reached to endosomal compartments following MGSA/GRO treatment. Colocalization of CXCR2 with the transferrin receptor in transfected HEK293 cells is consistent with the concept that both receptors utilize the same clathrin-dependent pathway. In the

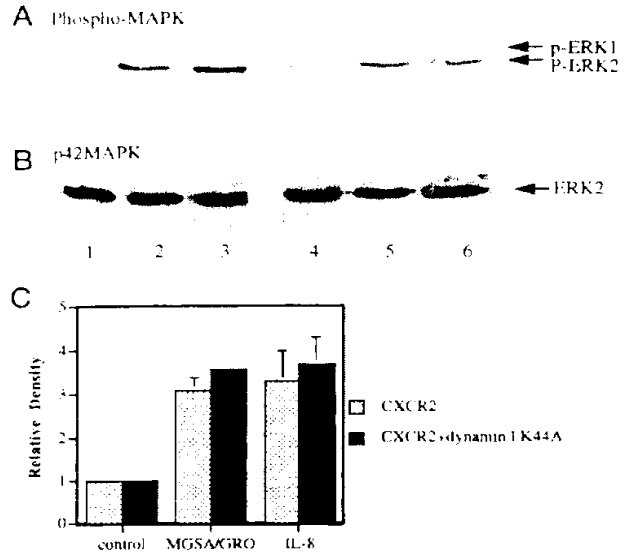

FIG. 5. **The effect of dynamin I K44A mutant on MGSA or IL-8-stimulated ERK activation in HEK293 cells.** *A*, HEK293 cells were transiently transfected with plasmids expressing CXCR2 with (*lanes 1–3*) or without (*lanes 4–6*) dynamin I K44A. The cells were harvested and plated equally onto 60-mm plates. The cells were then treated with buffer (*lanes 1* and *4*) or 100 ng/ml MGSA/GRO (*lanes 2* and *5*) or IL-8 (*lanes 3* and *6*) for 5 min. 30 μg of protein from clarified RIPA lysates were loaded per lane, and Western blot analysis was performed with a phosphospecific MAP kinase antibody and visualized by an horseradish peroxidase-conjugated secondary antibody. *B*, the blot from *A* was striped and reprobed with an antibody against ERK-2 to ensure the equal loading. *C*, the density of the bands (mean ± S.E.) representing phosphorylated ERK1 and ERK2 was determined by densitometric scanning. The results were obtained from three independent experiments. *Dotted bars*, CXCR2; *black bars*, CXCR2 plus dynamin I K44A.

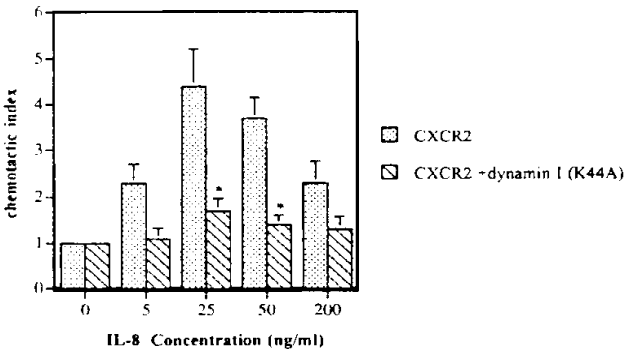

FIG. 6. **The effect of the dynamin I K44A mutant on IL-8-stimulated CXCR2-mediated chemotaxis of HEK293 cells.** HEK293 cells were transiently transfected with plasmids expressing CXCR2 with (*striped bars*) or without (*dotted bars*) rat dynamin I K44A. Two days after transfection, cells were compared for chemotaxis in response to IL-8 stimulation as described under "Experimental Procedures." Values represent the means ± S.E. of three independent experiments performed on different days. The data were analyzed using Student's paired *t* test (*, $p < 0.05$).

absence of agonist, a small but detectable portion of CXCR2 seems to be localized in the endosomes (Fig. 1*A*). This may be due to constitutive receptor internalization and recycling. This idea is supported by the finding that overexpression of dynamin I K44A reduces basal intracellular localization of CXCR2 (data not shown).

After internalization to the endosome, the receptor will be dephosphorylated and either recycled back to cell surface or degraded by proteolytic enzymes (11, 27). Using the dynamin I K44A mutant, we have shown that clathrin-mediated receptor internalization is a critical initial step for CXCR2 resensitization and down-regulation. Co-expression of dynamin I K44A resulted in significant diminution of both CXCR2 dephosphorylation and down-regulation. Although the exact mechanism responsible for dephoshorylation of GPCRs remains unclear, it is postulated that the conformational change of the receptor in the acidic environment facilitates dephosphorylation by a G protein-coupled receptor phosphatase (28). Recycling and resensitization of dephosphorylated receptor is believed to allow the chemokine receptors to sense and respond to a continuous gradient of chemokine stimulation.

The functional role of agonist-promoted CXCR2 endocytosis has long been elusive in the field of CXCR2 signal transduction. The result of MGSA/GRO and IL-8-mediated MAP kinase experiments suggests that CXCR2 endocytosis is not required for its immediate downstream signaling. These data are supported by the previous observation that a mutant CXCR2 deleting 31 carboxyl-terminal amino acids exhibited significantly impaired agonist-induced receptor endocytosis but not inhibition of adenylyl cyclase or MAP kinase activation (29). Further evidence suggesting the separation between CXCR2 endocytosis and immediate downstream signal transduction events came from the studies of another CXCR2 deletion mutant (30). Richardson *et al.* (30) demonstrated that a CXCR2 mutant (331T), exhibiting a deletion of the last 25 amino acid residues of the carboxyl-terminal domain, lost agonist-stimulated phosphorylation and sequestration when expressed in the placental cell RBL-2H3 cells. However, the immediate downstream signal transduction events such as GTPase activity, phosphatidylinositol hydrolysis, β-hexosaminidase release, and Ca^{2+} mobilization were not impaired. Studies of the β_2-AR indicate that the capacity of the receptor to signal through adenylyl cyclase remains intact following total inhibition of receptor endocytosis by dynamin K44A (17). However, others demonstrate that in HEK293 cells, the β_2-AR mediated activation of MAP kinase is inhibited by blocking receptor internalization although tyrosine phosphorylation-mediated activation of Shc and Raf kinase are unaffected (31). The reasons for the discrepancy in ligand-mediated receptor endocyrosis and downstream MAP kinase activation between CXCR2 and β_2-AR are not clear.

The chemotaxis assay is believed to be the most useful assay to evaluate the signal transduction capability of chemokine receptors, since it measures the ultimate result of a cascade of intracellular events that are activated by ligand-receptor interaction. More importantly, this assay also provides a functional read out for a process composed of sequential desensitization and resensitization events with respect to receptor activation. Our results clearly demonstrate that overexpression of dynamin I K44A abolished the CXCR2-mediated HEK293 cell chemotaxis toward both IL-8 and MGSA/GRO. The equal or similar cell surface expression of receptors has been confirmed in each experiment by immunofluorescence assay to exclude the possibility that the reduced chemotaxis in cells expressing dynamin I K44A is due to reduced receptor expression or cell surface targeting. The specific signal pathway responsible for chemotaxis is poorly understood. In human neutrophils, phosphatidylinositol 3-kinase activity is required for both induction of chemotaxis and MAP kinase activation (32). When phosphatidylinositol 3-kinase is blocked with wortmannin, IL-8-induced MAP kinase is also blocked (21). The fact that MAP kinase activation in cells expressing dynamin I K44A is normal

makes it unlikely that phosphatidylinositol 3-kinase activity is affected in these cells. Considering the fact that endocytosis permits CXCR2 dephosphorylation and resensitization, we therefore postulate that endocytosis, dephosphorylation, resensitization, and recycling of CXCR2 is required for graded response to ligand stimulation.

Blocking receptor internalization does not have major effects on the generation of immediate downstream signals but does alter the ability of cells to respond to a continuous signal generated over a concentration gradient, based upon the loss of receptor dephosphorylation and the subsequent receptor recycling. Another possible explanation for the blocking effects of dynamin I K44A on cell chemotaxis may be due to the inhibition of the redistribution of cell surface chemokine receptor and receptors for matrix attachment. One model of cell migration suggests that there is an increased exocytosis at the leading edge of moving cells (33, 34). This polarized exocytosis may be involved in delivery of fresh integrins and chemokine receptors to the cell front. This process enables the migrating cells to attach to the extracellular matrix and to sense the chemokine stimulation.

Following ligand-stimulated receptor phosphorylation, GPCRs bind to adaptor molecules that directly inhibit the interaction between receptor and G-protein (12, 13). In the case of the β_2-AR, the binding of β-arrestin and arrestin-3 is also an initial event required for receptor internalization (14, 15). Both β-arrestin and arrestin-3 can function as adaptors. The association of these molecules with phosphorylated receptor and clathrin is a key event in the formation of clathrin-coated pits. Recently, Aragay *et al.* (35) reported that β-arrestin associates with CCR2 shortly after agonist stimulation, suggesting that arrestins might play a universal role in mediating GPCR desensitization and internalization. Studies are currently in progress to test the role of arrestins and other adaptor molecules in CXCR2 desensitization and internalization.

In summary, we have established that agonist-promoted CXCR2 proceeds through the formation of clathrin-coated pits to endosomes. Furthermore, we demonstrated that the CXCR2 internalization is required for receptor dephosphorylation, resensitization, and down-regulation but not for immediate downstream signaling. More importantly, our chemotaxis experiments indicate that agonist-stimulated receptor endocytosis and dephosphorylation is essential for normal chemokine receptor-mediated chemotaxis in HEK293 cells.

Acknowledgments—We are grateful to Repligen Corp. for the generous supply of recombinant MGSA/GRO. We thank John MacDougall and Barbara Fingleton for critical reading of the manuscript.

REFERENCES

1. Baggiolini, M., Dewald, B., and Moser, B. (1994) *Adv. Immunol.* **55,** 97–179
2. Baggiolini, M., Loetscher, P., and Moser, B. (1995) *Int. J. Immunopharmacol.* **17,** 103–108
3. Oppenheim, J. J. (1993) *Adv. Exp. Med. Biol.* **351,** 183–186
4. Oppenheim, J. J., Zachariae, C. O., Mukaida, N., and Matsushima, K. (1991) *Annu. Rev. Immunol.* **9,** 617–648
5. Murphy, P. M., and Tiffany, H. L. (1991) *Science* **253,** 1280–1283
6. Cesarman, E., Nador, R. G., Bai, F., Bohenzky, R. A., Russo, J. J., Moore, P. S., Chang, Y., and Knowles, D. M. (1996) *J. Virol.* **70,** 8218–8223
7. Holmes, W. E., Lee, J., Kuang, W. J., Rice, G. C., and Wood, W. I. (1991) *Science* **253,** 1278–1280
8. Luster, A. D. (1998) *N. Engl. J. Med.* **338,** 436–445
9. Wu, D., LaRosa, G. J., and Simon, M. I. (1993) *Science* **261,** 101–103
10. Mueller, S. G., White, J. R., Schraw, W. P., Lam, V., and Richmond, A. (1997) *J. Biol. Chem.* **272,** 8207–8214
11. Koenig, J. A., and Edwardson, J. M. (1997) *Trends Pharmacol. Sci.* **18,** 276–87
12. Lohse, M. J., Benovic, J. L., Codina, J., Caron, M. G., and Lefkowitz, R. J. (1990) *Science* **248,** 1547–1550
13. Attramadal, H., Arriza, J. L., Aoki, C., Dawson, T. M., Codina, J., Kwatra, M. M., Snyder, S. H., Caron, M. G., and Lefkowitz, R. J. (1992) *J. Biol. Chem.* **267,** 17882–17890
14. Goodman, O. B., Jr., Krupnick, J. G., Santini, F., Gurevich, V. V., Penn, R. B., Gagnon, A. W., Keen, J. H., and Benovic, J. L. (1996) *Nature* **383,** 447–450
15. Ferguson, S. S., Downey, W. E. R., Colapietro, A. M., Barak, L. S., Menard, L., and Caron, M. G. (1996) *Science* **271,** 363–366
16. Gagnon, A. W., Kallal, L., and Benovic, J. L. (1998) *J. Biol. Chem.* **273,** 6976–6981
17. Zhang, J., Barak, L. S., Winkler, K. E., Caron, M. G., and Ferguson, S. S. (1997) *J. Biol. Chem.* **272,** 27005–27014
18. Zhang, J., Ferguson, S. S. G., Barak, L. S., Menard, L., and Caron, M. G. (1996) *J. Biol. Chem.* **271,** 18302–18305
19. Yang, W., Schraw, W. P., Mueller, S. G., and Richmond, A. (1997) *Biochemistry* **36,** 15193–15200
20. Mueller, S. G., Schraw, W. P., and Richmond, A. (1994) *J. Biol. Chem.* **269,** 1973–1980
21. Knall, C., Young, S., Nick, J. A., Buhl, A. M., Worthen, G. S., and Johnson, G. L. (1996) *J. Biol. Chem.* **271,** 2832–2838
22. Shpetner, H. S., and Vallee, R. B. (1992) *Nature* **355,** 733–735
23. Wang, L. H., Sudhof, T. C., and Anderson, R. G. (1995) *J. Biol. Chem.* **270,** 10079–10083
24. Hinshaw, J. E., and Schmid, S. L. (1995) *Nature* **374,** 190–192
25. van der Bliek, A. M., Redelmeier, T. E., Damke, H., Tisdale, E. J., Meyerowitz, E. M., and Schmid, S. L. (1993) *J. Cell Biol.* **122,** 553–563
26. Damke, H., Baba, T., Warnock, D. E., and Schmid, S. L. (1994) *J. Cell Biol.* **127,** 915–934
27. Dohlman, H. G., Thorner, J., Caron, M. G., and Lefkowitz, R. J. (1991) *Annu. Rev. Biochem.* **60,** 653–688
28. Krueger, K. M., Daaka, Y., Pitcher, J. A., and Lefkowitz, R. J. (1997) *J. Biol. Chem.* **272,** 5–8
29. Neptune, E. R., and Bourne, H. R. (1997) *Proc. Natl. Acad. Sci. U. S. A.* **94,** 14489–14494
30. Richardson, R. M., Pridgen, B. C., Haribabu, B., Ali, H., and Snyderman, R. (1998) *J. Biol. Chem.* **273,** 23830–23836
31. Daaka, Y., Luttrell, L. M., Ahn, S., Della Rocca, G. J., Ferguson, S. S., Caron, M. G., and Lefkowitz, R. J. (1998) *J. Biol. Chem.* **273,** 685–688
32. Knall, C., Worthen, G. S., and Johnson, G. L. (1997) *Proc. Natl. Acad. Sci. U. S. A.* **94,** 3052–3057
33. Bretscher, M. S. (1996) *Cell* **85,** 465–467
34. Hopkins, C. R., Gibson, A., Shipman, M., Strickland, D. K., and Trowbridge, I. S. (1994) *J. Cell Biol.* **125,** 1265–1274
35. Aragay, A. M., Mellado, M., Frade, J. M., Martin, A. M., Jimenez-Sainz, M. C., Martinez, A. C., and Mayor, F., Jr. (1998) *Proc. Natl. Acad. Sci. U. S. A.* **95,** 2985–2990

Regulation of the Expression of IL-8 Receptor A/B by IL-8: Possible Functions of Each Receptor

Anan Chuntharapai and K. Jin Kim[1]

Department of Bioanalytical Technology, Genentech, Inc., South San Francisco, CA 94080

We investigated the regulatory mechanism of the expression of IL-8R, IL-8R type A (IL-8RA), and IL-8R type B (IL-8RB) on human neutrophils by IL-8. The expression of IL-8RA/B was analyzed by flow cytometry using mAb specific for each receptor. IL-8 down-modulated >90% of IL-8RA and IL-8RB expression within 5 min. A related C-X-C chemokine, melanoma growth stimulatory activity, down-modulated IL-8RB but not IL-8RA. It required 7 to 13 times more IL-8 to down-modulate IL-8RA than IL-8RB, as determined by the half-maximal effective concentration of IL-8. Scatchard analysis showed that the affinity of IL-8RA for IL-8 was lower than that of IL-8RB. The possible functions of each IL-8R were explored by comparing 1) the expression levels of IL-8RA/B on migrated neutrophils during in vitro chemotaxis assay and 2) the recovery rate of IL-8RA/B expression after down-modulation by IL-8. Results obtained from the in vitro chemotaxis show that the expression level of IL-8RB, but not IL-8RA, on neutrophils that migrated into the chamber containing low concentrations (<1 nM) of IL-8 was significantly reduced compared with the control level. This suggests that IL-8RB may play an active role in the initiation of neutrophil migration distant from the site of inflammation, where the concentration of IL-8 is at the picomolar level. After down-modulation by 119 nM IL-8, the expression of IL-8RA fully recovered within 1.5 h, while the recovery rate of IL-8RB expression was slow and never reached more than 40% of the control level during a 3-h culture period. The rapid reexpression of IL-8RA suggests that the low affinity IL-8RA may play a more active role in mediating IL-8 signal at the site of inflammation, where the concentration of IL-8 is high. *The Journal of Immunology*, 1995, 155: 2587–2594.

Neutrophil accumulation in tissues has been recognized as a cardinal sign of inflammation. IL-8 is known to be a major neutrophil chemotactic factor (1–3). Two types of human IL-8R mediating transmembrane signals have been described: IL-8RA[2] and IL-8RB (4, 5). Both IL-8RA and IL-8RB are expressed not only on human blood neutrophils but also on monocytes (6, 7), a subset of NK cells, and a subset of T cells (6), although neutrophils express the highest level among these cells. A major question is the physiologic role of each receptor. To understand the role of IL-8RA/IL-8RB expressed on human neutrophils during inflammation, it is important to know the affinities of IL-8RA/IL-8RB for IL-8. It has been reported that both IL-8RA and IL-8RB bind to IL-8 with similar high affinities (3, 8–12), although the magnitudes of the affinities reported varied from 0.1 to 4 nM. However, these receptors have widely different affinities for MGSA. IL-8RA binds MGSA with low affinity in the range of 100 to 450 nM, while IL-8RB binds MGSA with high affinity in the range of 100 pM to 2 nM (3, 8–12). Thus, IL-8RB is referred to as a promiscuous receptor responding to various C-X-C chemokines in addition to IL-8, while IL-8RA is referred to as an IL-8- specific receptor. Both receptors coexist on human neutrophils; therefore, it has been difficult to precisely determine the affinity of each receptor for IL-8 on the neutrophil. In the past, much information on these affinities was obtained by using transfected cells expressing each receptor separately.

IL-8 has been shown to activate neutrophils through a single subunit interaction with its receptor (13). Alanine scanning mutagenesis (14) and synthesis of N-terminal-truncated variants (15) of IL-8 suggest that IL-8 residues E_4, L_5, and R_6 are essential for IL-8 binding to its receptors. In addition to this ELR sequence of IL-8, different portions of the IL-8 molecule interact with IL-8RA and

Received for publication March 27, 1995. Accepted for publication June 27, 1995.

The costs of publication of this article were defrayed in part by the payment of page charges. This article must therefore be hereby marked *advertisement* in accordance with 18 U.S.C. Section 1734 solely to indicate this fact.

[1] Address correspondence and reprint requests to K. Jin Kim, Ph.D., Department of Bioanalytical Technology, Genentech, Inc., 460 Point San Bruno Boulevard, South San Francisco, CA 94080.

[2] Abbreviations used in this paper: IL-8RA, IL-8R type A; EC_{50}, 50% effective concentration; IL-8RB, IL-8R type B; MGSA, melanoma growth stimulatory activity; FACS buffer, 1% FCS in PBS buffer.

0022-1767/95/$02.00

IL-8RB (16). A sequence between amino acid residues 7 to 50 was shown to be involved in binding to IL-8RA, while the C-terminal portion (residues 52–72) of IL-8 was shown to play a role in binding to IL-8RB (16).

It has been reported that [^{125}I]IL-8 bound to the IL-8R on neutrophils is rapidly internalized and degraded (17–19). More than 90% of the ligand-bound receptors are endocytosed within 10 min, and the receptors are recycled, as indicated by their reexpression on the cell surface (17). In this study, we further extended these observations by using IL-8RA- and IL-8RB-specific mAb to investigate the ability of IL-8 to differentially regulate the expression of the each receptor. Understanding the regulatory effect of IL-8 on IL-8RA/B expression on human neutrophils may provide insight into the physiologic role of each receptor during inflammation.

Materials and Methods

Down-modulation of the expression of IL-8R by IL-8

Human neutrophils were separated from whole blood by Ficoll-Hypaque gradient centrifugation (Mono-Poly Resolving Medium, ICN Biomedical, Inc., Aurora, OH) as described by the vendor, followed by lysis of erythrocytes with iso-osmotic NH_4Cl. Neutrophils were suspended to 10^6 cells/ml in HBSS plus 0.1% BSA, prewarmed at 37°C for 15 min, and then incubated with various concentrations of human IL-8 or MGSA for 15 min at 37°C. After washing twice in cold FACS buffer, cells were divided into two parts and stained with FITC-9H1 (anti-IL-8RA) (20) or FITC-10H2 (anti-IL-8RB) (6) for 30 min at 4°C. Cells were then washed twice in FACS buffer, and the level of FITC bound to the cells was analyzed by flow cytometry (FACScan, Becton Dickinson, Milpitas, CA).

Determination of the affinities of IL-8RA/B on human neutrophils for IL-8 and MGSA by Scatchard analysis

To determine the affinity of IL-8RA, human neutrophils were prewarmed at 37°C for 15 min and incubated with 127 nM MGSA for 15 min at 37°C to completely down-modulate IL-8RB. After washing twice in cold binding buffer (HBSS without Ca^{2+} and Mg^{2+}, with 25 mM HEPES and 0.5% BSA), cells were suspended to 4×10^6 cells/ml in the binding buffer. To determine the affinity of IL-8RB, cells resuspended to 4×10^6/ml in binding buffer were incubated with 200 μg/ml of mAb 9H1 (anti-IL-8RA) at 4°C for 30 min to block IL-8RA binding to IL-8. These pretreated cells were then used for the IL-8R binding assay, as described previously (20). Experiments were performed in triplicate. Briefly, cells were incubated with [^{125}I]IL-8 (spec. act., 2000 Ci/mM; Amersham Corp., Arlington Heights, IL) in the presence of various concentrations (0.005–11.9 nM) of IL-8 at 4°C for 1 h. The unbound [^{125}I]IL-8 was removed by sucrose gradient centrifugation. The level of [^{125}I]IL-8 bound to cells was determined by a gamma counter. The binding data were curve fit with the computer program Ligand (21), and the affinities of IL-8RA/B for IL-8 were determined by Scatchard analysis.

To determine the affinities of IL-8RB on human PMN for MGSA, PMN were incubated with [^{125}I]MGSA (sp. act., 2200 Ci/mM; DuPont Co., Biotechnology Systems, Wilmington, DE) in the presence of various concentrations (0.006–12.75 nM) of MGSA at 4°C for 1 h. The remaining steps were conducted as described above.

Neutrophil chemotaxis assays

Neutrophils were suspended to 10^6 cells/ml in HBSS plus 0.1% BSA. Two hundred milliliters of cells were loaded into the upper chamber (3.0-μm Nucleopore polycarbonate insert chamber, no. 3415, Costar, Cambridge, MA), and various concentrations of IL-8 were added to the lower chamber. After incubation at 37°C for 30 min in a CO_2 incubator, cells that migrated to the lower chamber were harvested and washed twice in cold FACS buffer. The expression level of IL-8RA/B on these migrated cells was determined by flow cytometry, as described above.

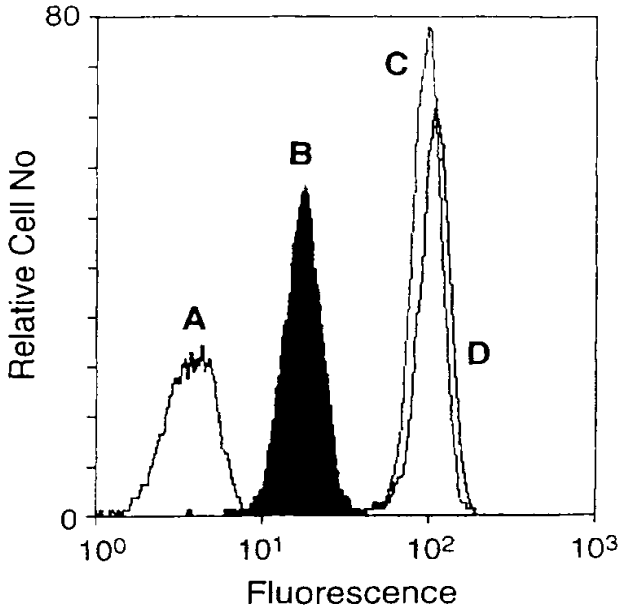

FIGURE 1. Flow cytometry analysis of IL-8RA expression on human neutrophils treated with or without IL-8 at 4 or 37°C. Cells were incubated with 119 nM human IL-8 for 30 min at 4°C (*C*) or 37°C (*B*), and the expression level of IL-8RA was detected by FITC-9H1 mAb. *D*, Cells at 4°C without IL-8; *A*, unstained control.

Determination of IL-8 concentrations by ELISA

The concentrations of IL-8 present in the culture supernatant were determined by the mAb-based IL-8-specific ELISA previously described (22).

Results

Blocking mAb to IL-8RA/B can detect IL-8R on human neutrophils that were preincubated with IL-8

To investigate the regulatory mechanisms of IL-8RA/B expression using mAb specific for each receptor, we first determined whether preincubation of cells with IL-8 would prevent the mAb from binding to the cell surface IL-8R. Human neutrophils were incubated with or without 119 nM IL-8 for 30 min at 4 or 37°C, washed, divided into two parts, stained with FITC-9H1 (anti-IL-8RA) or FITC-10H2 (anti-IL-8RB) at 4°C, and examined by flow cytometry. Figure 1 shows the result obtained with FITC-9H1 mAb. A similar finding was observed with FITC-10H2 mAb (data not shown). Under the conditions tested, the level of IL-8RA detected on neutrophils preincubated with IL-8 at 4°C (Fig. 1*C*) was similar to that on untreated cells (Fig. 1*D*). At this temperature, there was no down-modulation of receptors even though IL-8 bound to IL-8R on the cell membrane. This observation shows that mAb 9H1 could detect the IL-8RA on neutrophils that were preincubated with IL-8. When neutrophils were incubated with

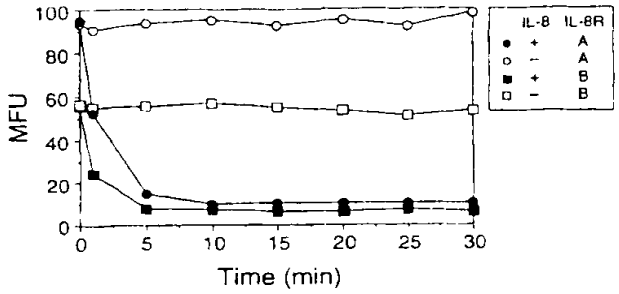

FIGURE 2. Rate of down-modulation of IL-8R on human neutrophils. Human neutrophils (5×10^5 cells/500 μl of medium) were incubated for various times at 37°C with or without 119 nM human IL-8. After washing in cold medium, cells were divided into two parts, stained with FITC-9H1 (anti-IL-8RA) or FITC-10H2 (anti-IL-8RB) for 30 min at 4°C, and analyzed by flow cytometry.

IL-8 at 37°C, there was a significant reduction in the IL-8RA level detected by FITC-9H1 (Fig. 1*B*), confirming the previous report that IL-8 down-modulated the expression of IL-8R (17). This experiment shows that FITC-9H1 and FITC-10H2 can be used to detect IL-8RA/B to achieve further understanding of the mechanism of receptor down-modulation by IL-8.

Differential down-modulation of IL-8RA/B expression on human neutrophils by IL-8 and MGSA

To determine the rate of down-modulation of IL-8RA/B expression by IL-8, neutrophils were incubated with 119 nM IL-8 for various times at 37°C. After incubation, the expression levels of IL-8RA/B were determined by staining cells with FITC-9H1 or FITC-10H2 at 4°C, respectively (Fig. 2). Within 5 min after the addition of IL-8, >80% of IL-8RA/B disappeared from the membrane, confirming the previous report of Samanta et al. (17).

We also determined the effects of various doses of IL-8 on the down-modulation of IL-8RA/B. Since these two receptors were reported to have similar affinities (3, 8–12), we expected similar dose responses of IL-8RA/B to IL-8. In fact, there were significant differences in the dose responses of these two receptors (Fig. 3, *top* and *middle panels*). The EC_{50} of IL-8 required to down-modulate 50% of the IL-8RA and IL-8RB were 1 and 0.2 nM in donor 1, and 1.5 and 0.2 nM in donor 3, respectively. As reported (6), we observed donor variation in the expression levels of IL-8RA/B and in the EC_{50} of IL-8 required for down-regulation of these receptors. However, regardless of the expression level of IL-8RA and IL-8RB among different donors (Fig. 3, donors 1 and 3), the EC_{50} of IL-8 required for the down-modulation of IL-8RA was higher than that of IL-8RB (Table I). Despite the high IL-8 concentration (>100 nM) or longer incubation time (>1 h), we could not completely down-modulate IL-8RA/B expression on neutrophils. This may be due to the two ongoing competitive processes: down-modulation of receptors by the ligand and reappearance of receptors after dissociation from the bound ligand.

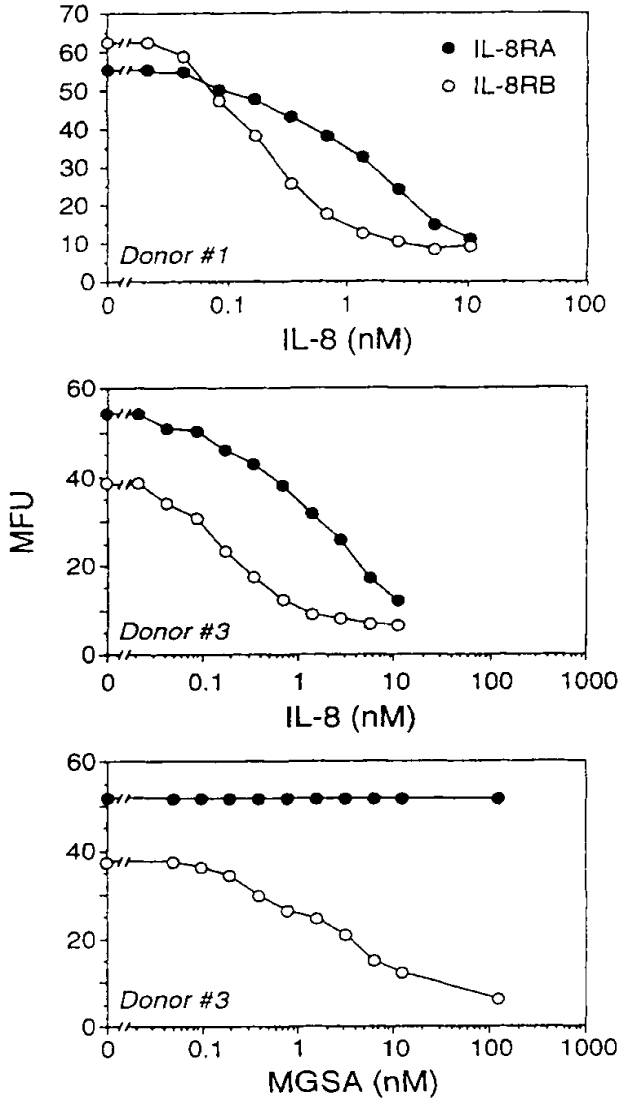

FIGURE 3. Comparison of the dose responses of IL-8RA/B to IL-8 and MGSA for down-modulation. Cells were incubated with various concentrations of human IL-8 or MGSA for 15 min at 37°C. At the end of the incubation, cells were stained with FITC-9H1 or FITC-10H2 and analyzed by flow cytometry.

We also investigated the effect of MGSA on the down-modulation of IL-8RA/B, since MGSA was reported to bind to IL-8RA with a low affinity and to IL-8RB with a high affinity similar to that of IL-8 (3, 8–12). The results in Figure 3 show that MGSA down-modulated IL-8RB but

Table I. *Affinity and EC_{50} of IL-8RA/B for IL-8*

Donor	IL-8RA		IL-8RB	
	EC_{50}	K_d [a]	EC_{50} [b]	K_d
1	1.950	0.168	0.150	0.031
2	1.300	0.096	0.195	0.027
3	1.250	0.266	0.180	0.130
4	ND	0.130	ND	0.032

[a] K_d (nM) was determined by using Scatchard analysis.
[b] EC_{50} (nM): the concentration of IL-8 which down-modulates IL-8R to be 50% of the fresh control level.

not IL-8RA, confirming the promiscuous nature of IL-8RB. In some donors, we found a slight down-modulation of IL-8RA at very high concentrations (>200 nM) of MGSA (data not shown). However, the concentration of MGSA is unlikely to reach this level even during inflammation. Therefore, we concluded that MGSA had little effect on the down-modulation of IL-8RA.

Affinities of IL-8RA/B on human neutrophils for IL-8 and MGSA

It has been generally accepted that IL-8RA/B have similar high affinities for IL-8, even though the reported affinities of IL-8RA/B for IL-8 vary from 0.1 to 4 nM (3, 8–12). However, results shown in Figure 3 showed that IL-8RB was more sensitive to IL-8 than IL-8RA, suggesting that IL-8RB had a higher affinity for IL-8 compared with IL-8RA. To confirm this affinity difference between IL-8RA and IL-8RB, we compared the affinities of these two receptors for IL-8 by Scatchard analysis (Fig. 4). Most affinity determination analysis for IL-8RA/B was performed using transfected cells, since both receptors are simultaneously expressed on human neutrophils. It is important to compare the affinities of these two receptors on neutrophils to understand the function of IL-8RA/B on neutrophils, rather than using transfected cells, because we do not know how other cell membrane components interact with IL-8R.

To determine the affinity of IL-8RA on human neutrophils for IL-8, we down-modulated IL-8RB with 127 nM MGSA, as shown in Figure 3 to avoid the problem of IL-8 binding to IL-8RB. This MGSA concentration was chosen because we observed slight down-modulation of IL-8RA at >200 nM MGSA in some donors. To determine the IL-8RB affinity for IL-8, we blocked the binding of IL-8 to IL-8RA by the addition of an excess amount of mAb 9H1, anti-IL-8RA, since we did not have an easy way to down-modulate IL-8RA without interfering with IL-8RB expression. Figure 4 shows a typical example of the Scatchard analysis of IL-8RA/B affinity for IL-8. The affinities of IL-8 binding to IL-8RA and IL-8RB were 168 and 31 pM, respectively. Scatchard analysis of the IL-8RA (Fig. 4*A*, *inset*) showed that most data points were well fitted to a one-binding site model. This suggests that the down-mod-

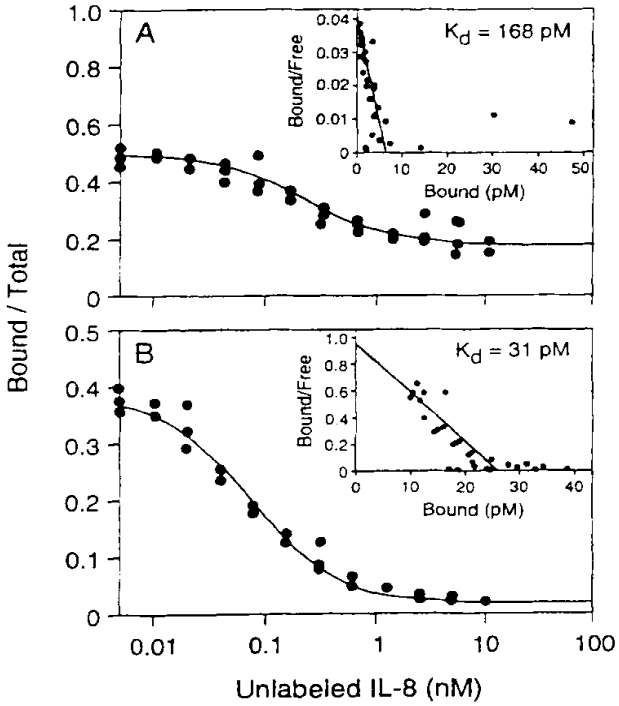

FIGURE 4. Comparison of the affinities of IL-8RA and IL-8RB on human neutrophils for IL-8 by Scatchard analysis. Human neutrophils were incubated with 127 nM MGSA (*A*) and 200 μg/ml of mAb 9H1 (*B*) to determine the affinities of IL-8RA, IL-8RB, and total IL-8R, respectively. Cells were then incubated with [^{125}I]IL-8 in the presence of various concentrations of IL-8 at 4°C for 1 h. The unbound [^{125}I]IL-8 was removed by sucrose gradient centrifugation. The level of [^{125}I]IL-8 bound to cells was determined by a γ-counter. The affinity of each receptor was determined by Scatchard analysis.

ulation of IL-8RB by MGSA was an effective way to block IL-8 binding to IL-8RB during the Scatchard analysis of the IL-8RA, even though the down-modulation of IL-8RB by 127 nM MGSA was not 100% complete, as shown in Figure 3. However, Scatchard analysis of the IL-8RB (Fig. 4*B*, *inset*) showed some deviation from a one-binding site model. This suggests that the inhibition of IL-8 binding of IL-8RA by mAb 9H1 was not 100% complete, and some of the IL-8A would participate in the affinity determination for IL-8RB. Since we observed donor variations in the expression level of each IL-8R (6, 10), we compared the affinities of IL-8RA/B for IL-8 in several donors (Table I). Results obtained from four donors showed that the affinity of IL-8RB for IL-8 was two- to fivefold higher than that of IL-8RA. Since the blocking of one receptor was not complete during Scatchard analysis of the other, the actual difference between two IL-8RA/B would be greater than what we observed. When we compared the EC_{50} of IL-8

Affinities of IL-8RB on human PMN for IL-8 and MGSA[a]

	Affinities (K_d in pM)			
	Donor 1	Donor 2	Donor 3	Mean + SD
	66.99	71.26	70.52	69.59 + 2.28
A	96.17	120.71	96.58	104.49 + 14.05

affinities of IL-8RB on human PMN for IL-8 were determined after preincubated with 200 μg/ml of mAb 9H1 (anti-IL-8RA) for 30 min contrast, the affinities of IL-8RB for MGSA were determined using cells.

down-modulation of IL-8RA/B there was a seven-old difference. From these results we concluded that re two classes of IL-8 binding sites on human PMN fferent affinities: IL-8RB is the high affinity recep-l IL-8RA is the low affinity receptor.

RB has been reported to have similar affinities for d MGSA (3, 8–12). However, we often observed EC_{50} of IL-8 required to down-modulate IL-8RB most 10 times lower than that of MGSA (Fig. 3, 3). This suggested that the affinity of IL-8RB for ight be higher than that for MGSA. To investigate ssibility, we compared the affinities of IL-8RB for d MGSA in competitive binding assays (Table II). obtained from three different donors showed that nity of IL-8RB for IL-8 (K_d = 69 pM) was only higher than that for MGSA (K_d = 104 pM), although alues were significantly different ($p < 0.05$).

ntial expression levels of IL-8RA/B on ophils that migrate to different ntrations of IL-8

portant question is the role each IL-8R plays during nation. Our results show that IL-8RB has a higher for IL-8 compared with IL-8RA. Therefore, we te that IL-8RB receives the IL-8 signal first at a site from the inflammation, where the IL-8 concentra-low, and this initiates neutrophil migration toward ammatory area. To investigate this possibility, we an in vitro chemotaxis assay. Neutrophils were into the upper chamber, and various concentrations were loaded into the lower chamber. After neu-were allowed to migrate into the lower chamber nin, migrated cells were harvested, and the expres-vels of IL-8RA/B were determined by flow cytom-g. 5). The level of IL-8RB, but not IL-8RA, on hils that migrated to the chamber with <1 nM IL-8 nificantly down-modulated. This supports the hy-s that IL-8RB may be the first receptor binding to d transmits the migratory signal of IL-8 to neutro-distant inflammation sites where the IL-8 concen-is low. The results shown in Figure 5 also suggest neutrophils migrate closer to the inflammatory area, the IL-8 concentration is high, fewer IL-8RB re-n the cell surface, and the low affinity IL-8RA re-

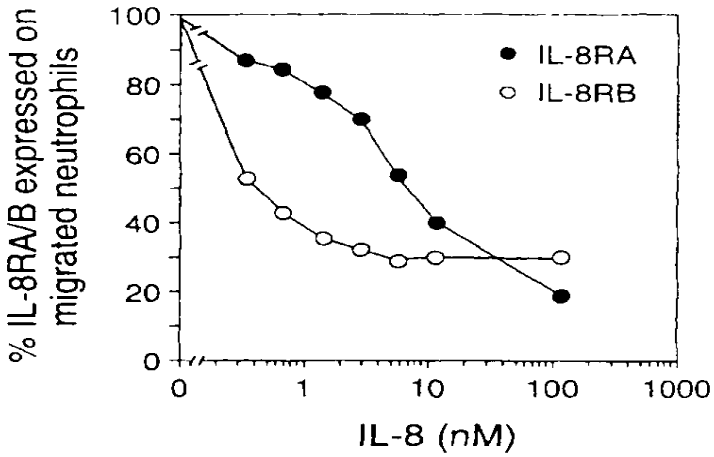

FIGURE 5. The expression levels of IL-8RA/B on human neutrophils after migration induced by IL-8 in vitro. Neutrophils were loaded into the upper chamber, and various concentrations of IL-8 were loaded into the lower chamber. After incubation at 37°C for 30 min, cells that migrated to the lower chamber were harvested, and the expression level of IL-8RA/B was analyzed by flow cytometry. The percent expression of IL-8RA/B was determined by dividing the mean fluorescence unit (MFU) of IL-8RA/B on migrated cells by the MFU of IL-8RA/B on untreated cells.

maining on the surface become an important participant in transmitting the IL-8 signal.

Reappearance of IL-8RA/B after down-modulation

It has been well documented that the low affinity receptor could be easily dissociated from the ligand compared with the high affinity receptor (23). Therefore, we postulated that the low affinity IL-8RA might play a more active role in mediating the IL-8 signal at the inflammatory area. To explore this possibility, we investigated the fate of IL-8RA/B after down-modulation by IL-8. Previously, it was reported that NH_4Cl, a lysosomotropic agent, inhibited the recycling of IL-8R on human neutrophils. Therefore, human neutrophils used in these experiments were prepared without NH_4Cl treatment. Cells were incubated with 119 nM IL-8 for 15 min to achieve maximum down-modulation, washed three times, incubated at 37°C for various times, and examined for the expression levels of IL-8RA/B during a 3-h culture period. As shown previously, most of the IL-8RA/B was down-modulated by 119 nM IL-8. However, once the exogenous IL-8 was removed, the level of IL-8RA continued to increase and reached 85% of the untreated fresh control level during a 1.5-h culture period. In contrast, the level of IL-8RB recovered to only ~40% of the control value during a 1-h culture period and then remained at that level throughout the experiment. The rapid reexpression of IL-8RA after complete down-modulation supports the hypothesis that IL-8RA may play a

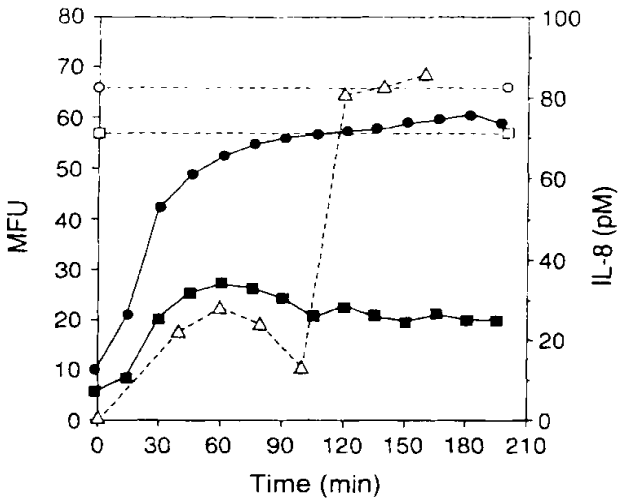

FIGURE 6. Rate of the reappearance of down-modulated IL-8Rs. Neutrophils (10^6 cells/ml) were incubated with or without 119 nM IL-8 at 37°C for 15 min. After washing, cells were aliquoted, incubated for various periods at 37°C, and analyzed for expression level of IL-8RA/B by flow cytometry. ●, IL-8RA with IL-8; ○, IL-8RA without IL-8; ■, IL-8RB with IL-8; □, IL-8RB without IL-8; △, IL-8 in the culture supernatants of neutrophils (5×10^5 cells/ml).

more active role in transmitting the IL-8 signal in the inflammatory area compared with IL-8RB. The slow recovery rate of IL-8RB may be due to the fact that IL-8RB has a high affinity for IL-8; therefore, it dissociates from IL-8 slowly.

It has been reported that neutrophils secrete IL-8 (22, 24, 25). We detected approximately 0.1 nM IL-8 by ELISA in culture supernatant incubated with neutrophils (10^6 cells/ml) for 1.5 h at 37°C (Fig. 6). This level of IL-8 would have some effect on the expression level of IL-8RB according to the results shown in Figure 3. To investigate this possibility, we added 10 μg/ml of neutralizing anti-human IL-8 mAb, 6G4 (26), to the culture containing neutrophils whose IL-8Rs were down-modulated by IL-8 and analyzed the recovery rate of IL-8RB at various times. The addition of 6G4 mAb enhanced IL-8RB expression; however, the recovery rate of IL-8RB was still slower than that of IL-8RA (data not shown).

Discussion

In the past, the regulatory mechanism of IL-8R expression on human neutrophils by IL-8 was investigated by detecting the remaining IL-8R on the cell surface with [^{125}I]IL-8 (17–19). The experiment shown in Figure 1 demonstrated that we could use FITC-9H1 and FITC-10H2 to detect IL-8RA/B on human neutrophils that were preincubated with IL-8. These mAb were originally selected for their abilities to inhibit [^{125}I]IL-8 binding to IL-8R A/B at 4°C (6, 20) and were shown to bind to the N-terminal portion of each receptor. Therefore, it may not be surprising that mAb 9H1 and 10H2 could detect almost all IL-8RA/B, respectively, even after neutrophils were preincubated with IL-8.

It has been generally accepted that IL-8RA/B have similar high affinities for IL-8 (3, 8–12). However, our results obtained from the comparison of the EC_{50} of IL-8 (Fig. 3 and Table I) and the K_d of each receptor for IL-8 (Fig. 4 and Table I) clearly demonstrate that IL-8RB has a higher affinity for IL-8 compared with IL-8RA: we detected seven- to 13-fold and two- to fivefold differences in the EC_{50} of IL-8 and the K_d values, respectively. Our finding of a two- to fivefold difference in the affinities (K_d) of IL-8RA/B for IL-8 does not necessarily contradict the previous findings for the following reasons. First, for other cytokines, the magnitude of difference in the affinities between a high and a low affinity receptor was at least in the range of 10- to 100-fold (23). Since the difference in affinities of IL-8RA and IL-8RB for IL-8 as determined by the Scatchard analysis is only in the range of two- to fivefold, the affinity might be concluded to be similar (or the same), especially compared with those for MGSA. For example, Cerrett et al. (10) reported the K_a of IL-8RA and IL-8RB to be 5.5×10^8 and 1.9×10^9, respectively, but they simply stated that IL-8RA/B had high affinities for IL-8 even though they observed biphasic patterns of ligand binding in some human donors. Second, during our Scatchard analysis, we tried to block the binding of IL-8 to one receptor to determine the affinity of the other receptor, but the blocking methods were not 100% effective. This incomplete blocking would narrow the measured difference between these two receptors. Therefore, the actual K_d difference between these two receptors would be greater than what we and others observed. A more accurate comparison of the relative affinities of IL-8RA/B might be obtained by evaluating the EC_{50} of IL-8 for receptor down-modulation, since these values were obtained without the extra IL-8-blocking step, and receptor modulation by the ligand may require an interaction at specific binding sites that may be more relevant in their physiologic functions.

The results presented in Figure 4 show that IL-8RB, but not IL-8RA, was down-modulated by MGSA, confirming the previous report of the promiscuous nature of IL-8RB and the IL-8 specificity of IL-8RA. The IL-8RA that has a lower affinity for IL-8 could not be down-modulated by MGSA, since its affinity for MGSA is much too low. For other hemopoietic growth factors, such as IL-3, IL-5, and GM-CSF, the high affinity receptor shows cross-reactivity to other related growth factors, while the low affinity receptor shows specificity for the particular growth factor (27, 28). Although no structural similarity exists between the IL-8R and other hemopoietic growth factor receptors, the principle that the high affinity receptor shows cross-reactivity to other related growth factors and the low affinity receptor shows specificity may also apply to IL-8R.

The EC_{50} of IL-8 required to down-modulate IL-8RB was almost 10 times lower than that of MGSA (Fig. 3, donor 3); however, we observed only a 1.5-fold difference in the affinities of IL-8RB for IL-8 and MGSA by Scatchard analysis (Table II) even though the difference was statistically significant ($p < 0.05$). The more drastic difference in the EC_{50} of IL-8 and that of MGSA could be due to the fact that IL-8RB modulation by the ligand may require an interaction at specific sites beyond the simple total binding, which was detected during the Scatchard analysis.

In the course of inflammation, resident macrophages and fibroblasts, located at the site of inflammation, secrete IL-8, and this secreted IL-8 gradually reaches nearby blood vessels. At a distant site, the concentration of IL-8 could be in the picomolar range; the IL-8 concentrations in the blood of burn patients (29) and early stage adult respiratory distress syndrome patients (30) were reported to be 27 and 770 pM, respectively. At the low picomolar concentrations of IL-8, IL-8RB would receive the IL-8 signal first and initiate the migration of neutrophils toward the inflammatory area, as shown in Figure 5. As neutrophils migrate closer to the site of inflammation, the IL-8 concentration can increase to the nanomolar range. The concentrations of IL-8 in the sputum (the site of inflammation) of patients with chronic inflammatory airway diseases are reported to be range from 1 to 9 nM (31). At these IL-8 concentrations, IL-8RA would be the major receptor involved in mediating the IL-8 signal, since few IL-8RB would remain on the cell membrane. This hypothesis is further supported by results obtained from patient samples (S. Fujishima manuscript in preparation).

The results presented in Figure 6 show that the recovery rate of IL-8RA expression was rapid after down-modulation, while that of IL-8RB was slow. This observation suggests that at the site of inflammation, the low affinity IL-8RA may play a major active role in transmitting the IL-8 signal due to its rapid recovery rate, while the high affinity IL-8RB would play a minor role due to its slow recovery rate. An important function of the high affinity receptors for the hemopoietic growth factors has been suggested to be the internalization and degradation of ligand, since the ligand-receptor affinities are high enough that the ligand is less likely to be dissociated from the receptor (23, 28). In the G protein-binding, seven-transmembrane domain thrombin receptor, it has been suggested that the receptor is then internalized shortly after activation, and the ligand bound to the receptor is dissociated and degraded in the lysosome (32). The resulting free receptor is then recycled to the cell surface membrane. IL-8 bound to the receptors was shown to be internalized and degraded in lysosomes (17). The slow recovery rate of IL-8RB suggests that the high affinity IL-8RB may bring IL-8 to the lysosome, where it is degraded. This subject needs further investigation.

Our present study shows the different affinities of IL-8RA/B for IL-8, which may result in differential function; the low affinity IL-8RA may play an active role in mediating IL-8 signal in the inflammatory area, while the high affinity IL-8RB may initiate the neutrophil migration in a distant area of infection. These findings may help in understanding the interaction of chemokines with their seven-transmembrane domain receptors and could facilitate the development of anti-inflammatory therapeutic drugs.

Acknowledgments

We thank Brian Fendly, Caroline Hebért, Peter Ralph, and William Wood for critical comments on the manuscript, Marcel Reichert for the IL-8 ELISA, and Henry Lowman for the single subunit IL-8.

References

1. Oppenheim, J. J., C. O. Zachariae, N. Mukaida, and K. Matsushima. 1991. Properties of the novel proinflammatory supergene "intercrine" cytokine family. *Annu. Rev. Immunol. 9:617.*
2. Hebert, C. A., and J. B. Baker. 1993. Interleukin-8: a review. *Cancer Invest. 11:743.*
3. Baggiolini, M., B. Dewald, and B. Moser. 1994. Interleukin-8 and related chemotactic cytokines-C-X-C and C-C chemokines. *Adv. Immunol. 55:97.*
4. Holmes, W. E., J. Lee, W.-J. Kuang, G. C. Rice, and W. I. Wood. 1991. Structure and functional expression of a human interleukin-8 receptor. *Science 253:1278.*
5. Murphy, P. M., and H. L. Tiffany. 1991. Cloning of complementary DNA encoding a functional human interleukin-8 receptor. *Science 253:1280.*
6. Chuntharapai, A., J. Lee, C. Hebert, and K. J. Kim. 1994. Monoclonal antibodies detect different distribution patterns of IL-8 receptor A and IL-8 receptor B on human peripheral blood leukocytes. *J. Immunol. 153:5682.*
7. Morohashi, H., T. Miyawaki, H. Nomura, K. Kuno, S. Murakami, K. Matsushima, and N. Mukaida. 1995. Expression of both types of human interleukin-8 receptors on mature neutrophils, monocytes and natural killer cells. *J. Leukocyte Biol. 57:180.*
8. Lee, J., R. Horuk, G. C. Rice, G. L. Bennett, T. Camerato, and W. I. Wood. 1992. Characterization of two high affinity human interleukin-8 receptors. *J. Biol. Chem. 267:16283.*
9. Moser, B., C. Schumacher, V. Von Tscharner, I. Clark-Lewis, and M. Baggiolini. 1991. Neutrophil-activating peptide 2 and gro/melanoma growth stimulatory activity interact with neutrophil-activating peptide 1/interleukin 8 receptors on human neutrophils. *J. Biol. Chem. 266:10666.*
10. Cerretti, D. P., C. J. Kozlosky, T. V. Bos, N. Nelson, D. P. Gearing, and M. P. Beckmann. 1993. Molecular characterization of receptors for human interleukin-8, GRO/melanoma growth stimulatory activity and neutrophil activating peptide-2. *Mol. Immunol. 30:359.*
11. Schnitzel, W., U. Monschein, and J. Besemer. 1995. Monomer-dimer equilibria of interleukin-8 and neutrophil-activating peptide 2. Evidence for IL-8 binding as a dimer and oligomer to IL-8 receptor B. *J. Leukocyte Biol. 55:763.*
12. Loetscher, P., M. Seitz, I. Clark-Lewis, M. Baggiolini, and B. Moser. 1994. Both interleukin-8 receptors independently mediate chemotaxis. Jurkat cells transfected with IL-8R1 or IL-8R2 migrate in response to IL-8, GROα and NAP-2. *FEBS Lett. 341:187.*
13. Rajarathnam, K., B. D. Sykes, C. M. Kay, B. Dewald, T. Geiser, M. Baggiolini, and I. Clark-Lewis. 1994. Neutrophil activation by monomeric Interleukin-8. *Science 264:90.*
14. Hébert, C., V. R. Vitangcol, and J. Baker. 1991. Scanning mutagenesis of interleukin-8 identifies a cluster of residues required for receptor binding. *J. Biol. Chem. 266:18989.*
15. Clark-Lewis, I., C. Schumacher, M. Baggiolini, and B. Moser. 1991. Structure-activity relationships of interleukin-8 determined using

chemically synthesized analogs. Critical role of NH_2-terminal residues and evidence for uncoupling of neutrophil chemotaxis, exocytosis, and receptor binding activities. *J. Biol. Chem. 266:23128.*

16. Schraufstatter, I. U., D. S. Barritt, M. Mia, Z. G. Oades, and C. G. Cochrane. 1993. Multiple sites on IL-8 responsible for binding to a and b IL-8 receptors. *J. Immunol. 151:6418.*
17. Samanta, A. K., J. J. Oppenheim, and K. Matsushima. 1990. Interleukin 8 (monocyte-derived neutrophil chemotactic factor) dynamically regulates its own receptor expression on human neutrophils. *J. Biol. Chem. 265:183.*
18. Besemer, J., A. Hujber, and B. Kuhn. 1989. Specific binding, internalization, and degradation of human neutrophil activating factor by human polymorphonuclear leukocytes. *J. Biol. Chem. 264:17409.*
19. Grob, P. M., E. David, T. C. Warren, R. P. DeLeon, P. R. Farina, and C. A. Homon. 1990. Characterization of a receptor for human monocyte-derived neutrophil chemotactic factor/interleukin-8. *J. Biol. Chem. 265:8311.*
20. Chunthrarapai, A., J. Lee, J. Burnier, W. I. Wood, C. Hebert, and K. J. Kim. 1993. Neutralizing monoclonal antibodies to human IL-8 receptor A map to the N-terminal region of the receptor. *J. Immunol. 152:1783.*
21. Munson, P. J., and D. Rodbard. 1980. Ligand: a versatile computerized approach for characterization of ligand-binding systems. *Anal. Biochem. 160:1085.*
22. Fujishima, S., A. R. Hoffman, T. Vu, K. J. Kim, H. Zheng, D. Daniel, Y. Kim, E. F. Wallace, J. W. Larrick, and T. A. Raffin. 1993. Regulation of neutrophil interleukin 8 gene expression and protein secretion by LPS, TNF-a, and IL-1b. *J. Cell. Physiol. 154:478.*
23. Nicola, N. A. 1991. Structural and functional characteristics of receptors for colony stimulating factors. In *Hematopoietic growth factors.* P. J. Quesenberry, S. Asano, and K. Saito, eds. Excerpta Medica, Amsterdam, p. 101.
24. Bazzoni, F., M. A. Cassatella, F. Rossi, M. Ceska, B. Dewald, and M. Baggiolini. 1991. Phagocytosing neutrophils produce and release high amounts of the neutrophil-activating peptide/interleukin 8. *J. Exp. Med. 173:771.*
25. Strieter, R. M., K. Kashara, R. Allen, H. J. Showell, T. J. Standiford, and S. L. Kunkel. 1990. Human neutrophils exhibit disparate chemotactic factor gene expression. *Biophys. Res. Commun. 173:725.*
26. Broaddus, V. C., A. M. Boylan, J. M. Hoeffel, K. J. Kim, M. Sadick, A. Chuntharapai, and C. A. Hébert. 1993. Neutralization of interleukin-8 inhibits intrapleural neutrophil influx in endotoxin pleurisy in rabbits. *J. Immunol. 152:2960.*
27. Guilbert, L. J., and E. R. Stanley. 1986. The interaction of ^{125}I-colony-stimulating factor-1 with bone marrow-derived macrophages. *J. Biol. Chem. 261:4024.*
28. Nicola, N. A., and D. Metcalf. 1991. Subunit promiscuity among hemopoietic growth factor receptors. *Cell 8:134.*
29. Fujishima, S., J.-J. Sasaki, Y. Shinozawa, K. Takuma, S. Hori, and N. Aikawa. 1993. Interleukin 8 in ARDS. *Lancet 342:237.*
30. Donnelly, S., R. M. Strieter, S. L. Kunkel, A. Walz, C. R. Robertson, D. C. Carter, I. S. Grant, A. J. Pollok, and C. Haslett. 1993. Interleukin-8 and development of adult respiratory distress syndrome in at-risk patient groups. *Lancet 341:643.*
31. Richman-Eisenstat, J. B. Y., P. G. Jorens, C. A. Hébert, I. Ueki, and J. A. Nadel. 1993. Interleukin-8: an important chemoattractant in sputum of patients with chronic inflammatory airway diseases. *Am. J. Physiol. 264:L413.*
32. Brass, L. F., S. Pizarro, M. Ahuja, E. Belmonte, N. Blanchard, J. M. Stadel, and J. A. Hoxie. 1994. Changes in the structure and function of the human thrombin receptor during receptor activation, internalization and recycling. *J. Biol. Chem. 269:2943.*